Identification of Signaling Pathways Dysregulated during Scrapie Pathogenesis using a Kinomics Approach

by

Rory Harry Shott

A thesis submitted in partial fulfillment of the requirements for the degree of

Doctor of Philosophy

Department of Biochemistry

University of Alberta

ABSTRACT

Prion diseases are a family of chronic lethal neurodegenerative diseases that affect humans and animals. The conversion of the cellular prion protein (PrP^{C}) to abnormal conformations (PrP^{Sc}) is accepted to be required for pathogenesis. However, the molecular mechanisms whereby PrP conversion ultimately results in neuronal death remains poorly understood.

Reversible protein phosphorylation by protein kinases and phosphatases regulates signal transduction. Dysregulated protein kinases are involved in the pathogenesis of many chronic diseases, including the neurodegenerative Alzheimer's and Parkinson's diseases. Consequently, protein kinases have become major therapeutic targets. Protein kinases are also involved in prion disease pathogenesis. However, the signaling pathways most critical to pathogenesis are yet unknown.

In this thesis, I describe the development of a multiplex Western blot-based kinomics approach to identify signaling pathways dysregulated during prion disease pathogenesis. This approach was validated using an *in vitro* model of prion pathogenesis, N2a neuroblastoma cells expressing cytoplasmic PrP mutants. The application of the kinomics approach to an *in vivo* model, mice infected with scrapie, revealed the dysregulation of two signaling pathways involved in neuronal survival or death at different times after infection. The pro-survival CaMK4β/CREB signaling pathway was activated at pre-clinical stages, but returned to mock-infected levels prior to the onset of clinical disease and the activation of pro-death MST1 signaling. My discovery that CaMK4β/CREB and MST1 signaling is dysregulated in mice infected with scrapie expands our understanding of the molecular mechanisms of prion-mediated neuronal death and identifies potential targets to further evaluate the roles of these pathways in prion disease pathogenesis.

PREFACE

A version of Chapter 3 has been published as RH Shott, C Appanah, C Grenier, G Tremblay, X Roucou, LM Schang, "Development of kinomic analyses to identify dysregulated signaling pathways in cells expressing cytoplasmic PrP". 2014. *Virology Journal* **11**:175. I designed, developed, and performed the kinomic analyses. I critically evaluated the results and wrote all drafts and final version of the manuscript under direct supervision by Luis M. Schang. Under my direct supervision, Cathy Appanah contributed the PKCθ data in the spiking experiments. Catherine Grenier and Guillaume Tremblay provided the constructs, performed the transfections, evaluated the transfection efficiencies and prepared the lysates. Xavier Roucou critically revised the manuscript. Luis M. Schang designed the study.

A version of Chapter 4 has been published as RH Shott, A Majer, KL Frost, SA Booth, LM Schang, "Activation of pro-survival CaMK4β/CREB and pro-death MST1 signaling at early and late times during a mouse model of prion disease". 2014. *Virology Journal* **11**:160. I prepared the homogenates and performed the kinomic analyses. I critically evaluated the results and wrote all drafts and final version of the manuscript under direct supervision by Luis M. Schang. Kathy L. Frost and Anna Majer performed the infections and collected and dissected the brains. Stephanie A. Booth and Anna Majer critically revised the manuscript. Luis M. Schang designed the study. All of the procedures involving live animals were approved by the Canadian Science Centre for Human and Animal Health – Animal Care Committee (CSCHAH-ACC) according to the guidelines set by the Canadian Council on Animal Care. The approval identifications for this study were animal use document (AUD) #H-08-009 and #H-11-020.

ACKNOWLEDGEMENTS

The work described here was supported by grants from PrioNet Canada, the Alberta Prion Research Institute, the Canadian Institutes for Health Research, and an award from the Burroughs Wellcome Fund. I would like to acknowledge financial support from the National Sciences and Engineering Research Council, the Government of the Province of Alberta (Queen Elizabeth II Doctoral Scholarship) and the University of Alberta Faculty of Medicine and Dentistry (75th Anniversary Graduate Student award). I would also like to acknowledge PrioNet Canada, Alberta Prion Research Institute, and the University of Alberta Faculty of Graduate Studies and Research for travel and training support.

The research presented here would not have been possible without the contributions of numerous individuals at various institutions. I would like to thank Dr. Deborah McKenzie, Camilo Duque Velásquez, Jacques van der Merwe from the University of Alberta Centre for Prions and Protein Folding Diseases (Edmonton, AB) for training and the use of, and accessibility to, materials, equipment and facilities. I thank Dr. Xavier Roucou, Catherine Grenier, and Guillaume Tremblay from the Université de Sherbrooke (Sherbrooke, QC) and Dr. Stephanie Booth, Anna Majer, Kathy Frost, and the staff from the National Microbiology Laboratory (Winnipeg, MB) for collaboration and the preparation of samples used in my studies. I would like to acknowledge all past and present members of the University of Alberta Signal Transduction Research Group for their training, and the staff and faculty of the University of Alberta Department of Biochemistry for their tireless efforts in providing a constructive research environment. I would like to thank my committee members Dr. Charles Holmes and Dr. David Westaway for their continued support throughout my program. I thank all current and past lab members for making these years of

research some of the most enjoyable to date (Kristen Conn, Rebecca Gibeault, Che Colpitts, Mi-Yao Hu, Abdullah Awadh, Esteban Flores, Sietske Speerstra, Rachael Erdmann, Michael Bildersheim, Emma Newman, Jonathan Lacasse, Mireille St.Vincent, Véronic Provencher, Furkat Mukhtarov, Bizhan Romani). Lastly, I give my deepest appreciation and thanks to my supervisor Dr. Luis M. Schang for his patience, dedication, and knowledge which was critical to the research I present here within this thesis.

TABLE OF CONTENTS

LIST OF TABLES

CHAPTER 1

CHAPTER 3

CHAPTER 4

LIST OF FIGURES

CHAPTER 1

CHAPTER 3

CHAPTER 4

LIST OF APPENDICES

CHAPTER 3

CHAPTER 4

LIST OF ABBREVIATIONS

ADAM	a disintegrin and metalloproteinase
Akt	protein kinase B
AMPA	alpha-amino-3-hydroxy-5-methyl-4-isoxazole propionic acid
AMPKα1	adenosine monophosphate-activated protein kinase catalytic subunit alpha-1
ATF6	activating transcription factor 6
Bax	Bcl-2 associated X protein
Bcl-2	B-cell lymphoma protein 2
BSE	bovine spongiform encephalopathy
c-Abl	Abelson leukemia oncogene cellular homolog
c-Kit	Hardy-Zuckerman 4 feline sarcoma virus oncogene cellular homolog
CaMK	calcium/calmodulin-dependent kinase
CaMK4β	calcium/calmodulin-dependent kinase 4, beta isoform
CC1	charged cluster 1 (region in PrP)
CC2	charged cluster 2 (region in PrP)
CDK	cyclin-dependent kinase
CREB	cAMP response element-binding protein
CWD	chronic wasting disease
CyPrP	cytoplasmic PrP
DLK	dual leucine zipper kinase
dpi	days post-inoculation
Dpl	Doppel
EGFP	enhanced green fluorescent protein
eIF2α	eukaryotic initiation factor 2 alpha
eIF4B	eukaryotic initiation factor 4B
EPSC	excitatory postsynaptic current
ERAD	ER-associated degradation
Erk	extracellular signal-regulated kinase
FFI	fatal familial insomnia
FK506	calcineurin/protein phosphatase 3 inhibitor (also known as tacrolimus)
FOXO3	forkhead box protein O3
Fyn	feline Gardner-Rasheed sarcoma virus oncogene cellular homolog/Yamaguchi 73 and Esh avian sarcoma virus oncogene cellular homolog-related novel protein kinase
GADD34	growth arrest and DNA damage-inducible protein 34 (also known as protein phosphatase 1 regulatory subunit 15A, PPP1R15A)

gCJD	genetic Creutzfeldt-Jakob disease
GFAP	glial fibrillary acid protein
GPI	glycosylphosphatinisitol
GSS	Gerstmann-Sträussler-Scheinker
H&E	hematoxylin and eosin
HD	hydrophobic domain (region in PrP)
Hsp70	heat shock protein 70
iCJD	iatrogenic Creutzfeldt-Jakob disease
IHC	immunohistochemistry
IRE1	inositol-requiring protein 1
JNK	c-Jun N-terminal kinase
KA	kainic acid
kDa	kilodalton
Lyn	v-yes-1 Yamaguchi sarcoma viral related oncogene homolog
MKK7	mitogen-activated protein kinase kinase 7
MST1	mammalian STE20-like protein kinase 1 (also known as STK4, serine/threonine protein kinase 4)
mTOR	mammalian target of rapamycin
mTORC	mammalian target of rapamycin complex
NICD	Notch-1 intracellular domain
NMDA	*N*-methyl-D-aspartate
NMDAR	*N*-methyl-D-aspartate receptor
NMR	nuclear magnetic resonance
nNOS	neuronal nitric oxide synthase
OR	octapeptide repeat (region in PrP)
p38γ	mitogen-activated protein kinase 12
p70S6K	ribosomal protein S6 kinase, 70 kilodalton, polypeptide 1
PDGFR	platelet-derived growth factor receptor
PDK	phosphoinositide-dependent kinase
PERK	PKR-like ER kinase
PIPLC	phosphatidylinositol-specific phospholipase C
PK	proteinase K
PKA	protein kinase A
PKC	protein kinase C
PMCA	protein misfolding cyclic amplification
PrP^{Ctm}	C-terminal transmembrane PrP
PrP^{sen}	protease-sensitive prion protein

PrP^{res}	protease-resistant prion protein
PSD-95	post-synaptic density protein 95
RML	Rocky Mountain Laboratory mouse-adapted scrapie strain
ROCK	Rho-associated coiled-coil-containing protein kinase
ROS	reactive oxygen species
RSK	ribosomal protein S6 kinase
sCJD	sporadic Creutzfeldt-Jakob disease
SDS	sodium dodecyl sulfate
Sho	Shadoo
STI571	'signal transduction inhibitor' 571 (also known as imatinib or Gleevec)
TME	transmissible mink encephalopathy
UPS	ubiquitin-proteasome system
UPR	unfolded protein response
vCJD	variant Creutzfeldt-Jakob disease
VEGFR	vascular endothelial growth factor receptor

CHAPTER 1: INTRODUCTION

Transmissible spongiform encephalopathies (TSEs), or prion diseases, are a family of chronic neurodegenerative diseases against which there are yet no preventative or therapeutic treatments (Colby et al., 2011; Chen et al., 2013). Prion diseases are invariably lethal to humans and other species such as cattle, goat, sheep, deer, elk and moose (Prusiner, 1998; Baeten et al., 2007). The characteristic neuropathology of prion diseases includes gliosis, spongiform degeneration, and neuronal death. The conversion of the cellular prion protein (PrP^{C}) to abnormal conformations (PrP^{Sc}) is widely accepted to be essential for pathogenesis. However, the molecular mechanisms whereby such conversion eventually leads to the consequent neurodegeneration are not yet fully understood.

1.1 Prion etiology

The study of prion diseases began with sheep scrapie. First described over 250 years ago, the disease was named for the salient behaviour of affected sheep to scrape excessively against stationary objects due to intense itch (pruritus), which frequently resulted in the loss of fleece (for review see Schneider et al., 2008). Death invariably followed 2-24 weeks of progressive clinical disease. Scrapie often appeared in flocks after the introduction of otherwise healthy sheep from infected flocks. Early attempts to experimentally transmit scrapie failed even after 9 months of observation. However, it was later noted that sheep on scrapie-affected farms rarely developed the disease before 18 months of age (Stockman, 1913). Thus, new experiments were performed in which healthy sheep (scrapie-free for 18 months) were inoculated with scrapie-infected brain homogenate and monitored for an extended period. Inoculated sheep developed scrapie 11-22

months later, depending on route of inoculation (Cuillé et al., 1936, as described by Hedlin et al., 2012). Scrapie was therefore an infectious disease with an unusually long incubation period (time from infection to the onset of clinical signs of disease). The infectious nature of scrapie was inadvertently verified when ~18,000 sheep were inoculated with a batch of louping-ill vaccine that unknowingly contained brain and spinal cord from scrapie-infected animals (Gordon, 1946). Approximately 5% of inoculated sheep not yet processed for consumption developed scrapie two years later, which was consistent with the incubation period (22 months) after subcutaneous inoculation observed previously by Cuillé and Chelle (1936).

Experimental transmission of scrapie to hamsters and mice reduced the incubation period to only 2 and 4 months, respectively (Chandler, 1961; Kimberlin et al., 1977). Size filtration experiments demonstrated that the scrapie agent was smaller than any bacteria (Gibbs, 1967; Kimberlin et al., 1971). The long incubation period of scrapie followed by death after a comparatively short clinical phase was like that of the slow viral diseases of sheep, *maedi* and *visna* (Sigurðsson., 1954; ter Meulen et al., 1978). Ultraviolet light (254 nm wavelength) damages nucleic acids largely through the formation of cyclobutane pyrimidine dimers or pyrimidine (6-4) pyrimidone photoproducts (for review see Sage, 1993; Batista et al., 2009). Surprisingly, the scrapie agent was more resistant to inactivation by ultraviolet light (254 nm wavelength) than any known virus (Alper et al., 1966; Alper et al., 1967), leading Alper to speculate that the agent may lack any nucleic acid (Alper et al., 1967). Pattison proposed the scrapie agent may be composed of protein (Pattison et al., 1967). This novel concept was developed into the protein-only hypothesis by Griffith, who theorized that an infectious protein could replicate without nucleic acid by inducing the conversion of a host protein into infectious one (Griffith, 1967). The newly formed

infectious protein would seed further conversion events resulting in exponential accumulation. Scrapie infectivity was reduced by treatments that hydrolyze or modify proteins (harsh proteinase K treatment, diethyl pyrocarbonate [DEP]/hydroxylamine, sodium dodecyl sulfate [SDS], chaotrophic ions, phenol, urea) but not by those that hydrolyze or modify nucleic acid (micrococcal nuclease, DNAse I, RNAses A and T1, divalent cations, hydroxylamine, psoralens, acid, ultraviolet light) (Millson et al., 1976; Cho, 1980; Prusiner et al., 1980a; Prusiner et al., 1980b; McKinley et al., 1981; Prusiner et al., 1981a; Prusiner et al., 1981b; McKinley et al., 1983b; Bellinger-Kawahara et al., 1987a; Bellinger-Kawahara et al., 1987b). Although these results could not exclude (and even supported) the possibility that the scrapie agent was a virus or virino (non-coding nucleic acid coated with host protein, Dickinson et al., 1979; Kimberlin, 1982) whose nucleic acid was encapsulated within a protein coat, scrapie-specific nucleic acids were not identified (Wietgrefe et al., 1985; Oesch et al., 1988; Duguid et al., 1988; Duguid et al., 1989). Prusiner would ultimately propose the scrapie agent to be a proteinaceous infectious particle, or prion (Prusiner, 1982), a concept for which he would later receive the Nobel Prize in Medicine in 1997.

Early purification experiments sedimented scrapie infectivity with cellular membrane fractions (Hunter et al., 1964; Millson et al., 1971). Further characterization of the sedimentation profile and biochemical behaviour of the scrapie agent allowed Prusiner to enrich for scrapie infectivity within these fractions by detergent extraction, micrococcal nuclease and proteinase K digestions, and discontinuous sucrose gradient sedimentation (Prusiner et al., 1977; Prusiner et al., 1978a; Prusiner et al., 1978b; Prusiner et al., 1981b; Prusiner et al., 1982). Fractions enriched for scrapie infectivity contained a host-encoded 27-30 kilodalton (kDa) protein (named PrP^{res}, for

protease-resistant prion protein) (Oesch et al., 1985; Chesebro et al., 1985), which was absent from uninfected or mock-infected controls (Prusiner et al., 1982; Bolton et al., 1982; Bendheim et al., 1984). PrP^{res} immunoblots of undigested scrapie-infected homogenates detected a detergent insoluble 33-35 kDa protein (named PrP^{Sc}, for prion protein scrapie) (Meyer et al., 1986). A detergent soluble 33-35 kDa protein detected in uninfected and scrapie-infected animals (named PrP^{C}, for prion protein cellular) was completely degraded by proteinase K (Oesch et al., 1985; Meyer et al., 1986). Although small nucleic acid fragments were also detected in fractions enriched for scrapie infectivity (Meyer et al., 1991; Kellings et al., 1992; Safar et al., 2005c), PrP^{Sc} was an alternative conformation of PrP^{C} that seeded its own conversion, consistent with the protein-only hypothesis (Pan et al., 1993; Stahl et al., 1993; Safar et al., 1993; Kocisko et al., 1994; Saborio et al., 2001). Moreover, the levels of PrP^{Sc} correlated with scrapie infectivity (McKinley et al., 1983a; Gabizon et al., 1988).

PrP^{Sc} was detected post-mortem in the brains of patients with the spongiform encephalopathy Gerstmann-Sträussler-Scheinker (GSS) (Roberts et al., 1986). GSS was experimentally transmissible (Tateishi et al., 1995b) but unlike scrapie, appeared to be dominantly inherited rather than acquired by infection. Following two families with GSS, the disease was linked to a proline (P) to leucine (L) substitution mutation at codon 102 of the gene encoding for PrP^{C}, denoted P102L PrP (Hsiao et al., 1989). Transgenic mice overexpressing mutant P101L PrP (corresponds to P102L in humans) accumulated PrP^{Sc} and developed neurodegenerative disease reminiscent of GSS at 150-200 days of age (Hsiao et al., 1990; Hsiao et al., 1994; Tremblay et al., 2004). Mice overexpressing wild-type PrP to similar levels remained healthy until 600 days of age (Telling et al., 1996). Neurological disease also spontaneously developed in transgenic mice

expressing other PrP mutations linked to GSS or other inherited spongiform encephalopathies of humans (fatal familial insomnia [FFI], genetic Creutzfeldt-Jakob disease [gCJD]) (Chiesa et al., 1998; Dossena et al., 2008; Yang et al., 2009; Jackson et al., 2009; Torres et al., 2013; Bouybayoune et al., 2015). The diseases induced in mice by the overexpression of mutant PrP P101L, D177N (aspartic acid [D] to asparagine [N] substitution mutation at codon 177 associated with FFI; corresponds to D178N in humans), and E199K (glutamic acid [E] to lysine [K] substitution mutation at codon 199 associated with gCJD; E200K in humans) were transmissible to wild-type mice or transgenic mice overexpressing wild-type PrP (Jackson et al., 2009; Friedman-Levi et al., 2011; Jackson et al., 2013). The expression of mutant PrP therefore induced the formation of infectious prions.

Mutant PrP were subsequently used to generate prions *in vitro*. Synthetic mutant P101L PrP folded into a PrP^{Sc}-like conformation induced transmissible neurodegenerative disease in transgenic mice (Tg196, which express P101L PrP at levels ~2-fold higher than endogenous PrP^{C}) (Kaneko et al., 2000; Tremblay et al., 2004). Recombinant PrP (recPrP) purified from *Escherichia coli* and folded into a PrP^{Sc}-like conformation was toxic to cultured cells and primary neurons (Novitskaya et al., 2006). Recombinant PrP in a PrP^{Sc}-like conformation induced transmissible neurodegenerative disease in transgenic mice overexpressing wild-type PrP (Tg4053) 470-700 days post-inoculation (dpi) (Colby et al., 2009). In similar experiments with transgenic mice overexpressing truncated PrP (Tg9949, which express PrP^{C} lacking residues 23-88 [PrPΔ23-88] at levels ~16-fold higher than endogenous PrP^{C}) transmissible neurodegenerative disease was induced 380-660 dpi (Legname et al., 2004; Colby et al., 2010). Uninoculated Tg9949 mice developed disease at ~600 days of age, but disease was not transmissible or associated with PrP^{Sc} accumulation

(Colby et al., 2010). Remarkably, purified PrP^C (in the presence of synthetic polyanions or synthetic phosphatidylethanolamine) or recombinant PrP (in the presence of synthetic phospholipid and total mouse liver RNA) subjected to repeated rounds of sonication and incubation also induced transmissible neurodegenerative disease in mice, suggesting *de novo* prion formation (Deleault et al., 2007; Wang et al., 2010a; Deleault et al., 2012; Zhang et al., 2013; Wang et al., 2015). Although nucleic acid was included in such reactions, scrapie infectivity was unaffected by nucleic acid degradation (Piro et al., 2011). Moreover, recombinant PrP alone also induced transmissible neurodegenerative disease in wild-type hamsters and mice after serial transmission resulted in sufficient PrP^{Sc} accumulation (Makarava et al., 2012; Raymond et al., 2012). Prions were therefore generated *de novo* from recombinant PrP. Together these findings demonstrate that prions are infectious agents consisting largely, if not solely, of PrP^{Sc}, an abnormal conformation of the cellular prion protein.

1.2 Prion protein (PrP^C)

The cellular prion protein (PrP^C) is a glycoprotein anchored to the outer leaflet of the plasma membrane by a glycosylphosphatinisitol (GPI) anchor (Stahl et al., 1987). PrP^C, or homologs thereof, are constitutively expressed in mammals, birds, fish, reptiles, and amphibians from early stages embryonic development (for review see Linden et al., 2008). Although transcript levels were unchanged, PrP^C protein levels in human brain decrease with age (McLennan et al., 2001; Williams et al., 2004; Whitehouse et al., 2010). Conversely, PrP^C levels in mice increased with age and higher levels of PrP^C were detected in the brain than in the heart, lung, liver, kidney, spleen, thymus, tongue, gut, testis, or skeletal muscle (Ford et al., 2002; Williams et al., 2004). Similar

distributions were observed in hamsters, sheep, and cattle (Bendheim et al., 1992; Horiuchi et al., 1995; Peralta et al., 2009). PrP^C is expressed on all cells within the brain (neurons and glia [astrocytes, microglia, oligodendrocytes]), although neurons express it to the highest levels (Barmada et al., 2004).

1.2.1 Structure

The secondary and tertiary structure of PrP^C was first determined by the Wüthrich group using nuclear magnetic resonance (NMR) analyses of recombinant PrP. Whereas physiologically expressed PrP^C may be di-, mono-, or unglycosylated, recombinant PrP was only unglycosylated. Recombinant PrP also lacked a GPI anchor. However, recombinant PrP was structurally equivalent to bovine PrP^C and could be purified to greater amounts than PrP^C from brains (Hornemann et al., 2004). The amino (N)-terminus (residues 23-124) of recombinant mouse PrP is flexible and disordered, whereas the carboxy (C)-terminus (residues 125-231) is globular and ordered, consisting of three α-helices (residues 144-154 [α1], 171-188 [α2], 199-228 [α3]) and a two-stranded anti-parallel β-sheet (residues 129-130 [β1], 162-163 [β2]) (Riek et al., 1996; Riek et al., 1997; Gossert et al., 2005) (Protein Data Bank ID code 1XYX [mouse PrP, residues 121-231]) (**Figure 1.1A**). A similar structure was determined for recombinant human PrP (Zahn et al., 2000). A disulphide bond between cysteine residues 178 and 213 connects α-helices 2 and 3 (**Figure 1.1B**). Five nearly identical 8-residue sequences form an octapeptide repeat (OR) region (residues 51-90, PQGGTWGQ followed by four PHGG[G/S]WGQ) (Westaway et al., 1987). Two regions rich in charged residues flank the OR, charged cluster 1 (CC1, residues 23-27) and charged cluster 2 (CC2, residues 100-110). Adjacent to CC2 is a region of hydrophobic residues, which form a

hydrophobic domain (HD, residues 111-134). Wüthrich received the Nobel Prize in Chemistry in 2002 for solving the three-dimensional structure of PrP^C (and other proteins).

1.2.2 Synthesis

The gene encoding PrP^C is on chromosome 2 in mice (*Prnp*) and chromosome 20 in humans (*PRNP*) (Sparkes et al., 1986). The open reading frame encoding PrP^C is within a single exon downstream of one or two short exons, depending on the species. The sequence of mouse PrP^C is nearly identical to human PrP^C, with exception to 17 substitutions, a single residue deletion preceding human PrP^C residue 55, and a two residue insertion following human PrP^C residue 226 (Schatzl et al., 1995). The N-terminus of the nascent PrP^C polypeptide encodes a 22 amino acid endoplasmic reticulum (ER)-targeting signal sequence (residues 1-22) (**Figure 1.1B**) (Turk et al., 1988). During translation, this signal sequence is recognized by the signal recognition particle (SRP). SRP interaction with the polypeptide and ribosome halts translation and targets the associated ribosome to the Sec61 translocation complex at the ER (for review see Rapoport, 2007). Translation is then resumed and the elongating polypeptide is inserted into the ER lumen. The ER signal sequence is subsequently cleaved off by a signal peptidase. The C-terminus contains a 23 amino acid GPI membrane anchor signal sequence that is also cleaved off within the ER to facilitate attachment of a GPI anchor to serine 231 in mouse PrP^C (serine 230 in human PrP^C). Additional post-translational modifications of the 208 amino acid polypeptide (207 amino acid polypeptide for human PrP^C) include variable *N*-linked glycosylation of asparagine (N) residues 180 and 196 (N181 and N197 in human PrP^C) (Haraguchi et al., 1989) and disulphide bond formation (**Figure 1.1B**) (Turk et al., 1988). Truncation of the ER-targeting signal sequence by in-

frame alternative translation initiation can result in cytoplasmic and nuclear PrP^C localization (Juanes et al., 2009; Lund et al., 2009). Out-of-frame alternative translation initiation generates a novel protein, termed alternative prion protein (AltPrP), which localizes to mitochondria (Vanderperre et al., 2011).

1.2.3 Trafficking

PrP^C traffics through the secretory pathway to the plasma membrane where it is localized to lipid rafts (Gorodinsky et al., 1995; Vey et al., 1996; Naslavsky et al., 1997), detergent-insoluble microdomains enriched for cholesterol and glycosphingolipids (Brown et al., 1992). PrP^C may localize to a specific subset of invaginated lipid rafts known as caveolae or caveloae-like domains (Ying et al., 1992; Vey et al., 1996; Peters et al., 2003). PrP^C is rapidly endocytosed from the plasma membrane (~90% within 2 minutes in primary neurons) via clathrin-dependent or -independent mechanisms (Shyng et al., 1994; Magalhaes et al., 2002; Sunyach et al., 2003; Taylor et al., 2005; Sarnataro et al., 2009; Kang et al., 2009). PrP^C endocytosis is promoted by copper and zinc ion binding to histidine residues within the octapeptide repeat region (Pauly et al., 1998; Perera et al., 2001). Internalized PrP^C traffics from early endosomes to late endosomes, from which the majority (~80% in primary neurons, Sunyach et al., 2003) are recycled back to the plasma membrane (Magalhaes et al., 2002; Pimpinelli et al., 2005). PrP^C not recycled to the plasma membrane is degraded in the lysosome (Borchelt et al., 1992). The half-life of PrP^C is 3-6 hours in cultured cells and approximately 18 hours in mouse brain (Caughey et al., 1989; Borchelt et al., 1990; Safar et al., 2005a). Meanwhile, the average turnover rate of proteins in the mouse brain is 9 days (Price et al., 2010).

1.2.4 Processing

PrP^C is physiologically cleaved at three regions. Endoproteolytic PrP^C cleavage between the mouse residues lysine 109/histidine 110, alanine 116/alanine 117, and alanine 119/valine 120 (central domain region), termed α-cleavage, generates a soluble N-terminal fragment (N1) and a GPI-anchored C-terminal fragment (C1) (Chen et al., 1995; Mange et al., 2004; McDonald et al., 2014; Vilches et al., 2015). Alpha(α)-cleavage is mediated by the peptidases ADAM (a disintegrin and metalloproteinase) 8, ADAM10, and ADAM17 within compartments of the secretory pathway or at the plasma membrane (Taraboulos et al., 1995; Vincent et al., 2001; Walmsley et al., 2009; Oliveira-Martins et al., 2010; Liang et al., 2012). PrP^C is alternatively cleaved between residues proline 59/histidine 60, proline 67/histidine 68, proline 75/histidine 76, and proline 83/histidine 84 (OR region) by ADAM8 or by reactive oxygen species (ROS) at the plasma membrane. This cleavage in the OR region is termed β-cleavage (McMahon et al., 2001; Watt et al., 2005; McDonald et al., 2014). Beta(β)-cleavage generates a soluble N2 fragment and a GPI-anchored C2 fragment. The levels of C2 were elevated in scrapie-infected mice and cells (Caughey et al., 1991b; Yadavalli et al., 2004) and in CJD patients (Chen et al., 1995). The similar electrophoretic mobilites of deglycosylated C2 and PrP^{res} suggest their formation results from cleavage at similar sites (Chen et al., 1995). The conformation of the OR region can be modulated by mutations (Lau et al., 2015) or interaction with copper ions (Chattopadhyay et al., 2005). Transgenic mice expressing mutant PrP with an OR region in a compact conformation resulted in elevated levels of C2, suggesting that OR flexibility modulates β-cleavage (Lau et al., 2015). PrP^C is also subject to γ-cleavage at a yet poorly defined region near the GPI anchor to generate N3/C3 fragments (Lewis et al., 2015). Soluble full length or C-terminal fragments are generated by

ADAM10-mediated cleavage adjacent to the GPI anchor (between residues glycine 227/arginine 288) (Borchelt et al., 1993; Harris et al., 1993; Taylor et al., 2009; Altmeppen et al., 2011; McDonald et al., 2014). Full length and C-terminal PrP^C fragments may also be released by exosomes with their GPI anchor intact (Fevrier et al., 2004; Vella et al., 2007; Alais et al., 2008; Wik et al., 2012).

1.2.5 Function

The early expression, rapid turnover, near ubiquitous distribution, and its conservation among species suggested that PrP^C held a critical function. However, no overt phenotype was observed in mice, cattle, or goat lacking PrP (Bueler et al., 1992; Manson et al., 1994; Richt et al., 2007; Yu et al., 2009). PrP knockout mice (*Prnp*$^{0/0}$ [Zurich I] and *Prnp*$^{-/-}$ [Edinburgh]) were fertile and developed normally, although some minor abnormalities, including impaired sleep regulation and neuronal differentiation were observed (Tobler et al., 1996; Steele et al., 2006). Recently, PrP has been characterized to function as a ligand for the G protein-coupled receptor Gpr126 (also known as adhesion G protein-coupled receptor G6, Adgrg6) on Schwann cells to promote peripheral neuron myelin maintenance (Bremer et al., 2010; Küffer et al., 2016). The most dramatic phenotype was observed in zebrafish (*Danio rerio*) lacking orthologs of mammalian PrP^C, PrP-1 and PrP-2. PrP-1 knockdown in zebrafish embryos via antisense *PrP-1* morpholino resulted in gastrulation arrest (Malaga-Trillo et al., 2009). The phenotype was rescued by the expression of PrP-1, PrP-2, or most interestingly, mouse PrP^C. The activation of compensatory mechanisms during development (otherwise absent in zebrafish) was proposed to account for the lack of phenotype after genetic ablation of PrP^C. However, RNA sequence analyses identified only 5

transcripts similarly dysregulated (all 2-fold higher levels or greater) in *Prnp*$^{0/0}$ mouse embryos at both days 6.5 and 7.5 relative to levels in wild-type mice (Khalifé et al., 2011). Microarray analyses comparing the transcript levels for ~14,000 genes in hippocampal homogenates from adult *Prnp*$^{0/0}$ and wild-type mice (12 weeks of age) identified only 3 differentially expressed transcripts (2-fold or greater), and none were the same as those dysregulated in mouse embryos (Benvegnù et al., 2011). Proteomic analyses of 1131 proteins from whole brain homogenates from *Prnp*$^{0/0}$ mice using 2-dimensional gel electrophoresis did not identify any proteins expressed to levels different (2-fold or greater) than in wild-type mice (Crecelius et al., 2008). No overt phenotype was observed in adult mice after conditional PrP knockout in neurons (Mallucci et al., 2002).

1.2.5.1 Neuroprotection

1.2.5.1.1 Hydrophobic domain

Proteins with similar sequence typically perform similar functions. In the absence of any obvious function for PrP^{C}, sequence analyses were performed to identify any genes with homology to *Prnp*. *Prnd* (prion gene complex, downstream) which shared ~25% sequence identity was identified 16 kb downstream of *Prnp* (Moore et al., 1999). *PRND* in humans was 20 kb downstream of *PRNP* (Makrinou et al., 2002). *Prnd* encodes for Doppel (German for "double"; Dpl, downstream prion protein-like), a GPI-anchored 179 amino acid glycoprotein with structural homology to the globular C-terminus of PrP^{C} (Silverman et al., 2000; Luhrs et al., 2003). Dpl expression in adult mice was restricted to the testes. Although no phenotype was observed in female Doppel knockout mice (*Prnd*$^{0/0}$), males were infertile as a result of impaired acrosome reaction (Behrens et al., 2002; Paisley et al., 2004). Aberrant Dpl overexpression in the brains of PrP knockout mice (*Prnp*$^{-/-}$

[Nagasaki, Rcm0, Zurich II, Rikn], Sakaguchi et al., 1996; Moore et al., 1999; Yokoyama et al., 2001; Rossi et al., 2001) resulted in ataxia with cerebellar neuronal degeneration (Moore et al., 1999; Genoud et al., 2004). The age of disease onset was inversely related to Dpl levels (Rossi et al., 2001; Anderson et al., 2004).

Doppel structurally mimicked a GPI-anchored PrP^{C} deletion mutant lacking residues 32-134 (PrPΔ32-134) (Luhrs et al., 2003). Transgenic mice expressing PrPΔ32-134 (in a *Prnp*$^{0/0}$ background) also developed ataxia with cerebellar neurodegeneration (Shmerling et al., 1998). The hydrophobic domain (HD; residues 111-134) is the most highly conserved PrP^{C} domain, suggesting a critical role in its function (van Rheede et al., 2003). Indeed, Dpl toxicity *in vivo* was inhibited by the introduction of the PrP^{C} HD (and CC2) region (Baumann et al., 2009). The expression of PrP mutants with more localized deletion of the HD region (PrPΔ94-134, PrPΔ105-125) were increasingly neurotoxic *in vivo* as indicated by reduced survival time (Baumann et al., 2007; Li et al., 2007). In mice expressing the same ΔHD mutant PrP (PrPΔHD), the age of disease onset was again inversely related to the level of mutant PrP expression. PrPΔHD toxicity did not result from partial or complete deletion of the adjacent charged cluster 2 region (CC2, residues 100-110) as mice expressing PrPΔ94-110 remained healthy (Bremer et al., 2010). Mice expressing PrPΔ23-134 or anchorless PrPΔ94-134 also remained healthy, indicating that PrPΔHD toxicity required the CC1 region (residues 23-27) and GPI membrane anchoring (Baumann et al., 2009; Westergard et al., 2011). PrPΔHD mutants trafficked to the plasma membrane like PrP^{C}, and PrP^{Sc} was not detected in any mice expressing PrPΔHD. PrPΔHD toxicity was therefore not the result of aberrant localization and PrPΔHD expression did not spontaneously induce the formation of prions.

Disease onset in mice expressing PrPΔHD or Dpl was dose-dependently inhibited by the expression of full-length PrP^C (Shmerling et al., 1998; Nishida et al., 1999; Anderson et al., 2004; Baumann et al., 2007; Li et al., 2007). For example, onset of terminal signs of disease occurred in transgenic mice expressing PrPΔ105-125 within 10 days in the absence of full-length PrP^C (in a *Prnp*$^{0/0}$ background), 160 days in the presence of physiological levels of PrP^C (*Prnp*$^{+/+}$ background), and greater than 300 days in mice expressing ~6 times the physiological levels of PrP^C (*tga20* mice; *Prnp*$^{0/0}$ background). The presence of the HD region in full-length PrP^C therefore protected against PrPΔHD or Dpl toxicity. Further support for this mechanism followed from the identification of *Sprn* (shadow of the prion protein gene) on chromosome 7 (chromosome 10 in humans) (Premzl et al., 2003). *Sprn* encodes for Shadoo (Japanese for "shadow"; Sho), a 98 amino acid GPI-anchored glycoprotein with an HD region homologous to that of PrP^C (Watts et al., 2007). The HD encoding region of mouse *Sprn* shares 48% sequence identity with *Prnp*. Sho protected *Prnp*$^{0/0}$ cultured neurons from PrPΔHD and Dpl induced toxicity (Watts et al., 2007; Sakthivelu et al., 2011). Deletion of the Sho HD region abolished its neuroprotective activity. ShoΔHD was not neurotoxic. Thus, the presence of even a HD region homologous to that of PrP^C impaired PrPΔHD and Dpl toxicity.

1.2.5.1.2 Amino terminus

Treatment with antibody specific for the N-terminus of PrP (POM2 antibody) prolonged survival time of transgenic mice expressing ΔHD mutant PrP (PrPΔ94-134), suggesting that interactions with the PrP N-terminus contribute to PrPΔHD toxicity (Sonati et al., 2013). PrPΔHD expression was toxic to human neuroblastoma SH-SY5Y cells, which express low levels of endogenous PrP^C

(Sakthivelu et al., 2011). PrPΔHD toxicity was inhibited in SH-SY5Y cells by co-expression of full-length PrP^C but not PrPΔ27-89, despite the presence of the HD region. In *Prnp*$^{0/0}$ cultured neurons, neuroprotection to Dpl toxicity was mapped to PrP residues 23-28, 51-90, 91-99, and 106-112 (Drisaldi et al., 2004; Watts et al., 2007). PrP^C neuroprotection against PrPΔHD and Dpl *ex vivo* therefore required the HD region and most N-terminal residues. The expression of N-terminal deletion mutants (PrPΔ23-88, PrPΔ27-89, PrPΔ28-89, PrPΔ32-80; collectively referred to as PrPΔN) was not neurotoxic in mice (Fischer et al., 1996; Muramoto et al., 1997; Shmerling et al., 1998).

PrP^C was also neuroprotective against other neurotoxic insults. Temporary occlusion of the middle cerebral artery blocks blood flow and serves as a model for ischemia-induced neuronal death. The degree of neuronal death is typically measured by infarct size in Nissl-stained brain sections. A larger infarct was detected in PrP knockout mice after ischemia than in wild-type mice (McLennan et al., 2004; Spudich et al., 2005), whereas PrP overexpression protected against ischemia (Shyu et al., 2005; Weise et al., 2008). Infarct lesions of similar size were observed in transgenic mice overexpressing PrPΔ32-93 and PrP knockout mice (Mitteregger et al., 2007). PrP^C neuroprotection against ischemic injury therefore requires most of its N-terminal residues.

Ischemia results in neuronal membrane depolarization, and subsequent inhibition of glutamate uptake and enhanced glutamate release (for review see Nishizawa, 2001). Glutamate is an agonist for excitatory *N*-methyl-D-aspartate (NMDA), α-amino-3-hydroxy-5-methyl-4-isoxazole propionic acid (AMPA), and kainate receptors. NMDA, AMPA, and kainate receptors are also activated preferentially by the ligands for which they are named after, NMDA, AMPA, and kainic acid (KA), respectively. Excessive stimulation of NMDA, AMPA, and kainate receptors is

neurotoxic. Consistent with increased sensitivity to ischemia, PrP knockout mice were more sensitive to neurotoxic levels of KA (Rangel et al., 2007; Walz et al., 1999). A greater number of degenerating hippocampal neurons were detected in *Prnp*$^{0/0}$ than wild-type mice after KA and NMDA treatment (Rangel et al., 2007; Khosravani et al., 2008). The expression of anchorless PrP or PrPΔN mutants (PrPΔ27-89, PrPΔ28-89) did not protect SH-SY5Y cells from neurotoxic levels of KA or glutamate (Rambold et al., 2008; Sakthivelu et al., 2011). In addition to most N-terminal residues, PrP^{C} neuroprotection against ischemia therefore also requires the presence of a GPI-anchor.

Sho also protected SH-SY5Y cells from neurotoxic levels of glutamate. Unexpectedly, deletion of the N-terminus of Sho, which lacked sequence homology to the neuroprotective N-terminus of PrP^{C}, also inhibited neuroprotection (Sakthivelu et al., 2011). Sho was protective against neurotoxic insults in the absence of PrP^{C}. Moreover, distribution within the brain overlapped that of PrP^{C}. Sho and PrP^{C} were thus proposed to be functionally redundant. In the absence of PrP^{C}, Sho expression levels were thus expected to increase to compensate. However, Sho levels were unchanged in brains of adult *Prnp*$^{0/0}$ mice and the phenotype of *Prnp*$^{0/0}$/*Sprn*$^{0/0}$ double knockout mice was no different from *Prnp*$^{0/0}$ mice (Watts et al., 2007; Daude et al., 2012).

1.2.5.1.3 Carboxy terminus

Transgenic mice expressing the C-terminus deletion mutant PrPΔ141-225 (in a *Prnp*$^{0/0}$ background) also developed ataxia with cerebellar neurodegeneration (Dametto et al., 2015). Higher levels of PrPΔ141-225 expression resulted in reduced survival time. Treatment with antibodies specific for the C-terminus of PrP^{C} were neurotoxic *ex vivo* and *in vivo* (Sonati et al.,

2013). Disruption of the C-terminus of PrP^C by antibody binding or deletion is therefore neurotoxic. However, the co-expression of full-length PrP failed to prevent death of mice expressing PrPΔ141-225.

1.2.5.1.4 PrP fragments

PrP^C α-cleavage occurs within the region spanning most of the HD region (residues 109-120; HD region, residues 111-134) (as described in **Section 1.2.4**). PrPΔHD mutants are therefore not susceptible to α-cleavage. Under physiological conditions, approximately 30-50% percent of PrP^C is cleaved into soluble N1 or anchored C1 fragments via α-cleavage (Chen et al., 1995). The ability of N1 and C1 fragments to rescue PrPΔHD toxicity has yet to be evaluated. However, the addition of recombinant N1 protected cultured rat retinal ganglionic cells from death mediated by oxygen-glucose deprivation, which models ischemia in culture (Guillot-Sestier et al., 2009). Although transgenic mice expressing only C1 (PrPΔ23-134 in a *Prnp*$^{0/0}$ background) remained healthy, ischemic injury generated infarcts of similar size in PrP knockout mice and mice expressing PrPΔ32-93, which may only be processed to generate C1 fragments (Mitteregger et al., 2007; Westergard et al., 2011). C1 is therefore not likely neuroprotective. Rather, C1 expression increased sensitivity of human embryonic kidney (HEK293) cells to staurosporine (a general protein kinase inhibitor from *Streptomyces staurospores*)-induced cell death, as indicated by higher levels of DNA fragmentation and activated caspase-3 than in mock-infected cells (Sunyach et al., 2007). The neuroprotective potential of C1 and N1 fragments requires further analyses. Meanwhile, some (PrPΔ105-125) but not all (PrPΔ32-134) PrPΔHD mutants were amenable to β-

cleavage, which occurs within the OR region (residues 59-84; OR region, residues 51-90). C2 and N2 fragments are therefore unlikely to contribute to PrPΔHD neurotoxicity.

1.3 Prion diseases

Prion diseases are a family of chronic neurodegenerative diseases affecting humans and animals (**Table 1.1**). Human prion diseases can be result from infection (acquired) or mutation (genetic). Prion disease in the absence of identifiable mutation or exposure to prion-infected material is termed sporadic. All prion diseases of animals appear to result from infection, although sporadic cases have been suspected. Rare prion diseases resulting from the feeding of BSE-contaminated products to domestic and captive animals, which are not further discussed in this thesis, include feline spongiform encephalopathy (FSE), exotic ungulate spongiform encephalopathy (EUE), and prion diseases of non-human primates (for review see Imran et al., 2011).

1.3.1 Etiology

Prion disease in humans has been attributed to ingestion of prion-infected human brain through cannibalism (kuru) or beef from BSE-infected cattle (variant CJD; vCJD) (Mathews et al., 1968; Will et al., 1996; Bruce et al., 1997). Prion disease has also been attributed to medical procedures (iatrogenic CJD; iCJD) using prion-contaminated neurosurgical instruments and the use of prion-containing corneal transplants, human growth hormone, and dura mater grafts (Duffy et al., 1974; Bernoulli et al., 1977; Koch et al., 1985; Tintner et al., 1986; Thadani et al., 1988). Genetic prion diseases of humans are associated with autosomal dominant *PRNP* mutations. Over 40 mutations have been identified to be associated with prion diseases, including a P102L mutation associated

with GSS, an E200K mutation associated with gCJD, and a D178N mutation associated with FFI or gCJD depending on the presence of methionine or valine at polymorphic codon 129 (for review see van der Kamp et al., 2009). No other diseases are associated with *PRNP* mutations. Lastly, sporadic or idiopathic prion diseases arise without identifiable exposure to prion-infected material and independent of *PRNP* mutation.

1.3.2 Transmissibility

Prion diseases are mediated by infectious prions. Consequently, prion diseases are transmissible. All transgenic mice overexpressing human PrP (Tg152, Tg45) developed prion disease after inoculation with brain homogenate from patients with kuru, iCJD, sCJD, and vCJD (Collinge et al., 1995b; Asante et al., 2002; Wadsworth et al., 2008). Transmission was less efficient in mice inoculated with inherited FFI brain homogenate (54%, Tg152; 78%, wild-type) (Collinge et al., 1995a; Tateishi et al., 1995a). Inherited prion diseases were also less efficiently transmitted to primates (Brown et al., 1994b). Spontaneous neurodegenerative disease in mice resulting from the expression of mutant PrP associated with inherited human prion diseases has proven difficult to transmit to wild-type mice (Friedman-Levi et al., 2011). Transmission to transgenic mice expressing lower levels of the same disease associated mutation (which otherwise remain healthy), or to mice overexpressing wild-type PrP^{C}, has been used to demonstrate infectivity of inherited prion diseases (Hsiao et al., 1994; Jackson et al., 2009; Jackson et al., 2013). However, not all mutations associated with inherited prion diseases have been analyzed. Acquired and sporadic prion disease therefore appear to be generally more transmissible than inherited prion diseases.

1.3.3 Susceptibility

Prion disease susceptibility in humans and animals is affected by polymorphisms in the prion protein gene. In humans, nucleotide polymorphisms at *PRNP* codon 129 encodes for methionine (M) or valine (V). Within the UK population, only approximately 50% of persons are codon 129 homozygous (~37% 129MM; ~12% 129VV). However, nearly 100% of sCJD and iCJD cases within the UK were in codon 129 homozygous persons (sCJD, 21/23 cases; iCJD 5/7 cases) (Palmer et al., 1991; Collinge et al., 1991). All definite or probable vCJD cases have been in 129 homozygous (129MM) persons, with exception to one recently identified case that was 129 heterozygous (National CJD Research and Surveillance Unit, 2016). Moreover, most surviving elderly women that had previously consumed kuru-infected brain were found to be 129 heterozygous (86/125 women) (Mead et al., 2008). Persons homozygous at *PRNP* codon 129 are therefore more susceptible to sporadic and infectious prion diseases than those who are heterozygous. The polymorphism at codon 129 may also affect susceptibility to some of the inherited prion diseases, as indicated by differences in the age of onset (younger in homozygotes than heterozygotes) (Dlouhy et al., 1992; Mead et al., 2006; Mead et al., 2007). Polymorphisms at *PRNP* codon 219 encodes for glutamic acid (E) or lysine (K). Although carried in 6% of the Japanese population, none of the 85 Japanese sCJD cases were in persons with the lysine allele at codon 219; all were 219EE homozygous (Shibuya et al., 1998). Prion disease susceptibility is also influenced by polymorphisms at codon 127, which encodes for glycine (G) or valine. All kuru cases were homozygous for glycine at codon 127 (152 cases) (Mead et al., 2009). The 127V allele was however detected in a proportion of surviving elderly women previously exposed to kuru (127GV, 6/125 women; the other 119 women were 127GG). Persons homozygous at *PRNP*

codon 127 are therefore more susceptible to kuru, and possibly other prion diseases (Asante et al., 2015).

In mice, polymorphisms in *Prnp* at codons 108 (leucine [L] or phenylalanine [F]) and 189 (valine or threonine [T]) modulate prion disease susceptibility. Disease onset was faster in mice expressing 108L/189T PrP (named *Prnp*^{a} or *sinc*^{s7}) inoculated with scrapie from an 108L/189T host, than from an 108F/189V host (named *Prnp*^{b} or *sinc*^{p7}) (Bruce et al., 1991). The converse was true for mice expressing 108F/189V PrP.

1.3.4 Diagnosis

Prion diseases are chronic diseases characterized by long incubation periods. The median incubation period of acquired human prion diseases ranges from 7-17 years, although incubation periods greater than 60 years have been estimated (Will, 2003; Collinge et al., 2008). In comparison, the median duration of the clinical phase of acquired human prion diseases ranges from 4-20 months. Clinical signs and symptoms of prion disease in humans include a lack of muscle coordination (ataxia), impaired memory, insomnia, anxiety, depression, dementia, and weight loss. Definite prion disease diagnosis requires the detection of PrP^{Sc}. Unfortunately, current methods of PrP^{Sc} detection require invasive tonsil or brain biopsy and are unreliable. More sensitive and specific antemortem diagnostic tests that detect PrP^{Sc} in samples collected by less invasive means, such as cerebrospinal fluid, olfactory epithelium brushings, and urine are still only in development (Atarashi et al., 2011; McGuire et al., 2012; Moda et al., 2014; Orru et al., 2014). Patients suspected to have prion disease are evaluated by computerized tomography (CT), magnetic resonance imaging (MRI), electroencephalogram (EEG), and analyses of 14-3-3 protein

levels in cerebrospinal fluid. The results from such analyses may support prion disease or identify alternative causes for the signs and symptoms (Paterson et al., 2012a). Patients suspected to have acquired or inherited prion disease may also be evaluated by epidemiological analyses for potential exposure to infected material or genetic testing for known mutations of prion protein gene associated with prion disease, respectively. Analyses of polymorphic codons 127, 129, and 219, which influence prion disease susceptibility, may also provide insight into the likelihood of distinct prion infections.

1.3.5 Impact on human health

There are yet no therapeutics available against prions diseases. Consequently, prion diseases are invariable lethal. The incidence of all human prion diseases is approximately 1-2 per million per year. An average of 247 new cases of human prion disease were diagnosed annually within the United States of America (USA) between 1979 and 2006 (Holman et al., 2010). The number of new cases in this time period only ranged from 172 in 1980 to 304 in 1997. Although most cases of human prion disease arise sporadically (~85%) or are attributed to *PRNP* mutation (~15%), prion diseases acquired by infection (less than 1% of new cases) remain a continuous concern for human health.

Prion diseases are often suspected only at late stages, largely due to their low prevalence and diagnostic difficulty. Unfortunately, the sterilization procedures used by most hospitals fail to inactivate prions (Rutala et al., 2010). At least 142 people may have been exposed to prion-contaminated surgical instruments in the USA within the last 15 years. Neurosurgical instruments used on a patient later diagnosed with CJD were subsequently used in neurosurgeries on 18 other

patients at the Novant Health Forsyth Medical Centre, North Carolina in 2014. Similar circumstances may have exposed 15 people to prion-contaminated surgical instruments at the Catholic Medical Centre, New Hampshire in 2013, 11 people at the Greenville Hospital System, South Carolina in 2012, and 98 people at the Emory University Hospital, Georgia in 2004. Although the last reported case of iatrogenic transmission by contaminated surgical instruments was in 1976, these exposures highlight the continuous risk.

Another concern for human health is a population exposed to BSE-contaminated meat products that pose a risk of human-to-human transmission. BSE was first described in Great Britain in 1986 and subsequently in 27 other countries, including Canada and the USA (Wells et al., 1987). Nearly 200,000 BSE cases have been confirmed worldwide, ~97% of which were within the United Kingdom (UK) (Office International des Epizooties, 2015a; Office International des Epizooties, 2015b). Although the origin of BSE remains unknown, the BSE epidemic resulted from the feeding of prion-contaminated meat and bone meal (MBM) to other cattle. The restrictions banning the use of ruminant MBM in livestock food production have gradually reduced the number of BSE cases since their implementation in 1996. These measures followed a less restrictive, and far less successful, feed ban implemented in 1988. Despite the MBM feed ban, new BSE cases continue to be identified. Most recently, one case of BSE was identified in France in March 2016. In 2015, both Norway and Slovenia reported their first cases of BSE. Variant CJD was first described in humans during the BSE epidemic (Will et al., 1996). All vCJD cases have been diagnosed in persons that have resided in BSE-affected countries. Transmission studies in mice and cynomolgus macaques (*Macaca fascicularis*) support the model that vCJD in humans results from ingestion of BSE-contaminated meat (Lasmezas et al., 1996b; Bruce et al., 1997;

Ritchie et al., 2009). As of April 2016, 230 vCJD cases have been reported worldwide (National CJD Research and Surveillance Unit, 2016). The majority (178 cases) were reported in the UK. It has been estimated that more than 10 million people were exposed to BSE in the UK, almost all prior to the modifications of animal processing procedures and banned usage of specified risk materials for human consumption. The ban temporary included consumption of any cattle older than 30 months of age (Chen et al., 2014). Surprisingly, analyses of 32,441 appendices collected from UK population between 2000-2012 identified 16 positive for PrP^{res} (Gill et al., 2013). None of the collected appendices were from confirmed vCJD cases. These results therefore suggest that 1 in 2000 people in the UK may be infected with vCJD but clinically healthy (subclinical). The prevalence may even be higher as PrP^{res} was not detected in all vCJD appendices (Joiner et al., 2002; Hilton et al., 2002). Variant CJD was transmitted intravenously by blood to cynomolgus macaques (Lacroux et al., 2014). Transgenic mice expressing bovine PrP developed prion disease after intracerebral inoculation with blood from a vCJD patient (Douet et al., 2014). Variant CJD infectivity was therefore present and transmissible by blood. This is a public health concern as there is yet no practical method to screen blood donations for prion infectivity. Five vCJD cases have been reported in which patients received blood products from clinically healthy persons who later developed vCJD (Peden et al., 2004; Llewelyn et al., 2004; Wroe et al., 2006; Peden et al., 2010). Patients with preclinical (or subclinical) vCJD infections therefore represent a potential source for secondary transmission. Prion infectivity was also detected in sCJD blood. However, no evidence has yet suggested that sCJD transmission via blood products is possible (Dorsey et al., 2009; Douet et al., 2014; Urwin et al., 2015).

Sheep, goat, deer, elk and moose are also susceptible to prion diseases and consumed by humans. Over 0.36% of all 339,968 sheep tested in the European Union (EU) in 2013 were infected with scrapie. Prevalences more than 2-fold greater were observed in previous years (0.85% in 2004, 0.83% in 2005) (European Commission Directorate-General for Health and Food Safety, 2015). Approximately 40% (140,491) of the sheep tested in the EU in 2013 were destined for human consumption, of which almost 0.07% were infected with scrapie. The prevalence of scrapie in sheep slaughtered for human consumption has increased every year in the EU since 2010. Although epidemiological evidence does not indicate that scrapie is transmissible to humans (Brown et al., 1987), scrapie-infected sheep brain homogenate intracerebrally inoculated into cynomolgus macaques resulted in prion disease 10 years later (Comoy et al., 2015). Intracerebral inoculation of sheep scrapie also induced disease in transgenic mice overexpressing human PrP (after second passage) (Cassard et al., 2014). Interestingly, the glycoform profile and distribution of PrP^{res} in scrapie-infected transgenic mice overexpressing human PrP was similar, if not identical, to that observed in the same mice inoculated with human sCJD brain homogenate (Cassard et al., 2014). However, oral transmission of scrapie to macaques (or other primates) or transgenic mice overexpressing human PrP has yet to be demonstrated.

In contrast to scrapie, which is restricted to farmed animals, CWD affects free-ranging cervids. The prevalence and distribution of CWD in the USA and Canada continues to increase (United States Geological Survey, National Wildlife Health Center, 2015). CWD has also been reported in South Korea but was restricted to imported deer and elk. Within endemic areas, CWD prevalence in free-ranging deer has been reported to be as high as 57% (Wyoming, USA; 2011). Surveillance programs found an overall prevalence of almost 0.6% in cervids tested from 1996-

2010 (Saunders et al., 2012). Similar to scrapie, there is no epidemiological evidence to indicate that CWD has been transmitted to humans (Belay et al., 2004; Mawhinney et al., 2006). However, CWD was experimentally transmitted via oral (and intracerebral) inoculation of squirrel monkeys (*Saimiri sciureus*) (Marsh et al., 2005; Race et al., 2009; Race et al., 2014). Human PrP was converted to PrP^{res} under cell-free conditions with CWD brain homogenate, even more efficiently than with scrapie brain homogenate (Raymond et al., 2000; Barria et al., 2014). Transgenic mice overexpressing human PrP remained healthy after inoculation with brain homogenate from CWD-infected deer and elk, although second passages were not performed (Tamgüney et al., 2006; Sandberg et al., 2010). Macaques inoculated with CWD-infected brain homogenate also remained healthy 10 years after inoculation (Race et al., 2014). CWD therefore represents a growing source of prions in animals consumed by humans. However, a risk to human health has yet to be demonstrated.

1.3.6 Strains

Prions exist in different strains. Strain differences for other etiological agents (such as bacteria and viruses) result from nucleic acid variation. As prions lacked detectable nucleic acid, prion strains must be independent of such nucleic acid variation. Rather, prion strains are attributed to PrP^{Sc} conformation (for review see Solforosi et al., 2013). Disease induced by different prion strains may be distinguished by differences in clinical presentation, incubation period, and neuropathology within a defined host.

1.3.7 PrP^{Sc}

The accumulation of pathological prion protein (PrP^{Sc}) is the defining feature of prion diseases. PrP^{Sc} is an alternative conformation of PrP^{C}. Infrared and circular dichroism spectroscopy demonstrated that PrP^{Sc} (and PrP^{res}) consists of higher proportions of β-sheet and lower proportions of α-helix than PrP^{C} (Caughey et al., 1991c; Pan et al., 1993; Gasset et al., 1993; Safar et al., 1993). PrP^{Sc} was not amenable to high resolution X-ray crystallography or NMR analyses, in large part due to its detergent insolubility. The structure of PrP^{Sc} therefore remains poorly defined. However, data gathered from lower resolution techniques have led to the generation of multiple PrP^{Sc} structure models, including an antiparallel intertwined β-helix, a parallel β-helix, a β-spiral, and an in-register β-sheet (for review see Diaz-Espinoza et al., 2012; Requena et al., 2014).

PrP^{Sc} is biochemically distinguished from PrP^{C} by its detergent insolubility and resistance to limited PK digestion (PrP^{res}). Nonetheless, PK-sensitive PrP^{Sc} (named PrP^{sen}, for protease-sensitive prion protein) also exists, and in many cases it constitutes the majority of PrP^{Sc} (Safar et al., 1998; Safar et al., 2005b). Like PrP^{C}, cellular PrP^{Sc} is localized to endosomal compartments and the plasma membrane. PrP^{Sc} is resistant to phosphatidylinositol-specific phospholipase C (PIPLC)-mediated cleavage of its GPI anchor, whereas PrP^{C} is released by PIPLC treatment (Stahl et al., 1987; Stahl et al., 1990). PrP^{Sc} has a half-life approximately twice as long as that of PrP^{C} in mice (~36h) and 5-10 times as long as PrP^{C} in scrapie-infected mouse N2a neuroblastoma cells (~30h), indicating slower or less effective clearance (Peretz et al., 2001b; Safar et al., 2005a). The levels of a reporter green fluorescent protein (GFP) under the control of the PrP promoter did not change during scrapie progression in mice (Jackson et al., 2014). PrP^{Sc} is further distinguished from PrP^{C} by an increased propensity to aggregate, which may contribute to the formation of

extracellular amyloid plaques containing PrP^{Sc}. Such amyloid plaques are observed upon histopathological analyses of some, but not all, prion diseases. Amyloid plaques in kuru-infected brains are stellate and fibrillar, whereas GSS plaques are multicentric, and vCJD plaques are surrounded by a halo of vacuoles (florid).

PrP^{Sc}, like PrP^{C}, is potentially glycosylated at two asparagine residues. PrP^{Sc} from different prion strains can be characterized by distinct glycosylation profiles, representing the proportions of di-, mono-, and unglycosylated PrP^{res}. Similar levels of di-, mono-, and unglycosylated PrP^{res} were detected in mice inoculated with mouse-adapted scrapie strain ME7, for example, whereas most PrP^{res} was mono- or unglycosylated in mice inoculated with strains RML or 139A (Kascsak et al., 1986; Thackray et al., 2007). PrP^{Sc} from different prion strains can also be characterized by distinct conformations. In the absence of high-resolution PrP^{Sc} structure, different PrP^{Sc} conformations may be distinguished by PrP^{res} fragment size, epitope presentation, and resistance to PK digestion or denaturation by chaotropic salts (Bessen et al., 1992a; Collinge et al., 1996; Safar et al., 1998; Peretz et al., 2001a). For example, PrP^{res} detected in immunoblots of human vCJD brain had a lower molecular weight than PrP^{res} in sCJD and iCJD brain (Hill et al., 2003). Similarly, distinct PrP^{Sc} conformations from two strains of hamster-adapted transmissible mink encephalopathy (TME) were characterized by differences in detergent solubility, resistance to PK digestion, PrP^{res} fragment sizes, and infrared spectroscopic analyses (Bessen et al., 1992a; Bessen et al., 1994; Caughey et al., 1998).

1.3.8 Neuropathology

Beyond PrP^{Sc} accumulation, prion disease neuropathology is further characterized by variable degrees of spongiform degeneration, gliosis, and neuronal loss (**Figure 1.2**). Prion disease neuropathology may also include synapse loss and the accumulation of tubulovesicular bodies.

1.3.8.1 Spongiform degeneration

A neuropathological hallmark of prion diseases is spongiform degeneration of the neuropil. There is also an increased number of round or oval vacuoles (2-20 μm in diameter) within neuron parikarya. Multilocular vacuoles may also be present. Such spongiform change is predominately localized to grey matter and is distinct from status spongiosis, in which irregular neuropil vacuoles are surrounded by a dense glial network (Masters et al., 1978). In formalin-fixed paraffin-embedded brain sections stained with hematoxylin and eosin (H&E), nucleic acids appear deep blue-purple, proteins appear pink, and vacuoles remain clear. Brain sections with extensive vacuolation therefore appear sponge-like upon histopathological analyses. Consequently, prion diseases were defined as spongiform encephalopathies - a disease of the brain resulting in sponge-like neuropathology.

Spongiform degeneration was critical for the definition of the host range of prion disease and the characterization of the etiological agent. Vacuolation was first observed in sheep that died from scrapie. Although scrapie etiology remained poorly understood at the time, vacuolar neuropathology suggested that the scrapie agent was present in the brain. Indeed, brain homogenate from scrapie-infected sheep was used to first demonstrate the infectious nature of the etiological agent (as described in **Section 1.1**). In humans, a neurodegenerative disease also

characterized by spongiform degeneration, known as kuru, was described in Eastern Highland populations of Papua New Guinea, particularly within the Fore linguistic group. In the Fore language, 'kuru' meant to shiver or shake, from fever or cold, thus describing the phenotype of affected individuals. Kuru was similar to scrapie in clinical and epidemiological presentation. Hadlow recognized that kuru and scrapie were also histopathologically similar, and suggested that kuru may also be mediated by an infectious agent (Hadlow, 1959). Indeed, when Gajdusek intracerebrally inoculated chimpanzees with kuru-infected brain homogenate, the animals developed kuru-like disease 18-21 months later (Gajdusek et al., 1966). It was for this and related work further characterizing the etiological agent of kuru that Gajdusek received the Nobel Prize in Medicine in 1976. Similar analyses based on spongiform degeneration observed in CJD brains also demonstrated the infectious nature of the etiological agent prior to the identification of PrP^{Sc} (Gibbs et al., 1968).

Different prion strains are characterized by differences in the extent and distribution of spongiform degeneration within the brain. Quantitative analyses of vacuolation (vacuolation scoring) was developed as a diagnostic tool, particularly for mouse-adapted scrapie strains. The lesion profile describes the extent of vacuolation and spongiform change within defined brain regions in a particular host genotype (Fraser et al., 1973). For example, most vacuolation was observed in cerebellar regions of C57BL/6 mice inoculated with scrapie strains RML, 139A, and ME7, while the degree of vacuolation was similar throughout all analyzed regions in mice inoculated with 79A (Castilla et al., 2008).

1.3.8.2 Reactive gliosis

Astrocytes are glial cells whose primary function is to maintain synapse homeostasis within the central nervous system (CNS) (for review see Sofroniew et al., 2010; Pekny et al., 2014). After CNS insult, astrocytes undergo a process known as reactive astrogliosis (also referred to as astrocytosis), the degree of which is directly related to the severity of the insult. Activated astrocytes are characterized by hypertrophy of the cell body and processes, and increased expression of multiple proteins, including the intermediate filament protein glial fibrillary acid protein (GFAP). Severe insults may result in astrocyte proliferation. CNS insults also activate resting (ramified) microglia, the resident immune cells of the CNS, through a process termed microgliosis (for review see Heneka et al., 2014). Similar to activated astrocytes, activated microglia are morphologically characterized by hypertrophy of the cell body and processes. Microgliosis may also result in microglia proliferation.

Reactive astrogliosis and microgliosis are a characteristic features of prion disease neuropathology. Little co-localization was observed in hippocampal sections from ME7-infected mice labelled with an antibody specific for GFAP and the cell proliferation marker Ki67 (Asuni et al., 2014). Astrocyte proliferation therefore contributes little to astrogliosis in prion disease. Conversely, increased numbers of microglia were detected in scrapie-infected mice by immunohistochemical (IHC) analyses, suggesting microglia proliferation in prion disease (Gómez-Nicola et al., 2013).

1.3.8.3 Neuronal loss

Neuronal loss is the neuropathological hallmark and the main cause of prion disease lethality. The anatomical regions of neuronal loss are associated with reactive gliosis. Histochemical analyses of mice infected with scrapie strain ME7 revealed the loss of ~50% of hippocampal neurons (CA1 sector) at terminal stages of disease (Jeffrey et al., 2000b). Some prion diseases are characterized by neuronal loss in distinct regions of the brain. In humans, for example, the brains of FFI patients had neuronal loss localized mostly to the thalamus, whereas most neuronal loss in gCJD brains was localized to the cerebral and cerebellar cortices (Gambetti et al., 2003). The mechanisms responsible for selective neuronal loss in prion diseases remains yet poorly understood but may include neuronal subtypes, PrP^{Sc} conformation, and the extent of glial activation.

1.3.8.4 Synapse loss

Synapses are the neuronal structures that mediate communication between neurons. Communication is mediated by neurotransmitters released from presynaptic axon terminals. Neurotransmitters cross the synaptic cleft to bind receptors on the postsynaptic dendrites and specialized protrusions along the dendritic shaft known as dendritic spines. Prion disease neuropathology is characterized by a reduced number of synapses (Jeffrey et al., 2000b). As synapse loss preceded neuronal loss *in vivo*, synapse loss is most evident prior to terminal stages of disease progression. Ultrastructural analyses detected 60% fewer synapses in the hippocampus of scrapie-infected than in mock-infected mice before the onset of clinical disease (~105 dpi; terminal at ~150 dpi) (Godsave et al., 2008). Similar reductions of dendritic spines were also observed prior to the onset of clinical disease in scrapie-infected mice (Brown et al., 2001).

1.3.8.5 Tubulovesicular structures

A unique hallmark of prion diseases are tubulovesicular structures (TVS; also known as tubulovesicular bodies/particles or scrapie-associated fibrils) detected upon ultrastructural analyses. TVS were observed at axonal and dendritic terminals as spheres or short tubules between 27-30 nm in diameter (for review see Liberski, 2008). Although their composition remains poorly defined, TVS are not composed of PrP (Liberski et al., 1997).

1.4 Pathogenesis

Prion disease pathogenesis describes the mechanisms whereby prion infection ultimately results in death. Prion diseases of different etiology (infectious, genetic, sporadic) share similar pathologies and clinical presentations, suggesting common pathogenic events. Although the extent and distribution of neuropathological changes in prion diseases mediated by different strains can vary, their onset is remarkably precise and predictable. Prion infection results in increased levels of prion infectivity and PrP^{Sc} in the CNS. The levels of infectivity and PrP^{Sc} can also increase in secondary lymphoid organs including the spleen, appendix, tonsils, lymph nodes, and intestinal Peyer's patches, albeit to much lower levels than in the CNS (Kimberlin et al., 1979; Hadlow et al., 1980; Hadlow et al., 1982; Hilton et al., 1998; Hill et al., 1999). Time-course microscopy of ME7-infected mice demonstrated that hippocampal PrP^{Sc} accumulation is sequentially followed by synapse loss, astrogliosis, vacuolation, and finally neuronal loss (Belichenko et al., 2000; Jeffrey et al., 2000b; Brown et al., 2001). Microglial activation also precedes vacuolation and neuronal loss (Williams et al., 1997; Giese et al., 1998). Tubulovesicular structures are first detected in scrapie-infected mice and hamsters at the time of synapse loss. However, their accumulation is also

associated with astrogliosis and vacuolation at later times (Liberski et al., 1990; Jeffrey et al., 2000a).

PrP^{Sc} accumulation during prion disease progression results in increased total PrP levels. Although the levels of *Prnp* transcripts were similar in uninfected and scrapie-infected animals throughout disease progression, PrP^{C} protein levels decreased during disease progression (Oesch et al., 1985; Chesebro et al., 1985; Kretzschmar et al., 1986; Hwang et al., 2009; Mays et al., 2014; Mays et al., 2015). Minor phenotypes of some prion diseases may be attributed to the reduction in the levels PrP^{C}, such as disrupted sleep regulation in FFI patients (Tobler et al., 1996). However, prion disease does not result from reduced PrP^{C} levels, as indicated by the absence of prion disease in PrP knockout mice (Bueler et al., 1992).

1.4.1 PrP conversion

PrP^{Sc} replication or propagation is mediated by autocatalytic template-assisted conversion of endogenous PrP^{C} to PrP^{Sc} (Kocisko et al., 1994; Bessen et al., 1995). Mice lacking PrP^{C} are resistant to scrapie infection (Bueler et al., 1993; Sailer et al., 1994). Prion disease pathogenesis therefore requires PrP conversion. PrP^{Sc} oligomers are most amenable to PrP conversion (Silveira et al., 2005). Consistently, PrP^{Sc} oligomers are also the most infectious species or aggregate of PrP^{Sc} (Silveira et al., 2005). PrP conversion is accelerated by the generation of PrP^{Sc} oligomers, which are proposed to serve as nuclei (or seeds) upon which PrP^{C} or a partially structured intermediate, PrP^{C*}, convert to PrP^{Sc} and polymerize to form fibrils. PrP^{Sc} seeds may be acquired from exogenous sources, or spontaneously formed by alternative folding or refolding mechanisms. Disease-associated mutations are proposed to promote PrP conversion by destabilization of PrP^{C} or

stabilization of PrP^{C*} (Swietnicki et al., 1998; Liemann et al., 1999; Apetri et al., 2004). The rate of accumulation of PrP^{Sc} oligomers slowed (Sasaki et al., 2009) and the level of prion infectivity reached a plateau (Sandberg et al., 2014) in scrapie-infected mice prior to significant PrP^{Sc} accumulation. PrP^{C} overexpression did not result in higher levels of prion infectivity (Sandberg et al., 2011; Mays et al., 2015). The accumulation of infectivity is therefore not likely limited by physiological levels of PrP^{C}.

PrP conversion occurs in lipid rafts on the plasma membrane (Taraboulos et al., 1995; Kaneko et al., 1997; Bate et al., 2004; Godsave et al., 2008; Goold et al., 2011; Godsave et al., 2013) or within endosomal compartments (Caughey et al., 1991a; Borchelt et al., 1992; Marijanovic et al., 2009; Yim et al., 2015). Although extracellular conversion is possible (Chesebro et al., 2005), PrP interaction with lipids induces conformational changes (Wang et al., 2007; Miller et al., 2013; Zurawel et al., 2014) and the generation of infectious PrP^{Sc} in cell-free conditions was promoted by phospholipids (and polyanions) (Deleault et al., 2007; Wang et al., 2010a; Deleault et al., 2012). Cofactor-induced conformational changes may therefore promote PrP conversion.

Transgenic mice expressing PrP deletion mutants (in a $Prnp^{0/0}$ background) were infected with scrapie to characterize the residues critical for PrP conversion and prion replication *in vivo*, or at least those critical for mouse-adapted scrapie. Mice expressing PrP lacking residues 23-93 (PrPΔ23-31, PrPΔ23-88, PrPΔ32-80, PrPΔ32-93) accumulated PrP^{Sc} and developed scrapie after inoculation with brain homogenate from scrapie-infected mice, albeit after a prolonged disease course, suggesting less efficient conversion (Fischer et al., 1996; Flechsig et al., 2000; Supattapone et al., 2001; Turnbaugh et al., 2012). Most N-terminal residues are therefore not required for PrP

conversion. These results were perhaps not surprising considering that limited PK digestion of PrP^{Sc} removes most N-terminal residues but does not affect infectivity (McKinley et al., 1983a). Deletion of the charged cluster 2 (CC2, residues 100-110) and hydrophobic domain (HD, residues 111-134) regions prevented PrP^{Sc} accumulation *in vitro* (PrPΔ23-88/Δ95-107, PrPΔ23-88/Δ108-121, PrPΔ105-125, PrPΔ112-119, PrPΔ113-133, PrPΔ114-121) (Muramoto et al., 1996; Holscher et al., 1998; Norstrom et al., 2005; Rambold et al., 2008) and scrapie onset *in vivo* (PrPΔ23-111 [equivalent to the C1 fragment], PrPΔ23-134) (Westergard et al., 2011). The CC2/HD regions alone or in combination with additional N-terminal residues may therefore be critical to PrP conversion. PrP conversion was inhibited in persistently infected scrapie mouse brain (SMB) cells by treatment with peptides corresponding to PrP HD region (mouse PrP119-136) (Chabry et al., 1999). The region downstream of the HD region may also be involved in PrP conversion as scrapie-infected mice treated with 6H4 antibody, which is specific for mouse PrP^{C} residues 141-155 and 201, did not accumulate PrP^{Sc} and remained healthy (Heppner et al., 2001; Doolan et al., 2015). This region primarily spans the α1-helix (residues 144-154), which is proposed to convert to β-sheet during PrP conversion (Govaerts et al., 2004). PrP lacking α1-helix did not convert to PrP^{res} when expressed in SMB cells (Vorberg et al., 2001). The heavy chain complementarity-determining region 3 of an antibody specific for the envelop glycoprotein gp120 of human immunodeficiency virus (HIV) was replaced with overlapping sequences of mouse PrP. Antibodies with sequences corresponding to charged cluster regions 1 and 2 and the α1-helix immunoprecipitated PrP^{Sc} (and prion infectivity) from scrapie-infected mouse brain (Moroncini et al., 2004; Solforosi et al., 2007). The charged cluster regions and α1-helix may therefore be involved in PrP^{C}-PrP^{Sc} interaction.

1.4.1.1 Transmission barrier

Transmission of prion diseases between different species is typically inefficient. Such transmission (or species) barriers may be overcome by PrP^{C} overexpression or PrP^{Sc} amplification, which promote PrP conversion (Sigurdson et al., 2006; Chianini et al., 2012). If PrP conversion is so inefficient that the incubation period is longer than the lifespan of the new host, then that species is resistant. In susceptible species, repeated passage results in increased infection (attack) rates and shortened incubation periods. During these passages, prions are proposed to adapt to the new host by selection of the PrP^{Sc} conformation that is most amenable to conversion from the available PrP^{Sc} population (Collinge, 1999; Collinge et al., 2007). As with intraspecies PrP conversion, interspecies PrP conversion is also modulated by PrP sequence homology. Although mouse and hamster PrP^{C} differ from each other at only 16 residues, mice inoculated with hamster-adapted scrapie strain Sc237 failed to develop disease (Scott et al., 1989). Transgenic mice expressing hamster PrP^{C} were susceptible to Sc237 scrapie, but resistant to mouse-adapted scrapie strain RML (Prusiner et al., 1990). Meanwhile, transgenic mice expressing mouse/hamster chimeric PrP (L108M, V111M, I138M, Y154N, S169N; named MH2M PrP) were susceptible to both Sc237 and RML (Scott et al., 1993). Complete PrP sequence homology is therefore not required for conversion. Similarly, mice which are otherwise resistant to human CJD (sCJD, iCJD) and elk CWD, were susceptible if they expressed chimeric mouse/human and mouse/elk PrP, respectively (Telling et al., 1994; Sigurdson et al., 2010). Mice were also susceptible to sCJD if limited to the synthesis of unglycosylated or N180 monoglycosylated PrP (expressing N196T mutant PrP) (Wiseman et al., 2015). Glycosylation deficient transgenic mice were also differentially

susceptibility to mouse- and hamster-adapted scrapie strains (DeArmond et al., 1997; Cancellotti et al., 2005). PrP glycosylation may therefore also modulate PrP conversion.

1.4.2 Prion toxicity

Although subclinical infections do occur (Thackray et al., 2002; Thackray et al., 2003), the accumulation of PrP^{Sc} and prion infectivity is lethal. Prion toxicity requires PrP^{C}-PrP^{Sc} interaction or conversion. Accordingly, the time to onset of clinical disease is modulated by PrP^{C} expression levels, PrP^{Sc} conformational stability, PrP sequence homology, and the route and dose of inoculation.

The most effective route of prion infection is intracerebral inoculation. Intraocular or peripheral routes of inoculation, such as intraperitoneal, intravenous, subcutaneous, or oral are comparatively less efficient (Kimberlin et al., 1978; Kimberlin et al., 1986). Lower levels of PrP^{res} were detected in the brains of mice inoculated with scrapie intraperitoneally than in those inoculated intracerebrally (Lasmezas et al., 1996a; Langevin et al., 2011). Prion disease incubation is also inversely related to PrP^{C} expression levels. Mice expressing PrP^{C} at levels approximately half of those in wild-type mice (*Prnp*$^{0/+}$) more than doubled the incubation period after inoculation with the same dose of scrapie (Büeler et al., 1994). At the same time, PrP^{res} levels in scrapie-infected *Prnp*$^{0/+}$ mice were less than half the levels in infected wild-type mice. Conversely, the incubation period in transgenic mice overexpressing PrP^{C} (*tga20*) was less than half of that in scrapie-infected wild-type mice (Fischer et al., 1996). Transgenic mice expressing anchorless PrP^{C} (*tg44*) were also resistant scrapie infection, although they accumulated PrP^{Sc} and prion infectivity (Chesebro et al., 2005). PrP^{C} is shed by ADAM10-mediated cleavage adjacent to the GPI anchor

(as described in **Section 1.2.4**). Conditional knockout of ADAM10 reduced survival time of scrapie-infected mice (Altmeppen et al., 2015). Prion toxicity is therefore dependent on the expression of GPI-anchored PrP^{C}. More specifically, the anchored PrP^{C} must be expressed on neurons. Neurodegeneration was restricted to grafts overexpressing PrP^{C} in scrapie-infected *Prnp*$^{0/0}$ mice, despite the accumulation of PrP^{Sc} throughout the brain (Brandner et al., 1996). PrP^{Sc} accumulated but disease progression and neuronal loss was inhibited in scrapie-infected mice by the conditional knockout of neuronal PrP^{C} (Mallucci et al., 2002). Moreover, transgenic mice expressing hamster PrP under control of neuron-specific enolase (NSE) promoter were susceptible to hamster-adapted scrapie (Race et al., 1995). Mice expressing PrP under control of the GFAP promoter were also susceptible scrapie, which suggests that astrocyte PrP^{C} expression may also suffice for prion toxicity (Raeber et al., 1997).

PrP^{Sc} conformation modulates the rate of PrP conversion and therefore influences prion toxicity. Two distinct PrP^{Sc} conformations were isolated from hamsters inoculated with TME (as described in **Section 1.3.7**). PrP^{Sc} associated with hamster-adapted TME strain 'hyper' converted PrP *in vitro* and *in vivo* faster than PrP^{Sc} from hamsters infected with 'drowsy' (Mulcahy et al., 2004). The incubation period was shorter in hamsters inoculated with 'hyper' than with 'drowsy' prion strains (Bessen et al., 1992b). PrP^{Sc} conformation may also be defined by resistance to guanidine hydrochloride denaturation using conformational-stability assay (Peretz et al., 2001a). PrP^{Sc} isolated from mice inoculated with natural and synthetic prions demonstrated that the incubation period was directly proportional to PrP^{Sc} conformational stability; the shortest incubation was observed after inoculation with the least stable PrP^{Sc} species (Legname et al., 2006; Colby et al., 2009). Prion disease incubation is therefore modulated by PrP^{Sc} conformation.

PrP sequence also modulates PrP conversion (as discussed in **Section 1.3.3**). For example, all but one clinical vCJD patients to date have been homozygous for methionine at *PRNP* codon 129. In another 129 heterozygous patient, vCJD PrP^{Sc} was detected only after death from non-neurological causes (Peden et al., 2004). Prions can be propagated *in vitro* by a process termed protein misfolding cyclic amplification (PMCA), wherein dilutions of infected brain homogenate (or other source of PrP^{Sc}) are used to seed PrP conversion in uninfected brain homogenate (or other source of PrP^{C}) by repeated round of sonication and incubation (Castilla et al., 2005). Higher levels of PrP^{res} were detected in vCJD-seeded PMCA reactions using brain homogenate from transgenic mice expressing 129MM human PrP, than from mice expressing 129MV or 129VV human PrP (Jones et al., 2007). These results suggest that 129M PrP is more efficiently converted by vCJD prions than 129V PrP.

1.4.2.1 PrP with neurotoxic potential

PrP^{C} localizes to the plasma membrane under physiological conditions. However, PrP^{C} may accumulate in the cytoplasm as a result of inefficient endoplasmic reticulum (ER)-targeting (Drisaldi et al., 2003; Rane et al., 2004; Levine et al., 2005), ER-associated degradation (Ma et al., 2001; Yedidia et al., 2001; Ma et al., 2002a), alternative translation initiation (Lund et al., 2009), or persistent pre-emptive quality control (Rane et al., 2008). Mice expressing a truncated PrP^{C} mutant lacking its N-terminal ER-targeting and C-terminal GPI-membrane-anchoring signals (named cytoplasmic PrP, or CyPrP) suffered from ataxia with gliosis and cerebellar degeneration (Ma et al., 2002b). The expression of CyPrP was also toxic to N2a cells (Ma et al., 2002b). The accumulation of PrP^{C} in the cytoplasm therefore has neurotoxic potential (Hegde et al., 2003).

However, low levels of cytoplasmic PrP have been observed in certain subpopulations of neurons without overt neurodegeneration (Mironov et al., 2003; Barmada et al., 2004; Bailly et al., 2004) and the roles of cytoplasmic PrP in prion infection are disputed (Norstrom et al., 2007; Thackray et al., 2014).

Incomplete translocation of PrP (Stewart et al., 2003) or post-translocational slippage out of the ER (Emerman et al., 2010) may result in transmembrane PrP (named C-terminal transmembrane PrP, or PrP^{Ctm}), wherein the C-terminus has translocated into the ER lumen but the N-terminus remains exposed to the cytosol. The expression of gCJD-associated G114V and GSS-associated A117V mutant PrP induced the formation of PrP^{Ctm} *in vitro* (Wang et al., 2011). Transgenic mice expressing PrP with mutations that promote PrP^{Ctm} formation (L9R-3AV, 3AV, KH-II) spontaneously developed neurodegenerative disease without PrP^{Sc} accumulation (Hegde et al., 1998; Hegde et al., 1999; Stewart et al., 2005). However, the expression of other disease-associated mutant PrP (P102L, E200K, V210I, PG14) did not induce PrP^{Ctm} synthesis *in vitro* or *in vivo* (Stewart et al., 2001; Emerman et al., 2010; Wang et al., 2011). Moreover, PrP^{Ctm} has yet to be detected in the brains of scrapie-infected (or even uninfected) mice or hamsters (Stewart et al., 2003). PrP^{Ctm} is therefore unlikely to contribute to prion disease neuronal death.

1.4.2.2 Neuronal death

As in most other neurodegenerative diseases, the mode of neuronal cell death remains incompletely defined in prion diseases. That prion infection is characterized by little or no immune response argues against necrosis as a major contributor to neuronal loss (Betmouni et al., 1999; Tribouillard-Tanvier et al., 2009). However, the role of apoptosis or programmed cell death in

prion disease pathogenesis is unclear. Apoptosis is characterized by cell shrinkage, chromatin condensation, apoptotic bodies (membrane-enclosed vesicles containing cellular components), and 180-200 bp fragments of nuclear DNA (for review see Taylor et al., 2008). Fragmented DNA and apoptotic morphology were detected in neurons of mice infected with scrapie and CJD, and in those of humans with FFI and CJD (sCJD, gCJD, iCJD, vCJD) (Giese et al., 1995; Lucassen et al., 1995; Jesionek-Kupnicka et al., 1997; Dorandeu et al., 1998; Jesionek-Kupnicka et al., 1999; Gray et al., 1999; Jesionek-Kupnicka et al., 2001; Siso et al., 2002). The induction of apoptosis typically results in the activation of cysteine proteases known as caspases. Activated caspases-2, -8, -9, -10, -11, and -12 cleave and activate downstream caspases-3, -6, and -7, which then mediate a series of apoptotic signaling events. Elevated levels of active caspase-3 were detected in the brains of scrapie-infected mice and CJD patients, and in cultured neurons treated with a neurotoxic peptide corresponding to human PrP residues 106-126 (PrP106-126) (Saez-Valero et al., 2000; White et al., 2001; Jamieson et al., 2001; Puig et al., 2001; Siso et al., 2002). However, similar levels of active caspase-3, albeit measured by immunohistochemistry without quantitation, were detected in mock- and scrapie-infected sheep (Lyahyai et al., 2006). Moreover, caspase-3 inhibition did not inhibit cell death *in vitro* or *ex vivo*, or affect survival time *in vivo* (Saez-Valero et al., 2000; White et al., 2001; Engelstein et al., 2005).

The activation of caspase-3 is mediated by the release of cytochrome *c* from the outer membrane of mitochondria. Permeabilization of the mitochondrial outer membrane is inhibited by B-cell lymphoma protein 2 (Bcl-2) and promoted by Bcl-2 associated X protein (Bax). Although the levels of pro-apoptotic Bax were elevated in scrapie-infected hamsters and sheep, Bax and Bcl-2 levels in scrapie-infected mice and CJD patients were unchanged relative to mock- or

uninfected controls (Park et al., 2000; Puig et al., 2001; Siso et al., 2002; Lyahyai et al., 2006). Mice lacking pro-apoptotic Bax or overexpressing anti-apoptotic Bcl-2 did not survive scrapie infection longer than wild-type mice (Steele et al., 2007b).

The activation of caspase-3 is also mediated by the activation of death receptors on the plasma membrane, such as the Fas receptor. However, the levels of the Fas receptor and corresponding ligand (FasL) were unchanged in scrapie-infected mice (Siso et al., 2002). Thus, apoptosis may contribute to prion disease neuronal death, but other modes are likely also involved.

1.4.2.3 Proposed mechanisms mediating neuronal death

1.4.2.3.1 Synaptic degeneration

Synaptic degeneration is an early neuropathological feature of prion diseases. Conditional knockout of PrP^C in neurons during early synaptic dysfunction of scrapie-infected mice prevented further disease progression (Mallucci et al., 2003). Early synaptic degeneration may therefore participate in prion pathogenesis.

The transmembrane receptor Notch-1 is cleaved by γ-secretase, releasing the transcriptional activator Notch-1 intracellular domain (NICD) (De Strooper et al., 1999; Mumm et al., 2000). NICD then translocates to the nucleus where it promotes transcription of genes encoding proteins that ultimately inhibit the maintenance of dendrites and axons, thus resulting in neuronal death (Arumugam et al., 2011). NICD levels were elevated in scrapie-infected mice, suggesting that synaptic degeneration may contribute to neuronal loss (Ishikura et al., 2005). However, inhibition of NICD formation by the γ-secretase inhibitor LY411575 [(2S)-2-[[(2S)-2-(3,5-difluorophenyl)-2-hydroxyacetyl]amino]-N-[(7S)-5-methyl-6-oxo-7H-benzo[d][1]benzazepin-7-yl]propanamide]

did not prevent dendrite degeneration in scrapie-infected mice. The inhibitor was too toxic to evaluate any potential effect on survival (Spilman et al., 2008). Treatment with the γ-secretase inhibitor CHF5074 [1-[4-(3,4-dichlorophenyl)-3-fluorophenyl]cyclopropane-1-carboxylic acid] prolonged survival of scrapie-infected mice, but the extent of dendrite degeneration was not evaluated (Poli et al., 2012). The mechanisms that mediate synaptic degeneration, and the role such degeneration has on neuronal loss during prion pathogenesis therefore remains unclear.

1.4.2.3.2 Dysregulated ion homeostasis

Dysregulated intracellular ion homeostasis has been proposed to contribute to neuronal death during prion disease pathogenesis. The expression of PrPΔ105-125 was neurotoxic *in vivo* (as discussed in **Section 1.2.5.1.1**). HEK293 cells expressing PrPΔ105-125 (and to a lesser degree PrPΔ32-134 and Dpl) were more sensitive to the cationic antibiotic G418 (Geneticin; (2R,3R,4R,5R)-2-[(1S,2S,3R,4S,6R)-4,6-diamino-3-[(2S,3R,4R,5S,6R)-3-amino-4,5-dihydroxy-6-[(1R)-1-hydroxyethyl]oxan-2-yl]oxy-2-hydroxycyclohexyl]oxy-5-methyl-4-(methylamino)oxane-3,5-diol) than cells expressing full-length PrP (Massignan et al., 2010). Patch-clamp analyses of HEK293, mouse N2a, and insect Sf9 (fall armyworm [*Spodoptera frugiperda*]) cells expressing PrPΔ105-125 detected spontaneous inward currents mediated by cation influx (Solomon et al., 2010). Similar currents were also detected in cultured neurons and cerebellar brain slices from mice expressing PrPΔ105-125 (Biasini et al., 2013). The expression of PrPΔ105-125 was therefore proposed to promote cell death by sustained ion receptor activation or through plasma membrane pore formation.

The synthetic peptide PrP106-126 also forms pores in lipid bilayer membranes (Lin et al., 1997; Kourie et al., 2000) and is neurotoxic *ex vivo* and *in vivo* (Forloni et al., 1993; Ettaiche et al., 2000; Bergström et al., 2005). Like PrP^{Sc}, PrP106-126 is PK resistance, β-sheet rich, and has a propensity to aggregate. Whereas the expression of PrP^{C} inhibits PrPΔ105-125 neurotoxicity, PrP106-126 neurotoxicity requires it (Selvaggini et al., 1993; Brown et al., 1994a; Forloni et al., 1994). Other neurotoxic peptides (PrP95-133, PrP105-132, PrP118-135, PrP120-133, PrP120-135, PrP127-147) that insert, or are predicted to insert, into membranes may also form pores (Pillot et al., 1997; Haïk et al., 2000; Rymer et al., 2000; Chabry et al., 2003; Vilches et al., 2013).

The ionotropic glutamate receptors are a family of ion receptors in the CNS that, with few exceptions, mediate the transport of cations. Prolonged stimulation of such glutamate receptors is neurotoxic, and neurons expressing PrPΔ105-125 were more sensitive to prolonged glutamate treatment than neurons expressing full-length PrP (Biasini et al., 2013). The death of cells expressing PrPΔ105-125 or cultured neurons treated with neurotoxic PrP peptides was inhibited by the noncompetitive NMDA receptor (NMDAR) antagonist MK-801 (dizocilpine; (5S,10R)-(+)-5-Methyl-10,11-dihydro-5H-dibenzo[a,d]cyclohepten-5,10-imine maleate) (Haïk et al., 2000; Biasini et al., 2013). NMDAR inhibition also protected against PrP^{Sc}-induced neuronal death and prolonged survival of scrapie-infected mice (Müller et al., 1993; Riemer et al., 2008; Resenberger et al., 2011).

As glutamate receptors are excitatory, neurotoxicity resulting from prolonged stimulation of glutamate receptors is termed excitotoxicity. Excitotoxic neuronal death can activate apoptotic or necrotic processes (for review see Wang et al., 2010b). Were excitotoxic neuronal death to contribute to prion disease pathogenesis it may therefore explain the inability to universally

attribute neuronal death to apoptosis (or any other single mode of neuronal cell death). However, excitotoxic stress, as indicated by spontaneous inward currents, was also detected in HEK293 cells expressing PrP mutants that lacked *in vivo* neurotoxicity (PrPΔ94-110, PrPΔ114-121) (Solomon et al., 2011). Moreover, the expression of only 3 of 10 disease-associated mutant PrP analyzed resulted in spontaneous currents *in vitro* (Solomon et al., 2010; Solomon et al., 2011). The insertional mutant PG14, which did not induce spontaneous currents *in vitro*, actually impaired calcium influx and reduced excitatory postsynaptic currents (EPSCs) *in vivo* (Senatore et al., 2012). The role of dysregulated ion homeostasis in neuronal death during prion disease pathogenesis is therefore not yet completely understood.

1.4.2.3.3 Impaired protein degradation

The accumulation of misfolded or unfolded proteins is inhibited by two degradation systems, lysosomal (via a process known as autophagy) and proteasomal. Endogenous PrP^{C} in degraded by both the lysosome and proteasome (Ma et al., 2001; Yedidia et al., 2001). The accumulation of PrP^{Sc} may therefore indicate impaired cellular protein degradation. Alternatively, PrP^{Sc} accumulation itself may overwhelm such degradation systems.

1.4.2.3.3.1 Impaired proteasomal degradation

The ubiquitin-proteasome system (UPS) is responsible for the degradation of more than 80% of intracellular proteins (for review see Wang et al., 2006). Polyubiquitination mediated by E1 ubiquitin-activating and E2 ubiquitin-conjugating enzymes, with an E3 ubiquitin ligase, targets most proteins for degradation by the 26S proteasome. The 26S proteasome consists of a 20S

catalytic and 19S regulatory particle. UPS inhibition promotes neuronal death and proteasome activity is reduced in scrapie-infected mouse N2a and hypothalamic GT-1 cells, and in scrapie-infected mice (Lowe et al., 1992; Qiu et al., 2000; Kang et al., 2004; Kristiansen et al., 2007). PrP^{Sc} directly impaired substrate entry into the proteasome, and consequently impaired proteasome function (Deriziotis et al., 2011). Neuronal death during prion disease pathogenesis may therefore result from UPS inhibition. As PrP is degraded by the UPS, UPS inhibition may increase the potential for PrP^{Sc} accumulation (Yedidia et al., 2001). Indeed, treatment with IU1 [1-[1-(4-fluorophenyl)-2,5-dimethyl-1H-pyrrol-3-yl]-2-(1-pyrrolidinyl)-ethanone], a small inhibitor of the deubiquitinating enzyme, ubiquitin carboxyl-terminal hydrolase 14 (Usp14), stimulated proteasome activation and promoted PrP^{Sc} clearance from infected mouse catecholaminergic CAD cells (McKinnon et al., 2015). Mice lacking the E3 ubiquitin ligase mahogunin ring finger-1 developed spongiform degeneration, astrogliosis, and neuronal loss, suggesting that UPS inhibition may also contribute to prion neuropathology (He et al., 2003). However, proteasome activity was unchanged or elevated in sheep infected with scrapie and the survival time of scrapie-infected mice was unaffected by mahogunin overexpression (Amici et al., 2010; Silvius et al., 2013).

1.4.2.3.3.1.1 Endoplasmic reticulum stress

The endoplasmic reticulum (ER) is the site for folding of secretory and transmembrane proteins. Misfolded or unfolded proteins are exported from the ER to the cytosol for degradation by the UPS, a processes termed ER-associated degradation (ERAD). Cellular stresses, which include UPS impairment, can induce the accumulation of misfolded and unfolded proteins in the ER lumen. The accumulation of proteins within the ER lumen can induce ER stress and consequently activate

the unfolded protein response (UPR). Mutant PrP associated with GSS (PG14) and gCJD (D177N/V128) accumulated within the ER lumen of neurons but did not induce ER stress *ex vivo* or *in vivo* (Drisaldi et al., 2003; Dossena et al., 2008; Quaglio et al., 2011; Senatore et al., 2012). ER stress can also result from excitotoxic stimuli (Ruiz et al., 2009), suggesting that UPR activation may also involve dysregulated ion homeostasis. Ultimately, the UPR acts to restore protein folding homeostasis by activation of the integral ER membrane proteins PKR-like ER kinase (PERK), inositol-requiring protein 1 (IRE1), and activating transcription factor 6 (ATF6) (for review see Ron et al., 2007; Walter et al., 2011).

PERK is activated by autophosphorylation. Active PERK phosphorylates and inhibits eukaryotic initiation factor 2 alpha (eIF2α). The levels of phosphorylated (activated) PERK and phosphorylated (inhibited) eIF2α were elevated in scrapie-infected mice and increased with PrP^{res} accumulation (Unterberger et al., 2006; Moreno et al., 2012). The eIF2α phosphatase, growth arrest and DNA damage-inducible protein 34 (GADD34, also known as protein phosphatase 1 regulatory subunit 15A [PPP1R15A]) dephosphorylates eIF2α. GADD34 overexpression reduced neuronal loss and prolonged survival of scrapie-infected mice, suggesting that PERK activation may participate in prion pathogenesis. Consistently, treatment with the PERK inhibitor GSK2606414 [1-[5-(4-amino-7-methylpyrrolo[2,3-d]pyrimidin-5-yl)-2,3-dihydroindol-1-yl]-2-[3-(trifluoromethyl)phenyl] ethanone] also reduced neuronal loss and prolonged survival time of scrapie-infected mice (Moreno et al., 2013). However, elevated levels of phosphorylated PERK and eIF2α were only detected in the brains of patients with human prion disease (vCJD, sCJD, iCJD, gCJD, GSS, FFI, kuru) if phosphorylated tau was also present, a feature not typically observed in prion disease (Unterberger et al., 2006).

AFT6 is translocated to the Golgi during ER stress and activated by proteolytic cleavage. Active ATF6 then translocates to the nucleus where it promotes the transcription of genes encoding for ER stress response proteins, including the ER chaperones glucose-regulated protein, 78 kDa (Grp78, also known as BiP) and Grp94 (also known as endoplasmin). Meanwhile, IRE1 is activated by dimerization and autophosphorylation. Active IRE1 mediates X-box-binding protein 1 (XBP1) mRNA cleavage to generate a transcript (XBP1s) encoding a transcriptional activator that also promotes the transcription of genes encoding Grp78 and Grp94, among others. The levels of Grp78 and Grp94 were elevated in PrP^{Sc}- or PrP106-126-treated cultured cells and CJD patients, but unchanged in scrapie-infected mice (Hetz et al., 2003; Ferreiro et al., 2006). Similar levels of activated (cleaved) ATF6 were detected in mock- and scrapie-infected mice. Moreover, conditional knockout of neuronal XBP1 in scrapie-infected mice did not affect PrP^{res} aggregation, neuronal loss, or survival time (Hetz et al., 2008). Neuronal death during prion disease is therefore independent of ATF6 activation and the IRE1-XBP1 branch of the ER stress response.

Active IRE1 also activates caspase-12 (in mice; caspase-4 in humans) and c-Jun N-terminal kinase (JNK) in response to ER stress (Urano et al., 2000). Elevated levels of activated JNK and activated (cleaved) caspase-12 were detected in scrapie-infected mice and hamsters (Hetz et al., 2003; Lee et al., 2005; Steele et al., 2007a). Consistently, elevated levels of activated the transcription factor c-Jun, a downstream JNK substrate, were also elevated at late stages of prion disease (Carimalo et al., 2005; Lee et al., 2005). Treatment with JNK inhibitors (JNK inhibitor II [2-methylanthra[1,9-cd]pyrazole-6(2H)-one] and SP600125 [anthra(1,9-cd)pyrazol-6(2H)-one]) or expression of a dominant-negative caspase-12 mutant inhibited PrP^{Sc}- and PrP106-126-mediated death *in vitro* and *ex vivo*, suggesting a role in neuronal death (Hetz et al., 2003;

Carimalo et al., 2005; Rambold et al., 2008). However, caspase-12 knockout mice did not survive scrapie infection (or accumulate less PrP^{res}) than wild-type mice (Steele et al., 2007a). The effect of JNK inhibition in prion disease pathogenesis *in vivo* has yet to be evaluated.

1.4.2.3.3.2 Impaired autophagy

Autophagy is a cellular process that degrades organelles and cytosolic proteins under conditions of stress or starvation (for review see Yang et al., 2010). Autophagy also degrades intracellular pathogens, a process termed xenophagy. Cellular components targeted for autophagic degradation may be trafficked to the lysosome within autophagosomes (macroautophagy), targeted to the lysosome by chaperones (chaperone-mediated autophagy), or result from lysosomal invagination (microautophagy). Autophagy also mediates degradation of ubiquitinated protein aggregates through interaction between p62 (also known as sequestosome 1 [SQSTM1]) and the autophagosomal membrane protein, microtubule-associated protein 1 light chain 3 (LC3-II) (Pankiv et al., 2007). Autophagy-related protein 5 (Atg5) and Atg7 are critical for macroautophagy (Kuma et al., 2004; Komatsu et al., 2005). Conditional knockout of neuronal Atg5 or Atg7 in mice resulted in growth retardation and neurodegeneration with ataxia (Hara et al., 2006; Komatsu et al., 2006). Autophagy is therefore proposed to participate in development and neuronal survival (or protection against neuronal death).

Increased numbers of autophagosomes and autophagic vacuoles were observed in *in vitro* and *in vivo* models of prion disease and in the brains of patients with FFI, sCJD, and gCJD (Boellaard et al., 1989; Boellaard et al., 1991; Liberski et al., 1992; Schatzl et al., 1997; Liberski et al., 2002; Sikorska et al., 2004; Liberski et al., 2005; Xu et al., 2012). Elevated levels of p62 and

LC3-II were detected in scrapie-infected mouse and hamster brain (Homma et al., 2014). Treatment with the autophagy inducers rapamycin (sirolimus; (7E,15E,17E,19E)-9,10,12,13,14, 21,22,23,24,25,26, 27,32,33,34aS-hexadecahydro-9R,27-dihydroxy-3S-[(1R)-2-[(1S,3R,4R)-4-hydroxy-3-methoxycyclohexyl]-1-methylethyl]-10R,21S-dimethoxy-6R,8,12R,14S,20,26R-hexamethyl-23S,27R-epoxy-3H-pyrido[2,1-c][1,4]oxaazacyclohentriacontine-1,5,11,28,29(4H, 6H,31H)-pentone) and lithium prolonged survival of scrapie-infected mice and transgenic mice expressing GSS-associated mutant PrP (Heiseke et al., 2009; Cortes et al., 2012). Treatment with astemizole (1-[(4-fluorophenyl)methyl]- N-[1-[2-(4-methoxyphenyl)ethyl]- 4-piperidyl] benzoimidazol-2-amine) also induced autophagy *in vitro* and appeared to prolong survival of scrapie-infected mice (Karapetyan et al., 2013). Autophagy may therefore be impaired or insufficiently activated to protect from neuronal death during prion disease pathogenesis. Proteins destined for degradation by the UPS may be reallocated to autophagic degradation during UPS inhibition (for review see Lilienbaum, 2013). Were this the case during prion disease pathogenesis, autophagic degradation may simply be unable to accommodate the increased protein load.

1.4.2.4 Glial cells in neurotoxicity

Activated microglia and astrocytes typically function to protect the CNS by clearance of apoptotic cells and neuronal debris. Microglia-mediated clearance of apoptotic bodies is promoted by milk fat globule epidermal growth factor 8 (Mfge8) opsonization (Fuller et al., 2008). Both microglia and astrocytes secrete Mfge8 (Boddaert et al., 2007). Mice lacking Mfge8 died faster after scrapie infection than wild-type mice, suggesting that activated microglia and astrocytes inhibit prion pathogenesis (Kranich et al., 2010). However, these effects appear to be dependent on the genetic

background of the mouse strains used. Gliosis may rather contribute to neuronal death during prion disease. For example, neuronal death *ex vivo* was reduced by the clearance of microglia with L-leucine methyl ester (LLME) treatment prior to scrapie infection (Brown et al., 1996; Giese et al., 1998). Moreover, inhibition of microglia proliferation during prion disease pathogenesis by treatment with the macrophage colony-stimulating factor 1 receptor (CSF1R) inhibitor GW2580 [5-(3-Methoxy-4-((4-methoxybenzyl)oxy)benzyl)pyrimidine-2,4-diamine] inhibited neuronal loss and prolonged survival of scrapie-infected mice (Gómez-Nicola et al., 2013).

Activated microglia produce and release toxic reactive oxygen species (ROS). Elevated levels of ROS were detected in scrapie-infected mice at terminal stages of disease (Sorce et al., 2014). The transmembrane electron carrier enzyme nicotinamide adenine dinucleotide phosphate oxidase (NOX) contributes to ROS production. Microglia express NOX2 and elevated levels of NOX2 were detected in the brains of CJD patients and scrapie-infected mice (Cooney et al., 2013; Sorce et al., 2014). However, the survival time of NOX2-deficient mice was not different from that of wild-type mice after infection with mouse-adapted scrapie strain 22L, despite inhibition of ROS production. The enzyme superoxide dismutase (SOD) catalyzes a dismutation reaction wherein two molecules of the ROS species superoxide (oxygen with an unpaired electron) are converted to oxygen (O_2) and hydrogen peroxide (H_2O_2). Hydrogen peroxide is then converted to water and oxygen by catalase or glutathione peroxidase. SOD therefore functions to protect from ROS toxicity. SOD overexpression prolonged survival time of scrapie-infected mice (Tamguney et al., 2008), while disease progression was accelerated in scrapie-infected mice lacking SOD ($Sod^{-/-}$) (Akhtar et al., 2013). ROS production may therefore contribute to prion pathogenesis.

Activated microglia and astrocytes also release cytokines that enhance (pro-inflammatory) or inhibit (anti-inflammatory) the immune response. The levels of both pro-inflammatory (interferon gamma [IFNγ], interleukin-1 alpha [IL-1α], and interleukin-1 beta [IL-1β]) and anti-inflammatory (interleukin-6 [IL-6] and transforming growth factor beta [TGFβ]) cytokines were elevated in scrapie-infected mice (Cunningham et al., 2002; Tribouillard-Tanvier et al., 2009). Although overexpression of the IL-1 receptor antagonist (IL-1Ra) had no effect on survival of scrapie-infected mice (Carroll et al., 2015), inhibition of IL-1 signaling by deletion of IL-1 receptor type 1 (IL-1R1) prolonged it (Schultz et al., 2004). Conversely, inhibition of anti-inflammatory TGFβ by adenovirus-mediated overexpression of the proteoglycan decorin promoted death of hippocampal neurons in mice infected with scrapie strain ME7 (Boche et al., 2006). Mice lacking the anti-inflammatory cytokine interleukin-10 (IL-10) died faster from scrapie infection than wild-type mice, suggesting that IL-10 expression inhibited prion disease pathogenesis (Thackray et al., 2004). Consistently, prolonged survival of scrapie-infected mice lacking the pro-inflammatory receptor cluster of differentiation 14 (CD14) was associated with elevated levels of IL-10 (and reduced levels of pro-inflammatory IL-1β) (Sakai et al., 2013). The levels of a subset of pro- and anti-inflammatory cytokines and chemokines were elevated in scrapie-infected mice but unchanged in mice lacking endogenous PrP (Tribouillard-Tanvier et al., 2009). Together, these findings suggest that the release of anti-inflammatory cytokines during prion disease pathogenesis is neuroprotective, but insufficient to protect against the neurotoxic pro-inflammatory factors also released.

1.4.2.5 PrP family proteins in prion pathogenesis

Shadoo (Sho) levels were reduced in the brains of prion-infected mice, hamsters, voles, and sheep at clinical stages of disease progression (Watts et al., 2007; Watts et al., 2011). Time-course analyses revealed that the levels of Sho decreased with increasing levels of PrP^{res}, leading to speculation that decreased Sho levels may contribute to prion disease pathogenesis (Watts et al., 2011). However, no change in scrapie survival time was observed in transgenic mice overexpressing (Tg24474, Tg24488) or in mice lacking Sho (*Sprn*$^{-/-}$) (Watts et al., 2011; Li et al., 2014). Doppel (Dpl) is not expressed in the brain under physiological conditions, or during prion disease, and did not affect survival time when expressed in the brain of prion-infected transgenic mice (Tuzi et al., 2002). The two other proteins in the PrP family, Sho and Dpl, therefore do not appear to contribute to prion disease pathogenesis.

1.5 Therapeutics

1.5.1 Inhibition of PrP conversion

There are no preventative or therapeutic treatments yet available against prion diseases (Colby et al., 2011). Inhibition of the accumulation of prions, the etiological agent, represents an attractive therapeutic target. Prions are composed largely, if not solely, of PrP^{Sc}. Neuronal death and disease progression were prevented in scrapie-infected mice by conditional ablation of PrP^{C} at the time when PrP^{Sc} was first detected (Mallucci et al., 2003). Inhibition of PrP^{C} conversion to PrP^{Sc} is thus a validated target for therapeutic intervention. Such inhibition may be mediated reduced levels of PrP^{C}, impaired PrP^{C}/PrP^{Sc} interaction, or enhanced clearance or digestion of PrP^{Sc}, by mechanisms that will be discussed below.

1.5.1.1 RNA interference

PrP^C expression levels can be reduced by RNA interference (RNAi) (**Figure 1.3**, 1). RNAi is a mechanism of post-transcriptional gene regulation that uses small interfering RNA (siRNA) to selectively degrade target mRNA (for review see Hannon, 2002; Davidson et al., 2011). siRNAs are 21-22 nucleotide long fragments of double-stranded RNA (dsRNA). The expression of synthetic siRNA specific for *Prnp* reduced PrP^C expression and cleared PrP^{res} from scrapie-infected N2a or GT-1 cells (Daude et al., 2003; Tilly et al., 2003). However, RNAi is usually not capable of reducing protein expression more than 90-95% and transgenic mice still succumbed to prion disease even when PrP^C levels were reduced to ~5% normal levels, albeit with a much prolonged incubation (Safar et al., 2005a). Not surprisingly, RNAi-mediated reduction in PrP^C levels, even up to 71%, prolonged survival of scrapie-infected mice but failed to fully protect them (Pfeifer et al., 2006; Lehmann et al., 2014)

1.5.1.2 Anti-PrP antibodies

Antibodies specific for PrP can inhibit PrP^C/PrP^{Sc} interactions and reduce the levels of PrP^C and PrP^{Sc} (**Figure 1.3**, 2 and 3). Anti-PrP antibody cleared PrP^{res} from N2a cells persistently infected with scrapie (ScN2a) (Peretz et al., 2001b; Enari et al., 2001; Perrier et al., 2004; Jones et al., 2010). The administration of purified antibodies (passive immunization) prolonged the survival of scrapie-infected mice (White et al., 2003), even when administered at clinical stages of disease (Song et al., 2008). Host tolerance inhibits the production of anti-PrP antibodies, but can be overcome by immune stimulation in the presence of a PrP antigen (active immunization). Mice immunized with live attenuated *Salmonella typhimurium* expressing recombinant mouse PrP

produced anti-PrP antibodies and survived ~200 days longer than control mice after oral scrapie infection (Goni et al., 2005; Goni et al., 2008). Mice immunized with recPrP, PrP peptides, plasmids encoding PrP fused to the lysosomal integral membrane protein type II, dendritic cells expressing PrP peptides, or native PrP^{Sc} bound to magnetic beads also survived longer after peripheral scrapie infection (Sigurdsson et al., 2002; Schwarz et al., 2003; Tayebi et al., 2004; Magri et al., 2005; Bade et al., 2006; Fernandez-Borges et al., 2006; Ishibashi et al., 2007; Tayebi et al., 2009; Bachy et al., 2010). The administration or generation of anti-PrP antibodies has therefore been demonstrated to prolong survival after scrapie infection *in vivo*. However, antibodies against host-encoded PrP^{C} have the potential to induce an autoimmune response. Indeed, treatment with the anti-PrP antibody POM1 was toxic to cultured organotypic cerebellar slices (Sonati et al., 2013). Only three PrP^{Sc}-specific epitopes have been identified (tyrosine-tyrosine-arginine [YYR] motif in β-strand 2, tyrosine-methionine-leucine [YML] motif in β-strand 1, rigid loop region between β-strand 2 and α-helix 2). The therapeutic potential of these epitopes has been little evaluated *in vivo* (Taschuk et al., 2014). Moreover, antibodies do not readily cross the blood-brain barrier. Consequently, active and passive immunotherapy was less effective after scrapie neuroinvasion (Sigurdsson et al., 2002; White et al., 2003; Tayebi et al., 2009; Ohsawa et al., 2013). The therapeutic potential of antibodies against prion diseases is thus far limited.

1.5.1.3 Heterologous PrP

PrP conversion is modulated by PrP sequence homology (as described in **Section 1.4.1.1**). The expression of mouse PrP with only a single amino acid substitution reduced PrP^{res} levels in transfected ScN2a cells (Priola et al., 1994). Mice are resistant to hamster-adapted scrapie strain

Sc237 (Scott et al., 1989) and conversely, hamsters are resistant to mouse-adapted scrapie strain RML (Prusiner et al., 1990). The sequence differences between mouse and hamster PrP is therefore sufficient to inhibit conversion. Indeed, the survival time of RML-infected transgenic mice was directly related to level of hamster PrP co-expression (Prusiner et al., 1990). Treatment with recombinant hamster PrP reduced prion neuropathology and prolonged survival time of scrapie-infected mice in a dose-dependent manner (Skinner et al., 2015). Although transgenic mice co-expressing human and mouse PrP were resistant to CJD infection (Telling et al., 1995), the therapeutic potential of treatment with mouse PrP (or other heterologous PrP) against prion diseases in humans has yet to be evaluated.

1.5.1.4 Small molecules

PrP conversion is also inhibited by many relatively small molecules including polyanions, polyamines, tetrapyrroles, tetracyclines, and polyene antibiotics (for review see Trevitt et al., 2006; Sakaguchi, 2009; Sim, 2012). The identification of such compounds is largely mediated by high-throughput screens (Kocisko et al., 2003; Kocisko et al., 2006). Consequently, the mechanisms by whereby most compounds inhibit PrP conversion remain poorly defined. Compounds that inhibit PrP^{res} accumulation *in vitro* are typically evaluated *in vivo* using scrapie-infected mice and hamsters. Although most effective when administered prophylactically or shortly after prion neuroinvasion, the compounds with the greatest therapeutic potential are those that also prolong survival when treatment is initiated later in disease progression. Pentosan polysulfate (PPS; [(2R,3R,4S,5R)-2-hydroxy-5-[(2S,3R,4S,5R)-5-hydroxy-3,4-disulfooxyoxan-2-yl]oxy-3-sulfooxyoxan-4-yl] hydrogen sulfate) treatment, for example, reduced PrP^{Sc} accumulation and

prolonged survival of scrapie-infected hamsters and mice when initiated at preclinical stages of disease progression, 35 and 49 days after intracerebral infection, respectively (Doh-ura et al., 2004). The 2-aminothiazole derivative IND24 [(4-biphenyl-4-yl-thiazol-2-yl)-(6-methyl-pyridin-2-yl)-amine] prolonged survival time of mice when treatment was initiated 60 days after intracerebral inoculation with scrapie strains RML and ME7 (Berry et al., 2013). Curcumin (diferoylmethane; (1E,6E)-1,7-bis(4-hydroxy-3-methoxyphenyl)hepta-1,6-diene-3,5-dione), simvastatin [(1S,3R,7S,8S,8aR)-8-2-[(2R,4R)-4-hydroxy-6-oxooxan-2-yl]ethyl-3,7-dimethyl-1,2,3,7,8,8a-hexahydronaphthalen-1-yl 2,2-dimethylbutanoate], and the fungal antibiotic amphotericin B [(1S,3R,4E,6E,8E,10E,12E,14E, 16E,18S,19R,20R,21S,25R,27R,30R,31R,33S, 35R,37S,38R)-3-[(2R,3S,4S,5S,6R)-4-amino-3,5-dihydroxy-6-methyloxan-2-yl]oxy-19,25,27,30, 31,33,35,37-octahydroxy-18,20,21-trimethyl-23-oxo-22,39-dioxabicyclo[33.3.1]nonatriaconta-4,6,8,10,12,14,16-heptaene-38-carboxylic acid] also prolonged survival time of scrapie-infected mice when administered even later within the preclinical stage of disease progression (Demaimay et al., 1997; Mok et al., 2006; Riemer et al., 2008). Most effectively, treatment with the diphenyl pyrazole derivative anle138b [3-(1,3-benzodioxol-5-yl)-5-(3-bromophenyl)-1H-pyrazole] or the conjugated polythiophene LIN5044 prolonged survival of scrapie-infected mice even when treatment was started after the onset of clinical signs (Wagner et al., 2013; Herrmann et al., 2015). Both these compounds appear to inhibit the formation of PrP^{Sc} oligomers, which otherwise enhance PrP conversion (as described in **Section 1.4.1**) (**Figure 1.3**, 4 and 5).

A number of steps within the PrP conversion process are therefore amenable to inhibition by various compounds. Unfortunately, the inhibition of PrP conversion mediated by most compounds is strain-specific. Treatment with compound B [(E)-5-(4-(2-(pyridin-4-ylmethylene)

hydrazinyl)phenyl)oxazole], for example, prolonged survival of mice infected with mouse-adapted scrapie strains RML, 22L, and Fukuoka-1, but not hamsters infected with hamster-adapted scrapie strain 263K (Kawasaki et al., 2007). IND24 and anle138b treatment did not affect survival time of transgenic mice infected with sCJD (Berry et al., 2013; Giles et al., 2015). Meanwhile, treatment with the quinacrine [4-N-(6-chloro-2-methoxyacridin-9-yl)-1-N,1-N-diethylpentane-1,4-diamine] cleared PrP^{res} from ScN2a cells, but increased levels of PrP^{res} in rabbit kidney epithelial cells expressing elk PrP ($Elk21^{+}$) persistently infected with CWD prions (Doh-Ura et al., 2000; Bian et al., 2014). Compounds that inhibit the conversion of PrP associated with one prion disease may therefore not be effective against others. Moreover, treatment with IND24, and a related derivative IND125, resulted in the accumulation of PrP^{Sc} biochemically distinct from that associated with the inoculating prion strain, suggesting that anti-PrP conversion compounds may select for alternative PrP^{Sc} conformations (Berry et al., 2013; Giles et al., 2015).

The therapeutic potential of a number of compounds has been evaluated in clinical trials of patients with prion disease. PPS treatment did not affect survival time of patients with CJD or GSS (Terada et al., 2010; Honda et al., 2012), despite one study suggesting otherwise (Bone et al., 2008). No difference in survival times were observed in two CJD patients treated with amphotericin B (Masullo et al., 1992). Treatment with quinacrine alone or in combination with chlorpromazine [3-(2-chlorophenothiazin-10-yl)-N,N-dimethylpropan-1-amine] did not prolong survival of CJD or FFI patients (Haik et al., 2004; Benito-Leon, 2004; Martínez-Lage et al., 2005; Collinge et al., 2009; Geschwind et al., 2013). Thus, no compound has yet been demonstrated to be effective when treatment is initiated after the onset of clinical signs of prion disease in humans.

1.5.2 Therapeutics targeting events downstream of PrP interaction/conversion

Human prion diseases can be infectious (acquired), inherited (genetic), or sporadic. The latter are the most common, accounting for approximately 85% of cases (Wadsworth et al., 2003). The inherited and acquired cases may be suspected from the risk facts before the onset of clinical symptoms. In contrast, the sporadic cases can only be diagnosed after the onset of clinical symptoms (Paterson et al., 2012b). PrP conversion occurs long before the onset of clinical signs of disease. In mice intracerebrally infected with scrapie strain ME7, for example, PrP^{res} was first detected at 70 dpi, almost 110 days before significant loss of CA1 hippocampal neurons, which occurred at 180 dpi, or the onset of clinical disease at 226 dpi (Jeffrey et al., 2000b). Consequently, therapeutics targeting PrP conversion were more effective when administered prophylactically or at preclinical stages of disease progression than at the onset of clinical disease. The direct delivery of anti-PrP antibody 31C6 to the CNS by intraventricular infusion, for example, prolonged survival of mice infected with scrapie strain Obihiro when administered at 60 dpi, but not when administered at 90 or 120 dpi (Song et al., 2008). Mice infected with scrapie strain ME7 survived 88 days longer when IND24 treatment was initiated at 1 dpi, but only 32 days longer when treatment was initiated at 60 dpi (Berry et al., 2013). Similarly, anle138b treatment initiated at the time of inoculation prolonged survival by 175 days, but only by 73 or 52 days when it was initiated at 80 or 120 dpi, respectively (Wagner et al., 2013). Therapeutics against PrP conversion therefore have limited application for sporadic prion disease.

Treatment with the calcineurin/protein phosphatase 3 inhibitor FK506 (tacrolimus; (1R,9S,12S,13R,14S,17R,18E,21S,23S,24R,25S,27R)-1,14-dihydroxy-12-[(1E)-1-[(1R,3R,4R)-4-hydroxy-3-methoxycyclohexyl]prop-1-en-2-yl]-23,25-dimethoxy-13,19,21,27-tetramethyl-17-

(prop-2-en-1-yl)-11,28-dioxa-4-azatricyclo[22.3.1.0^{4,9}]octacos-18-ene-2,3,10,16-tetrone) prolonged survival of scrapie-infected mice after the onset of clinical disease (Mukherjee et al., 2010). Although FK506 treatment reduced plasma membrane PrP^{C} levels in cultured cells (Karapetyan et al., 2013) and may affect the levels of PrP^{Sc} when administered preclinically (Nakagaki et al., 2013), treatment with FK506 at clinical onset did not affect the levels of PrP^{C} or the accumulation of PrP^{Sc} (Mukherjee et al., 2010). As FK506 is a (calcineurin) signaling inhibitor, these results suggest that dysregulated signaling downstream of PrP conversion is an alternative therapeutic target against prion diseases (**Figure 1.3**, 6). Unfortunately, however, such signaling pathways remain yet poorly characterized.

1.6 Protein kinases

Intracellular signal transduction allows for cells to interact with their extracellular environment. Proteins are critical mediators of intracellular signal transduction and subject to post-translational modifications. Such post-translational modifications include proteolytic cleavage and covalent modifications such as glycosylation, methylation, acetylation, sumoylation, palmitoylation, and phosphorylation (for review see Deribe et al., 2010). Protein phosphorylation is mediated by a family of enzymes known as protein kinases which, in eukaryotes, transfer a γ-phosphate from adenosine triphosphate (ATP) to the hydroxyl (-OH) group on serine, threonine, or tyrosine residue. Although less common, protein kinases can also use guanosine triphosphate (GTP) as a phosphoryl donor. The human genome encodes for 518 protein kinases, which comprise the human kinome (the protein kinase complement of the genome) (Manning et al., 2002). Another 145 genes within the human genome encode for protein phosphatases that mediate the removal of

phosphate (dephosphorylation) from serine, threonine, or tyrosine residues by hydrolysis (Alonso et al., 2004; Li et al., 2013).

Most protein kinases are intracellular or localized to the plasma membrane, where they may be anchored or transmembrane. Extracellular or secretory protein kinases have also been described (Tagliavini et al., 1993). Protein phosphorylation is mediated by a protein kinase catalytic domain, which is conserved in all but 32 (atypical) protein kinases. The protein kinase catalytic domain consists of a N-terminal lobe, consisting of mostly β-sheet, and a C-terminal lobe rich in α-helices (for review see Taylor et al., 2012). A hydrophobic cleft exists between these two lobes and is the active site where phosphotransfer occurs. The catalytic domain can be further divided into 12 subdomains (Hanks et al., 1995). Conserved sequence motifs within these subdomains facilitate protein kinase catalysis. ATP is anchored and properly oriented by interactions with a GxGxxGxV motif (where x is any amino acid) in subdomain I, the AxK motif in subdomain II, and the DFG motif in subdomain VII. Transfer of the γ-phosphate of ATP to the substrate protein is mediated by the aspartic acid (D) in the H/YRD catalytic loop in subdomain VIB.

Protein kinases have a defined set of substrate proteins. Substrate specificity is partly regulated by residues adjacent the acceptor serine, threonine, or tyrosine residue. Protein kinase A (PKA), for example, phosphorylates the serine or threonine residue within the consensus sequence RRxS/T, while ribosomal protein S6 kinase (RSK) recognizes the sequence RxRxxS/T (Pearce et al., 2010). Many substrates are other protein kinases, the phosphorylation of which modulates their activities. Protein kinase phosphorylation may also be mediated by autophosphorylation, wherein the kinase serves as its own substrate. Autophosphorylation reactions can be

intermolecular or intramolecular. Protein kinase activity is also modulated by multiple other mechanisms, including interactions with growth factors or with secondary messengers, such as calcium, diacylglycerol (DAG), inositol 1,4,5-trisphosphate (IP_3), and cyclic adenosine monophosphate (cAMP).

1.6.1 Protein kinases in prion diseases

Reversible protein phosphorylation modulates the function, localization, and activity of an estimated one-third of all cellular proteins (Johnson et al., 2005). Protein kinases (and phosphatases) are therefore critical regulators of signal transduction. It is thus not surprising that dysregulated protein kinase signaling is implicated in the pathogenesis of many chronic diseases, including cancer and neurodegenerative diseases such as Alzheimer's and Parkinson's (Cell Signaling Technology, 2015; Wood-Kaczmar et al., 2006; Martin et al., 2013). Dysregulated protein kinase signaling is also implicated in the pathogenesis of prion diseases (Combs et al., 1999; Jin et al., 1999; Mouillet-Richard et al., 2000; Chiarini et al., 2002; Schneider et al., 2003; Schwarz et al., 2004; Ertmer et al., 2004; Monnet et al., 2004; Kanaani et al., 2005; Lopes et al., 2005; Nixon, 2005; Lee et al., 2005; Nordstrom et al., 2005; Krebs et al., 2006; Weise et al., 2006; Lopes et al., 2007; Caetano et al., 2008; Aguib et al., 2009; Nordstrom et al., 2009; Roffe et al., 2010; Moreno et al., 2012; Allard et al., 2013; Harischandra et al., 2014). For example, feline Gardner-Rasheed sarcoma virus oncogene cellular homolog/Yamaguchi 73 and Esh avian sarcoma virus oncogene cellular homolog-related novel protein kinase (Fyn) knockout mice died faster than wild-type mice after scrapie infection (Schwarz et al., 2004). Conversely, inhibition of PERK by the overexpression of GADD34 prolonged survival of scrapie-infected mice (Moreno et al., 2012).

The activation of vascular endothelial growth factor receptor (VEGFR) inhibited death of cultured neurons treated with the neurotoxic prion peptide PrP106-126 (Arsenault et al., 2012). Death of PrP106-126-treated cultured neurons was also inhibited by Abelson leukemia oncogene cellular homolog (c-Abl) knockdown (Pan et al., 2014). Unfortunately, however, the protein kinase signaling pathways most critical to the pathogenesis of prion diseases remain yet poorly characterized.

1.7 Protein kinase inhibitors

Protein kinases are major therapeutic targets against chronic diseases. The first small molecule protein kinase inhibitor approved for clinical use was 'signal transduction inhibitor' 571 (STI571) (imatinib, Gleevec; 4-[(4-methylpiperazin-1-yl)methyl]-N-[4-methyl-3-[(4-pyridin-3-ylpyrimidin-2-yl)amino]phenyl]benzamide). STI571, an inhibitor of the protein kinases c-Abl, Hardy-Zuckerman 4 feline sarcoma virus oncogene cellular homolog (c-Kit) and platelet-derived growth factor receptor (PDGFR), was approved in 2001 for treatment against chronic myeloid leukemia (CML). Most patients with CML have constitutively active c-Abl as a result of chromosomal rearrangement. The gene encoding c-Abl (*abl*) on chromosome 9 has translocated and fused to the breakpoint cluster region (*bcr*) on chromosome 22 to produce what is referred to as the Philadelphia (Ph) chromosome (Heisterkamp et al., 1983; Groffen et al., 1984; Lugo et al., 1990). The Ph chromosome is under the control of the BCR promoter. Treatment with STI571 reduced white blood cell (and platelet) count to within normal physiological ranges and increased 5-year patient survival rate from approximately 30% to 90% (Druker et al., 2001; Druker et al., 2006).

The success of STI571 resulted in the increased investment into the development of protein kinase inhibitors as therapeutic agents. It is estimated that the pharmaceutical industry invests up to 30% of their research and development budget towards protein kinase inhibitors (Fabbro et al., 2012; Bamborough, 2012). Consequently, inhibitors of protein kinases are the largest group of new cancer therapeutics (Knight et al., 2010). As of August 2016, forty-one such inhibitors are now in clinical use, over 600 are involved in more than 3,800 clinical trials, and thousands more are in various stages of pre-clinical development (BioSeeker Group, 2016; United States National Institutes of Health, 2016c). Small molecule inhibitors have been identified for approximately 20% of protein kinases in the kinome (Wu et al., 2015). Protein kinase inhibitors therefore constitute a rapidly growing group of clinical drugs that have the potential to considerably impact the treatment of chronic diseases.

1.7.1 Therapeutic potential of protein kinase inhibitors against prion disease

Although the signaling pathways most critical to prion disease pathogenesis have yet to be fully characterized, PrP^{Sc} accumulation in scrapie-infected cultured cells was modulated by treatment with several protein kinase inhibitors (Ertmer et al., 2004; Nordstrom et al., 2005; Aguib et al., 2009; Heiseke et al., 2009; Nordstrom et al., 2009; Allard et al., 2013). Treatment with STI571 impaired scrapie neuroinvasion and prolonged survival of mice after intraperitoneal infection (Yun et al., 2007). Scrapie-infected mice treated with the phosphoinositide-dependent kinase 1 (PDK1) inhibitor BX912 [N-[3-[[5-bromo-4-[2-(1H-imidazol-5-yl)ethylamino]pyrimidin-2-yl]amino] phenyl]pyrrolidine-1-carboxamide] or the Rho-associated coiled-coil-containing protein kinase 1 (ROCK1) inhibitor Y-27632 [4-[(1R)-1-aminoethyl]-N-pyridin-4-ylcyclohexane-1-carboxamide]

just prior to the onset of clinical disease (130 dpi; clinical disease at 140 dpi) reduced PrP^{Sc} levels and prolonged survival time, suggesting that the PDK1-ROCK1 signaling pathway contributes to prion pathogenesis (Pietri et al., 2013; Alleaume-Butaux et al., 2015). Meanwhile, treatment with the PERK inhibitor GSK2606414 delayed disease onset in scrapie-infected mice without affecting PrP^{Sc} accumulation, indicating PERK dysregulation occurs downstream of PrP conversion (Moreno et al., 2013). Inhibitors of protein kinases therefore have potential as prion disease therapeutics.

1.8 RATIONALE

Prion diseases are chronic neurodegenerative diseases for which there are no therapeutic treatments available. Although much research into the development of such therapeutics has focused on inhibition of PrP conversion, the accumulation of PrP^{Sc} occurs before extensive neuronal death and presentation of clinical signs of disease. Most cases of prion disease in humans are sporadic and are therefore not diagnosed or suspected until the onset of clinical symptoms. Alternative therapeutic targets must be explored to identify those amenable to intervention after the onset of clinical signs. I propose that dysregulated signaling pathways downstream of PrP conversion, particularly those critical for neuronal death, may be a valid target for therapeutic intervention.

Protein kinases are critical mediators of signal transduction and modulate most intracellular processes. Dysregulated protein kinase signaling is involved in the pathogenesis of many diseases. Consequently, protein kinases have become major therapeutic targets. Forty-one protein kinase inhibitors are approved for clinical use against cancer and many more are in various stages of development, thus representing an expanding therapeutic source. Dysregulated protein kinase signaling is likely to also participate in the pathogenesis of prion diseases. Unfortunately, those signaling pathways most critical to prion pathogenesis remain poorly characterized. Protein kinases involved in pathways critical to pathogenesis have the potential to serve as novel therapeutic targets against prion disease.

Table 1.1 – List of human and animals prion diseases and their etiologies

Species	Etiology	Disease
Human	Acquired	Kuru
		Variant CJD (vCJD)
		Iatrogenic CJD (iCJD)
	Genetic	Genetic or familial CJD (gCJD, fCJD)
		Gerstmann-Sträussler-Scheinker syndrome (GSS)
		Fatal familial insomnia (FFI)
		PrP cerebral amyloid angiopathy (PrP-CAA)
		PrP systemic amyloidosis (PrP-SA)
	Sporadic	Sporadic CJD (sCJD)
		Sporadic fatal insomnia (sFI)
		Variable protease-sensitive prionopathy (VPSP)
Cattle	Acquired	Bovine spongiform encephalopathy (BSE; or 'Mad Cow' disease)
Deer, elk, moose	Acquired	Chronic wasting disease (CWD)
Sheep, goat	Acquired	Scrapie
Mink	Acquired	Transmissible mink encephalopathy (TME)

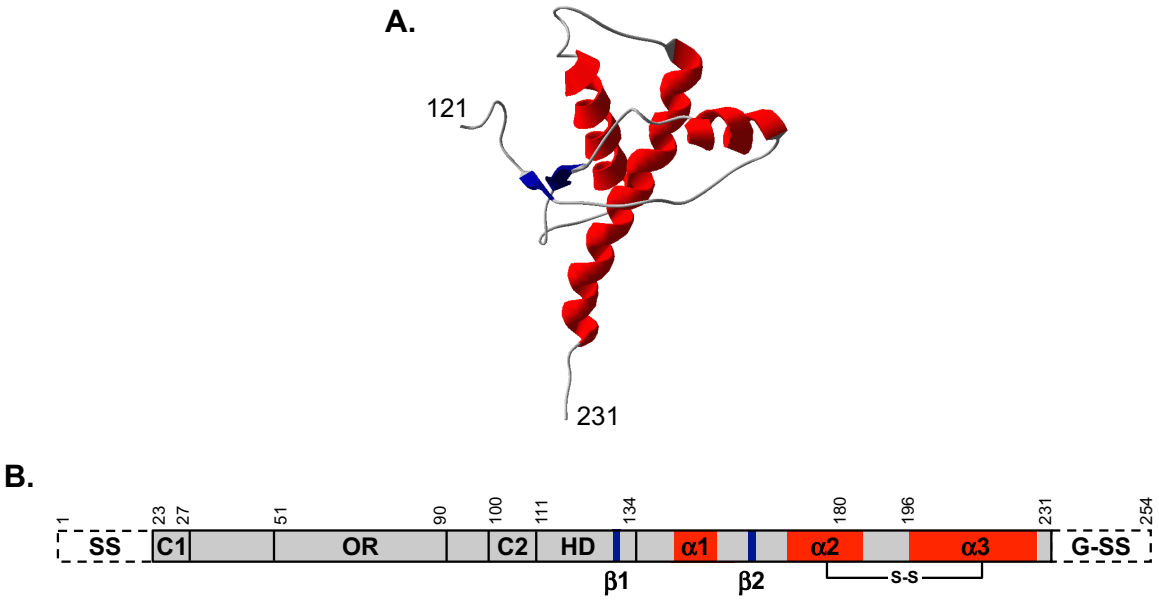

Figure 1.1 – Structure of mouse PrP^C. A) Ribbon diagram of the carboxy-terminus of recombinant mouse prion protein (residues 121-231) solved by nuclear magnetic resonance imaging (PDB ID code 1XYX) and analyzed using using Swiss-PdbViewer. Red, α-helices; blue, β-sheets. **B**) Schematic representation of nascent mouse PrP^C polypeptide. C1, charged cluster 1; OR, octapeptide repeat; C2, charged cluster 2; HD, hydrophobic domain; S-S, disulphide bond. Dashed regions indicate signal sequences that are cleaved during processing. SS, ER-targeting signal sequence; G-SS, GPI-anchor signal sequence.

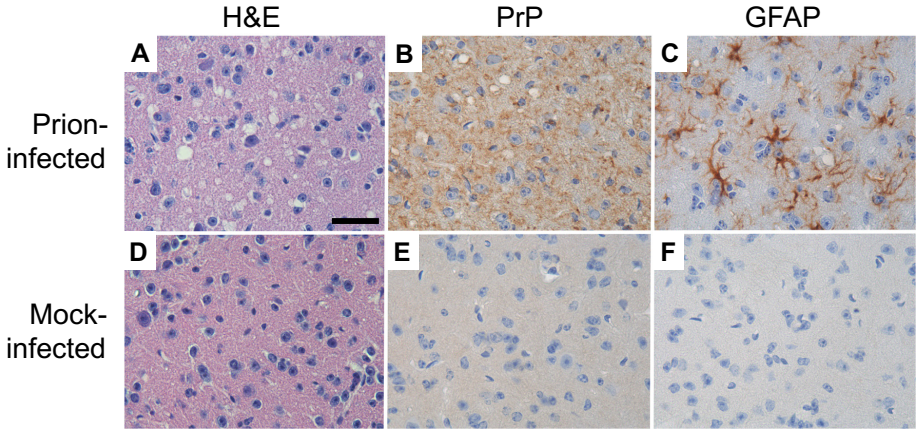

Figure 1.2 – Prion disease neuropathology. Brain sections from the superior colliculus of prion (TME hyper strain)-infected (**A-C**) or mock-infected (**D-F**) hamsters stained with hematoxylin and eosin (H&E) for vacuolation or probed with α-PrP and α-GFAP antibodies for PrP^{Sc} accumulation and astrogliosis, respectively. Scale bar, 100 μm. Image from Shikiya and Bartz, 2011. Reprinted with permission from the American Society for Microbiology.

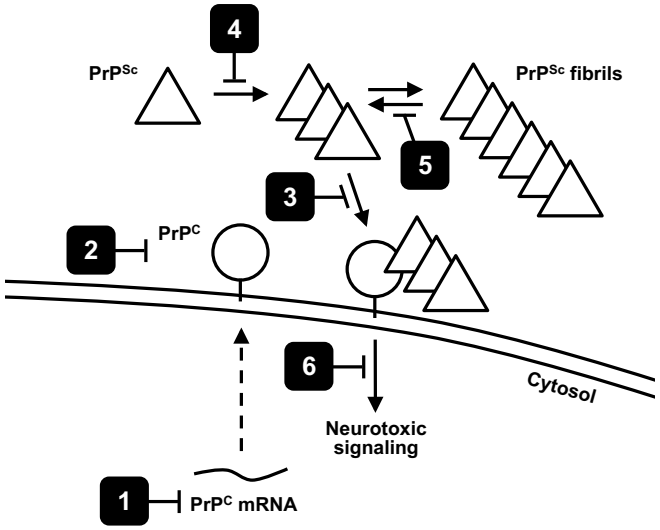

Figure 1.3 – Potential points of therapeutic intervention against prion diseases. The conversion of endogenous PrP^{C} to PrP^{Sc} can be inhibited by degradation of transcripts encoding PrP^{C} (1), reduced expression or improper localization of PrP^{C} (2), inhibition of PrP^{C}-PrP^{Sc} interaction (3), inhibition of PrP^{Sc} oligomerization (4), stabilization of PrP^{Sc} fibrils/inhibition of fragmentation (5; indirect inhibition of PrP^{Sc} oligomer formation), or the inhibition of neurotoxic signaling downstream of PrP conversion (6).

CHAPTER 2: MATERIALS AND METHODS

All experimental procedures involving prions were carried out at the National Microbiology Laboratory (Public Health Agency of Canada, Winnipeg, Manitoba) or the Centre for Prions and Protein Folding Diseases (University of Alberta) with strict adherence to approved safety protocols. I performed all procedures unless otherwise stated.

2.1 Cloning, cell culture, and transfections

Mouse N2a neuroblastoma cells were transfected by Catherine Grenier and Guillaume Tremblay (Department of Biochemistry, Faculty of Medicine, Université de Sherbrooke, Sherbrooke, Quebec).

Mouse 3T3 cells were propagated in Dulbecco's Modified Eagle's Medium (DMEM; Life Technologies Inc., Carlsbad, California, USA) supplemented with 5% (v/v) fetal bovine serum (FBS; PAA Laboratories GmbH, Pasching, Austria), 50 U/mL penicillin and 50 μg/mL streptomycin (Life Technologies Inc.), at 37°C in 5% CO_2. Cloning of human CyPrP^{EGFP}, CyPrP^{EGFP}124stop and CyPrP^{EGFP}124-230 in pCEP4β (Life Technologies Inc.) was previously described (Grenier et al., 2006). N2a cells were maintained in DMEM supplemented with 10% (v/v) FBS (Wisent, St. Bruno, Quebec, Canada) and transfected using Exgen (MBI Fermentas, Burlington, Ontario, Canada) or GeneCellin (BioCellChallenge, Toulon, France), according to the manufacturer's protocol. To monitor transfection, cells were harvested with trypsin/ethylene glycol-bis(2-aminoethylether)-N,N,N',N'-tetraacetic acid (EDTA) and centrifuged for 5 min at 500 × g. Following a wash with PBS, cells were fixed with 4% (w/v) paraformaldehyde/4% (w/v) sucrose solution for 20 min at room temperature, washed with PBS and analyzed on a cytometer for GFP expression.

2.2 Preparation of cell lysates

Transfected N2a cells were harvested by Catherine Grenier and Guillaume Tremblay (Université de Sherbrooke).

Mouse 3T3 and transfected N2a cells were cultured to approximately 85% confluency on 8 x 10 cm tissue culture dishes. All subsequent procedures were performed on ice or at 4°C, using reagents pre-chilled to 4°C. Each dish was washed twice with 2 mL of phosphate-buffered saline (PBS; 150 mM NaCl, 1 mM KH_2PO_4, 3 mM Na_2HPO_4, pH 7.4). Cells were collected by scraping into freshly prepared lysis buffer (0.2 mL per dish) (20 mM 4-morpholinepropanesulfonic acid [MOPS, pH 7.0], 2 mM EGTA, 5 mM ethylenedinitrilotetraacetic acid [EDTA], 1% [v/v] Nonidet P-40 [octyl phenoxypolyethoxylethanol], 0.001% [v/v] phosphatase inhibitor cocktail [catalog# 78420; Pierce, Rockford, Illinois, USA], 0.002% [v/v] protease inhibitor cocktail [catalog# P8340; Sigma-Aldrich, St. Louis, Missouri, USA], 1 mM dithiothreitol [DTT], pH 7.2). The lysates were passed twice through a 21 gauge needle, sonicated five times for 20 s intervals at 88 W output (XL-2020; Misonix, Farmingdale, New York, USA), and pre-cleared at 14,000 × g for 30 min (JA.14 rotor, Avanti J-E centrifuge; Beckman/Coulter, Brea, California, USA). Approximately 1 mL volumes of supernatant were aliquoted, snap frozen in liquid nitrogen, and then shipped on dry ice (N2a lysates) or stored immediately (3T3 lysates) at –80°C.

2.3 Animals and sample collection

All animal infections and sample collections were performed by Kathy L. Frost and Anna Majer (National Microbiology Laboratory, Public Health Agency of Canada, Winnipeg, Manitoba).

CD1 mice (Charles River Laboratories) between 4–6 weeks of age were infected intraperitoneally with the Rocky Mountain Laboratory (RML) mouse-adapted strain of scrapie. The inoculums consisted of 200 µl of 1% brain homogenate in PBS from either clinically ill or normal control mice. Animals were euthanized at 70, 90, 110, 130 days post-infection (dpi) and at terminal disease (155–190 dpi). Terminal disease was diagnosed by kyphosis, dull ruffled coat, weight loss of 20% or more and ataxia. Brain samples were collected and macrodissected into three sections, (*i*) cortical, (*ii*) subcortical (including thalamus, hypothalamus and hippocampus) and (*iii*) brainstem-cerebellum. Each section was flash frozen using a dry ice/methanol mixture, shipped on dry ice, and then stored at –80°C until processing. A total of 3 scrapie- and 3 mock-infected samples were collected per time point.

2.4 Preparation of brain homogenates

All procedures were performed at 4°C or on ice, and all reagents added were at 4°C. Weighed frozen whole brains (for antibody optimization), or brainstem-cerebellum, subcortical, and cortical regions from mock- or scrapie-infected mice, were homogenized in 3 mL of freshly prepared lysis buffer (20 mM MOPS [pH 7.0], 2 mM EGTA, 5 mM EDTA, 1% [v/v] Nonidet P-40, 0.01% [v/v] phosphatase inhibitor cocktail [catalog# 78420; Pierce], 0.02% [v/v] protease inhibitor cocktail [catalog# P8340; Sigma-Aldrich], 10 mM DTT, pH 7.2) (Pelech et al., 2003) per 250 mg of brain, using a tissue homogenizer with disposable tips (TH and hard tissue OMNI tip, respectively; OMNI International, Kennesaw, Georgia, USA). Brain homogenates were passed twice through a 21 gauge needle, sonicated five times for 20 s intervals at 88 W output (XL-2020; Misonix, Farmingdale, New York, USA [whole brains]; 431C1 cup horn probe, S-4000 sonicator;

Qsonica, Newtown, Connecticut, USA [mock- or scrapie-infected brain regions]), and pre-cleared by centrifugation for 30 min at 14,000 × g (JLA 16.250 BC or JA.14 rotor, Avanti J-E centrifuge; Beckman/Coulter, Brea, California, USA). Approximately 200 µL aliquots of supernatant were aliquoted into 1.5 mL tubes, snap frozen in liquid nitrogen, and stored at –80°C.

2.5 Protein quantitation

Protein concentration was determined by Bradford's assay (catalog# 500-0006; Bio-Rad Laboratories, Hercules, California, USA). Protein concentration and equal sample loading were re-tested in preliminary sodium dodecyl sulfate polyacrylamide gel electrophoresis (SDS-PAGE). Brain homogenates or cell lysates were mixed with equal volumes of 2X SDS loading buffer (125 mM Tris-Cl [pH 6.8], 20% [v/v] glycerol, 4% [w/v] SDS, 0.005% [w/v] bromophenol blue, 260 mM DTT), denatured at 100°C for 10 min, and loaded onto 10- or 15-well 8% SDS-PAGE gels (Mini-PROTEAN; Bio-Rad Laboratories) in electrophoresis tanks (Mini-PROTEAN II or Mini-PROTEAN Tetra; Bio-Rad Laboratories) filled with running buffer (190 mM glycine, 24.8 mM Tris, 0.1% [w/v] SDS, pH 8.3). Proteins were run through the stacking gel at 50 V, and then resolved for 90 min at 100 V, always at room temperature. Pre-stained protein standards (catalog# 161-0373; Bio-Rad Laboratories) were used to monitor protein resolution during electrophoresis. Proteins were stained with Coomassie blue G-250 (catalog# 161-0786, Bio-Safe Coomassie; Bio-Rad Laboratories) according to the manufacturer's instructions. Signal from Coomassie-stained protein was detected using an Odyssey infrared imaging system (LI-COR Biosciences, Lincoln, Nebraska, USA) in the 700 nm channel and quantitated using Odyssey 3.0 software (LI-COR

Biosciences). Protein amounts were calculated relative to a pre-quantitated standard brain homogenate.

2.6 Sodium phosphotungstic acid precipitation

Sodium phosphotungstic acid (NaPTA) precipitation was adapted from (Safar et al., 1998; Wadsworth et al., 2001). One milligram of mouse brain homogenate was mixed with an equal volume of 4% (w/v) sodium lauryl sarcosinate (sarkosyl) in PBS (prepared by Camilo Duque Velásquez, University of Alberta). Samples were incubated for 10 min at 37°C with constant agitation (1,000 rpm, Thermomixer; Eppendorf, Hamburg, Germany). A 37°C NaPTA solution (PBS, 4% [w/v] NaPTA, 170 mM $MgCl_2$, pH 7.4; prepared by Camilo Duque Velásquez, University of Alberta) was then added to a final concentration of 0.3% (w/v) NaPTA. Samples were incubated for 60 min at 37°C with constant agitation (1,000 rpm, Thermomixer; Eppendorf), then centrifuged at 37°C for 30 min at 16,000 × g (FA-45-18-11 rotor, 5418 microfuge; Eppendorf). Pellets were resuspended in 5 µL of 0.1% (w/v) sarkosyl/PBS and digested with 20 µg of proteinase K (PK; in 0.01 M $CaCl_2$) (catalog# 3115828001; Roche, Indianapolis, Indiana, USA) for 30 min at 37°C with a brief vortex after 15 min (Kumar et al., 2008). Digestion was stopped and PK-resistant protein was denatured by quickly adding an approximately equal volume 5X SDS loading buffer (300 mM Tris-Cl [pH 6.8], 50% [v/v] glycerol, 25% [v/v] β-mercaptoethanol, 10% [w/v] SDS, 1% [w/v] bromophenol blue; prepared by Florence Li, University of Alberta), and immediately incubating at 100°C for 10 min. Samples were then resolved by SDS-PAGE and analyzed by Western blot (**Section 2.7.3**).

2.7 Western blots

Proteins were denatured by incubating 10 min at 100°C with an equal volume of 2X, one-fourth volume of 5X, or one-fifth volume of 6X (375 mM Tris-Cl [pH 6.8], 60% [v/v] glycerol, 12% [w/v] SDS, 0.015% [w/v] bromophenol blue, 780 mM DTT) SDS-PAGE loading buffer prior to loading. All other procedures were performed at room temperature and all washes were performed using gentle rocking, unless otherwise indicated.

2.7.1 Western blots to evaluate EGFP and PrP expression

Lysate from N2a cells expressing empty vector (100 μg), or vector encoding EGFP (50 μg), CyPrP^{EGFP} (200 μg), CyPrP^{EGFP}124stop (100 μg), or CyPrP^{EGFP}124-230 (100 μg) was loaded onto 15-well 10% SDS-PAGE gels (Mini-PROTEAN; Bio-Rad Laboratories). Proteins were resolved as described in **Section 2.5** and the gels then equilibrated in transfer buffer (384 mM glycine, 49.6 mM Tris, 20% [v/v] methanol, 0.01% [w/v] SDS) (Otter et al., 1987) for 30 min. Meanwhile, polyvinylidene fluoride (PVDF) membranes (Immuno-Blot, 0.2 μm; Bio-Rad Laboratories) were soaked in methanol for 2 min, and equilibrated in transfer buffer for 20 min. For each membrane, four sheets of filter paper were equilibrated in transfer buffer for 5 min. Transfer cassettes were loaded into a transfer tank (TE22; Hoefer, Holliston, Massachusetts, USA) filled with transfer buffer at 4°C. Proteins were transferred for 23 h at 4°C; 1 h at 54 mA, 4 h at 189 mA, 8 h at 270 mA and finally 10 h at 378 mA. The temperature was maintained at 4°C by heat exchange (Isotemp 1016D; Thermo Fisher Scientific, Waltham, Massachusetts, USA) and gentle stirring of the transfer buffer. After transfer, membranes were dried, then soaked in methanol for 2 min before washing twice for 10 min each in Tris-buffered saline (TBS; 140 mM NaCl, 3 mM KCl, 25

mM Tris, pH 7.6). Membranes were blocked for 1 h in 10% (v/v) blocking buffer (catalog# B6429; Sigma-Aldrich) then simultaneously probed for 18 h at 4°C with primary antibodies specific for GFP (a kind gift from Dr. Luc Berthiaume, University of Alberta) and PrP (clone 3F4; a kind gift from Dr. Deborah McKenzie, University of Alberta) diluted to 1:10,000 and 1:2500, respectively, in 10% (v/v) blocking buffer/0.1% (v/v) Tween-20. Afterward, membranes were washed in TBS/0.1% (v/v) Tween-20 (TBST) once for 5 min and thrice for 10 min each. Membranes were incubated with donkey anti-mouse IRDye 680- (catalog# LIC-926-32222; LI-COR Biosciences) and donkey anti-rabbit IRDye 800- (catalog# LIC-926-32213; LI-COR Biosciences) labeled secondary antibodies, diluted to 1:20,000 in 10% (v/v) blocking buffer/0.1% (v/v) Tween-20/0.01% (w/v) SDS for 1 h. Membranes were washed thrice in TBST for 10 min each and once in TBS for 5 min. Signal from pre-stained protein standards and IRDye 680-labeled secondary antibody was detected at 700 nm, and from IRDye 800-labeled secondary antibody at 800 nm, using the Odyssey infrared imaging system. Signal was quantitated using Odyssey 3.0 software. To measure total protein, membranes were stained with Coomassie blue R-250 (catalog# 161-0400; Bio-Rad Laboratories) for 10 min and destained with 40% (v/v) methanol/10% (v/v) glacial acetic acid thrice for 10 min each, or until excess stain was removed. Signal from Coomassie-stained protein was detected at 700 nm using the Odyssey system and quantitated using Odyssey 3.0 software.

2.7.2 Western blots to evaluate GFAP and total PrP

Brain homogenate from mock- or scrapie-infected mice (100 μg per linear cm) was loaded onto 15-well 12% SDS-PAGE gels (Mini-PROTEAN; Bio-Rad Laboratories). Proteins were run

through the stacking gel at 50 V, and then resolved for 100 min at 100 V. Resolved proteins were transferred and blots performed as described in **Section 2.7.1**, with the exception that the membranes were incubated simultaneously with primary antibodies specific for PrP (clone SAF83; a kind gift from Dr. Deborah McKenzie, University of Alberta) and GFAP (catalog# ab7260; Abcam Inc., Cambridge, Massachusetts, USA) diluted to 1:10,000 and 1:20,000, respectively. Signal from secondary antibodies and Coomassie-stained protein was detected and quantitated as described in **Section 2.7.1**.

2.7.3 Western blots to evaluate PrP^{res}

NaPTA-enriched, PK-treated brain homogenate from mock- or scrapie-infected mice (1.0 mg) was loaded onto 15-well 12% SDS-PAGE gels (NuPAGE Novex Bis-Tris; Life Technologies Inc., Carlsbad, California, USA) in electrophoresis tanks (XCell II; Life Technologies Inc.). The running buffer (50 mM MOPS, 50 mM Tris, 1 mM EDTA, 0.1% [w/v] SDS, pH 7.7) within the upper (cathode) chamber contained 5 mM sodium bisulfite (from 1M stock prepared by Anthony Ness, University of Alberta). Proteins were run through the stacking gel at 60 V, and then resolved for 2.5 h at 120 V. Afterward, PVDF membranes (Immuno-Blot, 0.2 μm; Bio-Rad Laboratories) were soaked in methanol for 2 min, then equilibrated in transfer buffer (190 mM glycine, 24.5 mM Tris, 10% [v/v] methanol) for 20 min. For each membrane, two sheets of filter paper were equilibrated in transfer buffer for 5 min. Proteins were transferred at 4°C for 2 h at 30 V. After transfer, membranes were dried, soaked in methanol for 2 min and washed twice for 10 min each in TBS. Membranes were blocked in 5% (w/v) milk (non-fat skim milk powder)/TBST for 1 h, then probed with primary antibody specific for PrP (clone SAF83) diluted to 1:10,000 in 5%

(w/v) milk/TBST for 18 h at 4°C. Afterward, membranes were washed with TBST once for 5 min and thrice for 10 min each. Membranes were incubated with goat anti-mouse horseradish peroxidase (HRP)-labeled secondary antibody (catalog# 170-5047; Bio-Rad Laboratories) diluted to 1:40,000 in 5% (w/v) milk/TBST for 1 h. Membranes were washed in TBST once for 5 min and thrice for 15 min each, incubated for 5 min with enhanced chemiluminescent substrate (catalog# 34095, SuperSignal West Femto; Pierce) and then exposed to film (Super RX; Fujifilm, Tokyo, Japan). Exposed film was developed and scanned (CanoScan LiDE 200; Canon, Tokyo, Japan). Signal was quantitated using ImageJ (Version 1.47c; National Institutes of Health, Bethesda, Maryland, USA).

2.7.4 Multiplex Western blots

Proteins were resolved and transferred as described in **Section 2.7.1**. After transfer, membranes were dried and stored at –30°C, or soaked in methanol for 2 min and washed twice for 10 min each in TBS for immediate probing. Membranes were simultaneously probed with multiple antibodies using a multiscreen apparatus. After incubation with primary antibody, all membranes were briefly washed once with TBST within the multiscreen apparatus, then removed from the apparatus and further washed in TBST, once for 5 min and four times for 15 min each. After incubation with secondary antibody, all membranes were washed in TBST four times for 15 min each and once with TBS for 5 min. Signal from pre-stained protein standards and Alexa Fluor or IRDye 680-labeled secondary antibody was detected at 700 nm, and from IRDye 800-labeled secondary antibody at 800 nm, using the Odyssey infrared imaging system. Signal was quantitated using Odyssey 3.0 software.

Membranes with protein from cells expressing cytoplasmic PrP mutants or brain homogenate from scrapie-infected mice were stripped (only once) together and in parallel with the membranes from the control cells or mock-infected mice, respectively, under conditions to minimize protein loss (Yeung et al., 2009). Stripped membranes were washed with TBST and TBS once for 5 min each, then blocked and reprobed with a second set of primary antibodies, as described. No membrane was stripped more than once.

2.7.4.1 Multiplex Western blots of cell lysate spiked with brain homogenate

*Cathy Appanah (Department of Biochemistry, University of Alberta) performed the brain spike experiment for PKC*θ *under my supervision.*

For the spiking experiments, 85 μg (for p39 and TrkB) or 200 μg (for PKCγ, CaMK4, CDK1, CHK1, RSK2, CDK4, PDGFRβ, BTK and PKCθ) of total protein was loaded per linear cm of four- or five-well 8% SDS-PAGE gels. Membranes were then blocked for 1 h in 10% (v/v) blocking buffer (Sigma-Aldrich), then rinsed briefly with TBS and positioned within a 20-lane multiscreen apparatus (catalog# 170-4017, Bio-Rad Laboratories). Six hundred microlitres (600 μL) of primary antibody diluted in 10% (v/v) blocking buffer/0.1% (v/v) Tween-20 was loaded in the appropriate lane of the multiscreen apparatus and incubated for 18 h at 4°C. Mouse monoclonal primary antibodies were detected with goat anti-mouse Alexa Fluor 680-labeled secondary antibody (catalog# A21057, Molecular Probes, Eugene, Oregon, USA). Rabbit or goat polyclonal primary antibodies were detected with goat anti-rabbit (catalog# 611-132-122, Rockland, Gilbertsville, Pennsylvania, USA) or donkey anti-goat (catalog# 605-732-125, Rockland) IRDye 800-labeled secondary antibodies, respectively.

2.7.4.2 Multiplex Western blots of lysates from cells expressing cytoplasmic PrP mutants

Lysate from N2a cells expressing cytoplasmic PrP mutants (150 μg per linear cm) was loaded onto single-well 8% SDS-PAGE gels for primary blots; 8 or 10% gels loaded 150, 300, or 450 μg of protein per linear cm were used for secondary and tertiary blots. All primary blots were performed in one set, composed of one membrane each from cells transfected with empty vector or vector encoding CyPrP^{EGFP}, CyPrP^{EGFP}124stop, and CyPrP^{EGFP}124-230 for 24 h. All targeted secondary and tertiary blots were performed in three sets, each composed of one membrane from cells expressing EGFP and one from cells expressing CyPrP^{EGFP} for 12, 24, or 48 h. Membranes were blocked for 1 h in 10% (v/v) blocking buffer (Sigma-Aldrich) for evaluation of total protein levels, or in 3% (w/v) BSA (catalog# BSA-30, Rockland) for evaluation of phosphorylation levels. Membranes were rinsed briefly in TBS and positioned within a 20-lane multiscreen apparatus (Bio-Rad Laboratories). Combinations of primary antibodies were diluted in 10% (v/v) blocking buffer/0.1% (v/v) Tween-20 or 3% (w/v) BSA/0.1% (v/v) Tween-20, as appropriate. Six hundred microlitres (600 μL) of each dilution was loaded in the appropriate lane of the multiscreen apparatus and incubated for 18 h at 4°C. For primary blots, mouse monoclonal primary antibodies were detected with goat anti-mouse Alexa Fluor 680-labeled (catalog# A21057; Molecular Probes). Rabbit or goat polyclonal primary antibodies were detected with goat anti-rabbit (catalog# 611-132-122; Rockland) or donkey anti-goat (catalog# 605-732-125; Rockland) IRDye 800-labeled secondary antibodies, respectively. For secondary and tertiary blots, mouse monoclonal primary antibodies were detected with goat anti-mouse IRDye 680-labeled (catalog# LIC-926-32220; LI-COR Biosciences). Rabbit or goat polyclonal primary antibodies were detected with goat anti-

rabbit (catalog# LIC-926-32211; LI-COR Biosciences) or donkey anti-goat (catalog# LIC-926-32214; LI-COR Biosciences) IRDye 800-labeled secondary antibodies, respectively.

Membranes were stripped with a mild stripping buffer (25 mM glycine, 1% [w/v] SDS, pH 2.0) once for 5 min and twice for 15 min each. Membranes were then washed with TBST once and TBS once for 5 min each. Stripping of signal was verified by re-imaging the membranes using the Odyssey infrared imaging system. If necessary, membranes were further washed with mild stripping buffer for a maximum of six times of 15 min each. If still necessary, membranes were then incubated with harsh stripping buffer (50 mM Tris-Cl [pH 7.0], 2% [w/v] SDS, 50 mM DTT) (Harlow et al., 1999) for 15 min at 65°C with gentle rocking.

2.7.4.3 Multiplex Western blots of brain homogenates from scrapie-infected mice

Brain homogenate from mock- or scrapie-infected mice (200 μg per linear cm) was loaded onto single-well 8% SDS-PAGE gels (Mini-PROTEAN; Bio-Rad Laboratories). All blots were performed in three sets, each composed of one membrane from a mock- and one from a scrapie-infected mouse euthanized at 70, 90, 110, 130 dpi, or at terminal stage of disease. Membranes were blocked for 1 h in 10% (v/v) blocking buffer (Sigma-Aldrich) for evaluation of total protein levels, or in 3% (w/v) BSA (Rockland) for evaluation of phosphorylation levels. Membranes were rinsed briefly with TBS and positioned within a 24-lane multiscreen apparatus (catalog# 921-00000, MPX; LI-COR Biosciences). Combinations of primary antibody were diluted in 10% (v/v) blocking buffer/0.1% (v/v) Tween-20 or 3% (w/v) BSA/0.1% (v/v) Tween-20, as appropriate. One hundred and sixty microlitres (160 μL) of each antibody dilution was loaded in the appropriate lane of the multiscreen apparatus and incubated for 18 h at 4°C. Mouse monoclonal primary

antibodies were detected with donkey anti-mouse IRDye 680-labeled (catalog# LIC-926-32222; LI-COR Biosciences). Rabbit and goat polyclonal primary antibodies were detected with donkey anti-rabbit (catalog# LIC-926-32213; LI-COR Biosciences) or donkey anti-goat (catalog# LIC-926-32214; LI-COR Biosciences) IRDye 800-labeled secondary antibodies, respectively.

Membranes were stripped with mild stripping buffer once for 5 min and four times for 15 min each, then with harsh stripping buffer once for 15 min at 37°C.

2.8 Hierarchical cluster analysis

The integrated intensity levels (pixel volume) of proteins in cells expressing cytoplasmic PrP mutants or in brainstem-cerebellum homogenates of scrapie-infected mice were normalized to levels in cells expressing empty vector or in mock-infected mice, respectively. Relative protein kinase expression levels were then $\log_2$ transformed to avoid bias by proteins with extreme changes in expression and analyzed with Gene Cluster 3.0 (de Hoon et al., 2004) using city-block or Euclidean distance (similarity metric) and complete linkage (clustering method). Java Treeview was used to present the resulting clusters (Saldanha, 2004).

2.9 Time-course data normalizations

To evaluate the changes in total and phosphorylated protein levels in cells actually expressing $CyPrP^{EGFP}$, the raw levels (in the population containing expressing and non-expressing cells) were corrected for differences in transfection efficiency in each biological repeat and then expressed as relative to the levels in cells transfected with the EGFP expression construct using Equation 1:

$$\frac{G_i + \left[\frac{P_i - G_i}{TE}\right]}{G_i} \qquad (1)$$

where G_i and P_i are the pixel volumes (integrated intensity levels) in lysates from cells expressing EGFP and CyPrP^{EGFP}, respectively, in biological repeat *i*, and *TE* is the transfection efficiency (47%, repeat 1; 45%, repeat 2; 34%, repeat 3). This equation corrected for the fraction of cells in the CyPrP^{EGFP}-transfected population actually expressing the recombinant protein, which directly induce changes in signaling. These changes ($[P_i\text{-}G_i]/TE$) were then added to basal levels (those in the population of cells transfected with the vector encoding EGFP). The corrected levels in cells expressing CyPrP^{EGFP} were then normalized to the levels in cells expressing EGFP in the same biological repeat.

2.10 Statistical analyses

All data were analyzed using Prism (Version 5.0f; GraphPad Software Inc., La Jolla, California, USA). Multiplex Western blots of brain homogenates from scrapie-infected mice were performed in three experimental sets on different days. Each set consisted of one scrapie- and one mock-infected mouse from each time point. The ratios from each set were thus analyzed by paired *t*-test. The ratios were log transformed before analyses to transform the increased and decreased ratios (ratios greater or smaller than 1, respectively) to proportional values. For nonlinear regression analyses, curves of the normalized total and phosphorylated protein levels in cells expressing CyPrP^{EGFP} or in scrapie-infected mice were compared to no changes (a line with y-intercept = 1, slope = 0), representing the levels in cells expressing EGFP or in mock-infected mice, using a replicates test for lack-of-fit.

CHAPTER 3: DEVELOPMENT OF KINOMIC ANALYSES TO IDENTIFY DYSREGULATED SIGNALING PATHWAYS IN CELLS EXPRESSING CYTOPLASMIC PrP

*A version of this chapter has been published. RH Shott, C Appanah, C Grenier, G Tremblay, X Roucou, LM Schang. 2014. Virology Journal **11**:175. I designed, developed, and performed the kinomic analyses. I critically evaluated the results wrote all drafts and final version of the manuscript under direct supervision by Luis M. Schang. Under my supervision, Cathy Appanah contributed the PKCθ data in the spiking experiments. Catherine Grenier and Guillaume Tremblay provided the constructs, performed the transfections, evaluated the transfection efficiencies and prepared the lysates. Xavier Roucou critically revised the manuscript. Luis M. Schang designed the study.*

3.1 INTRODUCTION

Prion diseases are a family of chronic neurodegenerative diseases that are invariably lethal. Although dysregulated protein kinase signaling is implicated in the pathogenesis of prion diseases, most studies have focused on only a select number of protein kinases and thus evaluated the role of only a few signaling pathways during prion pathogenesis. The signaling pathways most critical to prion pathogeneses therefore remain poorly characterized.

Kinomics is the global analyses of protein kinases, akin to global analyses of mRNA (genomics), protein (proteomics), or metabolites (metabolomics) (Johnson et al., 2005). Kinomic analyses can be used to screen for dysregulated protein kinase signaling. Signaling pathways dysregulated in the pathogenesis of other chronic diseases result in, or are mediated by, changes in the protein (expression) levels of involved kinases (Altomare et al., 2005; Dhillon et al., 2007;

Freude et al., 2009; de la Monte, 2012). The analyses of such changes have been used to identify signaling pathways dysregulated in cancer (Mendes et al., 2007; Ye et al., 2009; Song et al., 2014) and neurodegenerative diseases, such as amyotrophic lateral sclerosis (ALS) (Yin et al., 2012). Kinomic analyses may thus also be useful to identify signaling pathways dysregulated during prion pathogenesis.

Although prion diseases are characterized by the accumulation of PrP^{Sc}, endogenous PrP^{C} is also required for pathogenesis (Brandner et al., 1996; Mallucci et al., 2003). PrP^{C} is physiologically anchored to the outside of the plasma membrane via a GPI anchor. PrP^{C} may also accumulate in the cytoplasm (as described in **Section 1.4.2.1**). Mice expressing a truncated PrP^{C} mutant which localized to the cytoplasm (named cytoplasmic PrP, or CyPrP) suffered from ataxia with gliosis and cerebellar degeneration (Ma et al., 2002b). The accumulation of PrP^{C} in the cytoplasm has therefore been considered a possible neurodegenerative mechanism, although this consideration had been questioned (Norstrom et al., 2007). The molecular mechanisms of such neurodegeneration can be studied in culture because CyPrP is also toxic to mouse N2a neuroblastoma cells (Ma et al., 2002b).

CyPrP expression inhibits heat shock protein 70 (Hsp70) synthesis in stressed N2a cells (Goggin et al., 2008). Hsp70 overexpression inhibits CyPrP-mediated toxicity, suggesting that the inhibition of Hsp70 synthesis may contribute to cell death (Rambold et al., 2006; Zhang et al., 2012). Hsp70 promotes the assembly and activation of mammalian target of rapamycin complex 2 (mTORC2; consisting of mTOR, rapamycin-insensitive companion of mTOR [rictor], mammalian lethal with SEC13 protein 8 [mLST8] and stress-activated protein kinase-interacting protein 1 [SIN1]), which then activates protein kinase B (Akt)/ribosomal protein S6 kinase, 70

kilodalton, polypeptide 1 (p70S6K)/eukaryotic initiation factor 4B (eIF4B) signaling (Martin et al., 2008; Rosner et al., 2009). Active eIF4B promotes protein synthesis, which is otherwise inhibited in cells expressing CyPrP (Goggin et al., 2008; Shahbazian et al., 2010).

Here, I describe the development of a kinomics approach to identify signaling pathways dysregulated during prion disease pathogenesis. I used a simple *in vitro* model to test the sensitivity of the approach to identify dysregulated signaling pathways, the accumulation of enhanced green fluorescent protein-tagged cytoplasmic PrP ($CyPrP^{EGFP}$) in N2a cells. The approach identified the Hsp70-regulated Akt/p70S6K/eIF4B signaling pathway to be inhibited in cells expressing $CyPrP^{EGFP}$, which is consistent with previously known consequences of $CyPrP^{EGFP}$ expression (Goggin et al., 2008). The results therefore support the ability of the kinomics approach to detect signaling pathways dysregulated in an *in vitro* model of prion pathogenesis.

3.2 RESULTS

3.2.1 Multiplex Western blots quantitate the expression levels of 137 protein kinases or regulatory subunits in only 1.2 mg of sample

I developed multiplex Western blots to analyze the expression levels of protein kinases potentially involved in prion pathogenesis. In these assays, protein extracts are run in SDS-PAGE in a single well, transferred to a membrane and simultaneously probed with multiple antibodies using a multiscreen apparatus.

The mice and human kinomes are well conserved, allowing the use of mice to identify and analyze protein kinases of potential importance in human disease. I performed an extensive literature search for human protein kinases that may be involved in prion or other

neurodegenerative diseases (Alzheimer's, Parkinson's, Huntington's, multiple sclerosis, or amyotrophic lateral sclerosis), and protein kinases involved in cellular pathologies associated with prion disease (neuronal apoptosis, gliosis, glial activation, neuronal degeneration, or neuronal survival). The search was restricted to protein kinases the mouse orthologs of which were detectable with the antibodies commercially available at the time. Following these criteria, I selected 145 protein kinases, almost 30% of the 540 or 518 protein kinases in the mouse or human kinomes, respectively (**Figure 3.1**) (Manning et al., 2002; Caenepeel et al., 2004). The selected protein kinases are distributed among the eight groups of protein kinases (AGC, CAMK, CMGC, CK1, STE, TK, TKL, and atypical) (Manning et al., 2002). The most under-represented kinases in the selection are involved in muscle contraction (myosin light chain kinases, MLCK), spermatogenesis (testis specific serine/threonine kinases, TSSK), or developmental processes (transforming growth factor-beta receptor kinases, TGF-β), which are not expected to be critical in prion disease. I also included the eleven cyclins or cyclin-like proteins (p25/p35, p39), which are the subunits required for the activity of the catalytic cyclin-dependent kinase (CDK) moiety of the active CDK/cyclin heterodimers.

The long-term objective of this project was to analyze the kinomic changes in brains of scrapie-infected mice (see **Chapter 4**). I therefore optimized the antibodies in multiplex Western blots with mouse brain homogenate. One hundred twenty-two (122) antibodies recognized their cognate proteins in 1.2 mg of mouse brain homogenate (200 μg loaded per linear cm) (**Table 3.1**). I selected the dilution of each antibody that resulted in maximum signal intensity, minimum background, and no antibody saturation, defined as no signal increase at higher antibody concentrations (**Figure 3.2**). Antibodies specific for calcium/calmodulin-dependent kinase 4

(CaMK4), mitogen-activated protein kinase/extracellular signal-regulated kinase 5 (MEK5), and c-Jun N-terminal kinase 2 (JNK2) detected two isoforms each. Fifteen (15) antibodies specific for proteins not recognized in mouse brain homogenate were optimized in Western blots using lysate from cultured 3T3 mouse fibroblasts (200 μg loaded per linear cm) (**Table 3.1**). The remaining 19 antibodies did not detect their cognate protein in mouse brain homogenate or 3T3 cell lysates and were omitted from further analyses.

The multiplex Western blots were tested for reproducibility. Mouse brain homogenate resolved throughout a single-well gel (1.2 mg; 200 μg per linear cm) was transferred to a single membrane and 16 lanes were isolated in the membrane with a multiscreen apparatus (**Figure 3.3**). Extracellular signal-regulated kinase 1 (Erk1) and Erk2 were probed in each of the 16 lanes. The standard deviation between all 16 lanes was only 2.2% or 1.0% of the average for Erk1 or Erk2, respectively, and the range was 8% of the average for Erk1 or 4% of Erk2.

To minimize the amount of sample required and limit blot-to-blot variability, multiple proteins were probed for in each multiscreen lane isolated on a single membrane. The 137 proteins optimized for detection by multiplex Western blot were combined into 32 groups, such that each group contained proteins of molecular weights clearly resolved in SDS-PAGE, detected by antibodies of different species, and recognized by antibodies giving weak or strong signals (Sets 1 or 2, respectively) (**Table 3.2**). The membranes were probed first for the 16 groups containing the proteins that resulted in the lowest signal intensities (**Figure 3.4**), stripped (only once) and reprobed for the remaining 16 groups with the second set of antibodies. All 122 protein kinases or regulatory subunits previously detected in standard Western blots of mouse brain homogenate were detected in the multiplex blots. The following protein kinases were detected in Set 1. **Lane 1:**

DAPK1 (not visible in this exposure, 145 kDa), non-specific (green, 95 kDa), Syk (not visible in this exposure, 74 kDa), CaMK4β (not visible in this exposure, 66 kDa), CaMK4 (red, 63 kDa), CK1γ1 (green, 45 kDa), non-specific (green, 42 kDa), cyclin D3 (red, 33 kDa), non-specific (green, 32, 25 kDa). **Lane 2:** HER2 (not visible in this exposure, 160 kDa), RSK1 (green, 85 kDa), AMPKα1 (not visible in this exposure, 64 kDa), CK1γ2 (not visible in this exposure, 55 kDa), non-specific (green, 45 kDa; red, 43, 40, 35 kDa; green, 25 kDa). **Lane 3:** ROCK1 (not visible in this exposure, 162 kDa), GRK2 (green, 80 kDa), p70S6K (red, 75 kDa), PCTAIRE3 (green, 48 kDa), non-specific (green, 40 kDa), cyclin H (not visible in this exposure, 37 kDa), non-specific (green, 27 kDa). **Lane 4:** JAK1 (red, 125 kDa), MARK4 (not visible in this exposure, 80 kDa), PLK1 (red, 66 kDa), non-specific (green, 65 kDa; red, 52 kDa), MAPKAPK2 (not visible in this exposure, 48 kDa), non-specific (red, 48, 45, 42, 40 kDa), p25/p35 (green, 35 kDa). **Lane 5:** HER3 (red, 185 kDa), Raf1 (red, 71 kDa), Fms/CSF1R (not visible in this exposure, 50 kDa), cyclin D1 (red, 36 kDa). **Lane 6:** CRIK (not visible in this exposure, 220 kDa), MSK1 (not visible in this exposure, 90 kDa), non-specific band (green, 65, 45, 38 kDa). **Lane 7:** Non-specific (green, 170 kDa), MLK3 (not visible in this exposure, 90 kDa), PDK1 (green, 60 kDa), CK1α (not visible in this exposure, 42 kDa), CK2α1 (not visible in this exposure, 40 kDa). **Lane 8:** Non-specific (green, 80 kDa), GRK5 (green, 65 kDa), non-specific (green, 52 kDa), p38α (not visible in this exposure, 42 kDa), non-specific (green, 40 kDa). **Lane 9:** Non-specific (red, 250 kDa), PKD2 (not visible in this exposure, 98 kDa), PKCβ (red, 82 kDa), non-specific (red, 60 kDa), DLK (green, 51 kDa), CDK7 (not visible in this exposure, 41 kDa). **Lane 10:** TrkB (red, 130 kDa), Erk5 (green, 110 kDa), MST1 (not visible in this exposure, 60 kDa), CK1ε (red, 44 kDa), non-specific (green, 34 kDa). **Lane 11:** PKD1 (green, 112 kDa), IKKβ (not

visible in this exposure, 88 kDa), Akt3 (green, 60 kDa), MKK7 (not visible in this exposure, 46 kDa), p38β (green, 42 kDa). **Lane 12:** EphA1 (not visible in this exposure, 180 kDa), InsR (not visible in this exposure, 130 and 88 kDa), non-specific (green, 80 kDa), RIPK2 (not visible in this exposure, 60 kDa), non-specific (green, 45, 35 kDa). **Lane 13:** ATM (not visible in this exposure, ~300 kDa), PRK2 (not visible in this exposure, 130 kDa), B-Raf (red, 90 kDa), non-specific (red, 65 kDa), Myt1 (green, 63 kDa), non-specific (red, 42, 35 kDa). **Lane 14:** c-Abl (not visible in this exposure, 130 kDa), PAK3 (green, 65 kDa), CaMK1α (green, 42 kDa). **Lane 15:** PKD3 (not visible in this exposure, 95 kDa), cyclin A (not visible in this exposure, 60 kDa). **Lane 16:** Non-specific (red, 120 kDa), Akt2 (green, 60 kDa), Lck (not visible in this exposure, 56 kDa). The following protein kinases were detected in Set 2. **Lane 1:** ROCK2 (red, 183 kDa), Akt1 (red, 60 kDa), SGK3 (green, 50 kDa), non-specific (green, 45 kDa), Erk2 (red, 42 kDa), non-specific (green, 36 kDa). **Lane 2:** TNIK (red, 180 kDa), PKCε (red, 90 kDa), MEK2 (red, 45 kDa). **Lane 3:** EphA7 (not visible in this exposure, 86 kDa), PKCδ (not visible in this exposure, 78 kDa), GSK3α (not visible in this exposure, 50 kDa). **Lane 4:** Non-specific (green, 140 kDa), DYRK1A (green, 90 kDa), IKKα (not visible in this exposure, 80 kDa), non-specific (green, 80 kDa), PKR (not visible in this exposure, 66 kDa), non-specific (green, 63 kDa), PKACβ (green, 53 kDa), non-specific (green, 42 kDa). **Lane 5:** TrkC (not visible in this exposure, 145 kDa), CaMK2γ (not visible in this exposure, 60 kDa), cyclin E1 (not visible in this exposure, 55 kDa), PKACα (red, 42 kDa). **Lane 6:** DDR1 (green, 109 kDa), PKCζ (red, 86 kDa), non-specific (green, 80 kDa), JNK2α2/β2 (red - partly covered by adjacent non-specific band, 52 kDa), non-specific (green, 44 kDa), JNK2α1/β1 (red, 42 kDa), MKK6 (green, 38 kDa), cyclin G1 (not visible in this exposure, 29 kDa). **Lane 7:** TrkA (not visible in this exposure, 138 kDa), PKCι (not visible in this exposure,

75 kDa), MEK5α (red, 55 kDa), MEK5β (red, 45 kDa). **Lane 8:** PKCγ (red, 80 kDa), CaMK1δ (not visible in this exposure, 44 kDa), non-specific (red, 45, 43 kDa). **Lane 9:** EphA3 (green, 140 kDa), non-specific (green, 120 kDa), CASK (red, 104 kDa), GSK3β (red, 46 kDa), p38γ (green, 43 kDa), CDK5 (red, 30 kDa). **Lane 10:** ASK1 (not visible in this exposure, 155 kDa), p39 (not visible in this exposure, 40 kDa). **Lane 11:** MEKK1 (not visible in this exposure, 205 kDa), PINK1 (not visible in this exposure, 66 kDa), Fyn (not visible in this exposure, 59 kDa), p38δ (not visible in this exposure, 43 kDa). **Lane 12:** EphA4 (red, 120 kDa), PAK1 (green, 68 kDa), Lkb1 (not visible in this exposure, 55 kDa), PKACγ (green, 40 kDa). **Lane 13:** HER4 (not visible in this exposure, 182 kDa), JAK2 (not visible in this exposure, 122 kDa), PKG1 (not visible in this exposure, 76 kDa), Src (not visible in this exposure, 60 kDa), Nek6 (green, 45 kDa). **Lane 14:** SLK (red, 220 kDa), HGK (green, 140 kDa), PKCα (red, 82 kDa), LIMK1 (green, 70 kDa), Erk1 (green, 44 kDa), non-specific (green, 40, 38 kDa). **Lane 15:** PRK1 (red, 120 kDa), CaMK2β (green, 66 kDa), MEK1 (red, 45 kDa), CDKL1 (not visible in this exposure, 42 kDa). **Lane 16:** Pyk2 (red, 115 kDa), CaMKK2 (not visible in this exposure, 66 kDa), JNK1 (green, 50 kDa), non-specific (green, 45 kDa).

Importantly, the multiplex Western blots allowed for the identification and resolution of (*i*) kinases yielding high or low intensity signals (for example, Set 1; Akt3 in lane 11 [green band at 60 kDa] versus Akt2 in lane 16 [green band at 60 kDa]), (*ii*) kinases of similar molecular weight in the same lanes (for example, Set 1, lane 3; GRK2 [green band at 80 kDa] and p70S6K [red band at 75 kDa]), and (*iii*) as many as 5 protein kinases in a single lane (for example, Set 2, lane 9; EphA3 [green band at 140 kDa], CASK [red band at 104 kDa], GSK3β [red band at 46 kDa], p38γ [green band at 43 kDa], CDK5 [red band at 30 kDa]; Set 2, lane 14; SLK [red band at 220

kDa], HGK [green band at 140 kDa], PKCα [red band at 82 kDa], LIMK1 [green band at 70 kDa], Erk1 [green band at 44 kDa]) (**Figure 3.4**).

In summary, multiplex Western blots were developed to quantitate 137 protein kinases or regulatory subunits involved in neurological diseases or pathologies using only 1.2 mg of sample on a single membrane stripped only once.

3.2.2 Multiplex Western blots are sensitive and linear, detecting incremental 6 (or 3)% changes in protein levels

I next tested the variability and linearity of the multiplex Western blots to changes in protein levels. Fifteen (15) of the 137 protein kinases or regulatory subunits were not detected in mouse brain homogenate but were detected in cell lysate from 3T3 mouse fibroblasts (**Table 3.1**). Mouse brain homogenate was thus spiked with incremental 6% (average of the range of the reproducibility of quantitations, as evaluated for Erk1 and Erk2) increases of 3T3 cell lysate, from 0 to 24%. Six of the proteins detected only in 3T3 cell lysates (CDK1, CDK4, PDGFRβ, ribosomal protein S6 kinase 2 [RSK2], checkpoint kinase 1 [CHK1], Bruton's tyrosine kinase [BTK]) were quantitated. Their levels increased linearly ($r^2 \geq 0.94$, $P < 0.001$) along the increases in 3T3 cell lysate, from 0 to 24% (**Figure 3.5A**). The levels of protein kinase C theta (PKCθ) increased linearly ($r^2 = 0.96$, $P < 0.0001$) even with incremental 3% increases of the 3T3 cell lysate, from 0 to 12%. To test the sensitivity to decreases in protein levels, I next analyzed the levels of four protein detected in mouse brain but not expressed in 3T3 cells (PKCγ, CaMK4, p39, and tropomyosin-related kinase B [TrkB]) (Cuadrado et al., 1990; Klein et al., 1991; Soppet et al., 1991; Alevizopoulos et al., 1997; Valin et al., 2009). Their levels decreased linearly ($r^2 \geq 0.87$, $P <$

0.01) along the incremental 6% (PKCγ, CaMK4) or 3% (TrkB, p39) decreases of mouse brain homogenate, from 100 to 76% (**Figure 3.5B**). The multiplex Western blots are therefore reproducible, sensitive and linear, detecting incremental 6% increases or decreases in protein levels.

3.2.3 Primary kinomic screens of N2a cells expressing cytoplasmic PrP mutants identified the mTOR signaling pathway as potentially dysregulated

To identify potentially dysregulated signaling pathways, protein kinases with similar changes in relative expression levels were blindly clustered by agglomerative unsupervised hierarchical clustering (**Figure 3.6**) (Deighton et al., 2009). Any clusters containing protein kinases involved in any given signaling pathways were next identified by literature and signal transduction database searches. The different treatments used in the clustering must affect the same signaling pathways differently, or affect different signaling pathways altogether, for this approach to detect relevant clusters.

The neurotoxicity of CyPrP expression requires residues 116–156 (Rambold et al., 2006). N2a neuroblastoma cells were transfected with human CyPrP or two mutants truncated within this region, CyPrP124stop and CyPrP124-230. The expression of CyPrP124stop is not toxic to N2a cells (Grenier et al., 2006), and cells expressing CyPrP124-230 also appear healthy, although the potential toxicity has not been quantitatively assessed. I expected cells expressing CyPrP to affect different subsets of signaling pathways than, or to differentially affect the same signaling pathways as, those expressing CyPrP124stop or CyPrP124-230. Such differentially affected signaling pathways might be involved in CyPrP-mediated neurotoxicity.

The cytoplasmic PrP mutants were tagged with enhanced green fluorescent protein (EGFP) to evaluate transfection efficiencies (**Figure 3.7**), as described previously (Grenier et al., 2006). The EGFP tag was inserted into CyPrP and CyPrP124stop between residues 38-39 and at the N-terminus of CyPrP124-230 (Gu et al., 2003). Lysates collected from N2a cells transfected for 24 h with empty vector (used as control) or vector encoding for human $CyPrP^{EGFP}$, $CyPrP^{EGFP}$124stop, or $CyPrP^{EGFP}$124-230 were subjected to primary multiplex Western blot (**Figures 3.8** and **3.9**). The densitometric data from the 76 protein kinases detected in cells expressing all mutants were normalized to the levels in the cells transfected with the empty vector (**Appendix 1**), $\log_2$ transformed and analyzed by unsupervised hierarchical clustering.

I first performed hierarchical clustering of the three PrP mutants to evaluate any potential (unexpected) similarities in changes in protein kinase expression (**Figure 3.10**). If two different cytoplasmic PrP mutants resulted in identical changes in protein kinase expression, the correlation would be 1; a correlation of 0 indicates no relationship. The city-block distance metric correlation between $CyPrP^{EGFP}$124stop and $CyPrP^{EGFP}$124-230 was 0.088, and between them and $CyPrP^{EGFP}$ was 0. The lack of the correlation indicated that, as expected, different signaling pathways were dysregulated in cells transfected with the different cytoplasmic PrP mutants.

I next performed hierarchical clustering of protein kinases by their expression levels in cells transfected with each of the three cytoplasmic PrP mutants (**Figure 3.11**). The $\log_2$ relative expression levels were grouped into categories each encompassing 18% changes in expression, three times the 6% changes that the tests detect linearly (**Figure 3.5**). I then identified the clusters that contained protein kinases involved in any given signaling pathways. I was most interested in clusters containing protein kinases that were expressed to different levels in cells expressing

CyPrP^{EGFP} than in cells expressing CyPrP^{EGFP}124stop or CyPrP^{EGFP}124-230. I excluded clusters containing protein kinases expressed to similar levels in cells expressing empty vector or CyPrP^{EGFP}. Five clusters were identified following these criteria (**Figure 3.11**, grey boxes). The mTOR signaling pathway includes the mTOR complex 2 (mTORC2), which activates Akt, PKCα, and serum/glucocorticoid-regulated kinase 1 (SGK1), and the mTOR complex 1 (mTORC1), which activates p70S6K and eukaryotic initiation factor 4E-binding protein (eIF4E-BP) (Foster et al., 2010). Two clusters containing protein kinases most affected in cells expressing CyPrP^{EGFP} included all the mTORC substrates included in the primary screens (PKCα, Akt, p70S6K) (**Figure 3.11**, ***i*** and ***ii***) (city-block distance metric correlation, cluster ***i***, 0.97; cluster ***ii***, 0.98 [0.99 between AMPKα1 and CK2α1]). PKCα and p70S6K clustered together because their levels were lowest in cells expressing CyPrP^{EGFP}. Adenosine monophosphate-activated protein kinase catalytic subunit alpha-1 (AMPKα1), which also regulates mTOR signaling, clustered together with Akt1 because its levels were highest in cells expressing CyPrP^{EGFP}. The mTOR signaling pathway regulates protein synthesis, which is inhibited in cells expressing CyPrP^{EGFP} (Goggin et al., 2008). The results from the primary kinomic screens therefore suggested that CyPrP-mediated neurotoxicity in N2a cells might involve dysregulated mTOR signaling.

3.2.4 The levels of proteins in the Akt1/p70S6K branch of the mTOR signaling pathway decreased synchronously with time of CyPrP^{EGFP} expression

If the changes in the levels of the proteins involved in mTOR signaling were the result of CyPrP^{EGFP} expression, then their levels would be expected to change in synchrony with time of expression. I therefore analyzed three independent samples (biological repeats) of N2a cell lysates

prepared 12, 24 and 48 h after transfection with the CyPrP^{EGFP}-expressing construct. Cells expressing EGFP were used as control.

The levels of EGFP increased from 12 to 48 h after transfection (**Figure 3.12**). In contrast, those of CyPrP^{EGFP} changed little (slightly decreased) with time. Targeted secondary analyses characterized the expression levels of 10 proteins involved in the mTOR signaling pathway (**Appendix 2**). Four of the antibodies used in these targeted multiplex Western blots had already been used in the primary screens (Akt1, p70S6K, PKCα, AMPKα1). New antibodies were selected to analyze two protein kinases (mTOR, mitogen-activated protein kinase-interacting kinase 1 [Mnk1]) and four downstream substrates (eIF4B, eukaryotic initiation factor 4E [eIF4E], ribosomal protein S6 [S6], eukaryotic elongation factor 2 [eEF2]), which were not included in the primary screens (**Table 3.3**). These antibodies were optimized as described in **Section 3.2.1**. The normalized expression levels were grouped into categories spanning 20% changes, slightly above 3 times the 6% changes that the tests detect linearly (**Figure 3.5**).

The levels of Akt1, mTOR, p70S6K, eEF2, and PKCα were higher at 12 h in all three samples (biological repeats) of cells expressing CyPrP^{EGFP} than in those of cells expressing EGFP (**Figure 3.13**). In contrast, the levels of all proteins analyzed were consistently lower than (or at the most, equal to) those in cells expressing EGFP at 24 h. Little change was observed from 24 to 48 h, with exception to PKCα, eIF4E, and eEF2, which were expressed to their highest levels in cells expressing the lowest levels of CyPrP^{EGFP} (biological repeat 1) (**Figure 3.12A**) (**Appendix 2**). I also performed a time-course analysis of the proteins in the Akt1/p70S6K branch of the mTOR signaling pathway (**Figure 3.14**). Akt1, mTOR, p70S6K, and eEF2, in the Akt1/p70S6K branch, were expressed to higher levels in cells expressing CyPrP^{EGFP} than in cells expressing EGFP at 12 h,

and then to lower levels at 24 or 48 h (except for Akt at 24 h). The levels of the other p70S6K substrates tested, S6 and eIF4B, also decreased with time. In summary, the levels of the proteins involved in Akt1/p70S6K signaling decreased synchronously after 12 h of CyPrP^{EGFP} expression.

3.2.5 Inhibition of Hsp70-regulated Akt/p70S6K/eIF4B signaling in cells expressing CyPrP^{EGFP}

To test whether Akt1/p70S6K signaling was dysregulated in cells expressing CyPrP^{EGFP}, I characterized the activation states of the 10 proteins previously tested. I optimized phosphorylation-specific antibodies for the sites directly phosphorylated by the relevant upstream protein kinases. Akt is activated by phosphorylation on serine residue 473 (S473) by mTORC2, and on threonine residue 308 (T308) by 3-phosphoinositide-dependent protein kinase 1 (PDK1) (Alessi et al., 1997; Sarbassov et al., 2005). The synthesis of Hsp70, which activates mTORC2, is inhibited in cells expressing CyPrP (Martin et al., 2008; Goggin et al., 2008). I therefore focused on Hsp70-regulated phosphorylation of Akt1. No available antibody was specific for phosphorylated S473 (P-S473) Akt1 only. I therefore used an antibody that detects S473 phosphorylation on all Akt isoforms (Akt1, Akt2, Akt2) (**Table 4.4**). Although mTOR phosphorylation is not required for mTORC1 activation, active mTORC1 typically contains S2448 phosphorylated mTOR (Copp et al., 2009). I included an antibody specific for this phosphorylation (P-S2448). I also included antibodies specific for the phosphorylation at activation-specific sites (activating phosphorylation) on AMPKα (P-T172), Mnk1 (P-T197/202), PKCα (P-S657), p70S6K (P-T389), S6 (P-S235/236; P-S240/244), eIF4B (P-S422) and eIF4E (P-S209), or the inhibition-specific site (inhibitory phosphorylation) on eEF2 (P-T56) (Ferrari et al., 1991; Redpath et al., 1993; Hawley et al., 1996; Burnett et al., 1998; Waskiewicz et al., 1999;

Raught et al., 2004; Sarbassov et al., 2004). The phosphorylation level of Akt (P-S473) at 12 h could be tested in only two of the three biological repeats due to limiting sample.

Active mTORC2 activates Akt by phosphorylation on S473, which then activates mTORC1 which, in turn, activates p70S6K by phosphorylation on T389. Active p70S6K activates eIF4B by phosphorylation on S422. The levels of activated Akt (P-S473), p70S6K (P-T389), and eIF4B (P-S422) were consistently lower in cells expressing CyPrP^{EGFP} than in cells expressing EGFP at all times (**Figure 3.15**). The levels of phosphorylated mTOR (P-S2448) in cells expressing CyPrP^{EGFP} were also lower than, or equal to, the levels in cells expressing EGFP, with exception to one sample at 48 h. I performed non-linear regression analyses (the regressions are non-linear) to test whether the changing phosphorylation levels of any proteins involved in the mTOR signaling pathway were different in cells expressing CyPrP^{EGFP} or EGFP. The levels of activated Akt (P-S473), p70S6K (P-T389), and eIF4B (P-S422) were different in cells expressing CyPrP^{EGFP} or EGFP (replicates test for lack-of-fit; Akt [P-S473], $P = 0.02$; p70S6K [P-T389], $P = 0.001$; eIF4B [P-S422], $P = 0.0002$) (**Figure 3.16**). In conclusion, Akt/p70S6K/eIF4B signaling is inhibited in cells expressing CyPrP^{EGFP}.

3.3 DISCUSSION

Here I describe the development of kinomic analyses aimed at identifying signaling pathways dysregulated during chronic pathologies. I designed and optimized multiplex Western blots to quantitate the expression of 137 protein kinases (including regulatory subunits) in a single membrane, and using only 1.2 mg of sample. These multiplex Western blots were reproducible, sensitive and linear, detecting 6% incremental changes in protein level. I tested the multiplex

Western blots in a kinomic screen of an *in vitro* model of prion pathogenesis, N2a neuroblastoma cells expressing cytoplasmic PrP mutants. The mTOR signaling pathway was identified in the primary screen. The levels of proteins involved in the Akt1/p70S6K branch of the mTOR signaling pathway changed synchronously and were phosphorylated or unphosphorylated to their inhibited states in $CyPrP^{EGFP}$-expressing cells.

Hsp70 overexpression inhibits CyPrP-mediated toxicity and the synthesis of Hsp70 is inhibited in cells expressing $CyPrP^{EGFP}$ (Rambold et al., 2006; Goggin et al., 2008; Zhang et al., 2012). The inhibition of Hsp70-regulated Akt/p70S6K/eIF4B signaling in cells expressing $CyPrP^{EGFP}$ is fully consistent with those previous data (Rambold et al., 2006; Goggin et al., 2008; Zhang et al., 2012), supporting the ability of the approach to detect kinomic changes. Inhibition of Hsp70-activated Akt/p70S6K/eIF4B signaling may also be important in CyPrP pathogenesis. Depletion of eIF4B by RNA interference promotes cell death (Shahbazian et al., 2010). Hsp70 overexpression protects against this cell death in part by promoting the expression of the anti-apoptotic protein B-cell lymphoma 2 (Bcl-2) (Kelly et al., 2002; Jiang et al., 2011). Active eIF4B is also required for the translation of Bcl-2 (and other proteins translated from mRNAs with highly structured 5' untranslated regions). CyPrP may therefore promote cell death by inhibiting Bcl-2 synthesis through the Akt/p70S6K/eIF4B pathway. Overexpression of Akt1, mTOR, and p70S6K in cells expressing $CyPrP^{EGFP}$ for 12 h may well be an ultimately fruitless early attempt to overcome neurotoxic inhibition of Akt/p70S6K/eIF4B signaling.

Active eIF4B promotes translation initiation by stimulating the helicase activity of eukaryotic initiation factor 4A (eIF4A) and promoting ribosome binding (Rozen et al., 1990; Methot et al., 1996a; Methot et al., 1996b; Rozovsky et al., 2008). Global protein synthesis is

inhibited in cells expressing CyPrP^{EGFP} (Goggin et al., 2008). Previous studies have indicated that eIF2α was inhibited in cells expressing CyPrP^{EGFP} in a protein kinase R (PKR)-dependent manner (Goggin et al., 2008). The inhibition of eIF4B also inhibits protein synthesis (Shahbazian et al., 2010), suggesting that the inhibition of Akt/p70S6K/eIF4B signaling may too contribute to the inhibition of protein synthesis in cells expressing CyPrP^{EGFP}.

In summary, the results presented are consistent with the previously reported inhibition of Hsp70 and global protein synthesis, suggesting that the inhibition of Akt/p70S6K/eIF4B signaling mediates cytoplasmic PrP pathogenesis. The kinomic analyses are therefore sensitive and specific in detection of signaling pathways dysregulated in a simple *in vitro* model of prion pathogenesis.

Table 3.1 – Accession numbers and antibody sources for the 127 protein kinases and 10 regulatory subunits optimized for analyses in primary multiplex Western blots.

Protein kinase	Accession Number	Antibody Source	Catalog Number
Akt1	P31749	Cell Signaling Technology	2967
Akt2	P31751	Cell Signaling Technology	2962
Akt3	Q9Y243	Cell Signaling Technology	4059
AMPKα1	Q13131	R&D Systems	MAB3197
ASK1	Q99683	Santa Cruz Biotechnology	sc-7931
ATM	Q13315	Abcam	ab78
B-Raf	P15056	Cell Signaling Technology	9434
BTK*	Q06187	Cell Signaling Technology	3532
c-Abl	P00519	BD Biosciences	554148
CaMK1α	Q14012	Abgent	AP7205a
CaMK1δ	Q8IU85	Abcam	ab22043
CaMK2β	Q13554	Abcam	ab34703
CaMK2γ	Q13555	Santa Cruz Biotechnology	sc-1541
CaMK4	Q16566	BD Biosciences	610275
CaMK4β	Q16566	BD Biosciences	610275
CaMKK2	Q96RR4	Santa Cruz Biotechnology	sc-9629
CASK	O14936	BD Biosciences	610782
CDK1*	P06493	BD Biosciences	610037
CDK2*	P24941	BD Biosciences	610145
CDK4*	P11802	Cell Signaling Technology	2906
CDK5	Q00535	Abcam	ab28441
CDK6*	Q00534	Cell Signaling Technology	3136
CDK7	P50613	Santa Cruz Biotechnology	sc-7344
CDKL1	Q00532	Abgent	AP7526b
CHK1*	O14757	Cell Signaling Technology	2360
CK1α	P48729	Santa Cruz Biotechnology	sc-6478
CK1ε	P49674	BD Biosciences	610446
CK1γ1	Q9HCP0	Santa Cruz Biotechnology	sc-13077
CK1γ2	P78368	Santa Cruz Biotechnology	sc-18499
CK2α1	P68400	Abcam	ab10468
CRIK	O14578	BD Biosciences	611376
DAPK1	P53355	Sigma Aldrich	D2178
DDR1	Q08345	Santa Cruz Biotechnology	sc-532
DLK	Q12852	Abcam	ab21682
DYRK1A	Q13627	Santa Cruz Biotechnology	sc-28899
EGFR*	P00533	Cell Signaling Technology	2232
EphA1	P21709	Santa Cruz Biotechnology	sc-925
EphA3	P29320	Santa Cruz Biotechnology	sc-919
EphA4	P54764	BD Biosciences	610471
EphA7	Q15375	Santa Cruz Biotechnology	sc-917
Erk1	P27361	Cell Signaling Technology	4372
Erk2	P28482	BD Biosciences	610103
Erk5	Q13164	Cell Signaling Technology	3372
FAK*	Q05397	BD Biosciences	610087
FGFR1*	P11362	Cell Signaling Technology	3472
Fms/CSF1R	P07333	Cell Signaling Technology	3152
Fyn	P06241	BD Biosciences	610164
GRK2	P25098	Cell Signaling Technology	3982
GRK5	P34947	Santa Cruz Biotechnology	sc-565
GSK3α	P49840	Cell Signaling Technology	9338
GSK3β	P49841	BD Biosciences	610201
HER2	P04626	Abcam	ab16901
HER3	P21860	EMD Millipore	05-390
HER4	Q15303	Abcam	ab38158
HGK	O95819	Santa Cruz Biotechnology	sc-25738
IKKα	O15111	EMD Millipore	05-536
IKKβ	O14920	EMD Millipore	05-535
InsR	P06213	BD Biosciences	610110

IRAK4*	Q9NWZ3	Cell Signaling Technology	4363
JAK1	P23458	BD Biosciences	610232
JAK2	O60674	Life Technologies	AHO1352
JNK1α1	P45983-2	EMD Millipore	06-748
JNK2α1/β1	P45984-2/-3	EMD Millipore	05-986
JNK2α2/β2	P45984-1/-4	EMD Millipore	05-986
Lck	P06239	EMD Millipore	05-435
LIMK1	P53667	Cell Signaling Technology	3842
Lkb1	Q15831	Abcam	ab37219
MAPKAPK2	P49137	Cell Signaling Technology	3042
MARK4	Q96L34	Cell Signaling Technology	4834
MEK1	Q02750	BD Biosciences	610121
MEK2	P36507	BD Biosciences	610235
MEK5α	Q13163-1	BD Biosciences	610956
MEK5β	Q13163-2	BD Biosciences	610956
MEKK1	Q13233	Santa Cruz Biotechnology	sc-437
MKK6	P52564	Cell Signaling Technology	9264
MKK7	O14733	BD Biosciences	611246
MLK3	Q16584	Cell Signaling Technology	2817
MSK1	O75582	Santa Cruz Biotechnology	sc-25417
MST1	Q13043	Cell Signaling Technology	3682
Myt1	O14731	Cell Signaling Technology	4282
Nek6	Q9HC98	Abgent	AP8077a
p38α	Q16539	BD Biosciences	612168
p38β	Q15759	Abcam	ab37993
p38δ	O15264	Cell Signaling Technology	9214
p38γ	P53778	EMD Millipore	07-139
p70S6K	P23443	BD Biosciences	611260
PAK1	Q13153	Cell Signaling Technology	2602
PAK3	O75914	Cell Signaling Technology	2609
PCTAIRE3	Q07002	Santa Cruz Biotechnology	sc-176
PDGFRβ*	P09619	Cell Signaling Technology	3175
PDK1	O15530	Cell Signaling Technology	3062
PINK1	Q9BXM7	Abcam	ab23707
PKACα	P17612	BD Biosciences	610980
PKACβ	P22694	Santa Cruz Biotechnology	sc-904
PKACγ	P22612	Santa Cruz Biotechnology	sc-905
PKCα	P17252	BD Biosciences	610107
PKCβ	P05771	BD Biosciences	610128
PKCδ	Q05655	BD Biosciences	610397
PKCε	Q02156	BD Biosciences	610085
PKCγ	P05129	BD Biosciences	611158
PKCι	P41743	BD Biosciences	610175
PKCθ*	Q04759	Cell Signaling Technology	2059
PKCζ	Q05513	Santa Cruz Biotechnology	sc-17781
PKD1	Q15139	Cell Signaling Technology	2052
PKD2	Q9BZL6	Abgent	AP7730b
PKD3	O94806	Abgent	AP7025a
PKG1	Q13976	Abcam	ab37709
PKR	P19525	Santa Cruz Biotechnology	sc-6282
PLK1	P53350	EMD Millipore	05-844
PRK1	Q16512	BD Biosciences	610686
PRK2	Q16513	Cell Signaling Technology	2612
Pyk2	Q14289	BD Biosciences	610548
Raf1	P04049	BD Biosciences	610151
RIPK2	O43353	Abgent	AP7818b
ROCK1	Q13464	BD Biosciences	611137
ROCK2	O75116	BD Biosciences	610623
RSK1	Q15418	Abcam	ab9365
RSK2*	P51812	Santa Cruz Biotechnology	sc-9986
SGK3	Q96BR1	Abgent	AP7949a
SLK	Q9H2G2	BD Biosciences	612466
Src	P12931	Cell Signaling Technology	2110

Syk	P43405	Cell Signaling Technology	2712
TNIK	Q9UKE5	BD Biosciences	612250
TrkA	P04629	Cell Signaling Technology	2505
TrkB	Q16620	BD Biosciences	610101
TrkC	Q16288	EMD Millipore	07-226
Yes*	P07947	BD Biosciences	610375
Regulatory subunit	**Accession Number**	**Antibody Source**	**Catalog Number**
cyclin A2	P20248	EMD Millipore	06-138
cyclin D1	P24385	Cell Signaling Technology	2926
cyclin D2*	P30279	Abcam	ab3085
cyclin D3	P30281	BD Biosciences	610279
cyclin E1	P24864	Cell Signaling Technology	4129
cyclin G1	P51959	Santa Cruz Biotechnology	sc-320
cyclin H	P51946	Santa Cruz Biotechnology	sc-1662
p25	Q15078	Cell Signaling Technology	2673
p35	Q15078	Cell Signaling Technology	2673
p39	Q13319	Santa Cruz Biotechnology	sc-28932

One hundred and twenty-two protein kinases or regulatory subunits included in our multiplex Western blots were detected in 200 μg of mouse brain homogenate per linear well cm. The other 15 (indicated by the asterisks) were detected in multiplex Western blots using an equivalent amount of cell lysate from cycling 3T3 mouse fibroblasts. The human accession number, antibody source, and catalog number for each protein is indicated.

Table 3.2 – Primary multiplex Western blots analyzed the levels of 137 protein kinases in N2a cells expressing cytoplasmic PrP mutants.

	Antibody Set 1					Antibody Set 2				
Group	Kinase	MW (kDa)	Dilution	Intensity	Type	Kinase	MW (kDa)	Dilution	Intensity	Type
1	cyclin D3	33	1:250	+++	MM	Erk2	42	1:2000	++++	MM
	CK1γ1	47	1:60	++	RP	SGK3	52	1:250	++++	RP
	CaMK4	63, 66 (β)	1:250	++	MM	Akt1	62	1:500	++++	MM
	Syk	74	1:125	+	RP	BTK	73	(1:60)	(++++)	RP
	DAPK1	145	1:2000	+	MM	ROCK2	183	1:125	++++	MM
2	CK1γ2	47	1:125	+	GP	MEK2	45	1:1000	++++	MM
	AMPKα1	64	1:125	+	MM	LIMK1	70	1:125	++++	RP
	RSK1	80	1:500	++++	RP	PKCε	90	1:2000	++++	MM
	HER2	185	1:125	+	MM	TNIK	184	1:2000	++++	MM
3	cyclin H	37	1:60	+	MM	CDK1	34	(1:500)	(++++)	MM
	PCTAIRE3	48	1:125	++	RP	GSK3α	50	1:125	+++	RP
	p70S6K	65, 88	1:250	+++	MM	PKCδ	78	1:125	+++	MM
	GRK2	80	1:60	++	RP	EphA7	86	1:125	+	RP
	ROCK1	162	1:125	+	MM	PDGFRβ	200	(1:500)	(++++)	MM
4	p25/p35	28, 38	1:125	+	RP	PKACβ	53	1:250	++++	RP
	MAPKAPK2	47	1:250	++	RP	PKR	66	1:125	+++	MM
	PLK1	66	1:125	+	MM	IKKα	82	1:500	++	MM
	MARK4	79	1:60	+	RP	DYRK1A	90	1:60	++++	RP
	JAK1	125	1:125	+	MM					
5	cyclin D1	36	1:60	++	MM	PKACα	42	1:250	++++	MM
	Fms/ CSF1R	49, 140	1:125	+	RP	cyclin E1	50	1:500	+++	MM
	Raf1	71	1:1000	++	MM	CaMK2γ	60	1:250	+++	GP
	PKCθ	80	1:125	+	RP	TrkC	145	1:125	+	GP
	HER3	185	1:60	+	MM					
6	CDK6	36	(1:500)	(+)	MM	cyclin G1	29	1:500	+	RP
	MSK1	92	1:125	++++	RP	MKK6	41	1:60	++++	RP
	CRIK	245	1:1000	+	MM	JNK2	42 (α1/β1), 52 (α2/β2)	1:125	+++	MM
						PKCζ	84	1:125	++++	MM
						DDR1	116	1:60	+++	RP
7	CK1α	38	1:125	+	GP	MEK5	45 (β), 56 (α)	1:125	++++	MM
	CK2α1	42	1:1000	++++	MM	PKCι	75	1:125	++++	MM
	PDK1	63	1:250	++	RP	TrkA	145	1:60	++++	RP
	RSK2	80	(1:500)	(++++)	MM					
	MLK3	90	1:60	+						
8	p38α	42	1:1000	+	MM	CaMK1δ	44	1:500	+	RP
	IRAK4	55	(1:60)	(++)	RP	CHK1	52	(1:500)	(++++)	MM
	GRK5	65	1:125	++++	RP	PKCγ	80	1:500	++++	MM
	IKKβ	87	1:125	+	MM	FGFR1	145	(1:60)	(+)	RP
9	CDK7	41	1:1000	+++	MM	CDK5	30	1:1000	++++	MM
	DLK	51	1:500	++++	RP	p38γ	43	1:125	+++	RP
	PKCβ	82	1:500	++++	MM	GSK3β	46	1:250	++++	MM
	PKD2	98	1:60	+	RP	CASK	104	1:500	++++	MM
						EphA3	148	1:125	++++	RP
10	CK1ε	44	1:500	++	MM	p39	42	1:1000	+++	RP
	MST1	60	1:60	+	RP	Yes	59	(1:500)	(+)	MM
	TrkB	85, 145	1:250	+	MM	FAK	115	(1:500)	(+++)	MM
	Erk5	110	1:125	++	RP	ASK1	155	1:250	++++	RP
11	p38β	42	1:125	+	MM	CDK4	30	(1:500)	(++++)	MM
	MKK7	47	1:500	++	RP	p38δ	43	1:125	+	RP
	Akt3	60	1:60	+	RP	Fyn	59	1:125	++	MM
	PKD1	112	1:125	++	RP	PINK1	63	1:250	+	RP
						MEKK1	205	1:125	+	RP
12	RIPK2	56	1:60	+	RP	PKACγ	40	1:1000	++++	RP
	InsR	88, 130	1:60	+	MM	Lkb1	55	1:250	+++	MM
	EphA1	180	1:250	+	RP	PAK1	66	1:125	++++	RP
						EphA4	125	1:250	++++	MM

13	Myt1	63	1:60	+	RP	Nek6	46	1:125	+	RP
	B-Raf	90	1:250	++	MM	Src	60	1:250	++	MM
	PRK2	130	1:125	+	RP	PKG1	76	1:60	+	RP
	ATM	350	1:60	+	MM	JAK2	122	1:2000	+++	MM
						HER4	182	1:250	+	RP
14	CaMK1α	42	1:60	++	RP	Erk1	44	1:250	++++	RP
	PAK3	65	1:125	++	RP	SLK	60, 124, 229	1:500	+++	MM
	c-Abl	135	1:500	+	MM	PKCα	82	1:500	++++	MM
						HGK	148	1:125	+++	RP
15	cyclin D2	36	(1:500)	(++)	MM	CDKL1	42	1:125	+	RP
	cyclin A2	60	1:250	+	MM	MEK1	45	1:500	++++	MM
	PKD3	95	1:60	+	RP	CaMK2β	66	1:60	++	RP
						PRK1	123	1:1000	+++	MM
16	CDK2	37	(1:500)	(+)	MM	JNK1	49	1:250	++++	RP
	Lck	56	1:1000	++++	RP	CaMKK2	68	1:125	+++	GP
	Akt2	62	1:60	++	RP	Pyk2	120	1:1000	++++	MM
	EGFR	175	(1:60)	(+)	RP					

Primary antibodies specific for 67 protein kinases (antibody set 1) were combined into 16 groups at optimized concentrations (dilutions) and loaded into the corresponding multiscreen lane. Blots were then stripped and reprobed with another 16 groups of antibodies specific for the remaining 70 protein kinases (antibody set 2). Parentheses indicate kinases detected in 3T3 lysate and not mouse brain homogenate. MW, molecular weight. Signal intensity; ++++, most intense; +, least intense. Antibody type; MM, mouse monoclonal; RP, rabbit polyclonal; GP, goat polyclonal.

Protein kinase	Accession Number	Antibody Source	Catalog Number
mTOR	P42345	Cell Signaling Technology	2983
Mnk1	Q9BUB5	Cell Signaling Technology	2195
eIF4B	P23588	Cell Signaling Technology	3592
eIF4E	P06730	Cell Signaling Technology	2067
eEF2	P13639	Cell Signaling Technology	2332
S6	P62753	Cell Signaling Technology	2317

Table 3.3 – Sources for the 6 new antibodies optimized for secondary multiplex Western blot analyses. The human accession number, antibody source, and catalog number for each protein is indicated.

Protein kinase	Antibody Source	Catalog Number
p-Akt (S473)	Cell Signaling Technology	4060
p-mTOR (S2448)	Cell Signaling Technology	2971
p-AMPKα (T172)	Cell Signaling Technology	2531
p-Mnk1 (T197/202)	Cell Signaling Technology	2111
p-PKCα (S657)	EMD Millipore	06-822
p-p70S6K (T389)	R&D Systems	AF8963
p-S6 (S235/236)	Cell Signaling Technology	4858
p-S6 (S240/244)	Cell Signaling Technology	4838
p-eIF4B (S422)	Cell Signaling Technology	3591
p-eIF4E (S209)	Cell Signaling Technology	9741
p-eEF2 (T56)	Cell Signaling Technology	2331

Table 3.4 – Sources for the 11 new antibodies optimized for tertiary multiplex Western blot analyses. The antibody source and catalog number for each protein is indicated.

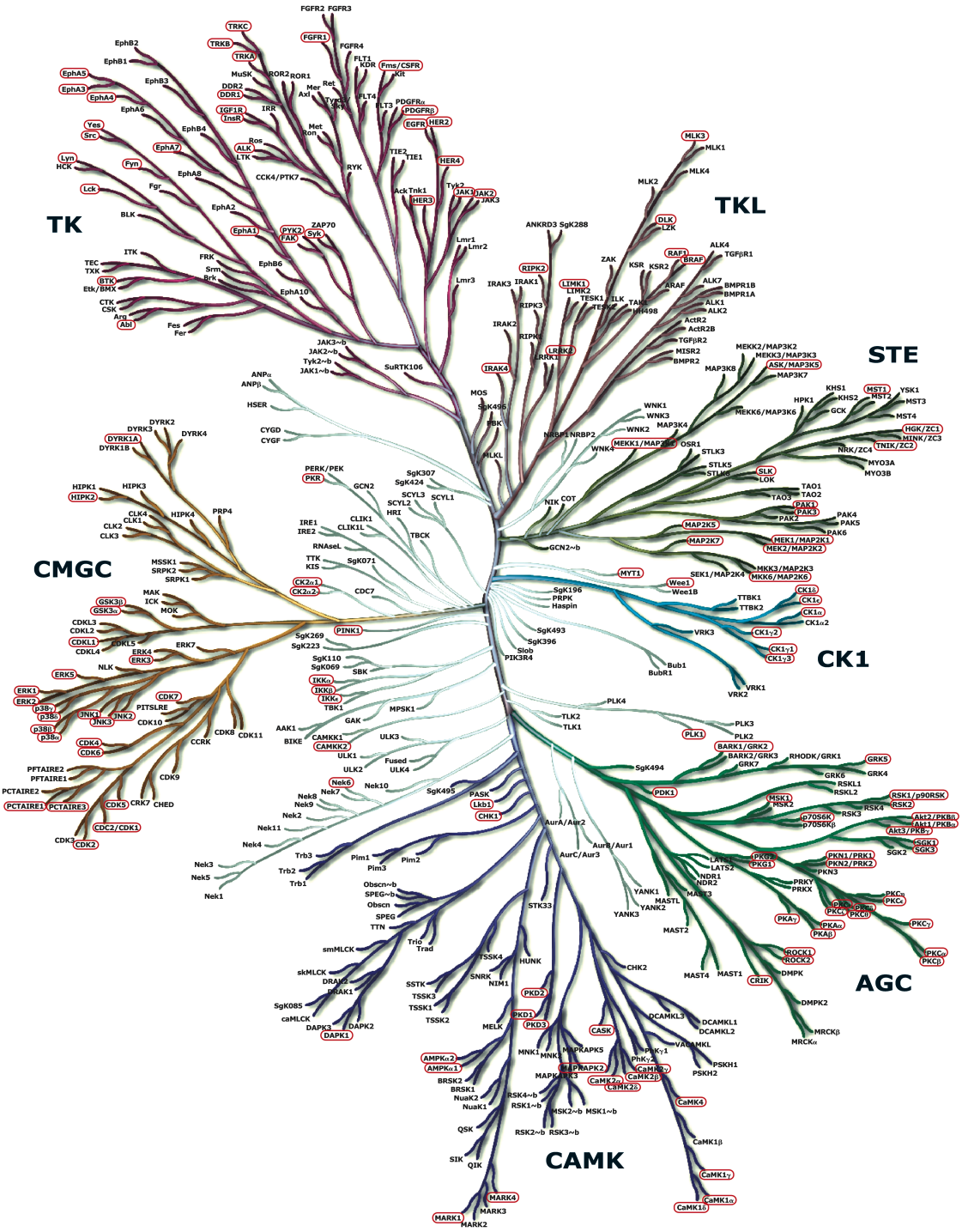

Figure 3.1 – The protein kinases selected for primary multiplex Western blots represent all major groups of the human protein kinases. The human kinome, the protein kinase complement of the human genome, clustered by protein kinase domain homology. The 145 protein kinases initially selected for analyses are outlined in red. ATM, which is a member of the atypical group of protein kinases, does not cluster with any group, and is therefore not presented. Figure modified from Manning et al., 2002.

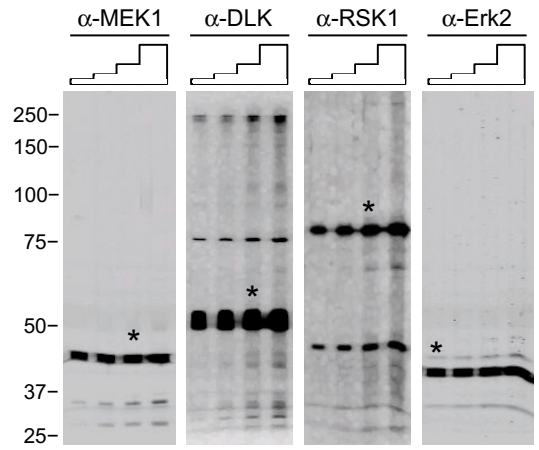

Figure 3.2 – Optimization of primary antibodies. Western blots optimizing α-MEK1, α-DLK, α-RSK1, and α-Erk2 primary antibodies. Resolved proteins from a single-well 8% SDS-PAGE gel loaded with 200 μg of mouse brain homogenate per linear cm were transferred and probed with 2-fold increasing concentrations (1:2000, 1:1000, 1:500, 1:250 dilutions) of primary antibody in separate lanes using a multi-screen apparatus. The asterisks indicate antibody saturation (1:500, α-MEK1, α-DLK, α-RSK1; 1:2000, α-Erk2). Molecular weights in kDa are indicated on the left.

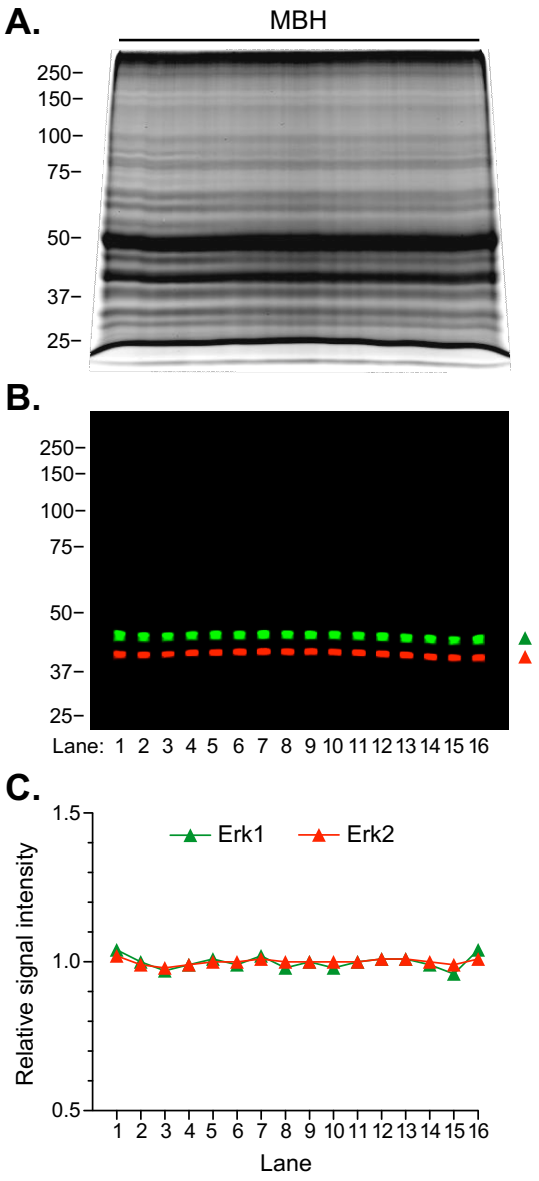

Figure 3.3 – Single-well 8% SDS-PAGE gels allow for homogeneous protein resolution and equivalent protein quantitation across all lanes. A) A Coomassie-stained single-well 8% SDS-PAGE gel loaded with 200 µg of mouse brain homogenate (MBH) per linear cm (1.2 mg total). Proteins are homogeneously resolved across the width of the gel. Molecular weights in kDa are indicated on the left. **B**) Protein from a duplicate gel was transferred and the membrane probed for Erk1 and Erk2 in 16 individual lanes isolated within the area of homogeneously resolved protein using a multi-screen apparatus. (**C**) Log_2 transformed levels of Erk1 and Erk2 in each lane relative to average. The mean ± SD and *P* values (two-tailed *t*-test compared to the expected value of 1) were: Erk1 = 1.0 ± 0.022, $P = 0.91$; Erk2 =1.0 ± 0.010, $P = 0.81$.

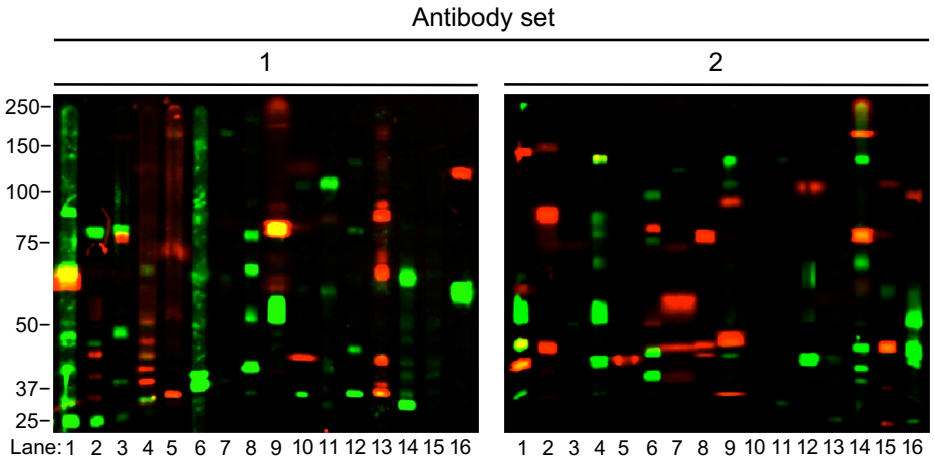

Figure 3.4 – Multiplex Western blots detect 122 selected protein kinases using only 1.2 mg of mouse brain. A single-well gel was loaded with 1.2 mg of mouse brain homogenate, and the proteins were resolved and transferred. A multi-screen apparatus isolated 16 individual lanes within the area of homogeneously resolved protein and probed with optimized antibodies specific for 122 selected protein kinases. Molecular weights in kDa are indicated on the left. Signal from secondary antibody labeled with Alexa Fluor 680 (red bands) and IRDye 800 (green bands) was detected using a LI-COR Odyssey infrared imaging system. Yellow bands, red-labeled goat anti-mouse secondary antibody detected by green-labeled anti-goat secondary antibody. Due to the wide range in expression levels, no single exposure of the blot can show all the bands. The bands that are visible in each lane at the exposure shown are listed (from top to bottom) in **Section 3.2.1**.

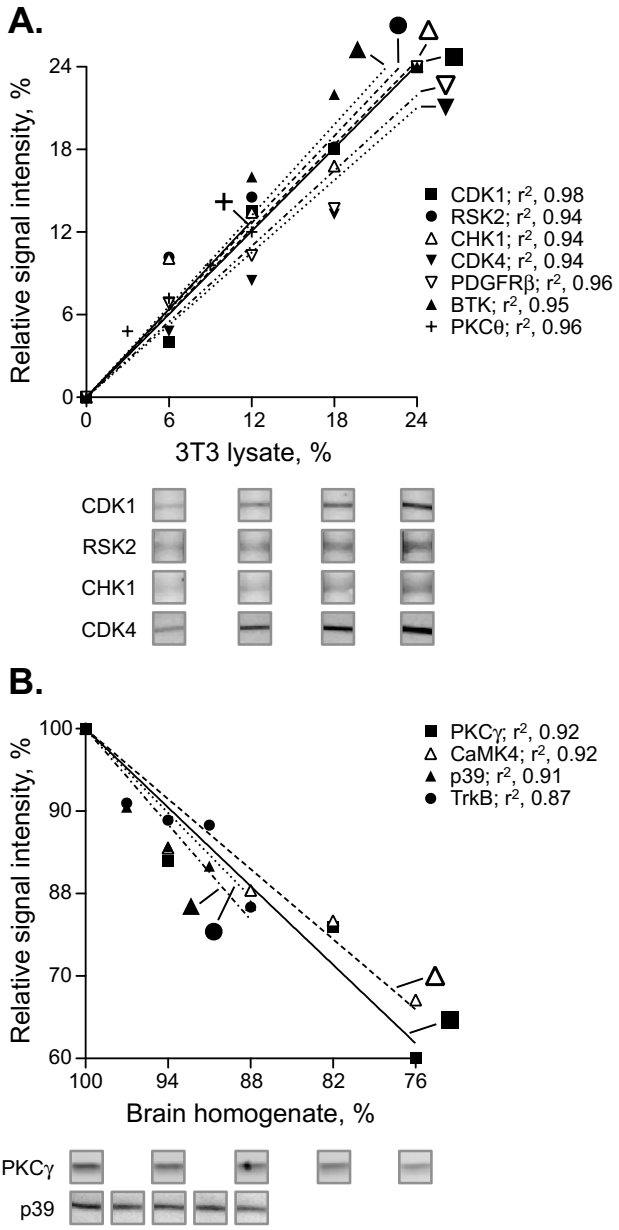

Figure 3.5 – Multiplex Western blots are sensitive and linear, detecting incremental 6 (or 3)% changes in protein levels. Line graphs presenting the relative signal intensity of the indicated protein kinases expressed in 3T3 cells but not in brain (**A**), plotted against the percentage of 3T3 lysate, or the protein kinases expressed in brain but not in 3T3 cells (**B**), plotted against the percentage of mouse brain homogenate. Mouse brain homogenate was spiked with incremental 3, 6, 9, or 12%, or 6, 12, 18, or 24% 3T3 cell lysate. The resolved proteins were transferred and probed by multiplex Western blot. The Western blots for CDK1, RSK2, CHK1, CDK4 (**A**), PKCγ (**B**) at 6% incremental changes, and p39 (**B**) at 3% incremental changes, are shown at the bottom of each graph as examples. The regression coefficient (r^2) for each protein is indicated. Due to a signal artifact, PKCγ in 88% brain homogenate was omitted from regression analyses.

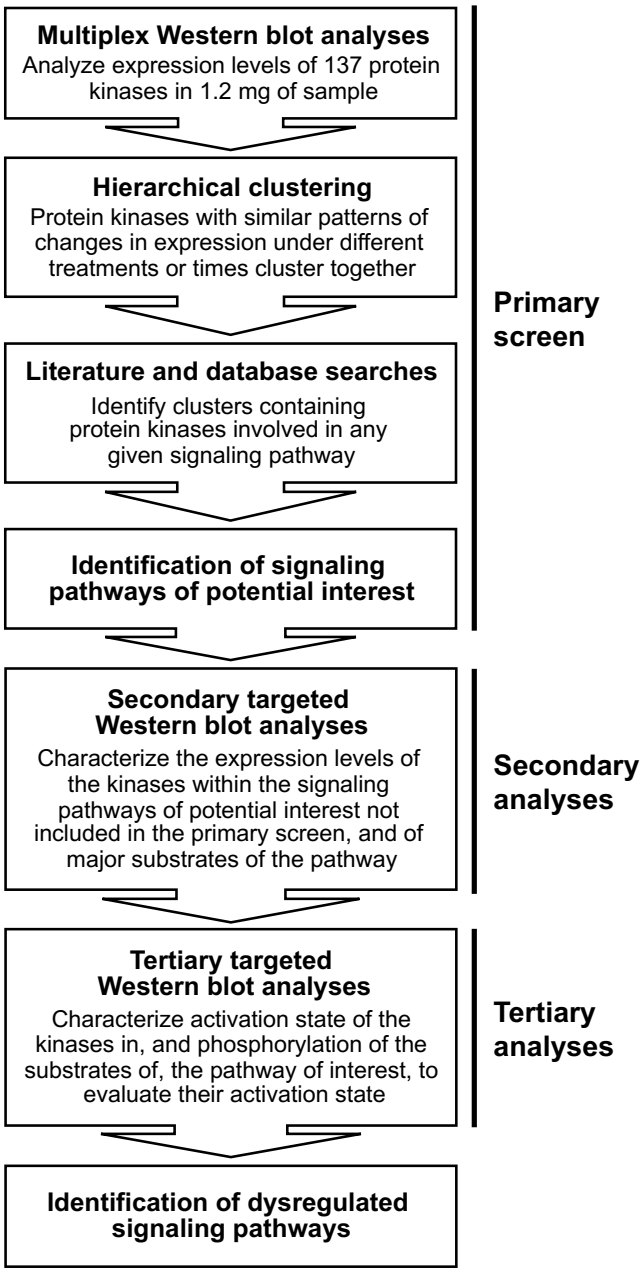

Figure 3.6 – Flow chart of the kinomic analyses. Algorithm used to identify dysregulated signaling pathways.

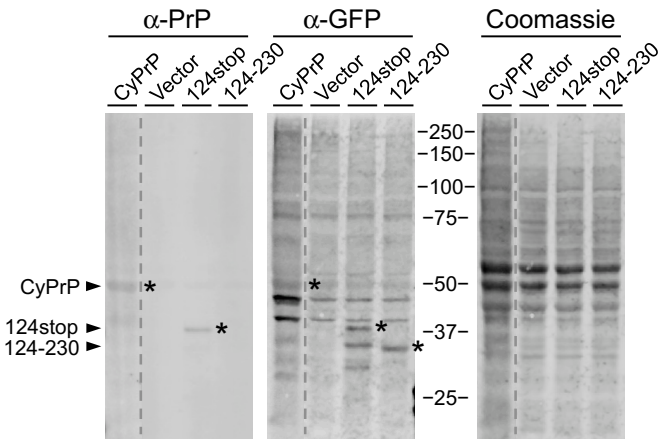

Figure 3.7 – Western blot for cytoplasmic PrP mutants in N2a cells. Proteins from N2a cell lysates transfected with empty vector, or vector encoding CyPrP^{EGFP} (CyPrP), CyPrP^{EGFP}124stop (124stop), or CyPrP^{EGFP}124-230 (124-230) were resolved, transferred to membranes and probed with α-PrP (which recognizes an epitope in residues 109-112) and α-GFP antibodies. Molecular weights in kDa are indicated to the right. The arrowheads to the left indicate the molecular weight of CyPrP^{EGFP} (48 kDa), CyPrP^{EGFP}124stop (38 kDa), and CyPrP^{EGFP} 124-230 (34 kDa). Asterisks indicate specific bands. CyPrP^{EGFP} and CyPrP^{EGFP}124stop were detected by α-PrP and α-GFP antibodies. CyPrP^{EGFP}124-230, which does not have the epitope recognized by the α-PrP antibody, was recognized only by the α-GFP antibody. A background band with a molecular weight close to that of CyPrP^{EGFP} cross-reacted with the α-GFP antibody. Membranes were stained with Coomassie to analyze total protein. Dashed lines separate different blots.

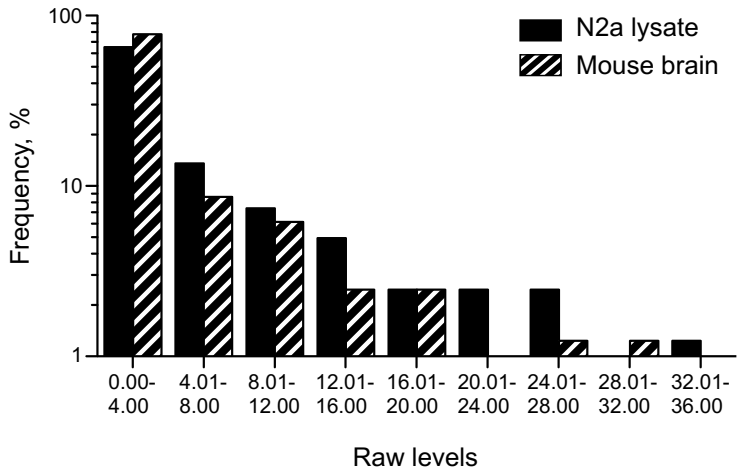

Figure 3.8 – Frequency distribution of signal intensity in N2a and mouse brain lysates. Signal for each protein kinase detected was quantitated after multiplex Western blots using 200 μg of mouse brain or 150 μg of N2a cell lysate per linear cm of gel. The number of protein kinases yielding signal intensities in each range is plotted. The frequency distribution of the signal intensity in both lysates is highly similar.

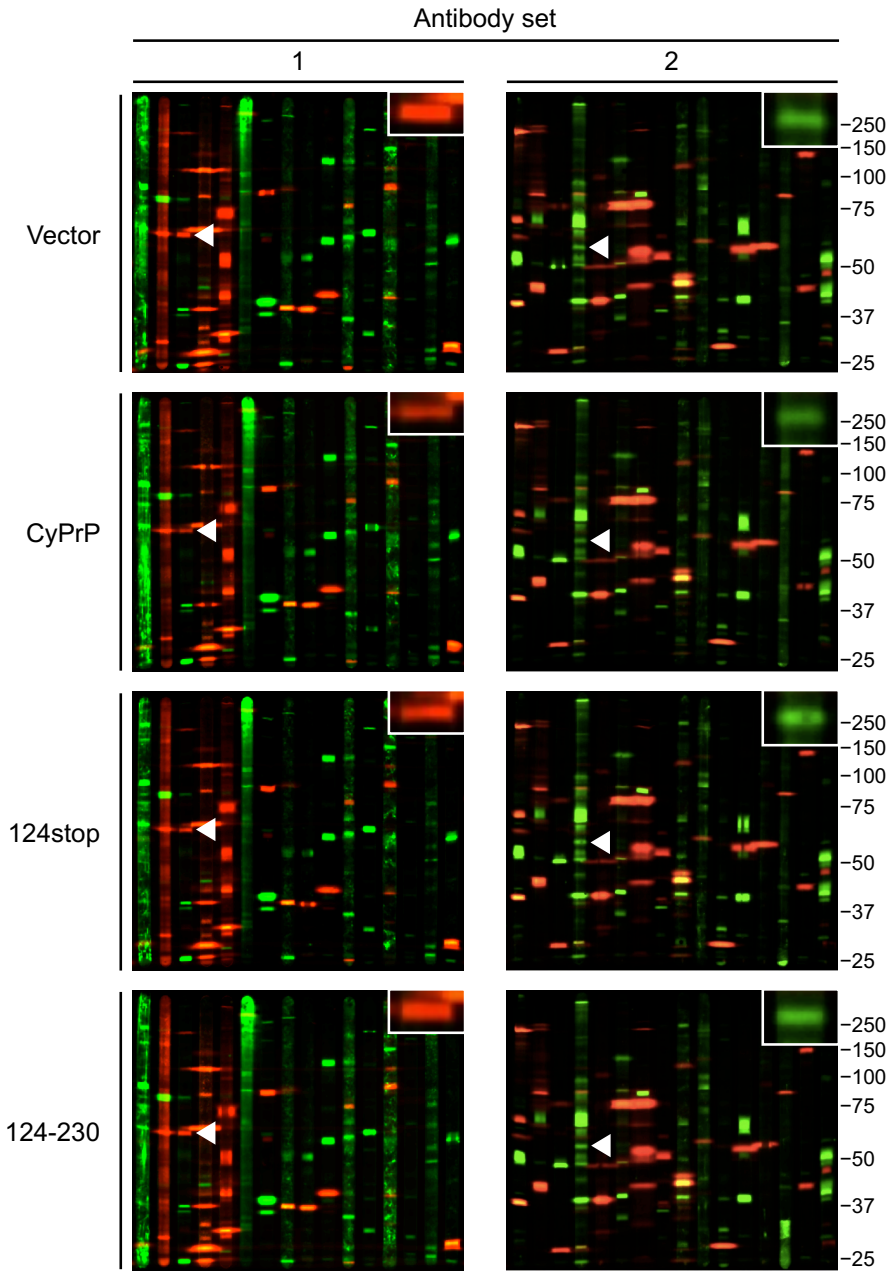

Figure 3.9 – Differential expression of protein kinases in N2a cells expressing different cytoplasmic PrP mutants. Multiplex Western blots of lysates from N2a cells transfected with empty vector (vector), or vector encoding CyPrP^{EGFP} (CyPrP), CyPrP^{EGFP}124stop (124stop), or CyPrP^{EGFP}124-230 (124–230). Molecular weights in kDa are indicated on the right. The protein kinases p70S6K (set 1) and PKACβ (set 2) are indicated by white arrowheads and enlarged, to illustrate their differential expression in cells expressing the different mutants.

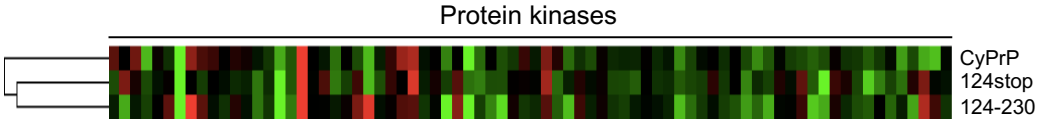

Figure 3.10 – No correlation between the expression levels of protein kinase in N2a cells expressing cytoplasmic PrP mutants. Hierarchical clustering of N2a cells expressing CyPrP^{EGFP} (CyPrP), CyPrP^{EGFP}124stop (124stop), or CyPrP^{EGFP}124-230 (124-230) using the normalized and $\log_2$ transformed densitometric data of the 76 protein kinases detected in primary multiplex Western blots. The city-block distance metric correlation between 124stop and 124-230 is 0.088, and between 124stop/124-230 and CyPrP is 0.

Figure 3.11 – Identification of the mTOR signaling pathway as potentially dysregulated in cells expressing CyPrP^{EGFP}. Hierarchical clustering of 76 protein kinases using the normalized and $\log_2$ transformed densitometric data from primary multiplex Western blots. Red, higher expression levels; green, lower expression levels. Each category encompasses changes in expression levels of 18% (0.23 in $\log_2$ scale), 3 times the 6% linear changes detected by the technique. Clusters were identified by city-block distance metric correlation with complete linkage. Grey boxes indicate clusters of protein kinases most differentially expressed in cells expressing CyPrP^{EGFP}. The clusters (***i***) and (***ii***) consist of PKCα, p70S6K, Akt1, and AMPKα1 involved in mTOR signaling. The protein kinases highlighted in **Figure 3.9**, p70S6K and PKACβ, are indicated by (●).

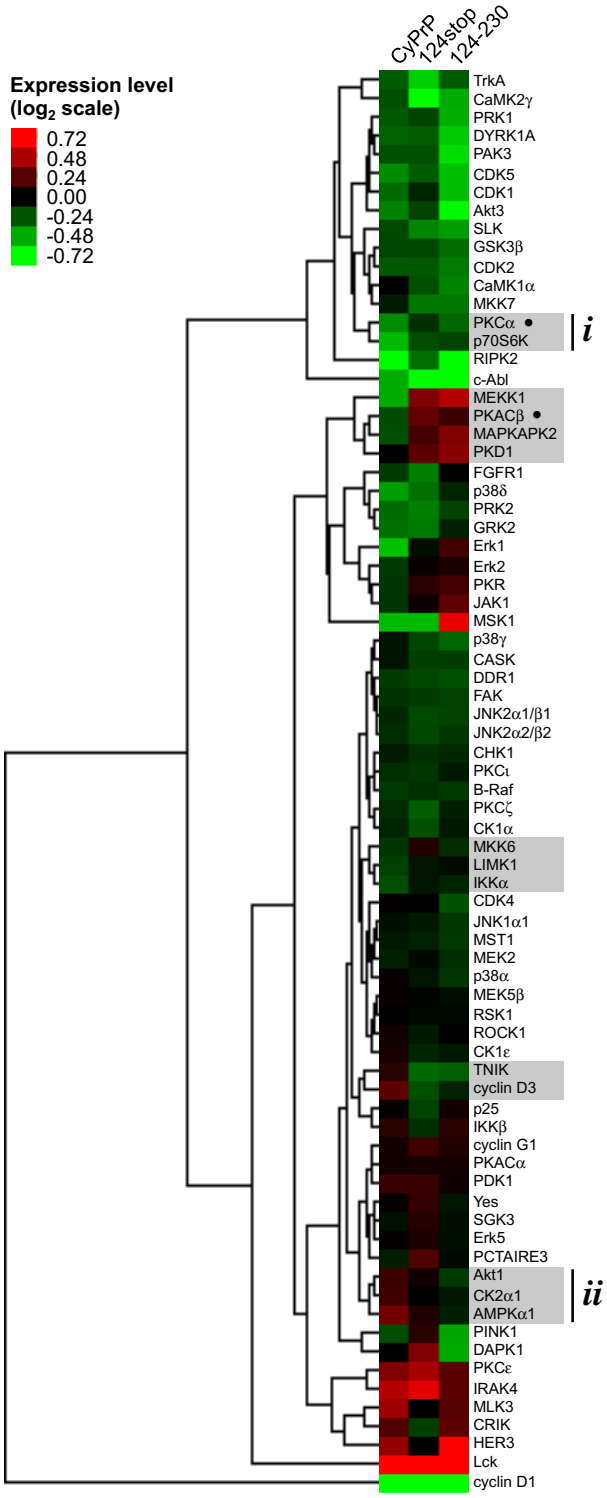
CyPrP
124stop
124-230
Expression level
(log2 scale)
0.72
0.48
0.24
0.00
-0.24
-0.48
-0.72
TrkA
CaMK2γ
PRK1
DYRK1A
PAK3
CDK5
CDK1
Akt3
SLK
GSK3β
CDK2
CaMK1α
MKK7
PKCα •
p70S6K
i
RIPK2
c-Abl
MEKK1
PKACβ •
MAPKAPK2
PKD1
FGFR1
p38δ
PRK2
GRK2
Erk1
Erk2
PKR
JAK1
MSK1
p38γ
CASK
DDR1
FAK
JNK2α1/β1
JNK2α2/β2
CHK1
PKCι
B-Raf
PKCζ
CK1α
MKK6
LIMK1
IKKα
CDK4
JNK1α1
MST1
MEK2
p38α
MEK5β
RSK1
ROCK1
CK1ε
TNIK
cyclin D3
p25
IKKβ
cyclin G1
PKACα
PDK1
Yes
SGK3
Erk5
PCTAIRE3
Akt1
CK2α1
AMPKα1
ii
PINK1
DAPK1
PKCε
IRAK4
MLK3
CRIK
HER3
Lck
cyclin D1

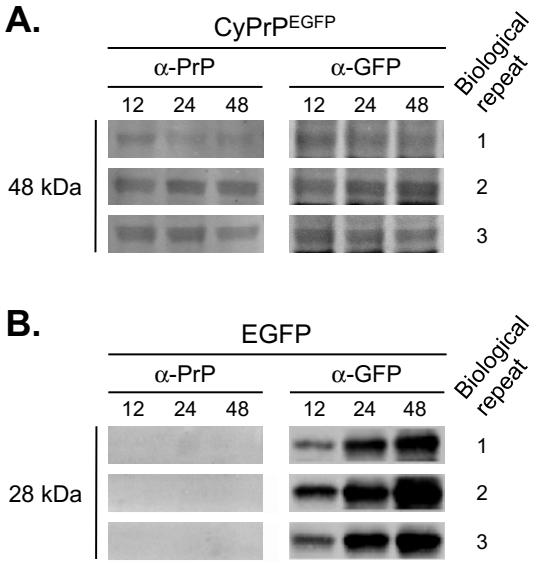

Figure 3.12 – Levels of CyPrP^{EGFP} and EGFP in the samples used for targeted secondary and tertiary analyses. Western blots of lysates from three biological repeats of N2a cells expressing CyPrP^{EGFP} (**A**) or EGFP (**B**) for 12, 24, and 48 h. CyPrP^{EGFP} (48 kDa) was detected by α-PrP and α-GFP primary antibodies, and EGFP (28 kDa) by α-GFP antibody only. Different exposures are shown for (**A**) and (**B**).

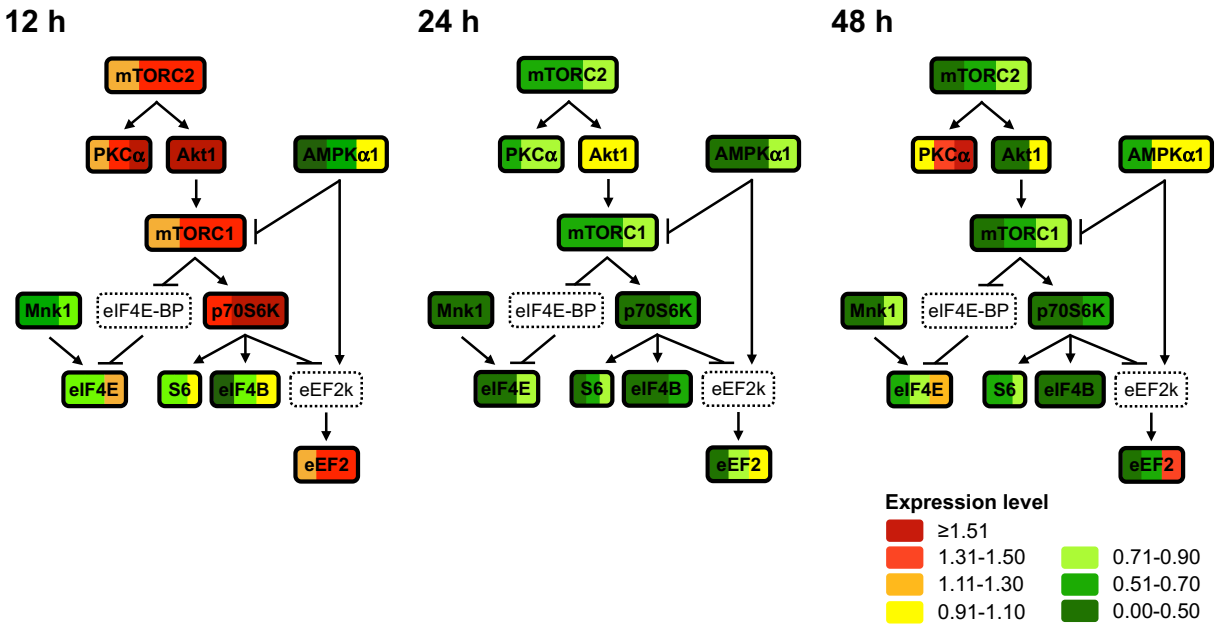

Figure 3.13 – Lower levels of mTOR signaling proteins in cells expressing CyPrP^{EGFP} for 24 and 48 h. Targeted secondary analyses of mTOR signaling in N2a cells expressing CyPrP^{EGFP} for 12, 24, or 48 h. The normalized expression levels of 10 protein kinases or substrates in each of the three biological repeats are shown by individual color bars. Each color-coded category encompasses 20% changes in the levels of expression, greater than 3 times the 6% linear changes detected by the technique. Proteins indicated by dashed lines were not analyzed. The expression levels of mTORC1 and mTORC2 represent the levels of mTOR.

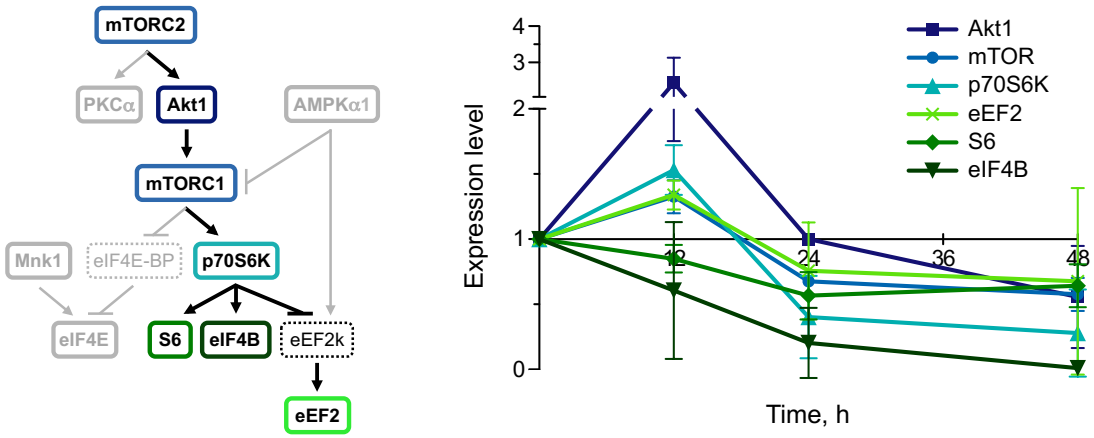

Figure 3.14 – The levels of proteins in the Akt1/p70S6K branch of the mTOR signaling pathway change coordinately. Time-course analyses of the normalized expression levels of Akt1, mTOR, p70S6K, S6, eIF4B, and eEF2 in N2a cells expressing CyPrP^{EGFP} for 12, 24, or 48 h. Mean ± SD; *n* = 3.

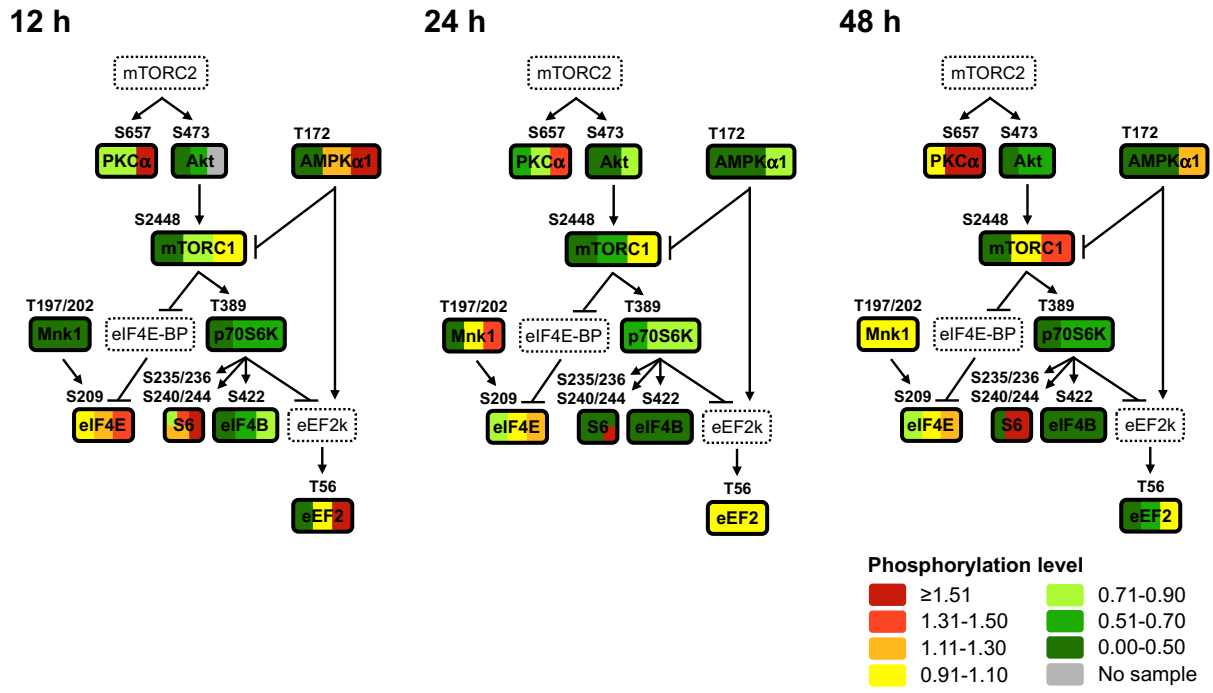

Figure 3.15 – Lower levels of activating phosphorylation of Akt, p70S6K, and eIF4B in cells expressing CyPrP^{EGFP}. Targeted tertiary analyses of mTOR signaling in N2a cells expressing CyPrP^{EGFP} for 12, 24, or 48 h. The normalized absolute phosphorylation levels of 10 protein kinases or substrates in each of the three biological repeats are shown by the color bars. The phosphorylation sites evaluated are indicated above each protein. Proteins indicated by dashed lines were not analyzed. Due to limited sample, the levels of p-Akt at 12 h were measured only in two of the three biological repeats. The color bars for S6 indicate the normalized phosphorylation levels of S235/236 (top) and S240/244 (bottom).

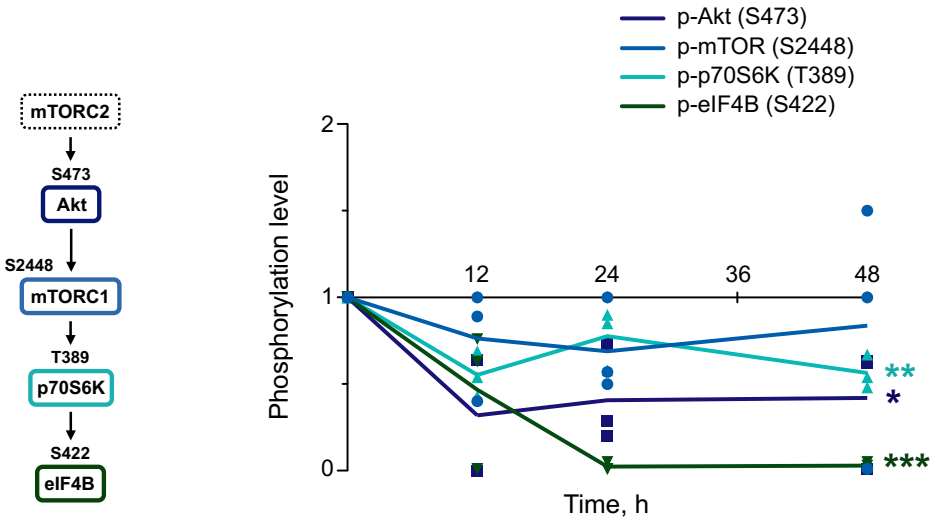

Figure 3.16 – Inhibition of the Akt/p70S6K/eIF4B signaling pathway in cells expressing CyPrP^{EGFP}. Time-course analysis of the normalized absolute levels of phosphorylated Akt (P-S473), mTOR (P-S2448), p70S6K (P-T389), and eIF4B (P-S422) in N2a cells expressing CyPrP^{EGFP} for 12, 24, or 48 h; individual data and mean (p-Akt, square; p-mTOR, circle; p-p70S6K, triangle; p-eIF4B, inverted triangle). Due to limited sample, the levels of p-Akt at 12 h were only measured in two biological repeats. The levels of all others were evaluated in three independent biological repeats. Differences in changes in phosphorylation levels in cells expressing CyPrP^{EGFP} and EGFP was analyzed by replicates test for lack-of-fit. *, $P < 0.05$; **, $P < 0.01$; ***, $P < 0.001$.

CHAPTER 4: KINOMIC ANALYSES IDENTIFY ACTIVATION OF PRO-SURVIVAL CaMK4β/CREB AND PRO-DEATH MST1 SIGNALING AT PRECLINICAL AND CLINICAL TIMES DURING A MOUSE MODEL OF PRION DISEASE

*A version of this chapter has been published. RH Shott, A Majer, KL Frost, SA Booth, LM Schang. 2014. Virology Journal **11**:160. I prepared the homogenates and performed the kinomic analyses. I critically evaluated the results wrote all drafts and final version of the manuscript under direct supervision by Luis M. Schang. Kathy L. Frost and Anna Majer performed the infections, collected and dissected the brains. Stephanie A. Booth and Anna Majer critically revised the manuscript. Luis M. Schang designed the study. All of the procedures involving live animals were approved by the Canadian Science Centre for Human and Animal Health – Animal Care Committee (CSCHAH-ACC) according to the guidelines set by the Canadian Council on Animal Care. The approval identifications for this study were animal use document (AUD) #H-08-009 and #H-11-020.*

4.1 INTRODUCTION

Prion diseases are characterized by a long incubation period followed by a comparatively short clinical phase. Most neuronal death occurs just prior to, or during, the clinical phase of disease progression. Studies of prion diseases pathogenesis have therefore largely focused on the molecular changes at this stage of disease progression. Unfortunately, however, such a targeted approach has not yet resulted in the identification of the signaling pathways most critical to prion disease pathogenesis.

PrP conversion is required for prion disease pathogenesis and is the earliest pathological event to occur during disease progression. The signaling pathways dysregulated by PrP conversion early in disease progression may also be critical to prion pathogenesis and distinct from signaling pathways dysregulated at later times. Microarray analyses have identified many genes and microRNA (miRNA) differentially expressed at preclinical and clinical time points in prion disease progression (Booth et al., 2004b; Skinner et al., 2006; Kim et al., 2008; Hwang et al., 2009; Majer et al., 2012; Boese et al., 2015). For example, only 6 of the 22 genes differentially expressed in scrapie-infected mice at pre-clinical stages of disease progression (104 days post-infection [dpi]) were also differentially expressed at clinical disease onset (146 dpi) (Skinner et al., 2006). However, such broad screen analyses of the changes in the expression levels of protein kinases during prion disease progression has yet to be performed.

Here, I applied my kinomics approach to mice infected with mouse-adapted scrapie at different stages of disease progression. I identified two dysregulated signaling pathways. The calcium/calmodulin-dependent protein kinase, beta isoform (CaMK4β)/cAMP response element-binding protein (CREB) signaling pathway, which promotes neuronal survival, was activated at earlier times but its activation state returned to that in mock-infected mice later on. Mammalian STE20-like protein kinase 1 (MST1) signaling, which promotes neuronal death, was, in contrast, activated at these later times. The dysregulation of CaMK4β/CREB and MST1 signaling pathways may therefore be critical to the neurodegeneration in scrapie-infected mice.

4.2 RESULTS

4.2.1 PrP^{res} is first detected in scrapie-infected mice at 130 dpi

Mock-infected mice or mice infected intraperitoneally with scrapie (mouse-adapted strain RML) were euthanized at 70, 90, 110, 130 dpi, or at terminal stages of disease (155–190 dpi). Brains were dissected into (*i*) cortical (cerebrum), (*ii*) subcortical (including thalamus, hypothalamus and hippocampus) and (*iii*) brainstem-cerebellum, as described (Allen Institute for Brain Science, 2015). Intraperitoneal inoculation route was used to avoid the acute induction of inflammatory signaling pathways and preclinical neuronal loss that can follow intracerebral inoculation (Betmouni et al., 1999).

I first analyzed the levels of total PrP (PrP^{C} and if present, PrP^{Sc}), protease-resistant PrP^{Sc} (PrP^{res}) and glial fibrillary acidic protein (GFAP) by Western blot. PrP^{res} was enriched by sodium phosphotungstic acid (NaPTA) precipitation prior to proteinase K (PK) treatment. In the absence of PK (total PrP), unglycosylated (~24 kDa), monoglycosylated (~27 kDa), and diglycosylated (~35 kDa) PrP were observed. PrP^{res} was only detected in scrapie-infected mice and its levels increased with time of infection (**Figure 4.1A**). As expected, RML strain PrP^{res} was predominately mono- or unglycosylated (Thackray et al., 2007). PrP^{res} was first detected in all regions at 130 dpi, and increased coordinately with the levels of GFAP from 130 dpi to terminal stages of disease (unpaired two-tail *t*-test; GFAP brainstem-cerebellum, $P = 0.0388$; subcortical, $P = 0.0008$; cortical, $P = 0.0414$) (**Figure 4.1B**), as expected (Lasmezas et al., 1996a; Yun et al., 2006). The levels of GFAP were also higher in the brainstem-cerebellum of scrapie-infected mice prior to PrP^{res} accumulation at 70 dpi ($P = 0.0041$) and showed a tendency to higher levels in the cortical region

at 90 dpi, as observed previously (Jendroska et al., 1991). The lower molecular weight form of GFAP has also been observed previously (Jang et al., 2008) and is likely the result of degradation.

4.2.2 Primary kinomic screens identified two signaling pathways of potential interest, which are involved in neuronal death and survival

After intraperitoneal infection, prion disease spreads in the brain caudal to rostral (from brainstem-cerebellum to cortical regions) (Kimberlin et al., 1982; Cole et al., 1985; Baldauf et al., 1997). The brainstem-cerebellum homogenates were therefore selected for the primary screens, for the greatest window of opportunity to identify signaling pathways dysregulated during pathogenesis. New antibody lots specific for calmodulin-dependent protein kinase 2 beta (CaMK2β), ephrin type-A receptor 1 (EphA1), receptor-interacting serine/threonine protein kinase 2 (RIPK2), and cyclin A2 failed to detect their cognate protein and were omitted from these primary screens. Ataxia telangiectasia mutated kinase (ATM; molecular weight, 350 kDa) was also omitted because the lanes of the 24-lane multiscreen could only probe for proteins whose molecular weights were between 25-250 kDa. Added to the primary screen were antibodies specific for 7 new protein kinases (adenosine monophosphate-activated protein kinase catalytic subunit alpha-2 [AMPKα2], checkpoint kinase 2 [CHK2], ephrin type-B receptor 3 [EphB3], v-yes-1 Yamaguchi sarcoma viral related oncogene homolog [Lyn], and MAP/microtubule affinity-regulating kinase 1 [MARK1], SGK1, and Wee1). These antibodies and 13 others, specific for protein kinases previously selected for analyses, were optimized and validated as described in **Section 3.2.1** (**Table 4.1**). Primary multiplex Western blots therefore analyzed the expression levels of 139 protein kinases (**Table 4.2**) in brainstem-cerebellum homogenates from 3 mock-infected and 3 scrapie-infected mice

euthanized at 70, 90, 110, 130 dpi or at terminal stages (155–190 dpi). I detected 109 protein kinases (78% of the 139 tested), most of which were differentially expressed in scrapie- as compared to mock-infected mice (**Figure 4.2**). For example, CaMK4β was expressed to higher levels in scrapie- than in mock-infected mice at 70 dpi (**Figure 4.2A**), and dual leucine zipper kinase (DLK) to lower levels at 130 dpi (**Figure 4.2D**). Ten protein kinases were not detected in one set of mock- and scrapie-infected mice at one time point (TrkB, Set 1 at 70 dpi; membrane-associated tyrosine/threonine-specific cdc2-inhibitory kinase [Myt1], Set 2 at 110 dpi; p70S6K, PKR, v-Raf murine sarcoma viral oncogene homolog B1 [B-Raf], serine/threonine-protein kinase D3 [PKD3], serine/threonine-protein kinase N2 [PRK2], STE20-like serine/ threonine-protein kinase [SLK], TRAF2 and NCK-interacting protein kinase [TNIK], and tropomyosin-related kinase C [TrkC], Set 3 at 130 dpi) (**Appendix 4**). Five other proteins (calcium/calmodulin-dependent protein kinase 1 alpha [CaMK1α], cyclin D1, cyclin G1, p25 and p35) were not resolved in one set at 70, 90, 110, and 130 dpi. Mitogen-activated protein kinase kinase kinase 5 (MAPKKK5, also known as ASK1) and mitogen-activated protein kinase kinase kinase 1 (MEKK1) were not quantitated in one set at 90 dpi, or two sets at terminal stages, due to transfer or blotting artifacts, respectively. The raw densitometric data obtained from all other protein kinases was normalized to data from the mock-infected mice, $\log_2$ transformed and analyzed by unsupervised hierarchical clustering.

I first blindly clustered the scrapie-infected mice to evaluate the changes in protein kinase expression during disease progression (**Figure 4.3**). The most distantly related cluster consisted of the two mice euthanized at 130 dpi with the highest levels of PrP^{res}, and one mouse euthanized at terminal stages of disease (130-1, 130-2, TER-1). The second most distantly related cluster

consisted of two mice euthanized at 70 dpi (70-2, 70-3). All other mice clustered in two subclusters. One of them consisted of the third mouse euthanized at 70 dpi (70-1), two mice euthanized at 90 dpi, and all three mice euthanized at 110 dpi. The other consisted of mice euthanized at 90 dpi, 130 dpi, and terminals stages of disease (90-1, 130-3, TER-2, TER-3). The mice therefore clustered largely based on time after infection, suggesting that levels of protein kinase expression in mice changed in response to scrapie pathogenesis.

I next clustered the data to identify protein kinases, the expression levels of which changed similarly in scrapie-infected mice during disease progression (**Figure 4.4A**). Protein kinases with similar changes in expression may, or may not, also be involved in the same signaling pathway (Deighton et al., 2009). To identify those that were, I performed literature and signal transduction database searches. Mitogen-activated protein kinase 12 (p38γ), ribosomal S6 kinase 1 (RSK1), Lyn, and CaMK4β, which clustered together because they were expressed to similarly higher levels in scrapie- than in mock-infected mice at 70 dpi, are all involved in an NMDAR-regulated CaMK4β signaling pathway that promotes neuronal survival (**Figure 4.4B**, ***i***). MST1, DLK, and JNK2 (p54; α2/β2 isoforms), which clustered together because they were expressed to similarly lower levels in scrapie- than in mock-infected mice at 130 dpi, are all involved in an MST1 signaling pathway that promotes neuronal death (**Figure 4.4B**, ***ii***). Although dual specificity mitogen-activated protein kinase kinase 7 (MKK7), which is also involved in this pathway, clustered distantly, its expression levels were also somewhat lower in scrapie- than in mock-infected mice at 130 dpi.

Primary screens of brainstem-cerebellum homogenates from scrapie-infected mice therefore identified two signaling pathways which may be dysregulated during pathogenesis. The NMDAR-

regulated CaMK4β signaling pathway promotes neuronal survival, and the expression levels of the protein kinases involved changed (increased) the most at earlier times. Conversely, the MST1 signaling pathway promotes neuronal death, and the expression levels of involved protein kinases were most affected (decreased) at later times.

4.2.3 CaMK4β/CREB signaling is activated at preclinical stages of scrapie in mice

The NMDAR-regulated CaMK4β signaling pathway promotes neuronal survival though the activation of CREB (Mabuchi et al., 2001). I therefore analyzed the expression levels of CREB (**Table 4.3**) (**Appendix 5**). I also analyzed the expression levels of neuronal nitric oxide synthase (nNOS) and the scaffold protein post-synaptic density protein 95 (PSD-95), which associate with, or are regulated by, RSK1, Lyn and p38γ at NMDARs (Kalia et al., 2003; Sabio et al., 2004; Song et al., 2007). CaMK4β, CREB, p38γ, RSK1, and PSD-95 levels in the brainstem-cerebellum of scrapie-infected mice were different from those in mock-infected mice (nonlinear regression analysis; CaMK4β, $P = 0.0404$; CREB, $P = 0.0372$; p38γ, $P = 0.0369$; RSK1, $P = 0.0471$; PSD-95, $P = 0.0147$). Consistent with the higher levels of RSK1, Lyn, p38γ, and CaMK4β in the brainstem-cerebellum of scrapie-infected mice at 70 dpi, the levels of nNOS and CREB were also higher at this time (two-tail paired ratio *t*-test; nNOS, $P = 0.0434$; CREB, $P = 0.0341$) (**Figure 4.5**). Conversely, the levels of PSD-95 were lower at 70 ($P = 0.0249$) and 130 dpi ($P = 0.0297$). I expanded the analyses to the subcortical and cortical regions. CREB levels were also significantly higher in the subcortical and cortical regions of scrapie-infected mice, but at 90 dpi (subcortical, $P = 0.0196$; cortical, $P = 0.0481$) (**Figure 4.5**). CaMK4β and CREB levels changed coordinately in

both the brainstem-cerebellum and subcortical regions (**Figure 4.5**). There was no coordinate change in the levels of p38γ, Lyn, RSK1, nNOS, and PSD-95 in any of the brain regions.

I next performed targeted tertiary (phosphorylation state-specific) analyses to characterize the activation state of (NMDAR-regulated) CaMK4β/CREB signaling in scrapie-infected mice. The activation of Lyn and RSK1 involves autophosphorylation on tyrosine residue 396 (Y396) or serine residue 380 (S380), respectively (Kmiecik et al., 1987; Kmiecik et al., 1988; Vik et al., 1997; Dalby et al., 1998). Activated RSK1 (P-S380) inhibits nNOS by phosphorylation on S847 (Song et al., 2007). Activated p38 (P-T180/Y182) phosphorylates PSD-95 on S290 (Sabio et al., 2004). Activated CaMK4β (P-T196; corresponding to human T200) phosphorylates CREB on S133 (Matthews et al., 1994; Ribar et al., 2000). Phosphorylated CREB promotes transcription of genes that encode proteins involved in neuronal survival (Zhang et al., 2009; Tan et al., 2012). There is no antibody specific for T180/Y182 phosphorylation on only p38γ. I therefore used an antibody that detects T180/Y182 phosphorylation on all p38 isoforms (p38α, p38β, p38γ, p38δ). In summary, I analyzed the levels of activating phosphorylation of p38 (P-T180/Y182), Lyn (P-Y396), RSK1 (P-S380), CaMK4β (P-T196), and CREB (P-S133), and the levels of inhibitory phosphorylation of nNOS (P-S847) (**Table 4.4**) (**Appendix 6**). No antibody specific for p38-phosphorylated PSD-95 (P-S290) was available.

As with their total levels, the levels of activated CaMK4β (P-T196) and CREB (P-S133) changed coordinately. Their levels were significantly higher in the brainstem-cerebellum of scrapie-infected than of mock-infected mice at 70 and 90 dpi (two-tail paired ratio *t*-test; CaMK4β, $P = 0.0256$ [70 dpi], 0.0248 [90 dpi]; CREB, $P = 0.0197$ [70 dpi], 0.0086 [90 dpi]) (**Figure 4.6**). The levels of phosphorylated CREB in the subcortical and cortical regions were also significantly

higher (subcortical, $P = 0.0412$ [90 dpi]; cortical $P = 0.0093$ [70 dpi], 0.0376 [90 dpi]), or at least there was a trend to higher levels in scrapie-infected than in mock-infected mice (subcortical, $P = 0.0936$ [70 dpi]) (**Figure 4.6**). The levels of activated CaMK4β in the subcortical and cortical regions at 70 and 90 dpi were similar in scrapie- and mock-infected mice. The levels of activated p38 (P-T180/T182) were significantly higher in scrapie-infected than in mock-infected mice at 70 and 90 dpi (brainstem-cerebellum, $P = 0.0225$ [90 dpi]; subcortical, $P = 0.0106$ [70 dpi]; cortical, $P = 0.0014$ [70 dpi]) but also at 110 and 130 dpi (brainstem-cerebellum, $P = 0.0465$ [110 dpi]; cortical, $P = 0.0116$ [130 dpi]) (**Figure 4.6**). There was no correlation between the levels of activated RSK1 (P-S380) and nNOS (P-S847) in any of the brain regions. The levels of activated Lyn (P-Y396) were mostly unchanged in scrapie-infected mice relative to mock-infected mice (**Figure 4.6**).

In summary, CaMK4β/CREB signaling was activated in scrapie-infected mice at preclinical times. The expression levels and the levels of phosphorylated CREB (P-S133) and activated CaMK4β (P-T196) were higher in scrapie- than in mock-infected mice at 70 and 90 dpi.

4.2.4 MST1 is activated at clinical stages of mouse scrapie

The MST1 signaling pathway mediates neuronal death by activating forkhead box protein O3 (FOXO3) (Lehtinen et al., 2006). I therefore analyzed the expression levels of FOXO3 in targeted secondary Western blots of brainstem-cerebellum homogenates from scrapie-infected mice at 70, 90, 110, 130 dpi or at terminal stages of disease (**Table 4.3**) (**Appendix 5**). Consistent with the lower expression levels of DLK (two-tailed paired ratio *t*-test; $P = 0.0182$), JNK2 ($P = 0.0063$), and MST1 ($P = 0.0095$), FOXO3 levels were also significantly lower ($P < 0.0001$) in the brainstem-

cerebellum of scrapie- than of mock-infected mice at 130 dpi (**Figure 4.7**). The levels of DLK, MKK7, and JNK2 were more similar in the subcortical and cortical regions of mock- and scrapie-infected mice than in their brainstem-cerebellum (**Figure 4.7**). However, MST1 and FOXO3 were still expressed to significantly lower levels in the cortical region of scrapie- than of mock-infected mice at 130 dpi (MST1, $P = 0.0384$; FOXO3, $P = 0.0090$) (**Figure 4.7**). MST1 levels also appeared to be different in the subcortical region of scrapie- or mock-infected mice (nonlinear regression analysis; MST1, $P = 0.0513$), but did not reach statistical significance at any single time point. The differential expression of MST1 and FOXO3 in the brainstem-cerebellum and cortical region, albeit to differing degrees, supports a model in which MST1/FOXO3 signaling is dysregulated during progression of scrapie.

To test this model, I performed targeted (phosphorylation state-specific) tertiary Western blots to characterize the activation state of MST1/FOXO3 signaling. MST1 is activated by autophosphorylation on T183 (Glantschnig et al., 2002). Activated MST1 (P-T183) phosphorylates FOXO3 in the cytosol on S208 (corresponding to S207 in human) (Lehtinen et al., 2006). Phosphorylated FOXO3 (P-S208) then translocates to the nucleus where it activates the transcription of genes that encode proteins involved in neuronal death. Activated MST1 is further activated by cleavage mediated by caspase-3. Cleaved MST1 further promotes cell death (Graves et al., 1998; Kakeya et al., 1998; Lee et al., 2001; Graves et al., 2001). I analyzed the levels of activating phosphorylation of MST1 (P-T183) and FOXO3 (P-S207) and activating cleavage of MST1 (**Table 4.4**) (**Appendix 6**). MST1 activation is promoted by JNK-mediated phosphorylation on S82 (Bi et al., 2010) and active JNK2 is phosphorylated on T183/Y185. As no antibody available was specific for P-T183/Y185 on only JNK2, I included an antibody that detects

T183/Y185 phosphorylation on all JNK isoforms (JNK1, JNK2, JNK3; p46 [JNK1α1, JNK1β1, JNK2α1, JNK2β1, JNK3α1] and p54 [JNK1α2, JNK1β2, JNK2α2, JNK2β2, JNK3β2]). No antibody specific for JNK-phosphorylated MST1 (P-S82) was available.

There was a trend to higher levels of activated JNK (p54; P-T183/Y185) and MST1 (P-T183) in the cortical region of scrapie-infected mice at 70 dpi (two-tail paired ratio *t*-test; JNK [p54], $P = 0.0851$; MST1, $P = 0.0880$) (**Figure 4.8**). The levels of activated JNK were significantly higher in the subcortical region at 70 dpi ($P = 0.0332$), whereas those of MST1 were not ($P = 0.2222$). Cleaved MST1 and phosphorylated FOXO3 (P-S208) levels were similar in scrapie- and mock-infected mice at this time (**Figure 4.8**). Levels of cleaved MST1 were significantly higher at 130 dpi in all brain regions (brainstem-cerebellum, $P = 0.0452$; subcortical, $P = 0.0237$; cortical, $P = 0.0243$), whereas activated JNK levels were similar in scrapie- and mock-infected mice at this time (**Figure 4.8**). The levels of activated MST1 (P-T183) were significantly higher ($P = 0.0215$) in the cortical region of scrapie-infected mice at terminal stages, when the levels of cleaved MST1 had returned to levels similar to those in mock-infected mice.

In summary, MST1 signaling was activated in scrapie-infected mice at clinical stages of disease. Levels of cleaved MST1 were higher at 130 dpi, when total levels of MST1 and FOXO3 were lower. At terminal stages of disease, levels of activated MST1 (P-T183) were higher in scrapie- than in mock-infected mice.

4.3 DISCUSSION

Here I describe the application of a my kinomics approach to an *in vivo* model of prion disease pathogenesis, mice intraperitoneally infected with scrapie strain RML. The primary screens

identified CaMK4β and MST1 signaling pathways as potentially dysregulated. Targeted analyses then tested the activation state of these pathways. CaMK4β/CREB signaling, which promotes neuronal survival, was activated at earlier times in scrapie-infected mice, but returned to the levels of mock-infected mice at later times. At these later times, MST1 signaling, which promotes neuronal death, was activated (**Figure 4.9**).

The activation of CaMK4β/CREB signaling at preclinical stages of prion disease had not been described. CREB is critical to neuronal survival. CREB/cAMP response element modulator (CREM) double knockout mice, or mice in which CREB is inhibited by overexpression of a dominant negative mutant or inhibitory peptides, suffer extensive neuronal loss (Mantamadiotis et al., 2002; Ao et al., 2006; Jancic et al., 2009). Active CREB promotes neuronal survival by regulating the transcription of 'activity-regulated inhibitor of death' (AID) genes, including *gadd45*β, *gadd45*γ, *btg2*, *npas4*, *nr4a1*, *inhba*, *atf3*, *ifi202b*, and *serpinb2* (Zhang et al., 2009; Tan et al., 2012). CREB also regulates the transcription of miR132-3p (Vo et al., 2005; Nudelman et al., 2010), which modulates synapse morphology (Magill et al., 2010). High-throughput analyses have identified changes in many mRNAs and miRNAs, including miR132-3p, in scrapie-infected mice prior to the accumulation of PrP^{res} or the onset of clinical disease (Booth et al., 2004b; Brown et al., 2005; Kim et al., 2008; Hwang et al., 2009; Moody et al., 2009; Majer et al., 2012). Elevated levels of miR132-3p and AID genes (*gadd45*β, *gadd45*γ, *btg2*, *npas4*, *nr4a1*) were observed at 70–110 dpi after infection with the same scrapie strain and by the same route of inoculation as described here (Majer et al., 2012). Activated CaMK4β/CREB signaling may well promote neuronal survival at preclinical stages of prion infection by upregulating the expression of miR132-3p and AID genes.

CaMK4β/CREB signaling returned to the activation levels of mock-infected mice at 110 dpi. Calcineurin (also known as protein phosphatase 2B, PP2B) regulates the activity of CaMK4 (Kasahara et al., 1999) and CREB (Bito et al., 1996), and elevated calcineurin activity was observed in scrapie-infected mice at clinical stages of disease (Mukherjee et al., 2010). Moreover, the calcineurin inhibitor FK506 prolonged survival of scrapie-infected mice and inhibited neuronal death in cultured neurons treated with PrP106-126 (Agostinho et al., 2003; Mukherjee et al., 2010; Nakagaki et al., 2013). CaMK4β/CREB signaling is therefore most likely neuroprotective in scrapie-infected mice. Decreased levels of activated CaMK4β (P-T196) and phosphorylated CREB (P-S133) were associated with decreased expression levels, suggesting that degradation may be involved in downregulation of this pathway. CaMK4 and CREB are degraded by calpain, a calcium-dependent protease (Watt et al., 1993; McGinnis et al., 1998). Active calpain degraded CaMK4 and CREB in cultured neurons treated with hydrogen peroxide after CREB (P-S133) dephosphorylation (See et al., 2001). Increased levels of calpain have been observed in *in vitro* and *in vivo* models of prion disease (O'Donovan et al., 2001; Guo et al., 2012), and calpain inhibition limited neuronal death in prion-infected cultured organotypic cerebellar slices or cultured neurons treated with PrP106-126 (Lopes et al., 2007; Falsig et al., 2012; Guo et al., 2012). Calpain inhibition also protected cultured organotypic cerebellar slices from neurotoxicity induced by anti-PrP antibody treatment (Sonati et al., 2013). CaMK4β/CREB signaling activation may therefore be inhibited in scrapie-infected mice after 90 days by calcineurin-mediated dephosphorylation and calpain-mediated degradation. CaMK4 and CREB are also dephosphorylated by protein phosphatase 2A (PP2A) (Wadzinski et al., 1993; Park et al., 1995; Westphal et al., 1998), the activity of which has yet to be evaluated during scrapie infection.

The activation of MST1 signaling at 130 dpi had not been described in prion disease either. MST1 is involved in other neurodegenerative diseases. Genetically modified mice that model ALS lose fewer neurons and survive longer if they are knocked out of MST1 (Lee et al., 2013). Active MST1 (P-T183) is cleaved by active (cleaved) caspase-3 (Graves et al., 1998; Kakeya et al., 1998; Lee et al., 2001; Graves et al., 2001), the levels of which are elevated in scrapie-infected mice (before the accumulation of PrP^{res}) and in cultured neurons or neuroblastoma cells exposed to PrP106-126 or PrP^{Sc} (White et al., 2001; Jamieson et al., 2001; Corsaro et al., 2003; Hetz et al., 2003). The elevated levels of cleaved MST1 at 130 dpi may therefore result from caspase-3-mediated cleavage. The activation of caspase-3, however, is not required for MST1 activation (Glantschnig et al., 2002) or neuronal death in prion disease (Saez-Valero et al., 2000; White et al., 2001; Engelstein et al., 2005). Although cleaved MST1 retains the T183 phosphorylation site, T183 phosphorylation is not required for cleavage (Glantschnig et al., 2002; Praskova et al., 2004), and I did not detect cleaved MST1 with the phosphorylation-specific antibody.

MST1 activates FOXO3, which is otherwise maintained in the cytosol in an inactive state by interaction with 14-3-3 proteins (Brunet et al., 1999). Caspase-mediated cleavage of MST1 removes its nuclear export signal. Cleaved MST1 is therefore predominately localized to the nucleus and thus unable to phosphorylate FOXO3 in the cytosol (Ura et al., 2001; Anand et al., 2008). The levels of phosphorylated FOXO3 (P-S208) might have been higher (but were not statistically different) after the levels of cleaved MST1 had returned to those in mock-infected mice. Active FOXO3 upregulates transcription of genes encoding pro-apoptotic proteins, including Bim (bcl-2 interacting mediator of cell death; *bcl2l11*), Puma (Bcl-2-binding component

3; *bbc3*) and Noxa (phorbol-12-myristate-13-acetate-induced protein 1; *pmaip1*) (You et al., 2006; Obexer et al., 2007; Czymai et al., 2010). The levels of Bim, Puma, *bcl2l11*, *bbc3* and *pmaip1* are elevated in scrapie-infected mice at late stages of disease progression (Steele et al., 2007b; Hetz et al., 2008; Majer et al., 2012), suggesting that neuronal death mediated by MST1 signaling could involve FOXO3.

The CaMK4β/CREB and MST1 signaling pathways were identified in primary screens because the expression levels of the involved protein kinases changed coordinately during prion disease progression (**Figures 4.5** and **4.7**). The CaMK4β/CREB signaling pathway promotes neuronal survival. CaMK4β and CREB were expressed to higher levels and activated at earlier stages of disease. Neurons may activate this pathway to protect themselves from prion-mediated death. Later (at 110 dpi), the neuroprotective CaMK4β/CREB signaling was lost and MST1 signaling was activated. Activation of MST1 signaling was associated with lower levels of full-length MST1 and FOXO3. The decrease in full-length MST1 was two-fold greater than the increase in the cleaved form (detected in the same blots with the same antibody). Cleaved MST1 may be less stable than full-length MST, or full-length MST1 may be processed by caspase-dependent and -independent pathways.

The opposing changes in expression and activation state suggest an attempt to prevent the neuronal death mediated by activated MST1 signaling. The levels of upstream kinases DLK, MKK7, and JNK2 were also lower in scrapie-infected mice at 130 dpi, albeit only in the brainstem-cerebellum (**Figure 4.7**), despite their similar levels of expression in most regions of the mouse brain (Yao et al., 1997; Lee et al., 1999; Pozniak et al., 2013). The cerebellum (in our brainstem-cerebellum samples) may contain ~50% of all neurons in an adult mouse brain (Fu et

al., 2013) and loses the most neurons in RML-infected mice, as indicated by nuclear DNA fragmentation (Siso et al., 2002). The changes in the total levels of proteins involved in the MST1 signaling pathway in each brain region may therefore reflect differences in the number of affected neurons.

Higher levels of total and phosphorylated CREB were expressed in all brain regions. CaMK4β in rat brain is predominately expressed in cerebellar granule neurons (Sakagami et al., 1999). Consistently, higher levels of CaMK4β were detected in brainstem-cerebellum than in the subcortical or cortical regions of scrapie-infected mice. The phosphorylation of CREB in subcortical and cortical regions is therefore likely mediated by other protein kinases. Although CaMK4 (P-T196) could also be responsible for CREB (P-S133) phosphorylation, there were no differences in the levels of activated CaMK4 (P-T196) in scrapie- versus mock-infected mice (**Appendix 6**). CREB is also phosphorylated on S133 by other protein kinases, including RSK, cAMP-dependent protein kinase (PKA), and mitogen-activated protein kinase-activated protein kinase 2 (MAPKAPK2) (for review see Johannessen et al., 2004). There was no correlation between the levels of active RSK1 (P-S380) and phosphorylated CREB (P-S133). I did not evaluate other protein kinases upstream of CREB because they were not identified in the primary screens.

Protein kinase	Accession Number	Antibody Source	Catalog Number
AMPKα2	P54646	R&D Systems	AF2850
ASK1	Q99683	Sigma Aldrich	PRS3677
c-Abl	P00519	Cell Signaling Technology	2862
CHK2	O96017	BD Biosciences	611570
CK1γ1	Q9HCP0	Abcam	ab87234
EphB3	P54753	R&D Systems	AF432
HER2	P04626	EMD Millipore	AHO1011
Lck	P06239	Santa Cruz Biotechnology	sc-13
Lyn	P07948	Cell Signaling Technology	2732
MARK1	Q9P0L2	Cell Signaling Technology	3319
MKK7	O14733	Cell Signaling Technology	4172
MSK1	O75582	R&D Systems	AF2518
Nek6	Q9HC98	Abcam	ab76071
p38β	Q15759	R&D Systems	MAB5885
PINK1	Q9BXM7	Santa Cruz Biotechnology	sc-37796
PKCγ	P05129	EMD Millipore	13-3800
PKD3	O94806	Cell Signaling Technology	5655
RSK2	P51812	R&D Systems	AF1518
SGK1	O00141	Abcam	ab18887
Wee1	P30291	EMD Millipore	06-972

Table 4.1 – Sources for the 20 new antibodies optimized for primary multiplex Western blot analyses. All proteins were detected in 200 μg of mouse brain homogenate per linear well cm. The human accession number, antibody source, and catalog number for each protein is indicated.

Table 4.2 – Primary multiplex Western blots analyzed the levels of 139 protein kinases in the brainstem-cerebellum of scrapie-infected mice.

	Antibody Set 1					Antibody Set 2				
Group	Kinase	MW (kDa)	Dilution	Intensity	Type	Kinase	MW (kDa)	Dilution	Intensity	Type
1	PKD2	98	1:60	+	RP	Yes	59	(1:500)	(+)	MM
	ROCK1	162	1:125	+	MM	ASK1	155	1:250	++++	RP
						TNIK	184	1:2000	++++	MM
2	CK1γ2	47	1:60	+	GP	MEK2	45	1:1000	++++	MM
	HER2	185	1:60	+	MM	DLK	51	1:500	++++	RP
						LIMK1	70	1:125	++++	RP
						PKCε	90	1:2000	++++	MM
						FAK	115	(1:500)	(+++)	MM
3	cyclin H	37	(1:60)	(+)	MM	CDK1	34	(1:500)	(++++)	MM
	PCTAIRE3	48	1:125	++	RP	GSK3α	50	1:125	+++	RP
	p70S6K	65, 88	1:250	+++	MM	PKCδ	78	1:125	+++	MM
	GRK2	80	1:60	++	RP	EphA7	86	1:60	+	RP
	PKD3	105	1:500	++	RP	PDGFRβ	200	(1:500)	(++++)	MM
4	p25/p35	28, 38	1:125	+	RP	PKACβ	53	1:250	++++	RP
	PLK1	66	1:125	+	MM	PKR	66	1:125	+++	MM
	JAK1	122	1:125	+	MM	IKKα	82	1:250	++	MM
	c-Abl	135	1:60	+	RP	DYRK1A	90	1:60	++++	RP
5	cyclin D1	36	1:60	++	MM	CHK1	52	(1:500)	(++++)	MM
	Fms/ CSF1R	49, 140	1:125	+	RP	CaMK2γ	60	1:250	+++	GP
	Raf1	71	1:1000	++	MM	PKCβ	82	1:500	++++	MM
	PKCθ	80	1:125	+	RP	EphA3	148	1:125	++++	RP
6	CDK6	36	(1:500)	(+)	MM	MKK6	41	1:60	++++	RP
	SGK1	46	1:250	++	RP	JNK2	42 (α1/β1), 52 (α2/β2)	1:125	+++	MM
						PKCζ	84	1:125	+++	MM
						TrkA	145	1:60	++++	RP
7	CK1α	38	1:60	+	GP	MEK5	45 (β), 56 (α)	1:125	++++	MM
	PDK1	63	1:250	++	RP	PKCι	75	1:125	++++	MM
	MLK3	90	1:60	+	RP	Wee1	100	1:125	++++	RP
8	p38α	42	1:1000	+	MM	PKACα	42	1:250	++++	MM
	PINK1	63	1:250	+	RP	CaMK1δ	44	1:125	++	RP
	IKKβ	87	1:125	+	MM	PAK3	65	1:125	++	RP
						PKCγ	80	1:1000	++	MM
						RSK2	80	1:2000	++++	RP
9	cyclin D3	33	1:250	+++	MM	CDK5	30	1:1000	++++	MM
	CK1γ1	47	1:250	++	RP	p38γ	43	1:125	+++	RP
	CaMK4	63, 66 (β)	1:250	++	MM	GSK3β	46	1:250	++++	MM
	Syk	74	1:125	+	RP	CASK	104	1:500	++++	MM
						EphB3	110	1:60	++++	GP
10	CK1ε	44	1:500	++	MM	Erk2	42	1:2000	++++	MM
	MAPKAPK2	47	1:250	++	RP	SGK3	52	1:250	++++	RP
	MARK4	79	1:60	+	RP	Akt1	62	1:500	++++	MM
	TrkB	85, 145	1:250	+	MM	BTK	73	(1:60)	(++++)	RP
	Erk5	110	1:125	++	RP					
11	Akt3	60	1:60	+++	RP	CDK4	30	(1:500)	(++++)	MM
	PKD1	112	1:125	++	RP	p39	42	1:250	+++	RP
	DAPK1	145	1:2000	+	MM					
12	cyclin G1	29	1:60	++	RP	PKACγ	40	1:1000	++++	RP
	InsR	88, 130	1:60	+	MM	Lkb1	55	1:250	+++	MM
						MSK1	92	1:125	++++	GP
						EphA4	125	1:250	++++	MM
13	Myt1	63	1:60	+	RP	CDK7	41	1:1000	+++	MM
						AMPKα1	64	1:125	+++	MM
						PAK1	66	1:125	++++	RP
14	MKK7	47	1:60	++++	RP	Erk1	44	1:250	++++	RP
	CHK2	65	1:60	++	MM	MST1	60	1:60	+	RP
	B-Raf	90	1:250	++	MM	SLK	60, 124, 229	1:500	+++	MM
						PKCα	82	1:500	++++	MM

15	HER4	182	1:250	+	RP	MEK1	45	1:500	++++	MM
	HER3	185	1:60	+	MM	Lck	56	1:250	++	RP
						PRK1	123	1:1000	+++	MM
16	CDK2	37	(1:500)	(+)	MM	JNK1	49	1:250	++++	RP
	CDKL1	42	1:60	+	RP	CaMKK2	68	1:125	+++	GP
	Akt2	62	1:60	++	RP	Pyk2	120	1:1000	++++	MM
	EGFR	175	(1:60)	(+)	RP					
17	cyclin D2	36	(1:500)	(++)	MM	p38β	42	1:60	++++	MM
	p38δ	43	1:125	+	RP	CaMK1α	42	1:125	+++	RP
	MARK1	90	1:60	+	RP	AMPKα2	63	1:60	++++	GP
						RSK1	80	1:250	++++	RP
18	Lyn	53	1:60	+	RP	DDR1	116	1:60	+++	RP
	PRK2	130	1:125	+	RP	JAK2	122	1:125	+	MM
	CRIK	245	1:1000	+	MM					
19	Nek6	46	1:250	+++	RP	GRK5	65	1:125	++++	RP
	Src	60	1:250	++	MM	ROCK2	183	1:125	++++	MM
	TrkC	145	1:125	+	GP					
20	Fyn	59	1:125	++	MM	CK2α1	42	1:1000	++++	MM
	PKG1	76	1:60	+	RP	IRAK4	55	(1:60)	(++)	RP
						FGFR1	145	(1:60)	(+)	RP
21	MEKK1	205	1:125	+	RP	cyclin E1	50	1:500	+++	MM
						HGK	148	1:125	+++	RP

Primary antibodies specific for 63 protein kinases (antibody set 1) were combined into 21 groups at optimized concentrations (dilutions) and loaded into the corresponding multiscreen lane. Blots were then stripped and reprobed with another 21 groups of antibodies specific for the remaining 76 protein kinases (antibody set 2). Parentheses indicate kinases detected in 3T3 lysate and not mouse brain homogenate. MW, molecular weight. Signal intensity; ++++, most intense; +, least intense. Antibody type; MM, mouse monoclonal; RP, rabbit polyclonal; GP, goat polyclonal.

Protein kinase	Accession Number	Antibody Source	Catalog Number
CREB	P16220	Cell Signaling Technology	9104
nNOS	P29475	Cell Signaling Technology	4231
PSD-95	P78352	Cell Signaling Technology	3409
FOXO3	O43524	Cell Signaling Technology	2497

Table 4.3 – Sources for the 4 new antibodies optimized for secondary multiplex Western blot analyses. The human accession number, antibody source, and catalog number for each protein is indicated.

Protein kinase	Antibody Source	Catalog Number
p-CaMK4β (T196)	Sigma Aldrich	SAB4504122
p-CREB (S133)	Cell Signaling Technology	9191
p-FOXO3 (S207)	Life Technologies	441230G
p-JNK (T183/Y185)	Cell Signaling Technology	4668
p-Lyn (Y396)	Abcam	40660
p-MST1 (T183)	Cell Signaling Technology	3681
p-nNOS (S847)	Abcam	16650
p-p38 (T180/Y182)	Cell Signaling Technology	4511
p-RSK1 (S380)	Cell Signaling Technology	9335

Table 4.4 – Sources for the 9 new antibodies optimized for tertiary multiplex Western blot analyses. The antibody source and catalog number for each protein is indicated.

Figure 4.1 – Levels of GFAP and PrP^{res} during scrapie progression. A) Western blots of GFAP, total PrP, and PrP^{res} in homogenates of brainstem-cerebellum, subcortical, and cortical regions of three mock- or three scrapie (RML)-infected mice at 70, 90, 110, 130 dpi or at terminal stage of disease (155–190 dpi). Molecular weights in kDa are indicated on the left. Black triangles, samples in which PrP^{res} was quantitated. **B**) Time-course changes in the levels of GFAP and PrP^{res}. Line graphs show the levels of GFAP in scrapie-infected mice normalized to the average levels in mock-infected mice at each time point. The levels of PrP^{res} are expressed as a percentage relative to the highest level detected in each region. Mean ± SD; $n = 3$ (mean ± range for PrP^{res} at 130 dpi where $n = 2$). Error bars on the x-axis, range in time of onset of terminal disease. The differences in GFAP levels in scrapie- versus mock-infected mice were analyzed by unpaired two-tail *t*-test. $^{*}P < 0.05$; $^{**}P < 0.01$; $^{***}P < 0.001$.

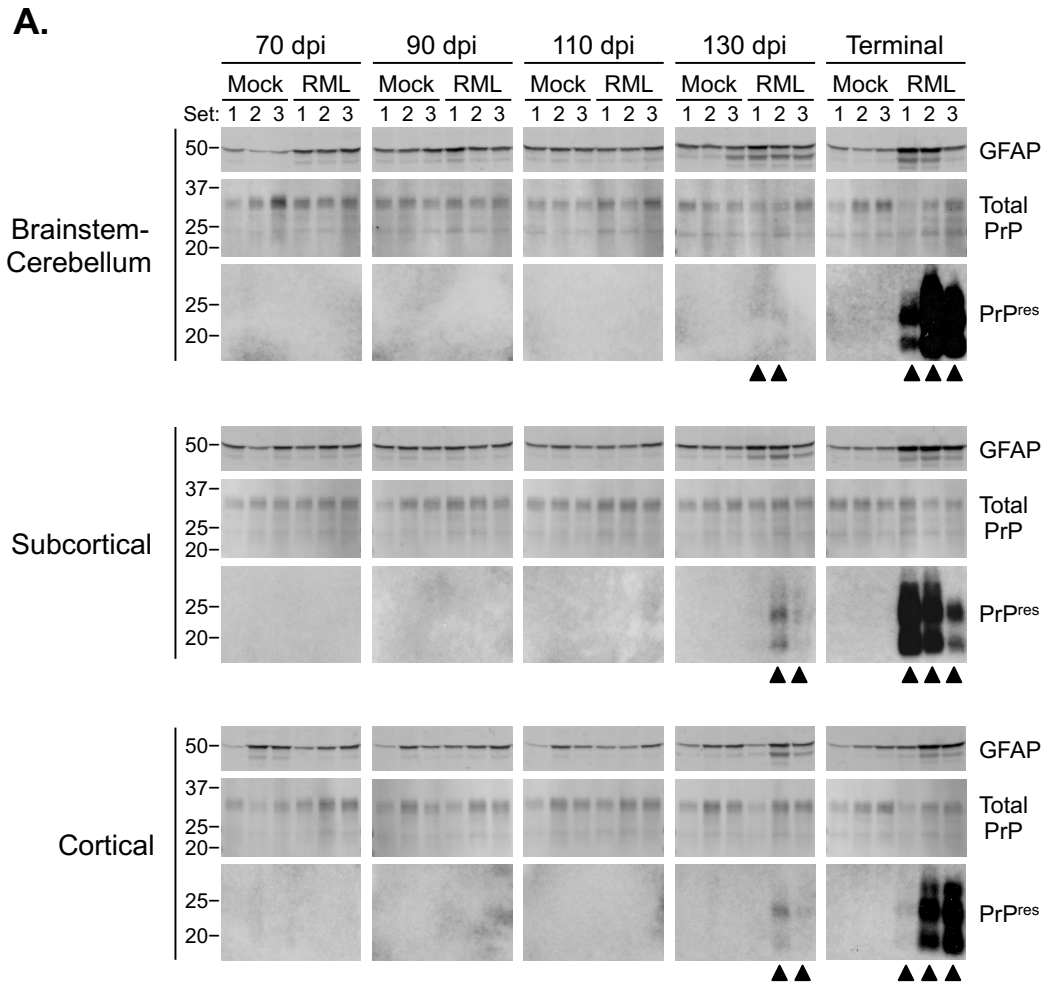
A.
70 dpi
90 dpi
110 dpi
130 dpi
Terminal
Mock
RML
Set: 1 2 3 1 2 3
Brainstem-Cerebellum
Subcortical
Cortical
50
37
25
20
GFAP
Total PrP
PrPres

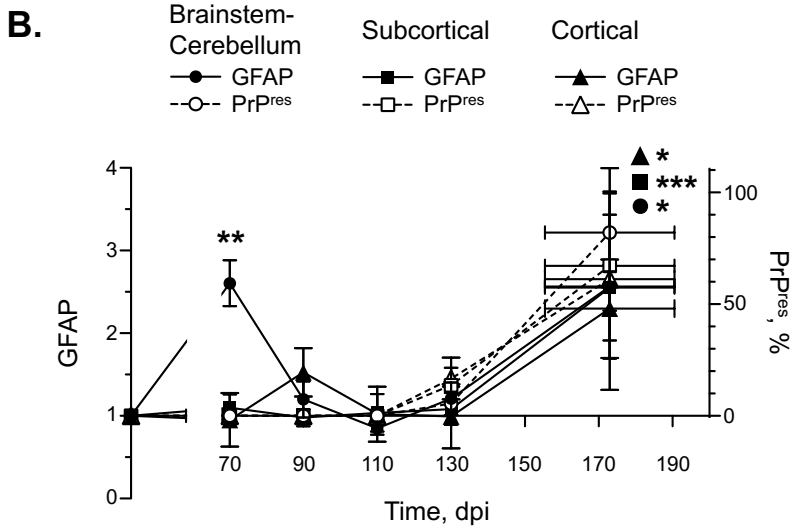
B.
Brainstem-Cerebellum
Subcortical
Cortical
GFAP
PrPres
**
*
***
*
GFAP
PrPres, %
Time, dpi
70
90
110
130
150
170
190

Figure 4.2 – Primary multiplex Western blots of brainstem-cerebellum from scrapie- and mock-infected mice at different stages of disease progression. The expression levels of 139 protein kinases were analyzed in three mock- or three scrapie (RML)-infected mice at 70 (**A, page 151**), 90 (**B, page 152**), 110 (**C, page 153**), 130 (**D, page 154**), or at terminal stage of disease (**E, page 155**). Mice identified by ID numbers; M, mock-infected; R, RML-infected. Molecular weights in kDa are indicated on the left. The protein kinases CaMK4β (probed with antibody set 1 [Set 1]) and DLK (probed with antibody set 2 [Set 2]) are indicated by white arrowheads and enlarged to illustrate their differential expression in scrapie- versus mock-infected mice. The antibody used to detect CaMK4β also detects CaMK4 (red band, indicated by the asterisks), the levels of which remain constant at 70 dpi when CaMK4β levels were most different. The expression levels of the other protein kinases tested in the same or adjacent lanes also remained constant or were expressed differently than CaMK4β and DLK (Set 1, CK1ε [red band] indicated by 1; Set 2, LIMK1 indicated by 1 and GSK3α indicated by 2). Apparent signal above GSK3α in mouse ID 11 M is an artifact.

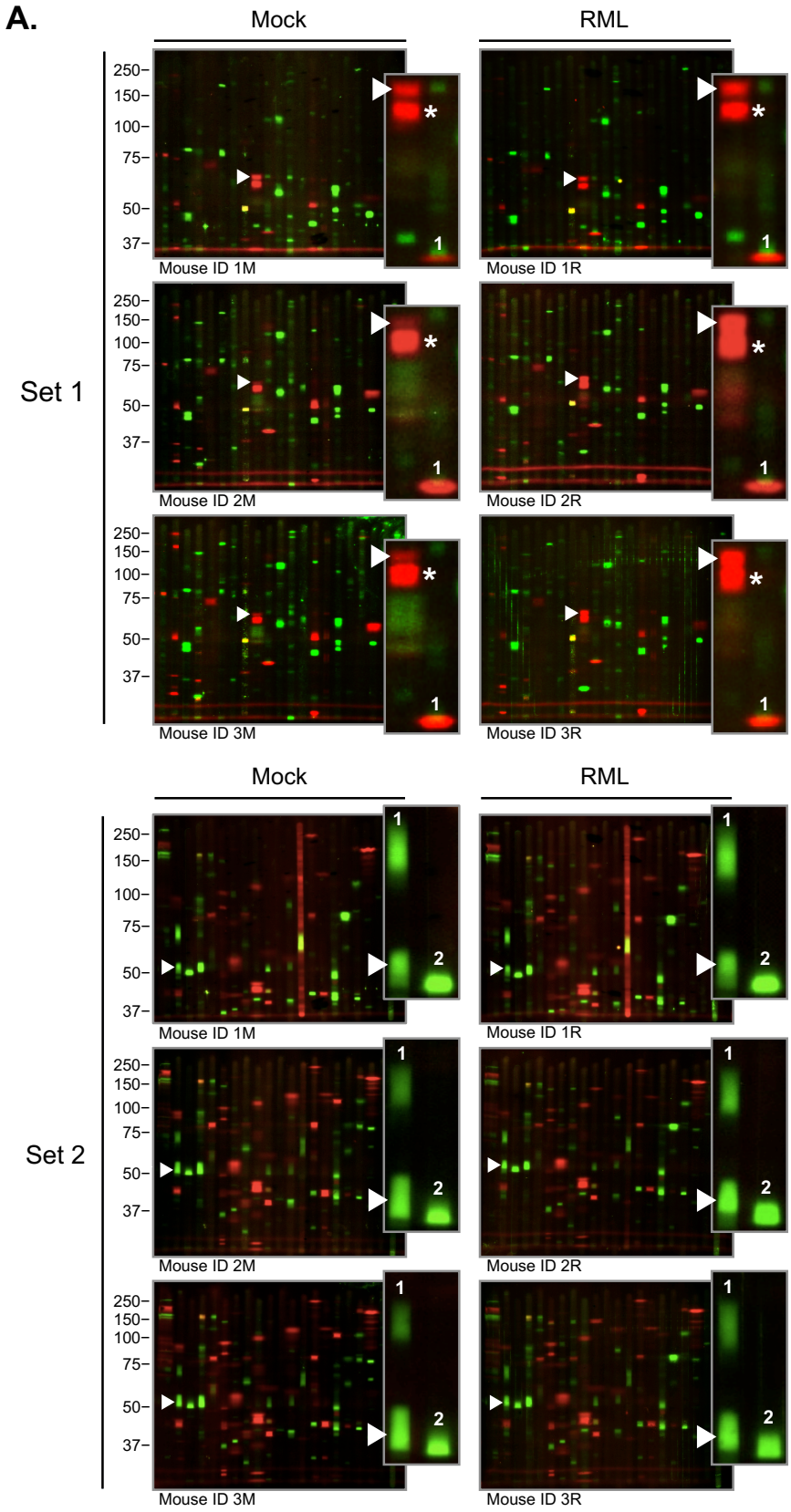
A.
Mock
RML
Set 1
250–
150–
100–
75–
50–
37–
Mouse ID 1M
Mouse ID 1R
Mouse ID 2M
Mouse ID 2R
Mouse ID 3M
Mouse ID 3R
Set 2
1
2

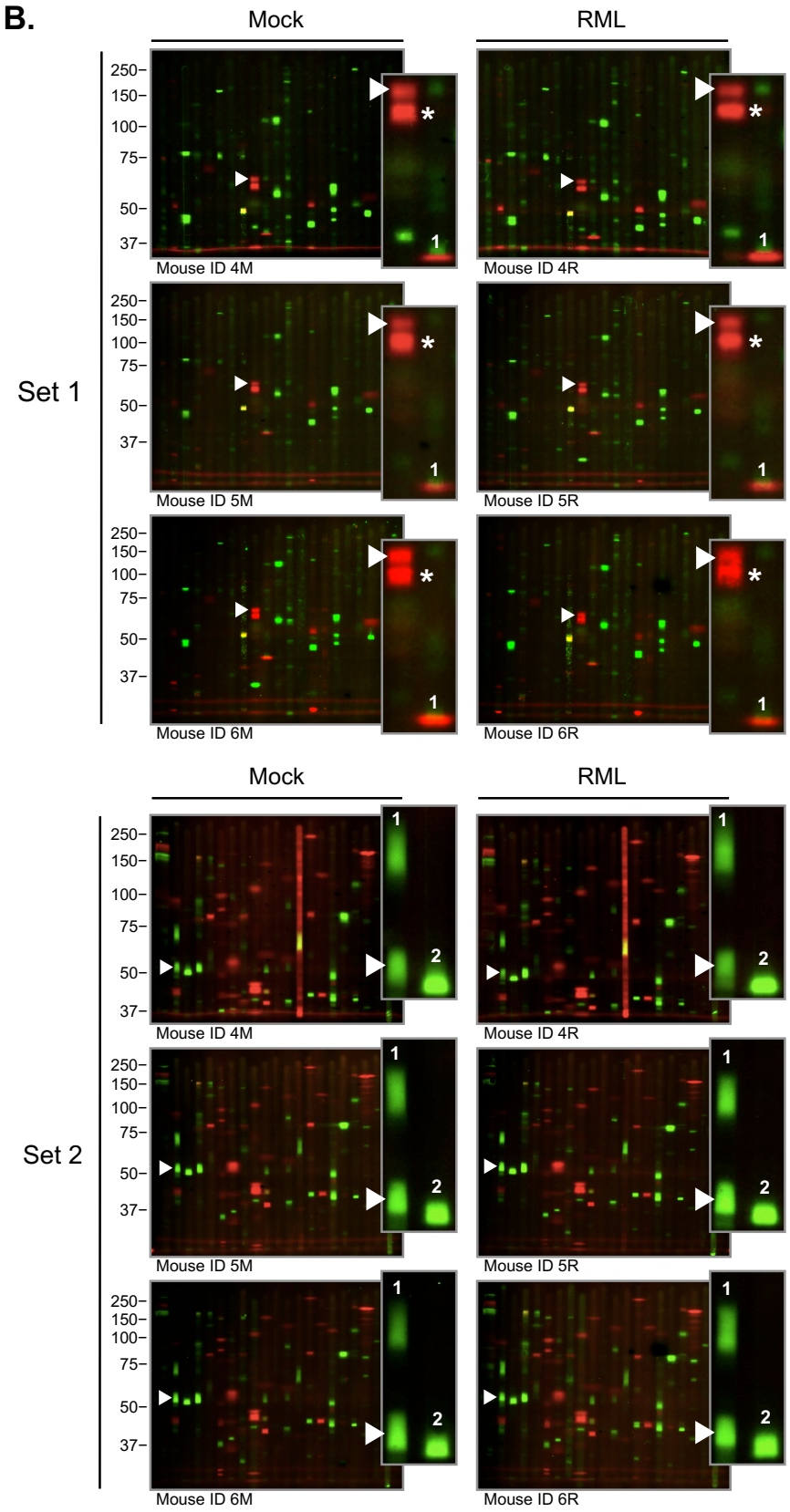
B.
Mock
RML
Set 1
250–
150–
100–
75–
50–
37–
Mouse ID 4M
Mouse ID 4R
Mouse ID 5M
Mouse ID 5R
Mouse ID 6M
Mouse ID 6R
Set 2
1
2

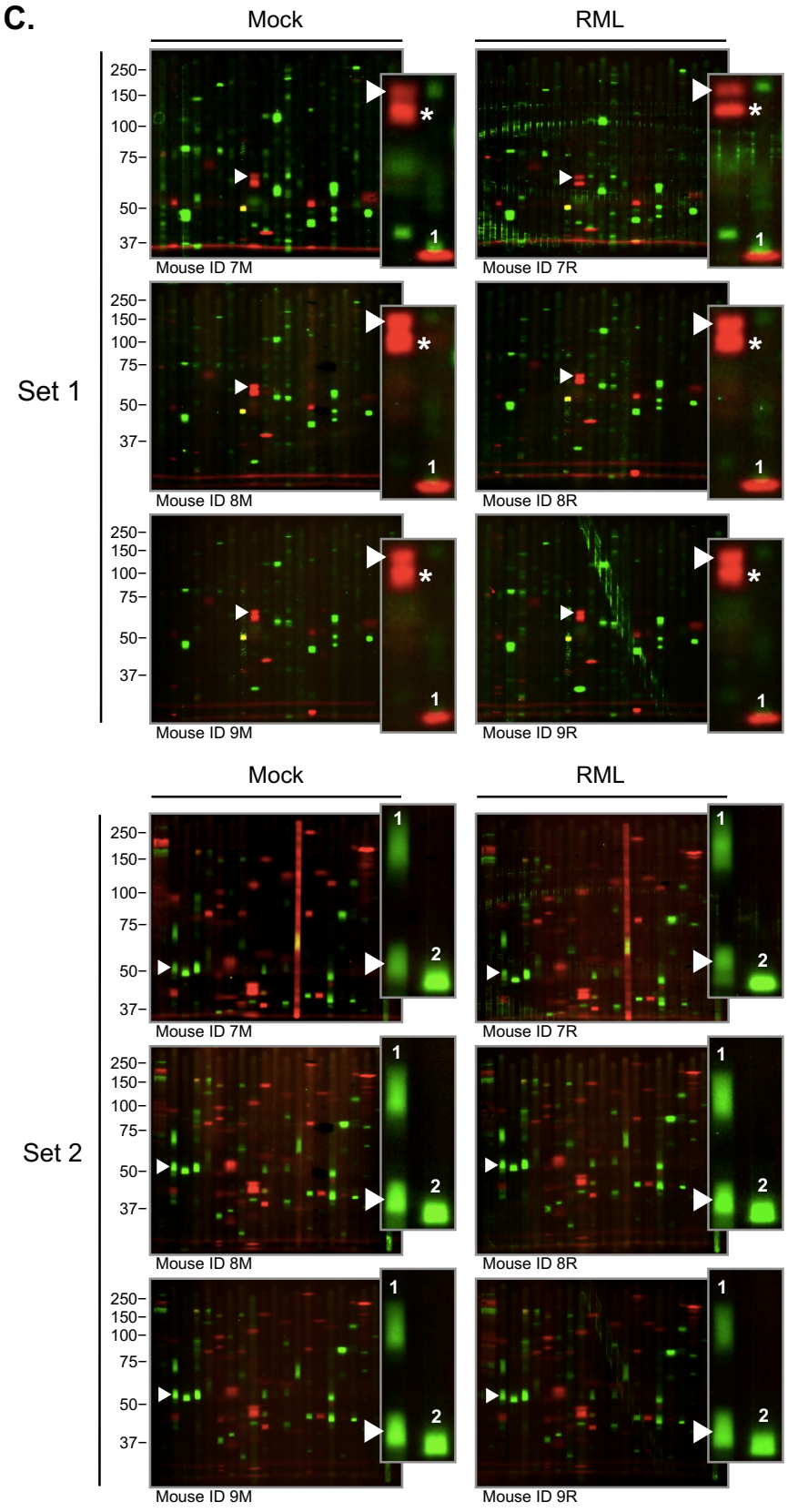
C.
Mock
RML
Set 1
250–
150–
100–
75–
50–
37–
Mouse ID 7M
Mouse ID 7R
Mouse ID 8M
Mouse ID 8R
Mouse ID 9M
Mouse ID 9R
Set 2
1
2

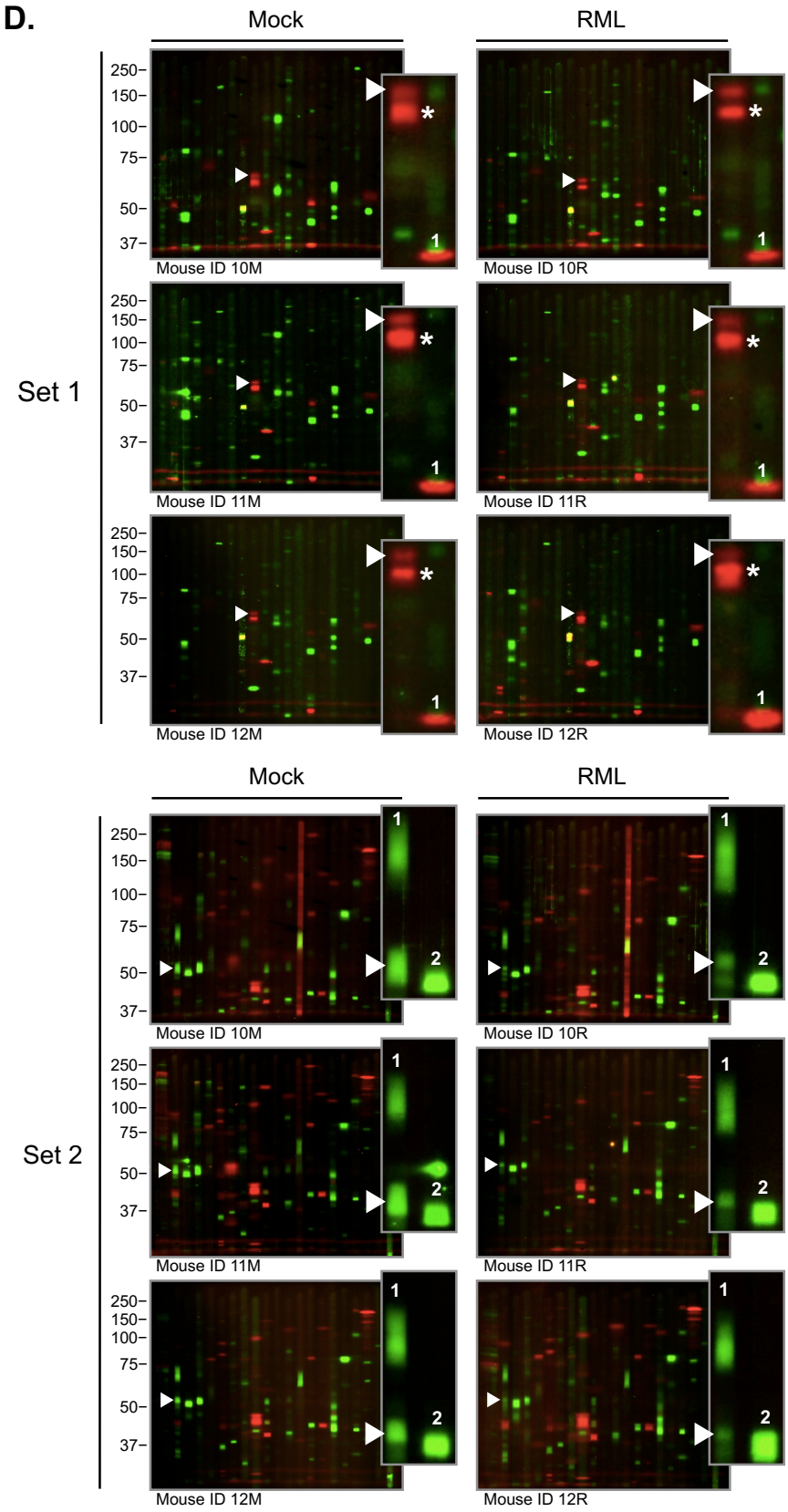
D.
Mock
RML
Set 1
250–
150–
100–
75–
50–
37–
Mouse ID 10M
Mouse ID 10R
Mouse ID 11M
Mouse ID 11R
Mouse ID 12M
Mouse ID 12R
Set 2
1
2

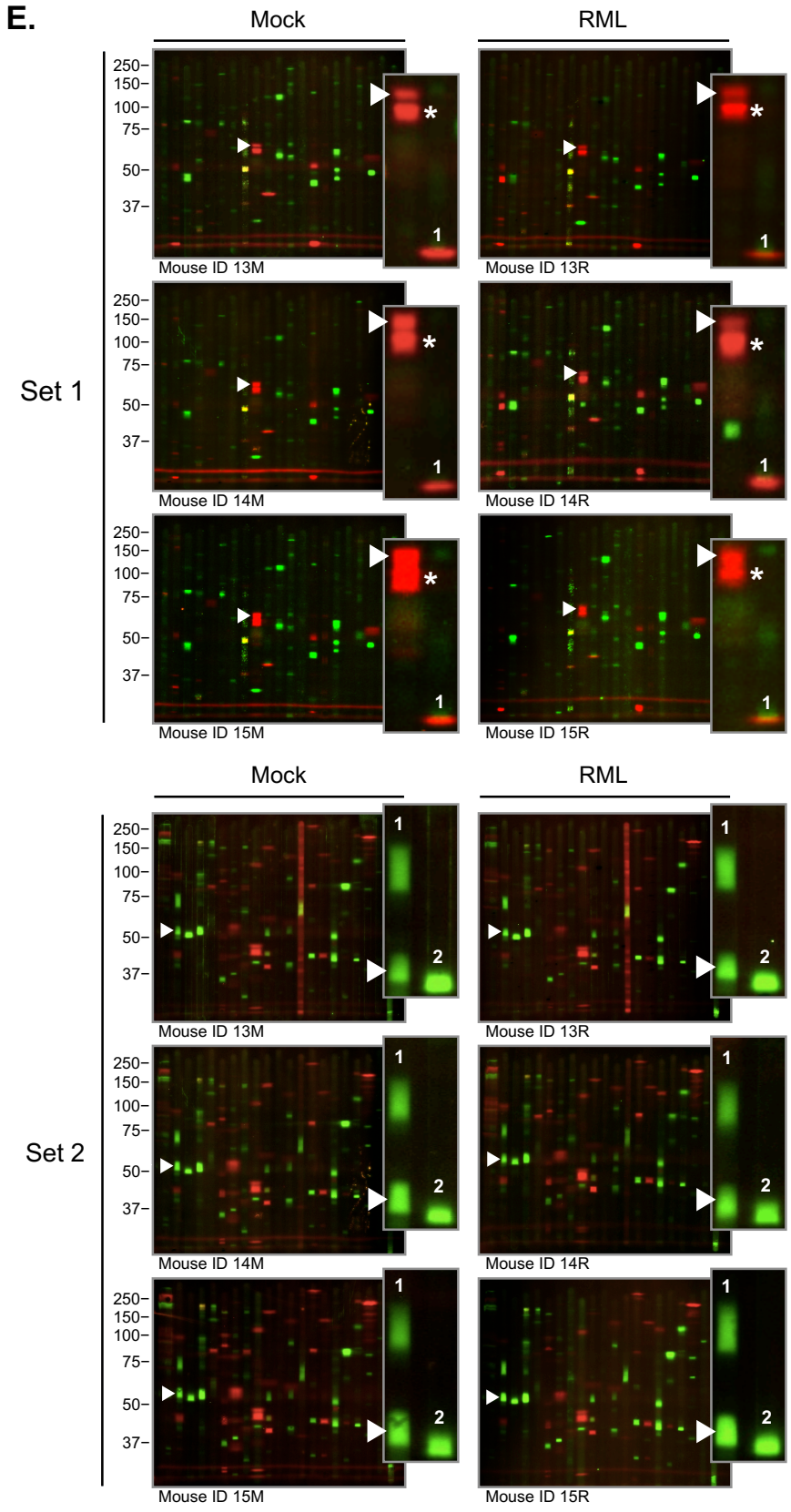
E.
Mock
RML
Set 1
250–
150–
100–
75–
50–
37–
Mouse ID 13M
Mouse ID 13R
Mouse ID 14M
Mouse ID 14R
Mouse ID 15M
Mouse ID 15R
Set 2
1
2

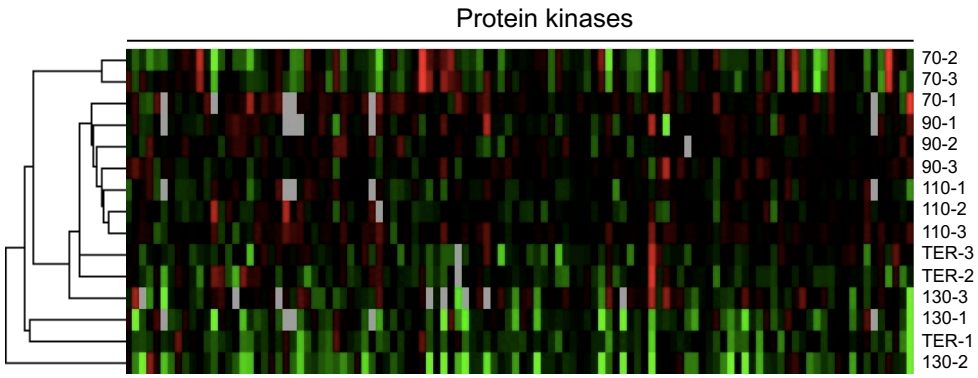

Figure 4.3 – Blind clustering of scrapie-infected mice groups them largely by time after infection. Hierarchical clustering of scrapie-infected mice euthanized at 70, 90, 110, 130 dpi or at terminal stage of disease (TER) using the densitometric data of the 109 protein kinases detected in primary multiplex Western blots. The normalized and $\log_2$ transformed levels of protein kinase expression for each set (1, 2, 3 - consisting of one scrapie-and one mock-infected mouse euthanized at each time point) Clusters were identified by Euclidean distance metric correlation with complete linkage.

Figure 4.4 – Identification of two signaling pathways of potential interest involved in neuronal survival and death. A) Hierarchical clustering the normalized and $\log_2$ transformed densitometric data of the expression levels of 109 protein kinases detected in primary multiplex Western blots of brainstem-cerebellums of scrapie-infected mice at 70, 90, 110, 130 dpi or at terminal stage of disease (TER). Red, higher expression level; green, lower expression level; grey, no data (protein kinases that were not resolved, not detected, or not quantitated due to transfer or blotting artifacts). Clusters were identified by Euclidean distance metric correlation with complete linkage. Cluster (***i***) consists of protein kinases involved in the NMDAR-regulated CaMK4β signaling pathway. Cluster (***ii***) consists of protein kinases involved in the MST1 signaling pathway with MKK7, indicated by (◆). The protein kinases highlighted in **Figure 4.2**, CaMK4β and DLK, are indicated by (●). **B**) Expression levels of protein kinases involved in the CaMK4β and MST1 signaling pathways, and included in the primary multiplex Western blots, at 70 dpi (top panel) and 130 dpi (bottom panel), respectively. Color bars indicate the levels in each of the three scrapie-infected mice normalized to those in mock-infected mice.

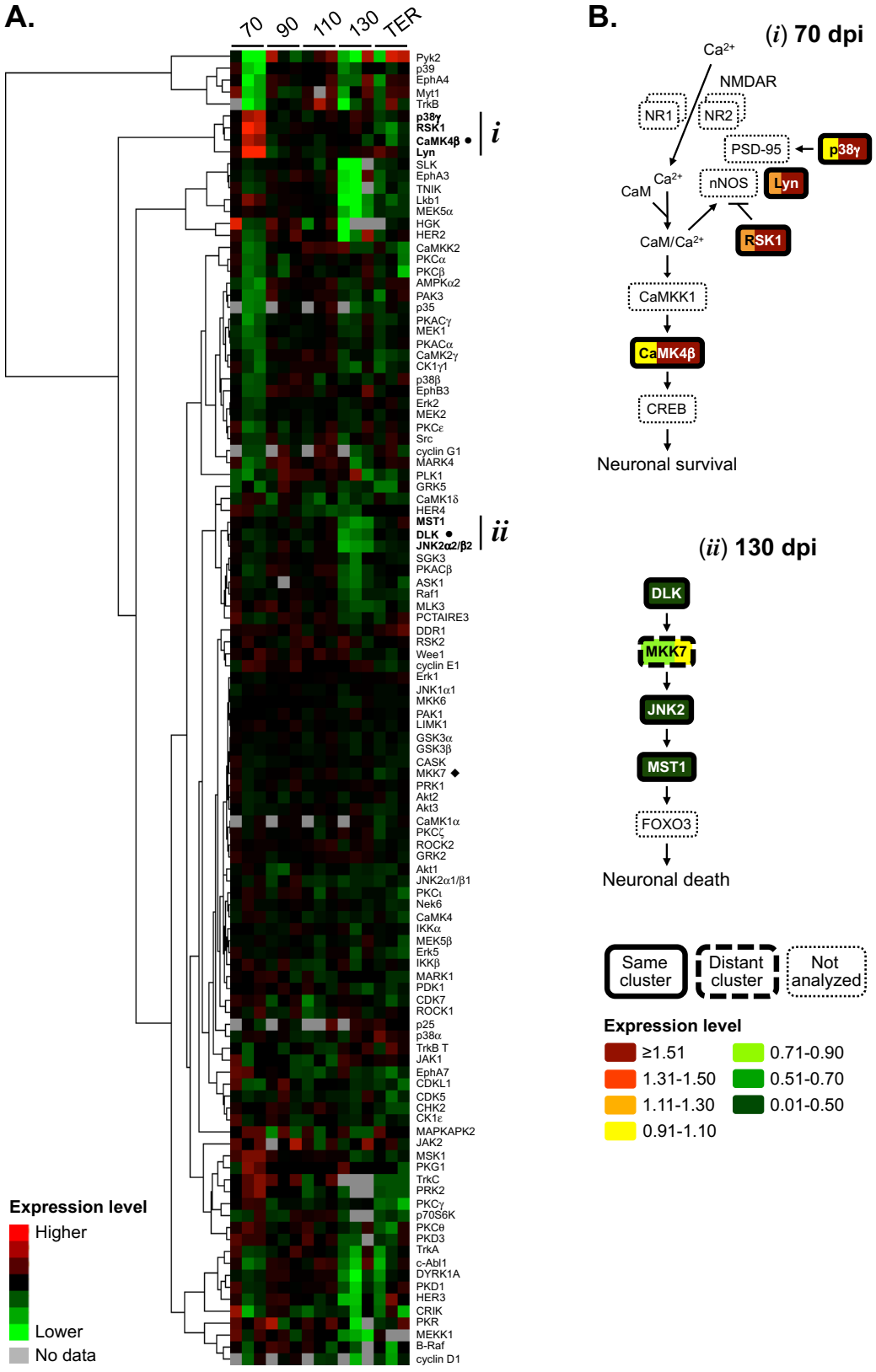
A.
70
90
110
130
TER
Pyk2
p39
EphA4
Myt1
TrkB
p38γ
RSK1
CaMK4β ●
Lyn
i
SLK
EphA3
TNIK
Lkb1
MEK5α
HGK
HER2
CaMKK2
PKCα
PKCβ
AMPKα2
PAK3
p35
PKACγ
MEK1
PKACα
CaMK2γ
CK1γ1
p38β
EphB3
Erk2
MEK2
PKCε
Src
cyclin G1
MARK4
PLK1
GRK5
CaMK1δ
HER4
MST1
DLK ●
JNK2α2/β2
ii
SGK3
PKACβ
ASK1
Raf1
MLK3
PCTAIRE3
DDR1
RSK2
Wee1
cyclin E1
Erk1
JNK1α1
MKK6
PAK1
LIMK1
GSK3α
GSK3β
CASK
MKK7 ◆
PRK1
Akt2
Akt3
CaMK1α
PKCζ
ROCK2
GRK2
Akt1
JNK2α1/β1
PKCι
Nek6
CaMK4
IKKα
MEK5β
Erk5
IKKβ
MARK1
PDK1
CDK7
ROCK1
p25
p38α
TrkB T
JAK1
EphA7
CDKL1
CDK5
CHK2
CK1ε
MAPKAPK2
JAK2
MSK1
PKG1
TrkC
PRK2
PKCγ
p70S6K
PKCθ
PKD3
TrkA
c-Abl1
DYRK1A
PKD1
HER3
CRIK
PKR
MEKK1
B-Raf
cyclin D1
Expression level
Higher
Lower
No data
B.
(i) 70 dpi
Ca2+
NMDAR
NR1
NR2
PSD-95
p38γ
Ca2+
CaM
nNOS
Lyn
CaM/Ca2+
RSK1
CaMKK1
CaMK4β
CREB
Neuronal survival
(ii) 130 dpi
DLK
MKK7
JNK2
MST1
FOXO3
Neuronal death
Same cluster
Distant cluster
Not analyzed
Expression level
≥1.51
1.31-1.50
1.11-1.30
0.91-1.10
0.71-0.90
0.51-0.70
0.01-0.50

Figure 4.5 – CREB is expressed to higher levels in scrapie- than in mock-infected mice at 70 and 90 dpi. Targeted secondary analyses of the NMDAR-regulated CaMK4β signaling pathway in brainstem-cerebellum, subcortical and cortical regions of scrapie-infected mice at 70, 90, 110, 130 dpi or at terminal stage of disease (TER; 155–190 dpi). **A**) Expression levels of p38γ, Lyn, RSK1, CaMK4β, nNOS, CREB, and PSD-95 in three scrapie-infected mice at each time point, normalized to those in the mock-infected mice, shown by color bars. The proteins in dashed lines were not analyzed. **B**) Normalized levels of CaMK4β and CREB, or p38γ, Lyn, RSK1, nNOS, and PSD-95, shown as time series. Mean ± SD; $n = 3$ (mean ± range for Lyn at 90 dpi [subcortical], 110 dpi [cortical], and terminal [subcortical], nNOS at terminal [brainstem-cerebellum], and PSD-95 at 90 dpi and terminal [brainstem-cerebellum]; $n = 2$). Error bars on the x-axes, range in time of onset of terminal disease. The differences in the expression levels in scrapie- versus mock-infected mice were analyzed by two-tailed paired ratio *t*-test. $^{*}P < 0.05$, $^{**}P < 0.01$.

A.

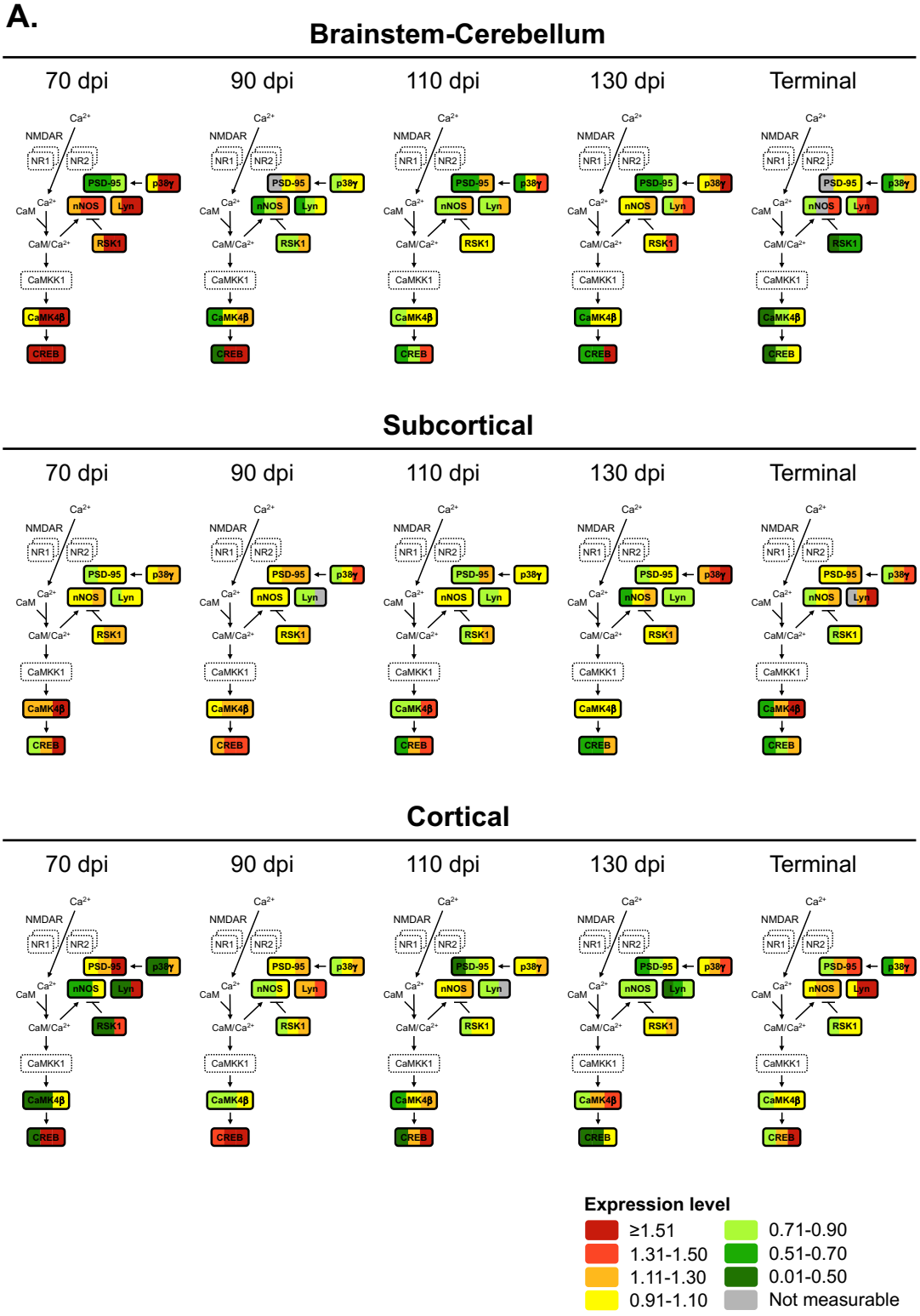
Brainstem-Cerebellum
70 dpi
90 dpi
110 dpi
130 dpi
Terminal
Subcortical
70 dpi
90 dpi
110 dpi
130 dpi
Terminal
Cortical
70 dpi
90 dpi
110 dpi
130 dpi
Terminal
Ca2+
NMDAR
NR1
NR2
PSD-95
p38γ
CaM
nNOS
Lyn
CaM/Ca2+
RSK1
CaMKK1
CaMK4β
CREB
Expression level
≥1.51
1.31-1.50
1.11-1.30
0.91-1.10
0.71-0.90
0.51-0.70
0.01-0.50
Not measurable

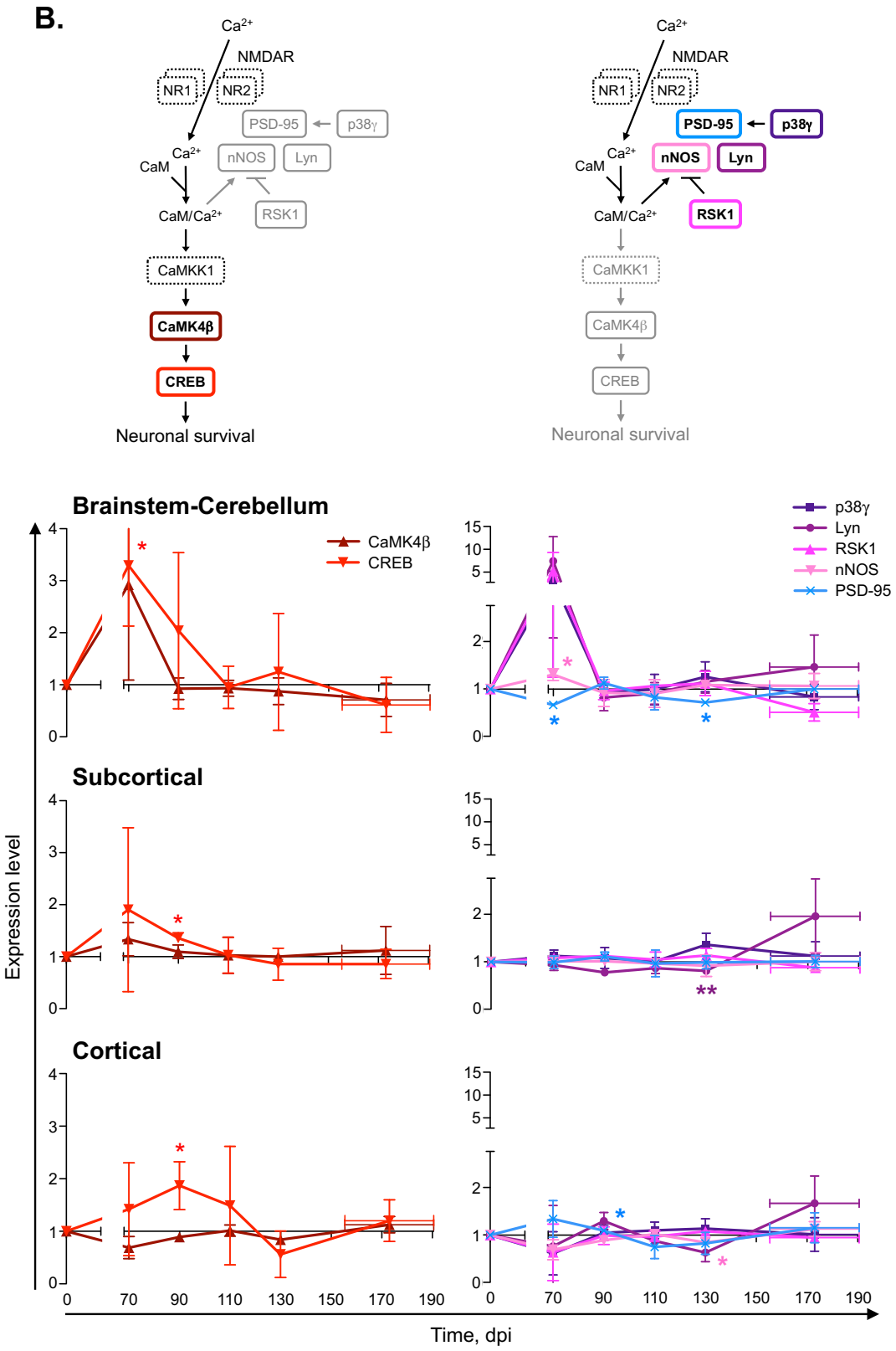
B.
Ca2+
NMDAR
NR1
NR2
PSD-95
p38γ
CaM
Ca2+
nNOS
Lyn
CaM/Ca2+
RSK1
CaMKK1
CaMK4β
CREB
Neuronal survival
Brainstem-Cerebellum
Subcortical
Cortical
CaMK4β
CREB
p38γ
Lyn
RSK1
nNOS
PSD-95
Expression level
Time, dpi
0
70
90
110
130
150
170
190

Figure 4.6 – Activation of CaMK4β/CREB signaling in scrapie-infected mice at preclinical stages of disease. Targeted tertiary analyses of the NMDAR-regulated CaMK4β signaling pathway in brainstem-cerebellum, subcortical and cortical regions of scrapie-infected mice at 70, 90, 110, 130 dpi or at terminal stage of disease (TER; 155–190 dpi). **A**) Levels of phosphorylated p38 (T180/Y182), Lyn (Y396), RSK1 (S380), nNOS (S847), CaMK4β (T196), and CREB (S133) in the three scrapie-infected mice at each time, normalized to those in the mock-infected mice, shown by color bars. The proteins in dashed lines were not analyzed. **B**) Normalized levels of phosphorylated CaMK4β (T196) and CREB (S133), or p38 (T180/Y182), Lyn (Y396), RSK1 (S380), nNOS (S847), shown as time series. Mean ± SD; $n = 3$ (mean ± range for CaMK4β (P-T196) at 90 dpi [subcortical] and 110 dpi [brainstem-cerebellum], CREB (P-S133) at 130 dpi [brainstem-cerebellum], Lyn (P-Y396) at terminal [subcortical and cortical], and nNOS (P-S847) at 70 dpi and terminal [subcortical]; $n = 2$). Error bars on the x-axes, range in time of onset of terminal disease. The differences in phosphorylation levels in scrapie- versus mock-infected mice were analyzed by two-tailed paired ratio *t*-test. $^{*}P < 0.05$; $^{**}P < 0.01$.

A.

Brainstem-Cerebellum

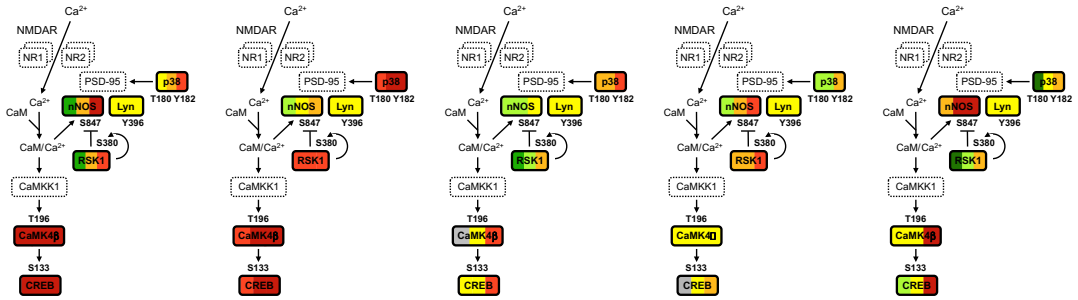

Subcortical

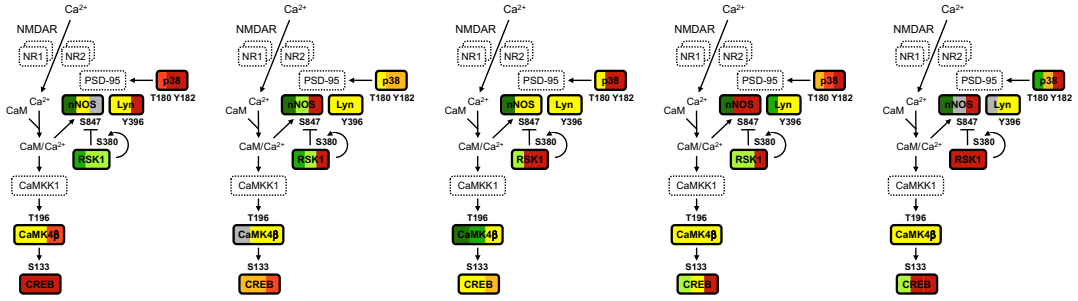

Cortical

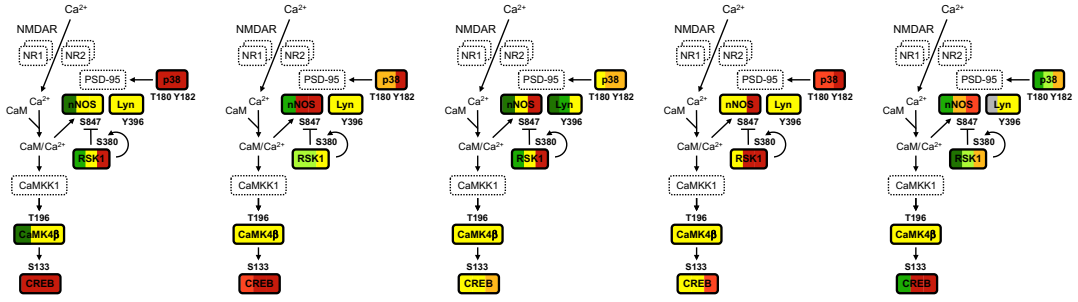

Phosphorylation level

≥1.51	0.71-0.90
1.31-1.50	0.51-0.70
1.11-1.30	0.01-0.50
0.91-1.10	Not measurable

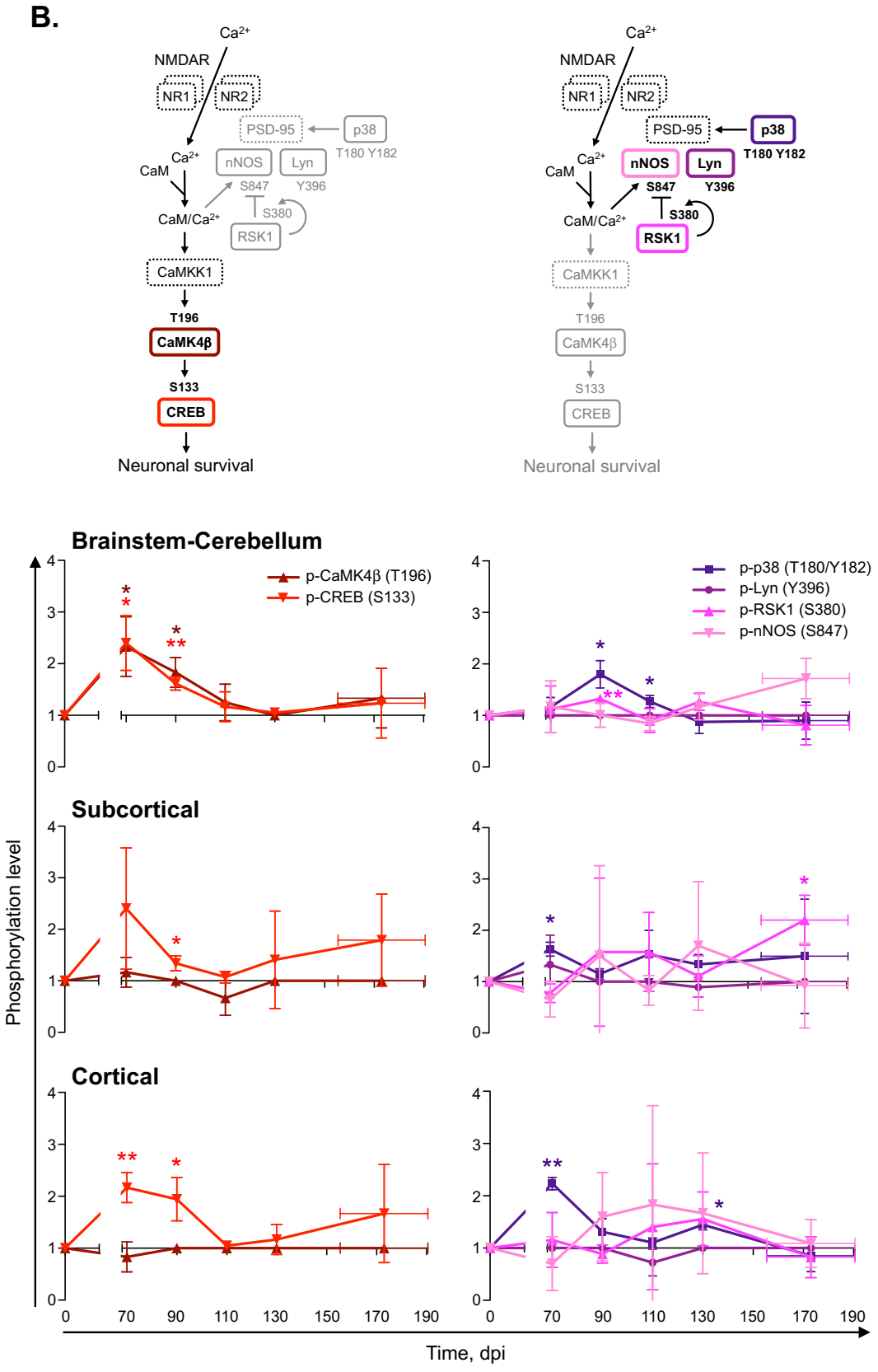
B.
Ca2+
NMDAR
NR1
NR2
PSD-95
p38
T180 Y182
CaM
Ca2+
nNOS
Lyn
S847
Y396
CaM/Ca2+
S380
RSK1
CaMKK1
T196
CaMK4β
S133
CREB
Neuronal survival
Brainstem-Cerebellum
Subcortical
Cortical
p-CaMK4β (T196)
p-CREB (S133)
p-p38 (T180/Y182)
p-Lyn (Y396)
p-RSK1 (S380)
p-nNOS (S847)
Phosphorylation level
Time, dpi
0
70
90
110
130
150
170
190

Figure 4.7 – MST1 and FOXO3 are expressed to lower levels in scrapie-infected mice at 130 dpi. Targeted secondary analyses of the MST1 signaling pathway in brainstem-cerebellum, subcortical and cortical regions of scrapie-infected mice at 70, 90, 110, 130 dpi or at terminal stage of disease (TER; 155–190 dpi). Expression levels of DLK, MKK7, JNK2, MST1, and FOXO3 in three scrapie-infected mice at each time point, normalized to those in the mock-infected mice, shown by color bars (**A**) and as a time series (**B**). Mean ± SD; $n = 3$ (mean ± range for FOXO3 at 90 dpi [brainstem-cerebellum] and TER [brainstem-cerebellum, subcortical region]; $n = 2$). Error bars on the x-axes, range in time of onset of terminal disease. The differences in expression levels in scrapie- versus mock-infected mice were analyzed by two-tailed paired ratio *t*-test. $^{*}P < 0.05$; $^{**}P < 0.01$; $^{****}P < 0.0001$.

A.

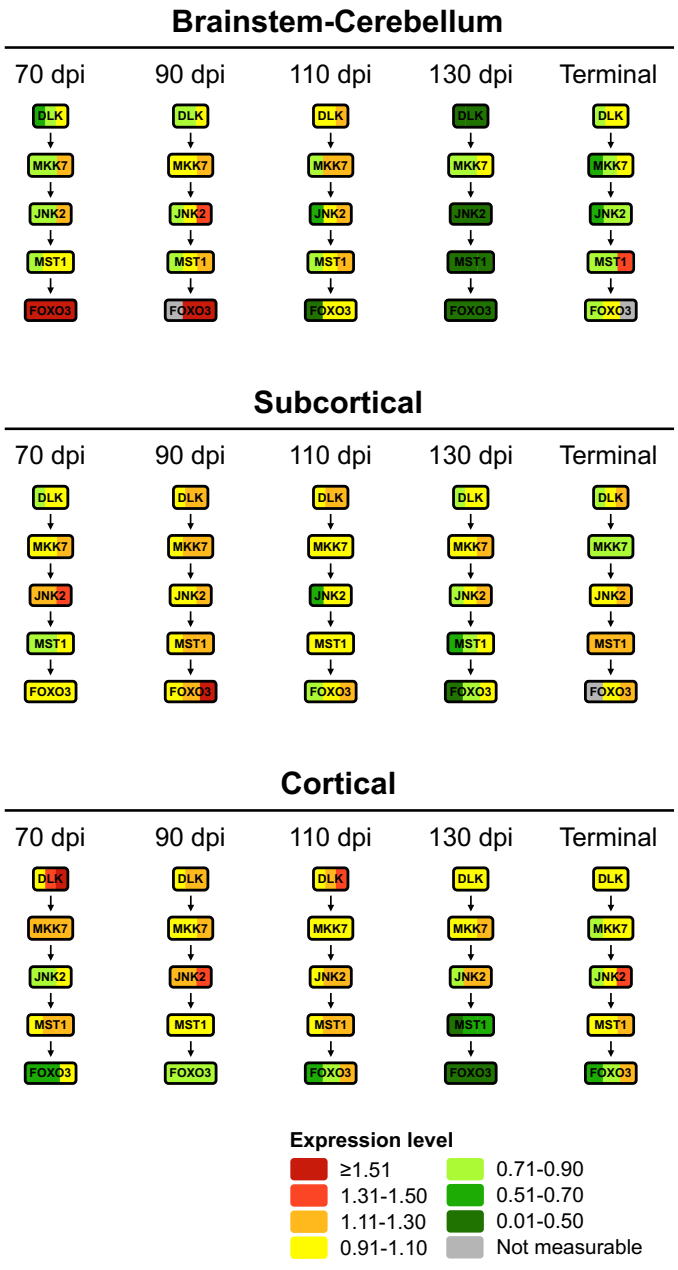
Brainstem-Cerebellum
70 dpi
90 dpi
110 dpi
130 dpi
Terminal
DLK
MKK7
JNK2
MST1
FOXO3
Subcortical
Cortical
Expression level
≥1.51
1.31-1.50
1.11-1.30
0.91-1.10
0.71-0.90
0.51-0.70
0.01-0.50
Not measurable

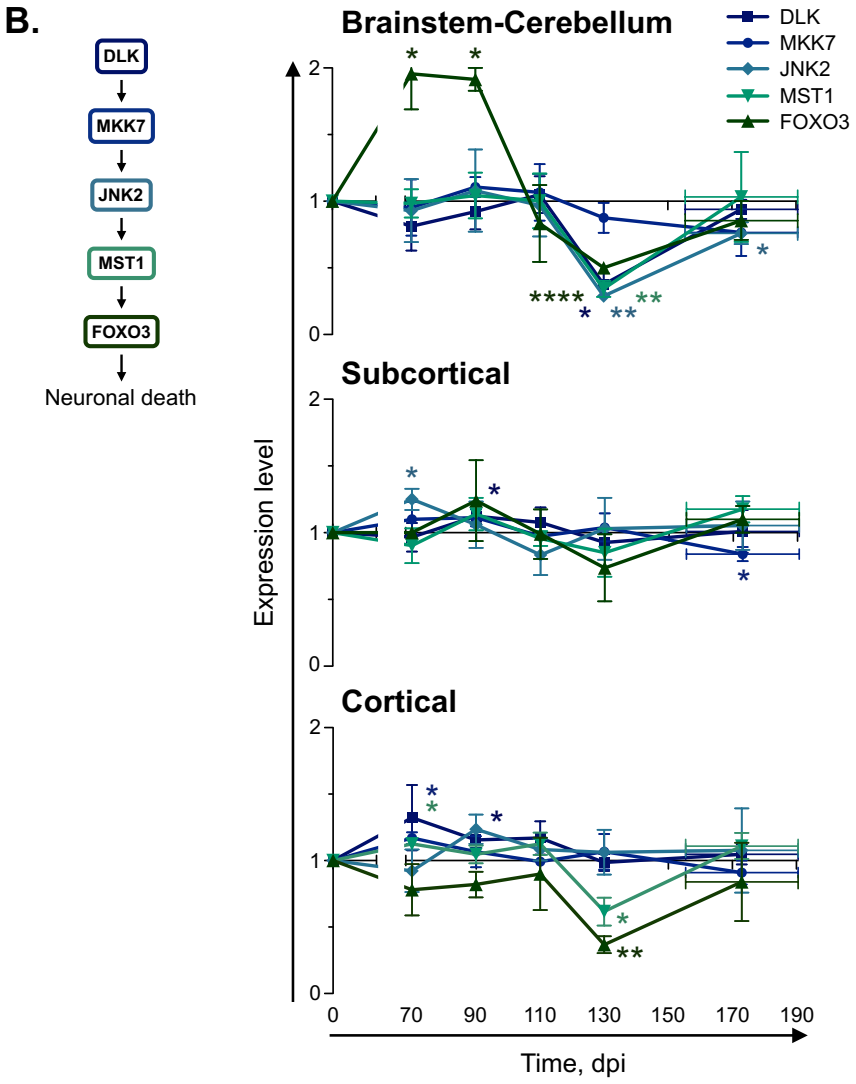
B.
DLK
MKK7
JNK2
MST1
FOXO3
Neuronal death
Brainstem-Cerebellum
Subcortical
Cortical
DLK
MKK7
JNK2
MST1
FOXO3
Expression level
0
1
2
0
70
90
110
130
150
170
190
Time, dpi

Figure 4.8 – Activation of MST1 in scrapie-infected mice at clinical stages of disease. Targeted tertiary analyses of MST1 signaling in brainstem-cerebellum, subcortical region, and cortical regions of scrapie-infected mice at 70, 90, 110, 130 dpi or at terminal stage of disease (TER; 155–190 dpi). Levels of phosphorylated JNK (T183/Y185), MST1 (T183), FOXO3 (S208), and cleaved MST1 in three scrapie-infected mice at each time point, normalized to those in the mock-infected mice, shown by color bars (**A**) and as a time series (**B**). The proteins in dashed lines were not analyzed. Mean ± SD; $n = 3$ (mean ± range for MST1 (T183) at 110 dpi [subcortical region] and TER [brainstem-cerebellum], and FOXO3 (S208) at 130 dpi [brainstem-cerebellum] and TER [cortical region]; $n = 2$). Error bars on the x-axes, range in time of onset of terminal disease. The differences in the phosphorylation levels, or levels of cleaved MST1, in scrapie- versus mock-infected mice were analyzed by two-tailed paired ratio *t*-test. $^{*}P < 0.05$ (cleaved MST1, $^{\#}P < 0.05$).

A.

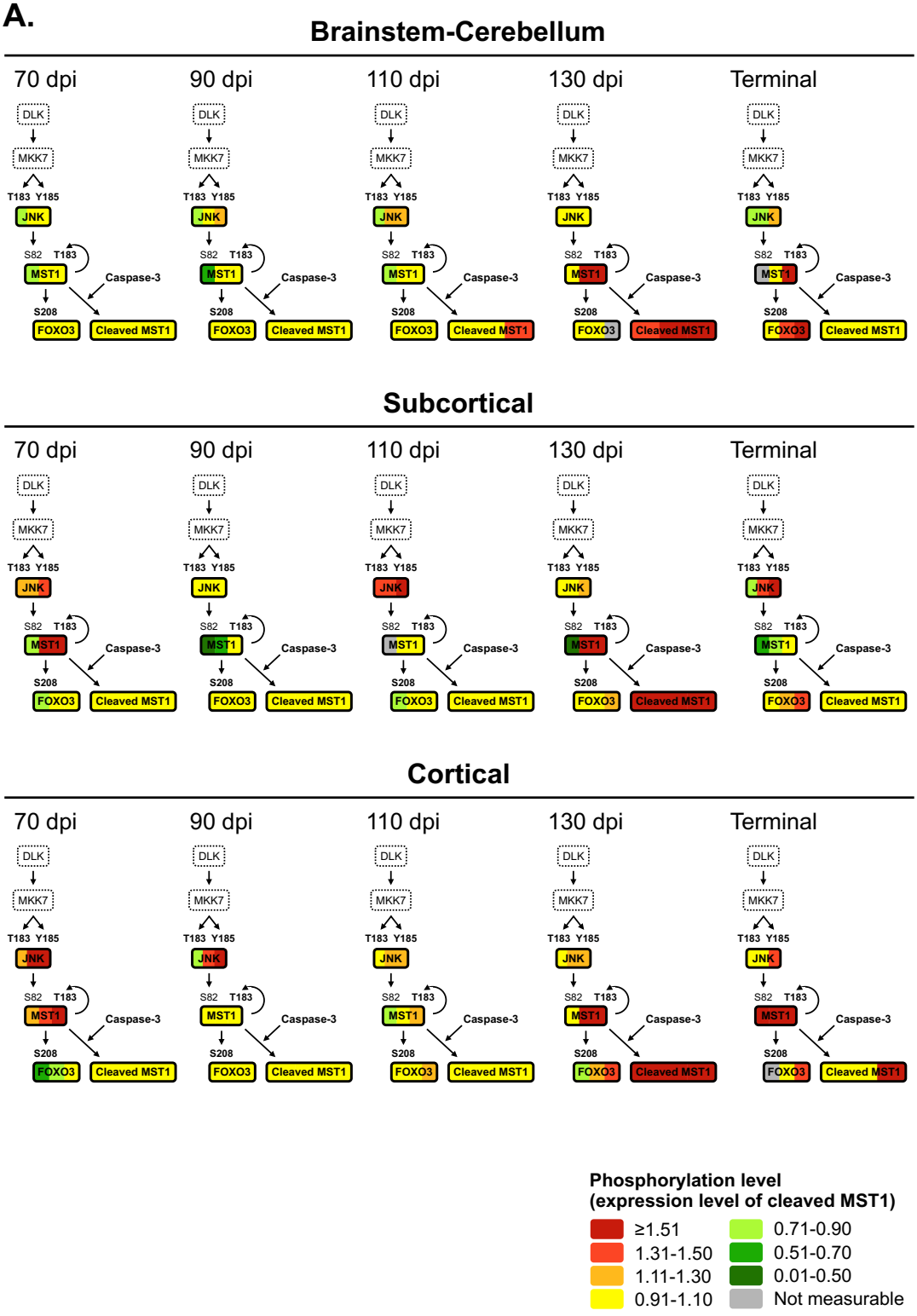
Brainstem-Cerebellum
70 dpi
90 dpi
110 dpi
130 dpi
Terminal
DLK
MKK7
T183 Y185
JNK
S82 T183
MST1
Caspase-3
S208
FOXO3
Cleaved MST1
Subcortical
70 dpi
90 dpi
110 dpi
130 dpi
Terminal
DLK
MKK7
T183 Y185
JNK
S82 T183
MST1
Caspase-3
S208
FOXO3
Cleaved MST1
Cortical
70 dpi
90 dpi
110 dpi
130 dpi
Terminal
DLK
MKK7
T183 Y185
JNK
S82 T183
MST1
Caspase-3
S208
FOXO3
Cleaved MST1
Phosphorylation level
(expression level of cleaved MST1)
≥1.51
1.31-1.50
1.11-1.30
0.91-1.10
0.71-0.90
0.51-0.70
0.01-0.50
Not measurable

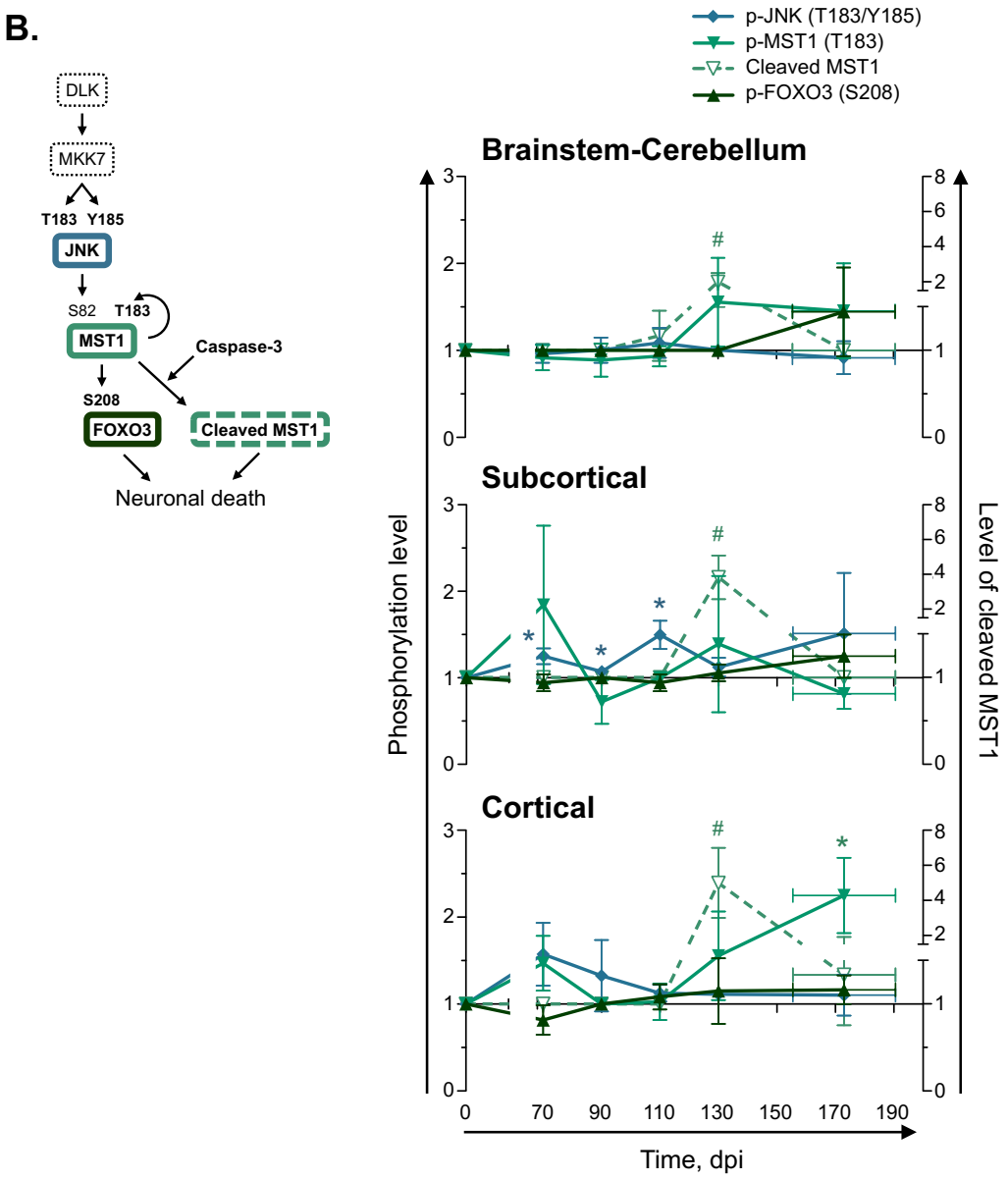
B.
DLK
MKK7
T183 Y185
JNK
S82 T183
MST1
Caspase-3
S208
FOXO3
Cleaved MST1
Neuronal death
p-JNK (T183/Y185)
p-MST1 (T183)
Cleaved MST1
p-FOXO3 (S208)
Brainstem-Cerebellum
Subcortical
Cortical
Phosphorylation level
Level of cleaved MST1
Time, dpi
0
70
90
110
130
150
170
190

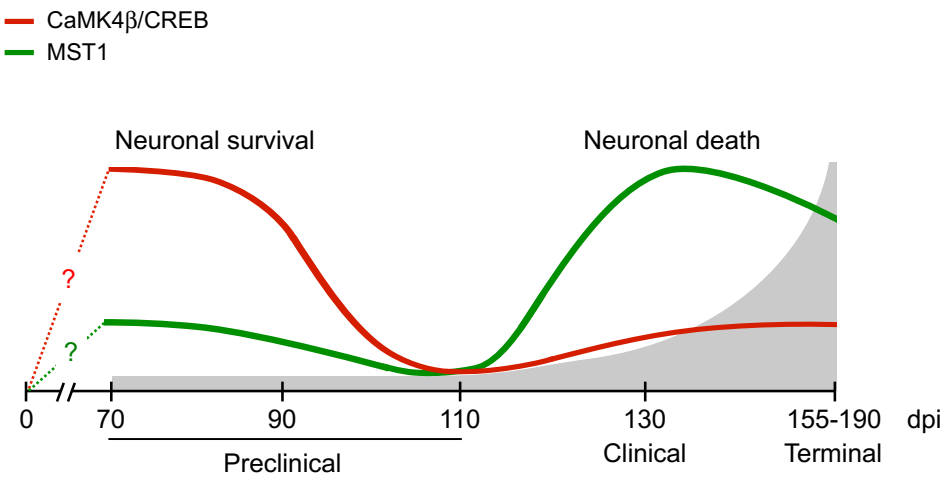

Figure 4.9 – A model for the activation of signaling pathways involved in neuronal survival and death during scrapie pathogenesis. Relative activation states of CaMK4β/CREB (red line) and MST1 (green line) signaling in scrapie-infected mice during disease progression, indicated in grey. Between 90 and 130 dpi, there is a switch from signaling involved in neuronal survival (activated CaMK4β/CREB) to that involved in neuronal death (activated MST1). Figure adapted from Majer et al., 2012.

CHAPTER 5: DISCUSSION

In this thesis, I describe the development and application of a kinomics approach to identify signaling pathways dysregulated during prion disease pathogenesis. I demonstrated the kinomics approach to be sensitive enough to detect 6 (or 3)% changes in protein kinase expression levels. The kinomics approach was validated using an *in vitro* model of prion pathogenesis, N2a cells expressing cytoplasmic PrP mutants. The application of the kinomics approach to scrapie-infected mice then identified dysregulated CaMK4β/CREB and MST1 signaling at preclinical and clinical times in disease progression, respectively.

The kinomics approach identified the inhibition of Akt/p70S6K/eIF4B signaling in N2a cells expressing $CyPrP^{EGFP}$. These results were consistent with the previously observed inhibition of Hsp70 synthesis, and suggest that inhibition of Hsp70-regulated Akt/p70S6K/eIF4B signaling promotes cell death (as discussed in **Section 3.3**). The Akt/p70S6K/eIF4B signaling pathway regulates protein synthesis, which is inhibited in cells expressing $CyPrP^{EGFP}$ (Goggin et al., 2008). Hsp70 would still be expected to be expressed (and even upregulated) during a global inhibition of protein synthesis (Zhao et al., 2002; Zhang et al., 2015). Global protein synthesis is also inhibited in the hippocampus of RML-infected mice (Moreno et al., 2012) and may contribute to prion pathogenesis *in vivo* (Moreno et al., 2013), yet the levels of Hsp70 were unchanged or elevated in scrapie- or CJD-infected brain (Hetz et al., 2003; Zhang et al., 2012). Moreover, Hsp70 overexpression did not significantly prolong survival of scrapie-infected mice (Tamguney et al., 2008), and unlike the changes detected in cells expressing $CyPrP^{EGFP}$, I did not detect synchronous changes in the levels of Akt1, Akt2, Akt3, and p70S6K in brainstem-cerebellum homogenates of

scrapie-infected mice (**Figure 4.4**). It is therefore unlikely that dysregulated Akt/p70S6K/eIF4B signaling contributes to prion pathogenesis *in vivo*.

Transgenic mice expressing mutant CyPrP spontaneously developed ataxia with gliosis and cerebellar degeneration (Ma et al., 2002b). However, no PrP^{Sc} was detected and brain homogenate from these mice did not transmit disease (Norstrom et al., 2007). Although toxic to N2a cells, the expression of mutant CyPrP was not toxic to human primary neurons or neuroblastoma cells (BE[2]-M17, SK-N-SH) (Roucou et al., 2003). In uninfected mice, low levels of cytoplasmic PrP were observed in subpopulations of neurons which otherwise appeared healthy (Mironov et al., 2003; Barmada et al., 2004; Bailly et al., 2004), and the levels of cytoplasmic PrP were not elevated in scrapie-infected mice (Godsave et al., 2008). The accumulation of PrP in the cytoplasm, while potentially neurotoxic, therefore appears to contribute little to prion pathogenesis. This model was used in this thesis to evaluate and validate the kinomics approach that I developed.

To study prion pathogenesis, I applied the kinomics approach to mice infected with scrapie. Scrapie-infected mouse brains were divided into brainstem-cerebellum, subcortical, and cortical regions, a potential source of variability. Nonetheless, the levels of proteins involved in CaMK4β/CREB and MST1 signaling were most affected in brainstem-cerebellum, not subcortical or cortical regions of scrapie-infected mice. These regional differences thus allowed for the identification of the CaMK4β/CREB and MST1 signaling pathways as pathways of potential interest.

The CaMK4β/CREB signaling pathway was activated at preclinical times in scrapie-infected mice (70 and 90 dpi) (**Figure 4.6**). The molecular mechanisms whereby CaMK4β/CREB

signaling is dysregulated during pathogenesis have yet to be elucidated. CaMK4β (and CaMK4) are expressed in neurons, but not astrocytes or microglia (Murray et al., 2009; Carriba et al., 2012). Dysregulated CaMK4β/CREB signaling is therefore most likely to affect neurons. The protein kinase CaMK4β is activated by phosphorylation on threonine 196 (T200 in humans) by upstream calcium/calmodulin-dependent protein kinase kinase 1 (CaMKK1) or CaMKK2. The levels of CaMKK2 were analyzed in primary screens. CaMKK2 was expressed to lower levels in scrapie- than in mock-infected mice at 70 dpi, when all other proteins involved in CaMK4β/CREB signaling were expressed to higher levels (**Figure 4.4**). CaMKK2 was thus not likely involved in dysregulated CaMK4β/CREB signaling and was not further evaluated in the targeted analyses. Although the levels of CaMKK1 were not analyzed, elevated levels of total (and activated) CaMKK1 would be expected. The activation of CaMKK1 and downstream CaMK4 is promoted by interaction with calcium-bound calmodulin (Ca^{2+}/CaM) (Chatila et al., 1996; Tokumitsu et al., 1996). The levels of Ca^{2+}/CaM increase proportionally with the levels of intracellular calcium. The activation of the CaMK4β/CREB signaling pathway is therefore regulated by the levels of intracellular calcium, suggesting that the levels of intracellular calcium are elevated at preclinical stages of prion disease progression.

5.1 Regulation of CaMK4β/CREB signaling during prion disease

The levels of intracellular calcium are regulated by multiple mechanisms. Increased levels of intracellular calcium can result from increased influx/decreased efflux of extracellular calcium or increased release/decreased import of calcium from intracellular stores. The influx of extracellular calcium in neurons is mediated by the activation of voltage-gated calcium channels (VGCCs),

store-operated calcium channels (SOCCs), and ligand-gated calcium channels such as the ionotropic glutamate receptors (NMDA, AMPA, kainate) (for review see Grienberger et al., 2012). Intracellular calcium is removed from the cell by plasma membrane calcium ATPases (PMCAs) and sodium/calcium exchangers (NCXs). Primary analyses of brainstem-cerebellum homogenates from scrapie-infected mice identified that the levels of p38γ, RSK1, Lyn, and CaMK4β were expressed to similarly higher levels in scrapie- than in mock-infected mice at 70 dpi (**Figure 4.4**). All these proteins associate with NMDARs, or can be activated by the downstream influx of extracellular calcium via NMDARs, suggesting the involvement of an NMDAR-regulated CaMK4β signaling pathway. The levels of nNOS and CREB were also expressed to higher levels of brainstem-cerebellum homogenates from scrapie-infected mice at 70 dpi (**Figure 4.5**). The levels of the NMDAR-associated scaffold protein PSD-95, however, were lower. PSD-95 promotes NMDAR surface expression (Lin et al., 2004). Although the influx of extracellular calcium mediated by physiological NMDAR stimulation can activate CaMK4/CREB signaling (Impey et al., 2002), NMDAR overactivation is excitotoxic (as described in **Section 1.4.2.3.2**). NMDAR activity is regulated by PrP^{C} (Khosravani et al., 2008) and treatment with the NMDAR antagonist memantine [1-amino-3,5-dimethyladamantane] protected against PrP^{Sc}-induced neuronal death and prolonged survival of scrapie-infected mice, suggesting that NMDAR overactivation contributes to prion pathogenesis (Müller et al., 1993; Riemer et al., 2008; Resenberger et al., 2011). NMDAR-mediated excitotoxicity was inhibited in cultured cortical neurons by PSD-95 knockdown (Sattler et al., 1999). The lower expression levels of PSD-95 in scrapie-infected mice may therefore be neuroprotective. Impaired association between PSD-95 and NMDAR promoted sustained activation of CaMK4/CREB signaling and protected neurons *ex vivo* and *in vivo* from

ischemia-induced cell death (Bell et al., 2013). The lower expression of PSD-95 in scrapie-infected mice may therefore contribute to the activation of CaMK4β/CREB signaling, potentially mediated by extracellular calcium influx via NMDARs. VGCC-mediated calcium influx is impaired in cerebellar granule neurons treated with PrP106-126 and in transgenic mice expressing the PrP mutant PG14 (Thellung et al., 2000; Senatore et al., 2012). VGCCs are therefore not likely to contribute to extracellular calcium influx in prion pathogenesis. The role of other extracellular calcium transporters in prion pathogenesis has yet to be extensively evaluated.

The levels of intracellular calcium are also regulated by release from the endoplasmic (and sarcoplasmic) reticulum. The transport of calcium into the ER is mediated by sarcoplasmic/ endoplasmic reticulum calcium ATPase (SERCA), while ER calcium release is mediated by activation of ryanodine receptors and inositol 1,4,5-trisphosphate (IP_3)-gated receptors. Higher levels of intracellular calcium were detected in N2a cells treated with PrP^{Sc} than in cells treated with recombinant PrP^{C} or uninfected mouse brain homogenate (Hetz et al., 2003). The cells were cultured in the absence of extracellular calcium, suggesting that the elevated calcium levels came from intracellular stores. Treatment with PrP106-126 also stimulated release of calcium from intracellular stores in SH-SY5Y cells (O'Donovan et al., 2001). SERCAs transport intracellular calcium into the ER for storage. N2a cells transfected to overexpress SERCA were more susceptible to PrP^{Sc}-induced cell death than mock-transfected cells (Torres et al., 2010). Release of calcium from intracellular stores activates CaMK4β/CREB signaling. Treatment with the IP_3 receptor inhibitor 2-aminoethoxy diphenylborate (2-APB) inhibited phosphorylation of CREB in BDNF-stimulated cultured neurons (Spencer et al., 2008). Increased release of calcium from intracellular stores via IP_3 receptors activated CaMK4β/CREB signaling in an *in vitro* model of Alzheimer's

disease, SH-SY5Y and PC12 cells expressing mutant presenilin (Müller et al., 2011). The release of calcium from intracellular stores may therefore also contribute to the activation of CaMK4β/CREB signaling in scrapie-infected mice.

The levels of total and phosphorylated CREB were also elevated in subcortical and cortical homogenates from scrapie-infected mice at preclinical stages of disease progression (**Figures 4.5** and **4.6**). However, the levels of CaMK4β in scrapie-infected mice remained similar to levels in mock-infected mice, consistent with the predominant cerebellar expression of CaMK4β (Sakagami et al., 1999). The phosphorylation of CREB on serine 133 can also be mediated by Akt, CaMK1, CaMK2, DYRK1A, LIMK1, PKA, PKC, PKG, MAPKAPK2, MSK1, MSK2, p70S6K, RSK1 and RSK2. The levels of RSK1 were evaluated in targeted analyses of subcortical and cortical homogenates but did not correlate with changes in levels of phosphorylated CREB. The levels of Akt1, Akt2, Akt3, CaMK1α, CaMK1δ, CaMK2γ, DYRK1A, LIMK1, PKACα, PKACβ, PKACγ, PKCα, PKCβ, PKCγ, PKCε, PKCζ, PKCθ, PKCι PKG1, MAPKAPK2, MSK1, p70S6K, and RSK2 were only analyzed in brainstem-cerebellar homogenates (primary analyses) (**Appendix 4**). Western blot analyzes to characterize the expression levels and the activation states of these protein kinases (and others with the ability to phosphorylate CREB) in subcortical and cortical homogenates are required. Protein kinases with elevated expression and activation levels in scrapie-infected mice from subcortical and cortical homogenates at preclinical stages of disease progression (70 and 90 dpi) may contribute to CREB phosphorylation.

The activation state of CaMK4β/CREB signaling in scrapie-infected mice returned to levels similar to that in mock-infected mice at 110 dpi (**Figure 4.6**). These changes are likely mediated by calcineurin and calpain activation (as discussed in **Section 4.3**). Further analyses are

required to evaluate the levels of total calcineurin and calpain, which may be elevated at times prior to, and later than, 110 dpi. Inhibitors of proteases and phosphatases (including calcineurin) were added during homogenization to inhibit protein degradation and preserve kinase phosphorylation. Homogenates from this set of scrapie-infected mice are therefore not amenable to calpain or calcineurin activity analyses.

5.2 Regulation of MST1 signaling during prion disease

The MST1 signaling pathway was activated after the activation state of CaMK4β/CREB signaling returned to that in mock-infected mice (**Figures 4.7** and **4.8**). The MST1 signaling pathway was identified as potentially dysregulated from the similarly reduced expression levels of DLK, JNK2, and MST1 in scrapie-infected mice at 130 dpi. Targeted analyses revealed elevated levels of activated MST1 (P-T183) and cleaved MST1. However, the levels of activated JNK (P-T183/Y185) in scrapie-infected mice were similar to those in mock-infected mice. Similar results were observed in subcortical and cortical regions of scrapie-infected mice at 130 dpi. Although these findings suggest that MST1 activation may occur independently of JNK2, no antibody specific for JNK-phosphorylated MST1 (P-S82) was available. I was thus unable to evaluate the levels of JNK-phosphorylated MST1. I was also unable to evaluate the levels of activated JNK2 only since the phosphorylation-specific antibody used also detects activated JNK1 and JNK3, which are both expressed to higher levels than JNK2 in most areas of the mouse brain (Lee et al., 1999). Were the levels of activated JNK1 and JNK3 to be reduced in scrapie-infected mice, it would impair detection of elevated levels of activated JNK2. In addition to JNK, the activation of MST1 is also modulated by the protein kinases c-Abl, Akt, TAOK3, by the protein phosphatases

PP2A and Pleckstrin homology domain leucine-rich repeat containing protein phosphatases 1/2 (PHLPP1/2), and by interactions with thioredoxin-1, peroxiredoxin-1, and Ras-associated domain family (RASSF) proteins (for review see Rawat et al., 2015). The levels of c-Abl, Akt1, Akt2, and Akt3 were only analyzed in the brainstem-cerebellum of scrapie-infected mice (primary analyses) (**Appendix 4**). Western blot analyses to characterize the total and activated levels of these protein kinases in subcortical and cortical homogenates are required, as are Western blot analyses of the other proteins that may contribute to MST1 activation in homogenates from all regions.

MST1 signaling mediates neuronal death by FOXO3 activation. The relatively unchanged levels of phosphorylated FOXO3 (P-S208) when the levels of activated MST1 were elevated in scrapie-infected mice (130 dpi) could partly be a consequence of the elevated levels of cleaved MST1 (**Figure 4.8**). Cleaved MST1 localizes to the nucleus and is thus unable to phosphorylate cytoplasmic FOXO3 (as discussed in **Section 4.3**). MST1 also promotes neuronal death by FOXO1 activation (Yuan et al., 2009). The levels of FOXO1 were not analyzed in scrapie-infected mice. However, the phosphorylation-specific FOXO3 antibody that I used also detects MST1-phosphorylated FOXO1 (P-S212), suggesting that levels of phosphorylated FOXO1 were not elevated at 130 dpi either. Cleaved MST1 may also contribute to neuronal death by the phosphorylation of serine residue 14 (S14) on histone H2B (Cheung et al., 2003). The phosphorylation of histone H2B on S14 promotes chromatin condensation, and chromatin condensation has been observed in scrapie-infected GT1 cells and mice (Giese et al., 1995; Williams et al., 1997; Schatzl et al., 1997; Siso et al., 2002). Western blot analyses could be used to evaluate the levels of total and S14 phosphorylated H2B. Although no available antibody is

specific for it, levels of phosphorylated histone H2B (P-S14) would be expected to be elevated in scrapie-infected mice at 130 dpi.

5.3 Validation of dysregulated CaMK4β/CREB and MST1 signaling during scrapie pathogenesis

Proteins involved in the same intracellular signaling pathway are expressed in the same cell type, and colocalize to the same subcellular region or compartment. Immunohistochemical analyses (IHC) of stored fixed and frozen brain slices from the same scrapie- and mock-infected used in the experiments described here are part of the experimental design. Thus, IHC analyses could be used to test the dysregulation of the CaMK4β/CREB and MST1 signaling pathways in scrapie-infected mice. Primary antibodies of different origin (mouse, rabbit, goat) can be distinguished by differently labelled secondary antibodies. Thus, primary antibodies to brain cell markers and proteins involved in CaMK4β/CREB and MST1 signaling may be simultaneous detected in a single sample by IHC analyses, as in the multiplex Western blots. Primary antibodies from the same origin may also be used if required, which can be differentiated by various techniques (Frisch et al., 2011; Manning et al., 2012). The transcription factor CREB is ubiquitously expressed throughout the brain (Chen et al., 1999; Blom et al., 2002) while CaMK4β is predominately expressed in cerebellar granule neurons (Sakagami et al., 1999). Most CaMK4 in neurons is localized to the nucleus, independent of T196 phosphorylation (Deisseroth et al., 1998; Lemrow et al., 2004). CaMK4β may therefore colocalize with CREB in the nuclei of neurons from the brainstem-cerebellum brain region, independently of its activation state. The upstream protein kinases contributing the most to the phosphorylation of CREB in neurons from the subcortical and cortical brain regions are yet unknown, but could be identified by additional Western blot

analyses (as described above) and would be expected to colocalize with CREB in the nuclei of neurons from these brain regions. MST1 signaling promotes neuronal cell death, but the activation of MST1 signaling also promotes the death of astrocytes and microglia (Yun et al., 2011; Lee et al., 2014) Prion pathogenesis is characterized rather by the activation and proliferation of astrocytes and microglia (as discussed in **Section 1.3.7.2**), suggesting that astrocytes and microglia are not affected by pro-death MST1 signaling during prion disease. Neurons affected by dysregulated MST1 signaling in scrapie-infected mice at 130 dpi would be expected to have elevated levels of activated MST1 (P-T183), and perhaps phosphorylated FOXO3 (P-S208). Higher levels of cleaved MST1 are also expected at 130 dpi in neurons with dysregulated MST1 signaling, as detected by increased levels of total MST1 in the nucleus. Neurons with elevated levels of activated MST1 and cleaved (nuclear) MST1 could also have reduced levels of total MST1 (cytoplasmic) and FOXO3, suggesting an attempt to protect from death mediated by activated MST1 signaling. Neurons within these same regions may or may not have activated CaMK4β/CREB signaling at earlier times in disease progression.

Immunohistochemical analyses can also evaluate the level and distribution of PrP^{Sc} and prion neuropathology. PrP^{Sc} accumulation after intraperitoneal infection spreads along with disease progression, caudal to rostral (as discussed in **Section 4.2.2**). The medulla and pons are the first regions to accumulate PrP^{Sc}, followed by the hypothalamus and thalamus, and lastly the hippocampus, cerebellum, and cortex. The spread of prion infectivity from medulla to cortex takes approximately 21 days (Kimberlin et al., 1982). I first detected PrP^{res} in all regions from scrapie-infected mice at 130 dpi (**Figure 4.1**). The dilution of PrP^{Sc} in the medulla and pons with the cerebellum (brainstem-cerebellum homogenate) and the differential rate of PrP^{Sc} accumulation in

subcortical brain regions likely impaired detection of temporal differences in PrP^{res} by Western blot. Such differences in PrP^{res} accumulation in specific regions could, however, be detected by IHC analyses. Spongiform degeneration and reactive gliosis should only be detected in scrapie-infected mice, and like PrP^{res} accumulation, should spread caudal to rostral with disease progression. PrP^{Sc} accumulation in RML-infected CD1 mice at clinical stage of disease is widely distributed in most brain regions, albeit with lower levels in the hippocampus, amygdala, and hypothalamus. In contrast, most spongiform degeneration is in the thalamus and septum (DeArmond et al., 1997; Moda et al., 2012). Neurodegeneration can be evaluated histologically by various methods (Yamaguchi et al., 2013). For example, neuronal loss could be evaluated in sections from scrapie-infected mice by Nissl stain or with antibodies specific for neuronal markers, such as NeuN. To detect degenerating neurons, brain sections could be silver-stained or labelled with anionic fluorescein derivatives, such as Fluoro-Jade C (Schmued et al., 2005). Neuronal loss in RML-infected mice may be most prevalent in the cerebellum, which contains ~50% of all neurons in an adult mouse brain (as discussed in **Section 4.3**). As the MST1 signaling pathway promotes neuronal death, neurons with higher levels of activated MST1 and cleaved (nuclear) MST1 may also stain preferentially with Fluoro-Jade C.

5.4 Role of dysregulated CaMK4β/CREB and MST1 signaling in scrapie pathogenesis

Further analyses are required to evaluate whether CaMK4β/CREB and MST1 signaling mediate prion disease pathogenesis or is dysregulated as a consequence of it. If the CaMK4β/CREB signaling pathway promotes neuronal survival during prion pathogenesis, then sustained activation of CaMK4β/CREB signaling would be expected to prolong survival of scrapie-infected mice.

Conversely, if neuronal death involves the activation of the MST1 signaling pathway, then inhibition of MST1 signaling would be expected prolong survival of mice infected with scrapie. The return of activated CaMK4β/CREB signaling in scrapie-infected mice to mock-infected levels may result from increased calpain and calcineurin activities (as discussed in **Section 4.3**). Indeed, RML-infected mice treated with the calcineurin inhibitor FK506 at the onset of clinical signs of disease had higher levels of phosphorylated CREB (P-S133) and survived longer than mice treated with vehicle (Mukherjee et al., 2010). I found that the levels of activated CaMK4β (P-T196) and phosphorylated CREB (P-S133) returned to the levels in mock-infected levels by 110 dpi, prior to the onset of clinical disease. Initiating treatment with a calcineurin inhibitor such as FK506 at ~90 dpi after intraperitoneal RML infection of CD1 mice may therefore preserve activated CaMK4β/CREB signaling. Unfortunately, preclinical treatment with FK506 may also impair PrP^{Sc} accumulation and thus confound the interpretation of the potential contribution of CaMK4β/CREB signaling in prion pathogenesis (Nakagaki et al., 2013). Another calcineurin inhibitor, cyclosporin A, has not yet been tested against prion pathogenesis *in vivo*. Cultured pancreatic beta cells treated with FK506 and cyclosporin A resulted in elevated levels of phosphorylated c-Jun, a downstream substrate of DLK/JNK (and potentially MST1) signaling (Oetjen et al., 2006; Plaumann et al., 2008). Although further analyses are required to evaluate whether MST1 signaling in scrapie-infected mice involves DLK/JNK activation, these results suggest that calcineurin inhibition by FK506 or cyclosporin A may stimulate both pro-survival (CaMK4β/CREB) and pro-death (MST1) signaling pathways. The effect of calpain inhibitor treatment on scrapie pathogenesis *in vivo* has not been evaluated either. I found that the levels of total CaMK4β and CREB were reduced to levels in mock-infected mice by 110 dpi. Preclinical

treatment with a calpain inhibitor, starting, for example, at ~90 dpi after intraperitoneal inoculation, could be used to evaluate the role of calpains in CaMK4β/CREB signaling and survival of scrapie-infected mice. While such approaches indirectly evaluate the role of CREB signaling in prion pathogenesis, transgenic mice with sustained or inducible CREB overexpression could be used to directly evaluate CREB signaling. The application of these mice, however, may be limited. Elevated levels of CREB in transgenic mice with inducible CREB overexpression was mostly restricted to the nucleus accumbens and dorsal striatum (Chen et al., 1998), whereas the transcription of CREB-regulated genes was actually impaired in mice with sustained CREB overexpression (Brodie et al., 2004).

The MST1 signaling pathway was activated at 130 dpi, as indicated by elevated levels of activated MST1 (P-T183) and cleaved MST1. A more precise analysis of the temporal changes in MST1 signaling from 110 dpi until terminal stages of disease could evaluate whether activated MST1 signaling occurs prior to or after clinical onset. Such analyses will be critical to better characterize the therapeutic potential of MST1 signal inhibition. Treatment with the small molecule MST1 inhibitor 9E1 inhibited phosphorylation of histone H2B *in vitro* (Anand et al., 2009). Treatment with the inhibitor LP-945706 lowered levels of activated MST1 (P-T183) (Salojin et al., 2014). T183 phosphorylation is not required for MST1 cleavage (Glantschnig et al., 2002; Praskova et al., 2004). Separate inhibition of activated MST1 (P-T183) or cleaved MST1 could evaluate the contribution of each to prion pathogenesis. If activated MST1 signaling was involved in neuronal death and prion pathogenesis, the initiation of treatment with MST1 inhibitors at ~110 dpi after intraperitoneal infection would be expected to reduce neuronal loss and prolong survival. The contribution of MST1 signaling to prion pathogenesis could also be

evaluated using mice lacking MST1 (*Mst1*$^{-/-}$), which exhibit reduced numbers of peripheral naive T cells but are otherwise fertile and develop normally (Zhou et al., 2008; Oh et al., 2009) and have been used to evaluate the role of MST1 signaling in ALS (Lee et al., 2013).

Were further analyses to identify MST1 signaling as critical to prion pathogenesis, it would provide a potential therapeutic target against sporadic prion diseases. Patients with sporadic prion disease are only diagnosed after the onset of clinical symptoms. While such symptoms are the result of previous neuronal loss, further neuronal loss could be inhibited by treatment with a small molecule inhibitor of MST1 signaling. Treatment should be combined with a PrP conversion inhibitor (as described in **Section 1.5.1**) to reduce the levels of PrP^{Sc}. Unfortunately, the early symptoms of sporadic prion disease are non-specific (such as dizziness, fatigue, headaches, incoordination, mood swings, loss of interest). In the absence of an adequate antemortem diagnostic test, diagnosis is often delayed. A retrospective analysis of 97 sCJD patients identified a mean of 7.9 months before diagnosis with 373 alternative diagnoses during that time (Paterson et al., 2012b). Thus, the benefits of effective therapeutics may be restricted by the current delay in diagnosis during which neuronal loss continues. In contrast to patients with sporadic prion disease, those with infectious or genetic prion disease are often identified prior to the onset of clinical signs. In these patients, the application of combined MST1 signaling and PrP conversion inhibitors would have even greater benefit (greater inhibition of neuronal loss).

5.5 Suitability of the kinomics approach to identify signaling pathways dysregulated during prion pathogenesis

The kinomics approach that I developed is dependent on the primary screens to first identify signaling pathways of potential interest. These primary screens used multiplex Western blots for targeted proteomic analyses of protein kinase levels. Although two commercial multiplex Western blot services were available at the time of development (Kinexus Bioinformatics Corporation, Kinetworks; BD Biosciences, Powerblot), the use of such commercial services was not feasible with prion-infected material due to biosafety restrictions. In comparison to these services, my primary screens were also designed to specifically analyze protein kinases with potential roles in prion or other neurodegenerative diseases, or in pathologies associated with prion disease. Moreover, my primary screens were very extensive, evaluating the levels of almost one-third the protein kinases in the mouse (or human) genome. The activation state of any signaling pathways identified from these primary screens are then analyzed using phosphorylation-specific antibodies. Where possible, these analyses evaluated the sites directly phosphorylated by the relevant upstream protein kinases.

Previous kinomic analyses have evaluated for dysregulated signaling using peptide arrays. Although they have yet to be applied to prion disease *in vivo*, peptide arrays have identified signaling pathways differentially induced by PrP^C stimulation with PrP antibody (6H4) or PrP106-126 *in vitro* (Arsenault et al., 2012). At the time this project was designed, however, few peptide arrays were available, and those that were evaluated the activities of only a limited number protein kinases (Peppelenbosch, 2012). The activities of many protein kinases towards the small peptides used in these arrays is similar to that towards their physiological protein substrates (Daigle et al., 2014). However, the degree of this specificity still remains incompletely characterized (Arsenault et

al., 2011). Thus, the results of such peptide arrays are typically validated by Western blot with phosphorylation-specific antibodies. Other previous studies have analyzed limited numbers of protein kinases (c-Abl, Src, Fyn, Yes, Lck, Lyn, Syk, Akt, mTOR, p70S6K, CaMK2α, CDK5, PYK2, PKA, PKC, PKR, PERK, MEK1/2 and MAPKs) and thus characterized the selected signaling pathways only (as described in **Section 3.1**). High-throughput reverse-phase protein arrays can also be used to analyze changes in protein kinase levels (Spurrier et al., 2008). This approach requires highly specific antibodies, however, as cross-reactivity cannot be differentiated from specific signal. In comparison, Western blot analyses can discriminate specific detection from cross-reactivity, as most cross-reacting proteins have different molecular weights than the actual target proteins. Western blot analyses are therefore amenable to analyses of a larger number of proteins than protein arrays with the existing antibodies.

High-throughput gene arrays have identified hundreds of genes expressed differentially during, and a number of cellular processes affected by, prion disease (Booth et al., 2004a; Booth et al., 2004b; Brown et al., 2004; Xiang et al., 2004; Riemer et al., 2004; Brown et al., 2005; Skinner et al., 2006; Sawiris et al., 2007; Xiang et al., 2007; Kim et al., 2008; Sorensen et al., 2008; Hwang et al., 2009; Tang et al., 2009; Tang et al., 2010; Filali et al., 2011; Majer et al., 2012; Barbisin et al., 2014; Herbst et al., 2015). However, only 518 or 540 of the ~30,000 genes in the human or mouse genomes, respectively, encode for protein kinases. Hierarchical clustering of gene array data thus results in very few clusters with multiple protein kinases, impairing the identification of any particular signaling pathway. Moreover, protein kinases are extensively regulated post-transcriptionally and therefore their mRNA levels and activities often do not correspond well (Gygi et al., 1999). Global analyses of changes in miRNA, which may post-

transcriptionally regulate as many as 60% of human genes (Friedman et al., 2009), have also been performed during prion pathogenesis and have identified potentially dysregulated signaling pathways (Saba et al., 2008; Montag et al., 2009; Majer et al., 2012; Boese et al., 2015). However, the biological roles of most miRNAs have yet to be characterized, thus complicating the interpretation of the effects mediated by many identified miRNAs. Despite these limitations, the results from gene and miRNA analyses of mice infected with the same scrapie strain and by the same route of inoculation (CD1 mice intraperitoneally inoculated with scrapie strain RML) (Majer et al., 2012) were consistent with the Western blot analyses that I present here.

5.6 Application of the kinomics approach to other neurodegenerative diseases

The signaling pathways most critical to the pathogenesis of other neurodegenerative diseases also remain poorly characterized. The most prevalent human neurodegenerative disease, Alzheimer's, affects an estimated 28.5 million people in the world (World Health Organization, 2016). Like prion diseases, there are no preventative or therapeutic treatments available against Alzheimer's disease (for review see Folch et al., 2016). However, protein kinases are proposed to participate in Alzheimer's disease pathogenesis. Treatment with the JNK inhibitor SP600125, for example, reduced synapse loss in an Alzheimer's mouse model (Zhou et al., 2015). Synapse loss was also inhibited in an Alzheimer's mouse model by treatment with the Src family kinase inhibitor saracatinib (AZD0350; N-(5-chlorobenzo[d][1,3]dioxol-4-yl)-7-(2-(4-methylpiperazin-1-yl)ethoxy)-5-(tetrahydro-2H-pyran-4-yloxy)quinazolin-4-amine) (Kaufman et al., 2015). Saracatinib and another protein kinase inhibitor, masitinib (AB1010; 4-((4-methylpiperazin-1-yl)methyl)-N-(4-methyl-3-((4-(pyridin-3-yl)-1,3-thiazol-2-yl)amino)phenyl)benzamide), are even

in clinical trials for treatment against Alzheimer's disease (saracatinib [phase 2a], NCT02167256; masitinib [phase 3], NCT01872598) (United States National Institutes of Health, 2016a; United States National Institutes of Health, 2016b). Many of protein kinases with proposed roles in Alzheimer's disease (and other neurodegenerative diseases) are analyzed in my primary kinomic screens (as described in **Section 3.2.1**). The kinomics approach that I developed therefore has the potential to identify novel therapeutic targets against Alzheimer's and other neurodegenerative diseases.

5.7 Limitations of the kinomics approach

The kinomics approach that I developed of course has its limitations. First, the primary screens identify signaling pathways of potential interest using hierarchical clustering and literature and signal transduction database searches. The identification of any potentially dysregulated signaling pathway therefore requires multiple kinases in the pathway to be included in the screen. Most protein kinases included in the screen are involved in well characterized signaling pathways. This approach is therefore unable to detected signaling pathways that are less well characterized, or for which only one or very few kinases are included in the primary screen. The development of more sophisticated platforms for the analyses of kinomic data allows for complimentary or alternative methods of analyses (Trost et al., 2013). Such platforms were at primitive stages of development when I designed the kinomics approach described in this thesis. Second, although dysregulated signaling in chronic conditions often results in, of is the result of, changes in the expression levels of involved proteins, protein kinases are extensively regulated post-translationally. Consequently, the primary screens can only detect signaling pathways regulated mostly post-translationally if the

post-translational regulation is at the level of degradation. Post-translational covalent modifications are more likely to modulate, or differentially affect, acute changes in protein function and less likely to modulate chronic changes. Third, the kinomic approach that I developed evaluates the role of protein dephosphorylation in prion pathogenesis only indirectly. Protein phosphatases are proposed to participate in the pathogenesis of prion and other neurodegenerative diseases (Mukherjee et al., 2010; Braithwaite et al., 2012; Das et al., 2015). The results presented here support a role for calcineurin in dysregulated CaMK4β/CREB signaling during prion pathogenesis. Lastly, the kinomics approach is unable to differentiate signaling pathways dysregulated as a result of disease from those critical in its pathogenesis. This differentiation requires additional analyzes.

5.8 Summary

To summarize, I developed a kinomic approach to identify signaling pathways dysregulated during prion pathogenesis. I discovered that CaMK4β/CREB and MST1 signaling is dysregulated in mice infected with scrapie. The involved protein kinases are targets to further evaluate the roles of CaMK4β/CREB and MST1 signaling in prion pathogenesis.

REFERENCES

Agostinho, P., & Oliveira, C. R. (2003). Involvement of calcineurin in the neurotoxic effects induced by amyloid-beta and prion peptides. *Eur J Neurosci*, *17*(6), 1189-1196.

Aguib, Y., Heiseke, A., Gilch, S., Riemer, C., Baier, M., Schätzl, H. M., & Ertmer, A. (2009). Autophagy induction by trehalose counteracts cellular prion infection. *Autophagy*, *5*(3), 361.

Akhtar, S., Grizenkova, J., Wenborn, A., Hummerich, H., Fernandez de Marco, M., Brandner, S., Collinge, J., & Lloyd, S. E. (2013). Sod1 deficiency reduces incubation time in mouse models of prion disease. *PLoS One*, *8*(1), e54454.

Alais, S., Simoes, S., Baas, D., Lehmann, S., Raposo, G., Darlix, J. L., & Leblanc, P. (2008). Mouse neuroblastoma cells release prion infectivity associated with exosomal vesicles. *Biol Cell*, *100*(10), 603-615.

Alessi, D. R., James, S. R., Downes, C. P., Holmes, A. B., Gaffney, P. R., Reese, C. B., & Cohen, P. (1997). Characterization of a 3-phosphoinositide-dependent protein kinase which phosphorylates and activates protein kinase Balpha. *Curr Biol*, *7*(4), 261-269.

Alevizopoulos, A., Dusserre, Y., Ruegg, U., & Mermod, N. (1997). Regulation of the transforming growth factor beta-responsive transcription factor CTF-1 by calcineurin and calcium/calmodulin-dependent protein kinase IV. *J Biol Chem*, *272*(38), 23597-23605.

Allard, E. K., Grujic, M., Fisone, G., & Kristensson, K. (2013). Prion formation correlates with activation of translation-regulating protein 4E-BP and neuronal transcription factor Elk1. *Neurobiol Dis*, *58*, 116-122.

Alleaume-Butaux, A., Nicot, S., Pietri, M., Baudry, A., Dakowski, C., Tixador, P., Ardila-Osorio, H., Haeberlé, A. M., Bailly, Y., Peyrin, J. M., Launay, J. M., Kellermann, O., & Schneider, B. (2015). Double-Edge Sword of Sustained ROCK Activation in Prion Diseases through Neuritogenesis Defects and Prion Accumulation. *PLoS Pathog*, *11*(8), e1005073.

Allen Institute for Brain Science. Allen Brain Atlas. Retrieved October 25, 2015, from http://www.brain-map.org/.

Alonso, A., Sasin, J., Bottini, N., Friedberg, I., Friedberg, I., Osterman, A., Godzik, A., Hunter, T., Dixon, J., & Mustelin, T. (2004). Protein tyrosine phosphatases in the human genome. *Cell*, *117*(6), 699-711.

Alper, T., Cramp, W. A., Haig, D. A., & Clarke, M. C. (1967). Does the agent of scrapie replicate without nucleic acid? *Nature*, *214*(5090), 764-766.

Alper, T., Haig, D. A., & Clarke, M. C. (1966). The exceptionally small size of the scrapie agent. *Biochem Biophys Res Commun*, *22*(3), 278-284.

Altmeppen, H. C., Prox, J., Krasemann, S., Puig, B., Kruszewski, K., Dohler, F., Bernreuther, C., Hoxha, A., Linsenmeier, L., Sikorska, B., Liberski, P. P., Bartsch, U., Saftig, P., & Glatzel, M. (2015). The sheddase ADAM10 is a potent modulator of prion disease. *Elife*, *4*.

Altmeppen, H. C., Prox, J., Puig, B., Kluth, M. A., Bernreuther, C., Thurm, D., Jorissen, E., Petrowitz, B., Bartsch, U., De Strooper, B., Saftig, P., & Glatzel, M. (2011). Lack of a-disintegrin-and-metalloproteinase ADAM10 leads to intracellular accumulation and loss of shedding of the cellular prion protein in vivo. *Mol Neurodegener*, *6*, 36.

Altomare, D. A., & Testa, J. R. (2005). Perturbations of the AKT signaling pathway in human cancer. *Oncogene*, *24*(50), 7455-7464.

Amici, M., Cecarini, V., Cuccioloni, M., Angeletti, M., Barocci, S., Rossi, G., Fioretti, E., Keller, J. N., & Eleuteri, A. M. (2010). Interplay between 20S proteasomes and prion proteins in scrapie disease. *J Neurosci Res*, *88*(1), 191-201.

Anand, R., Kim, A. Y., Brent, M., & Marmorstein, R. (2008). Biochemical analysis of MST1 kinase: elucidation of a C-terminal regulatory region. *Biochemistry*, *47*(25), 6719-6726.

Anand, R., Maksimoska, J., Pagano, N., Wong, E. Y., Gimotty, P. A., Diamond, S. L., Meggers, E., & Marmorstein, R. (2009). Toward the development of a potent and selective organoruthenium mammalian sterile 20 kinase inhibitor. *J Med Chem*, *52*(6), 1602-1611.

Anderson, L., Rossi, D., Linehan, J., Brandner, S., & Weissmann, C. (2004). Transgene-driven expression of the Doppel protein in Purkinje cells causes Purkinje cell degeneration and motor impairment. *Proc Natl Acad Sci U S A*, *101*(10), 3644-3649.

Ao, H., Ko, S. W., & Zhuo, M. (2006). CREB activity maintains the survival of cingulate cortical pyramidal neurons in the adult mouse brain. *Mol Pain*, *2*, 15.

Apetri, A. C., Surewicz, K., & Surewicz, W. K. (2004). The effect of disease-associated mutations on the folding pathway of human prion protein. *J Biol Chem*, *279*(17), 18008-18014.

Arsenault, R., Griebel, P., & Napper, S. (2011). Peptide arrays for kinome analysis: new opportunities and remaining challenges. *Proteomics*, *11*(24), 4595-4609.

Arsenault, R. J., Li, Y., Potter, A., Griebel, P. J., Kusalik, A., & Napper, S. (2012). Induction of ligand-specific PrP (C) signaling in human neuronal cells. *Prion*, *6*(5), 477-488.

Arumugam, T. V., Cheng, Y. L., Choi, Y., Choi, Y. H., Yang, S., Yun, Y. K., Park, J. S., Yang, D. K., Thundyil, J., Gelderblom, M., Karamyan, V. T., Tang, S. C., Chan, S. L., Magnus, T., Sobey, C. G., & Jo, D. G. (2011). Evidence that gamma-secretase-mediated Notch signaling induces neuronal cell death via the nuclear factor-kappaB-Bcl-2-interacting mediator of cell death pathway in ischemic stroke. *Mol Pharmacol*, *80*(1), 23-31.

Asante, E. A., Linehan, J. M., Desbruslais, M., Joiner, S., Gowland, I., Wood, A. L., Welch, J., Hill, A. F., Lloyd, S. E., Wadsworth, J. D., & Collinge, J. (2002). BSE prions propagate as either variant CJD-like or sporadic CJD-like prion strains in transgenic mice expressing human prion protein. *EMBO J*, *21*(23), 6358-6366.

Asante, E. A., Smidak, M., Grimshaw, A., Houghton, R., Tomlinson, A., Jeelani, A., Jakubcova, T., Hamdan, S., Richard-Londt, A., Linehan, J. M., Brandner, S., Alpers, M., Whitfield, J., Mead, S., Wadsworth, J. D., & Collinge, J. (2015). A naturally occurring variant of the human prion protein completely prevents prion disease. *Nature*, *522*(7557), 478-481.

Asuni, A. A., Gray, B., Bailey, J., Skipp, P., Perry, V. H., & O'Connor, V. (2014). Analysis of the hippocampal proteome in ME7 prion disease reveals a predominant astrocytic signature and highlights the brain-restricted production of clusterin in chronic neurodegeneration. *J Biol Chem*, *289*(7), 4532-4545.

Atarashi, R., Satoh, K., Sano, K., Fuse, T., Yamaguchi, N., Ishibashi, D., Matsubara, T., Nakagaki, T., Yamanaka, H., Shirabe, S., Yamada, M., Mizusawa, H., Kitamoto, T., Klug, G., McGlade, A., Collins, S. J., & Nishida, N. (2011). Ultrasensitive human prion detection in cerebrospinal fluid by real-time quaking-induced conversion. *Nat Med*, *17*(2), 175-178.

Bachy, V., Ballerini, C., Gourdain, P., Prignon, A., Iken, S., Antoine, N., Rosset, M., & Carnaud, C. (2010). Mouse vaccination with dendritic cells loaded with prion protein peptides overcomes tolerance and delays scrapie. *J Gen Virol*, *91*(Pt 3), 809-820.

Bade, S., Baier, M., Boetel, T., & Frey, A. (2006). Intranasal immunization of Balb/c mice against prion protein attenuates orally acquired transmissible spongiform encephalopathy. *Vaccine*, *24*(9), 1242-1253.

Baeten, L. A., Powers, B. E., Jewell, J. E., Spraker, T. R., & Miller, M. W. (2007). A natural case of chronic wasting disease in a free-ranging moose (Alces alces shirasi). *J Wildl Dis*, *43*(2), 309-314.

Bailly, Y., Haeberle, A. M., Blanquet-Grossard, F., Chasserot-Golaz, S., Grant, N., Schulze, T., Bombarde, G., Grassi, J., Cesbron, J. Y., & Lemaire-Vieille, C. (2004). Prion protein (PrPc) immunocytochemistry and expression of the green fluorescent protein reporter gene under control of the bovine PrP gene promoter in the mouse brain. *J Comp Neurol*, *473*(2), 244-269.

Baldauf, E., Beekes, M., & Diringer, H. (1997). Evidence for an alternative direct route of access for the scrapie agent to the brain bypassing the spinal cord. *J Gen Virol*, *78*(Pt 5), 1187-1197.

Bamborough, P. (2012). System-based drug discovery within the human kinome. *Expert Opin Drug Discov*, *7*(11), 1053-1070.

Barbisin, M., Vanni, S., Schmädicke, A. C., Montag, J., Motzkus, D., Opitz, L., Salinas-Riester, G., & Legname, G. (2014). Gene expression profiling of brains from bovine spongiform encephalopathy (BSE)-infected cynomolgus macaques. *BMC Genomics*, *15*, 434.

Barmada, S., Piccardo, P., Yamaguchi, K., Ghetti, B., & Harris, D. A. (2004). GFP-tagged prion protein is correctly localized and functionally active in the brains of transgenic mice. *Neurobiol Dis*, *16*(3), 527-537.

Barria, M. A., Balachandran, A., Morita, M., Kitamoto, T., Barron, R., Manson, J., Knight, R., Ironside, J. W., & Head, M. W. (2014). Molecular barriers to zoonotic transmission of prions. *Emerg Infect Dis*, *20*(1), 88-97.

Bate, C., Salmona, M., Diomede, L., & Williams, A. (2004). Squalestatin cures prion-infected neurons and protects against prion neurotoxicity. *J Biol Chem*, *279*(15), 14983-14990.

Batista, L. F., Kaina, B., Meneghini, R., & Menck, C. F. (2009). How DNA lesions are turned into powerful killing structures: insights from UV-induced apoptosis. *Mutat Res*, *681*(2-3), 197-208.

Baumann, F., Pahnke, J., Radovanovic, I., Rulicke, T., Bremer, J., Tolnay, M., & Aguzzi, A. (2009). Functionally relevant domains of the prion protein identified in vivo. *PLoS One*, *4*(9), e6707.

Baumann, F., Tolnay, M., Brabeck, C., Pahnke, J., Kloz, U., Niemann, H. H., Heikenwalder, M., Rulicke, T., Burkle, A., & Aguzzi, A. (2007). Lethal recessive myelin toxicity of prion protein lacking its central domain. *EMBO J*, *26*(2), 538-547.

Behrens, A., Genoud, N., Naumann, H., Rülicke, T., Janett, F., Heppner, F. L., Ledermann, B., & Aguzzi, A. (2002). Absence of the prion protein homologue Doppel causes male sterility. *EMBO J*, *21*(14), 3652-3658.

Belay, E. D., Maddox, R. A., Williams, E. S., Miller, M. W., Gambetti, P., & Schonberger, L. B. (2004). Chronic wasting disease and potential transmission to humans. *Emerg Infect Dis*, *10*(6), 977-984.

Belichenko, P. V., Brown, D., Jeffrey, M., & Fraser, J. R. (2000). Dendritic and synaptic alterations of hippocampal pyramidal neurones in scrapie-infected mice. *Neuropathol Appl Neurobiol*, *26*(2), 143-149.

Bell, K. F., Bent, R. J., Meese-Tamuri, S., Ali, A., Forder, J. P., & Aarts, M. M. (2013). Calmodulin kinase IV-dependent CREB activation is required for neuroprotection via NMDA receptor-PSD95 disruption. *J Neurochem*, *126*(2), 274-287.

Bellinger-Kawahara, C., Cleaver, J. E., Diener, T. O., & Prusiner, S. B. (1987a). Purified scrapie prions resist inactivation by UV irradiation. *J Virol*, *61*(1), 159-166.

Bellinger-Kawahara, C., Diener, T. O., McKinley, M. P., Groth, D. F., Smith, D. R., & Prusiner, S. B. (1987b). Purified scrapie prions resist inactivation by procedures that hydrolyze, modify, or shear nucleic acids. *Virology*, *160*(1), 271-274.

Bendheim, P. E., Barry, R. A., DeArmond, S. J., Stites, D. P., & Prusiner, S. B. (1984). Antibodies to a scrapie prion protein. *Nature*, *310*(5976), 418-421.

Bendheim, P. E., Brown, H. R., Rudelli, R. D., Scala, L. J., Goller, N. L., Wen, G. Y., Kascsak, R. J., Cashman, N. R., & Bolton, D. C. (1992). Nearly ubiquitous tissue distribution of the scrapie agent precursor protein. *Neurology*, *42*(1), 149-156.

Benito-Leon, J. (2004). Combined quinacrine and chlorpromazine therapy in fatal familial insomnia. *Clin Neuropharmacol*, *27*(4), 201-203.

Benvegnù, S., Roncaglia, P., Agostini, F., Casalone, C., Corona, C., Gustincich, S., & Legname, G. (2011). Developmental influence of the cellular prion protein on the gene expression profile in mouse hippocampus. *Physiol Genomics*, *43*(12), 711-725.

Bergström, A. L., Cordes, H., Zsurger, N., Heegaard, P. M., Laursen, H., & Chabry, J. (2005). Amidation and structure relaxation abolish the neurotoxicity of the prion peptide PrP106-126 in vivo and in vitro. *J Biol Chem*, *280*(24), 23114-23121.

Bernoulli, C., Siegfried, J., Baumgartner, G., Regli, F., Rabinowicz, T., Gajdusek, D. C., & Gibbs, C. J. J. (1977). Danger of accidental person-to-person transmission of Creutzfeldt-Jakob disease by surgery. *Lancet*, *1*(8009), 478-479.

Berry, D. B., Lu, D., Geva, M., Watts, J. C., Bhardwaj, S., Oehler, A., Renslo, A. R., DeArmond, S. J., Prusiner, S. B., & Giles, K. (2013). Drug resistance confounding prion therapeutics. *Proc Natl Acad Sci U S A*, *110*(44), E4160-9.

Bessen, R. A., Kocisko, D. A., Raymond, G. J., Nandan, S., Lansbury, P. T., & Caughey, B. (1995). Non-genetic propagation of strain-specific properties of scrapie prion protein. *Nature*, *375*(6533), 698-700.

Bessen, R. A., & Marsh, R. F. (1992a). Biochemical and physical properties of the prion protein from two strains of the transmissible mink encephalopathy agent. *J Virol*, *66*(4), 2096-2101.

Bessen, R. A., & Marsh, R. F. (1992b). Identification of two biologically distinct strains of transmissible mink encephalopathy in hamsters. *J Gen Virol*, *73*(Pt 2), 329-334.

Bessen, R. A., & Marsh, R. F. (1994). Distinct PrP properties suggest the molecular basis of strain variation in transmissible mink encephalopathy. *J Virol*, *68*(12), 7859-7868.

Betmouni, S., & Perry, V. H. (1999). The acute inflammatory response in CNS following injection of prion brain homogenate or normal brain homogenate. *Neuropathol Appl Neurobiol*, *25*(1), 20-28.

Bi, W., Xiao, L., Jia, Y., Wu, J., Xie, Q., Ren, J., Ji, G., & Yuan, Z. (2010). c-Jun N-terminal kinase enhances MST1-mediated pro-apoptotic signaling through phosphorylation at serine 82. *J Biol Chem*, *285*(9), 6259-6264.

Bian, J., Kang, H. E., & Telling, G. C. (2014). Quinacrine promotes replication and conformational mutation of chronic wasting disease prions. *Proc Natl Acad Sci U S A*, *111*(16), 6028-6033.

Biasini, E., Unterberger, U., Solomon, I. H., Massignan, T., Senatore, A., Bian, H., Voigtlaender, T., Bowman, F. P., Bonetto, V., Chiesa, R., Luebke, J., Toselli, P., & Harris, D. A. (2013). A mutant prion protein sensitizes neurons to glutamate-induced excitotoxicity. *J Neurosci*, *33*(6), 2408-2418.

BioSeeker Group. Protein Kinase Inhibitors in Oncology Drug Pipeline - Update 2016. Retrieved September 28, 2016, from http://www.researchandmarkets.com/reports/1196697/protein_kinase_inhibitors_in_oncology_drug.

Bito, H., Deisseroth, K., & Tsien, R. W. (1996). CREB phosphorylation and dephosphorylation: a Ca(2+)- and stimulus duration-dependent switch for hippocampal gene expression. *Cell*, *87*(7), 1203-1214.

Blom, J. M., Tascedda, F., Carra, S., Ferraguti, C., Barden, N., & Brunello, N. (2002). Altered regulation of CREB by chronic antidepressant administration in the brain of transgenic mice with impaired glucocorticoid receptor function. *Neuropsychopharmacology*, *26*(5), 605-614.

Boche, D., Cunningham, C., Docagne, F., Scott, H., & Perry, V. H. (2006). TGFbeta1 regulates the inflammatory response during chronic neurodegeneration. *Neurobiol Dis*, *22*(3), 638-650.

Boddaert, J., Kinugawa, K., Lambert, J. C., Boukhtouche, F., Zoll, J., Merval, R., Blanc-Brude, O., Mann, D., Berr, C., Vilar, J., Garabedian, B., Journiac, N., Charue, D., Silvestre, J. S., Duyckaerts, C., Amouyel, P., Mariani, J., Tedgui, A., & Mallat, Z. (2007). Evidence of a role for lactadherin in Alzheimer's disease. *Am J Pathol*, *170*(3), 921-929.

Boellaard, J. W., Kao, M., Schlote, W., & Diringer, H. (1991). Neuronal autophagy in experimental scrapie. *Acta Neuropathol*, *82*(3), 225-228.

Boellaard, J. W., Schlote, W., & Tateishi, J. (1989). Neuronal autophagy in experimental Creutzfeldt-Jakob's disease. *Acta Neuropathol*, *78*(4), 410-418.

Boese, A. S., Saba, R., Campbell, K., Majer, A., Medina, S., Burton, L., Booth, T. F., Chong, P., Westmacott, G., Dutta, S. M., Saba, J. A., & Booth, S. A. (2015). MicroRNA abundance is altered in synaptoneurosomes during prion disease. *Mol Cell Neurosci*, *71*, 13-24.

Bolton, D. C., McKinley, M. P., & Prusiner, S. B. (1982). Identification of a protein that purifies with the scrapie prion. *Science*, *218*(4579), 1309-1311.

Bone, I., Belton, L., Walker, A. S., & Darbyshire, J. (2008). Intraventricular pentosan polysulphate in human prion diseases: an observational study in the UK. *Eur J Neurol*, *15*(5), 458-464.

Booth, S., Bowman, C., Baumgartner, R., Dolenko, B., Sorensen, G., Robertson, C., Coulthart, M., Phillipson, C., & Somorjai, R. (2004a). Molecular classification of scrapie strains in mice using gene expression profiling. *Biochem Biophys Res Commun*, *325*(4), 1339-1345.

Booth, S., Bowman, C., Baumgartner, R., Sorensen, G., Robertson, C., Coulthart, M., Phillipson, C., & Somorjai, R. L. (2004b). Identification of central nervous system genes involved in the host response to the scrapie agent during preclinical and clinical infection. *J Gen Virol*, *85*(Pt 11), 3459-3471.

Borchelt, D. R., Rogers, M., Stahl, N., Telling, G., & Prusiner, S. B. (1993). Release of the cellular prion protein from cultured cells after loss of its glycoinositol phospholipid anchor. *Glycobiology*, *3*(4), 319-329.

Borchelt, D. R., Scott, M., Taraboulos, A., Stahl, N., & Prusiner, S. B. (1990). Scrapie and cellular prion proteins differ in their kinetics of synthesis and topology in cultured cells. *J Cell Biol*, *110*(3), 743-752.

Borchelt, D. R., Taraboulos, A., & Prusiner, S. B. (1992). Evidence for synthesis of scrapie prion proteins in the endocytic pathway. *J Biol Chem*, *267*(23), 16188-16199.

Bouybayoune, I., Mantovani, S., Del Gallo, F., Bertani, I., Restelli, E., Comerio, L., Tapella, L., Baracchi, F., Fernández-Borges, N., Mangieri, M., Bisighini, C., Beznoussenko, G. V., Paladini, A., Balducci, C., Micotti, E., Forloni, G., Castilla, J., Fiordaliso, F., Tagliavini, F., Imeri, L., & Chiesa, R. (2015). Transgenic fatal familial insomnia mice indicate prion infectivity-independent mechanisms of pathogenesis and phenotypic expression of disease. *PLoS Pathog*, *11*(4), e1004796.

Braithwaite, S. P., Stock, J. B., Lombroso, P. J., & Nairn, A. C. (2012). Protein phosphatases and Alzheimer's disease. *Prog Mol Biol Transl Sci*, *106*, 343-379.

Brandner, S., Isenmann, S., Raeber, A., Fischer, M., Sailer, A., Kobayashi, Y., Marino, S., Weissmann, C., & Aguzzi, A. (1996). Normal host prion protein necessary for scrapie-induced neurotoxicity. *Nature*, *379*(6563), 339-343.

Bremer, J., Baumann, F., Tiberi, C., Wessig, C., Fischer, H., Schwarz, P., Steele, A. D., Toyka, K. V., Nave, K. A., Weis, J., & Aguzzi, A. (2010). Axonal prion protein is required for peripheral myelin maintenance. *Nat Neurosci*, *13*(3), 310-318.

Brodie, C. R., Khaliq, M., Yin, J. C., Brent Clark, H., Orr, H. T., & Boland, L. M. (2004). Overexpression of CREB reduces CRE-mediated transcription: behavioral and cellular analyses in transgenic mice. *Mol Cell Neurosci*, *25*(4), 602-611.

Brown, A. R., Rebus, S., McKimmie, C. S., Robertson, K., Williams, A., & Fazakerley, J. K. (2005). Gene expression profiling of the preclinical scrapie-infected hippocampus. *Biochem Biophys Res Commun*, *334*(1), 86-95.

Brown, A. R., Webb, J., Rebus, S., Williams, A., & Fazakerley, J. K. (2004). Identification of up-regulated genes by array analysis in scrapie-infected mouse brains. *Neuropathol Appl Neurobiol*, *30*(5), 555-567.

Brown, D., Belichenko, P., Sales, J., Jeffrey, M., & Fraser, J. R. (2001). Early loss of dendritic spines in murine scrapie revealed by confocal analysis. *Neuroreport*, *12*(1), 179-183.

Brown, D. A., & Rose, J. K. (1992). Sorting of GPI-anchored proteins to glycolipid-enriched membrane subdomains during transport to the apical cell surface. *Cell*, *68*(3), 533-544.

Brown, D. R., Herms, J., & Kretzschmar, H. A. (1994a). Mouse cortical cells lacking cellular PrP survive in culture with a neurotoxic PrP fragment. *Neuroreport*, *5*(16), 2057-2060.

Brown, D. R., Schmidt, B., & Kretzschmar, H. A. (1996). Role of microglia and host prion protein in neurotoxicity of a prion protein fragment. *Nature*, *380*(6572), 345-347.

Brown, P., Cathala, F., Raubertas, R. F., Gajdusek, D. C., & Castaigne, P. (1987). The epidemiology of Creutzfeldt-Jakob disease: conclusion of a 15-year investigation in France and review of the world literature. *Neurology*, *37*(6), 895-904.

Brown, P., Gibbs, C. J. J., Rodgers-Johnson, P., Asher, D. M., Sulima, M. P., Bacote, A., Goldfarb, L. G., & Gajdusek, D. C. (1994b). Human spongiform encephalopathy: the National Institutes of Health series of 300 cases of experimentally transmitted disease. *Ann Neurol*, *35*(5), 513-529.

Bruce, M. E., McConnell, I., Fraser, H., & Dickinson, A. G. (1991). The disease characteristics of different strains of scrapie in Sinc congenic mouse lines: implications for the nature of the agent and host control of pathogenesis. *J Gen Virol*, *72*(Pt 3), 595-603.

Bruce, M. E., Will, R. G., Ironside, J. W., McConnell, I., Drummond, D., Suttie, A., McCardle, L., Chree, A., Hope, J., Birkett, C., Cousens, S., Fraser, H., & Bostock, C. J. (1997). Transmissions to mice indicate that 'new variant' CJD is caused by the BSE agent. *Nature*, *389*(6650), 498-501.

Brunet, A., Bonni, A., Zigmond, M. J., Lin, M. Z., Juo, P., Hu, L. S., Anderson, M. J., Arden, K. C., Blenis, J., & Greenberg, M. E. (1999). Akt promotes cell survival by phosphorylating and inhibiting a Forkhead transcription factor. *Cell*, *96*(6), 857-868.

Bueler, H., Aguzzi, A., Sailer, A., Greiner, R. A., Autenried, P., Aguet, M., & Weissmann, C. (1993). Mice devoid of PrP are resistant to scrapie. *Cell*, *73*(7), 1339-1347.

Bueler, H., Fischer, M., Lang, Y., Bluethmann, H., Lipp, H. P., DeArmond, S. J., Prusiner, S. B., Aguet, M., & Weissmann, C. (1992). Normal development and behaviour of mice lacking the neuronal cell-surface PrP protein. *Nature*, *356*(6370), 577-582.

Büeler, H., Raeber, A., Sailer, A., Fischer, M., Aguzzi, A., & Weissmann, C. (1994). High prion and PrP^{Sc} levels but delayed onset of disease in scrapie-inoculated mice heterozygous for a disrupted PrP gene. *Mol Med*, *1*(1), 19-30.

Burnett, P. E., Barrow, R. K., Cohen, N. A., Snyder, S. H., & Sabatini, D. M. (1998). RAFT1 phosphorylation of the translational regulators p70 S6 kinase and 4E-BP1. *Proc Natl Acad Sci U S A*, *95*(4), 1432-1437.

Caenepeel, S., Charydczak, G., Sudarsanam, S., Hunter, T., & Manning, G. (2004). The mouse kinome: discovery and comparative genomics of all mouse protein kinases. *Proc Natl Acad Sci U S A*, *101*(32), 11707-11712.

Caetano, F. A., Lopes, M. H., Hajj, G. N., Machado, C. F., Pinto Arantes, C., Magalhaes, A. C., Vieira Mde, P., Americo, T. A., Massensini, A. R., Priola, S. A., Vorberg, I., Gomez, M. V., Linden, R., Prado, V. F., Martins, V. R., & Prado, M. A. (2008). Endocytosis of prion protein is required for ERK1/2 signaling induced by stress-inducible protein 1. *J Neurosci*, *28*(26), 6691-6702.

Cancellotti, E., Wiseman, F., Tuzi, N. L., Baybutt, H., Monaghan, P., Aitchison, L., Simpson, J., & Manson, J. C. (2005). Altered glycosylated PrP proteins can have different neuronal trafficking in brain but do not acquire scrapie-like properties. *J Biol Chem*, *280*(52), 42909-42918.

Carimalo, J., Cronier, S., Petit, G., Peyrin, J. M., Boukhtouche, F., Arbez, N., Lemaigre-Dubreuil, Y., Brugg, B., & Miquel, M. C. (2005). Activation of the JNK-c-Jun pathway during the early phase of neuronal apoptosis induced by PrP106-126 and prion infection. *Eur J Neurosci*, *21*(9), 2311-2319.

Carriba, P., Pardo, L., Parra-Damas, A., Lichtenstein, M. P., Saura, C. A., Pujol, A., Masgrau, R., & Galea, E. (2012). ATP and noradrenaline activate CREB in astrocytes via noncanonical Ca(2+) and cyclic AMP independent pathways. *Glia*, *60*(9), 1330-1344.

Carroll, J. A., Striebel, J. F., Race, B., Phillips, K., & Chesebro, B. (2015). Prion infection of mouse brain reveals multiple new upregulated genes involved in neuroinflammation or signal transduction. *J Virol*, *89*(4), 2388-2404.

Cassard, H., Torres, J. M., Lacroux, C., Douet, J. Y., Benestad, S. L., Lantier, F., Lugan, S., Lantier, I., Costes, P., Aron, N., Reine, F., Herzog, L., Espinosa, J. C., Beringue, V., & Andréoletti, O. (2014). Evidence for zoonotic potential of ovine scrapie prions. *Nat Commun*, *5*, 5821.

Castilla, J., Morales, R., Saá, P., Barria, M., Gambetti, P., & Soto, C. (2008). Cell-free propagation of prion strains. *EMBO J*, *27*(19), 2557-2566.

Castilla, J., Saa, P., Hetz, C., & Soto, C. (2005). In vitro generation of infectious scrapie prions. *Cell*, *121*(2), 195-206.

Caughey, B., Race, R. E., Ernst, D., Buchmeier, M. J., & Chesebro, B. (1989). Prion protein biosynthesis in scrapie-infected and uninfected neuroblastoma cells. *J Virol*, *63*(1), 175-181.

Caughey, B., & Raymond, G. J. (1991a). The scrapie-associated form of PrP is made from a cell surface precursor that is both protease- and phospholipase-sensitive. *J Biol Chem*, *266*(27), 18217-18223.

Caughey, B., Raymond, G. J., & Bessen, R. A. (1998). Strain-dependent differences in beta-sheet conformations of abnormal prion protein. *J Biol Chem*, *273*(48), 32230-32235.

Caughey, B., Raymond, G. J., Ernst, D., & Race, R. E. (1991b). N-terminal truncation of the scrapie-associated form of PrP by lysosomal protease(s): implications regarding the site of conversion of PrP to the protease-resistant state. *J Virol*, *65*(12), 6597-6603.

Caughey, B. W., Dong, A., Bhat, K. S., Ernst, D., Hayes, S. F., & Caughey, W. S. (1991c). Secondary structure analysis of the scrapie-associated protein PrP 27-30 in water by infrared spectroscopy. *Biochemistry*, *30*(31), 7672-7680.

Cell Signaling Technology. Kinase-Disease Associations. Retrieved October 25, 2015, from http://www.cellsignal.com/common/content/content.jsp?id=science-tables-kinase-disease.

Chabry, J., Priola, S. A., Wehrly, K., Nishio, J., Hope, J., & Chesebro, B. (1999). Species-independent inhibition of abnormal prion protein (PrP) formation by a peptide containing a conserved PrP sequence. *J Virol*, *73*(8), 6245-6250.

Chabry, J., Ratsimanohatra, C., Sponne, I., Elena, P. P., Vincent, J. P., & Pillot, T. (2003). In vivo and in vitro neurotoxicity of the human prion protein (PrP) fragment P118-135 independently of PrP expression. *J Neurosci*, *23*(2), 462-469.

Chandler, R. L. (1961). Encephalopathy in mice produced by inoculation with scrapie brain material. *Lancet*, *1*(7191), 1378-1379.

Chatila, T., Anderson, K. A., Ho, N., & Means, A. R. (1996). A unique phosphorylation-dependent mechanism for the activation of Ca2+/calmodulin-dependent protein kinase type IV/GR. *J Biol Chem*, *271*(35), 21542-21548.

Chattopadhyay, M., Walter, E. D., Newell, D. J., Jackson, P. J., Aronoff-Spencer, E., Peisach, J., Gerfen, G. J., Bennett, B., Antholine, W. E., & Millhauser, G. L. (2005). The octarepeat domain of the prion protein binds Cu(II) with three distinct coordination modes at pH 7.4. *J Am Chem Soc*, *127*(36), 12647-12656.

Chen, B., Thompson, M., Louth, J., & Guo, K. (2013). Prion chemical biology: on the road to therapeutics? *Curr Top Med Chem*, *13*(19), 2441-2464.

Chen, B., Wang, J. F., Hill, B. C., & Young, L. T. (1999). Lithium and valproate differentially regulate brain regional expression of phosphorylated CREB and c-Fos. *Brain Res Mol Brain Res*, *70*(1), 45-53.

Chen, C. C., & Wang, Y. H. (2014). Estimation of the exposure of the UK population to the bovine spongiform encephalopathy agent through dietary intake during the period 1980 to 1996. *PLoS One*, *9*(4), e94020.

Chen, J., Kelz, M. B., Zeng, G., Sakai, N., Steffen, C., Shockett, P. E., Picciotto, M. R., Duman, R. S., & Nestler, E. J. (1998). Transgenic animals with inducible, targeted gene expression in brain. *Mol Pharmacol*, *54*(3), 495-503.

Chen, S. G., Teplow, D. B., Parchi, P., Teller, J. K., Gambetti, P., & Autilio-Gambetti, L. (1995). Truncated forms of the human prion protein in normal brain and in prion diseases. *J Biol Chem*, *270*(32), 19173-19180.

Chesebro, B., Race, R., Wehrly, K., Nishio, J., Bloom, M., Lechner, D., Bergstrom, S., Robbins, K., Mayer, L., Keith, J. M., & et, A. (1985). Identification of scrapie prion protein-specific mRNA in scrapie-infected and uninfected brain. *Nature*, *315*(6017), 331-333.

Chesebro, B., Trifilo, M., Race, R., Meade-White, K., Teng, C., LaCasse, R., Raymond, L., Favara, C., Baron, G., Priola, S., Caughey, B., Masliah, E., & Oldstone, M. (2005). Anchorless prion protein results in infectious amyloid disease without clinical scrapie. *Science*, *308*(5727), 1435-1439.

Cheung, W. L., Ajiro, K., Samejima, K., Kloc, M., Cheung, P., Mizzen, C. A., Beeser, A., Etkin, L. D., Chernoff, J., Earnshaw, W. C., & Allis, C. D. (2003). Apoptotic phosphorylation of histone H2B is mediated by mammalian sterile twenty kinase. *Cell*, *113*(4), 507-517.

Chianini, F., Fernandez-Borges, N., Vidal, E., Gibbard, L., Pintado, B., de Castro, J., Priola, S. A., Hamilton, S., Eaton, S. L., Finlayson, J., Pang, Y., Steele, P., Reid, H. W., Dagleish, M. P., & Castilla, J. (2012). Rabbits are not resistant to prion infection. *Proc Natl Acad Sci U S A*, *109*(13), 5080-5085.

Chiarini, L. B., Freitas, A. R., Zanata, S. M., Brentani, R. R., Martins, V. R., & Linden, R. (2002). Cellular prion protein transduces neuroprotective signals. *EMBO J*, *21*(13), 3317-3326.

Chiesa, R., Piccardo, P., Ghetti, B., & Harris, D. A. (1998). Neurological illness in transgenic mice expressing a prion protein with an insertional mutation. *Neuron*, *21*(6), 1339-1351.

Cho, H. J. (1980). Requirement of a protein component for scrapie infectivity. *Intervirology*, *14*(3-4), 213-216.

Colby, D. W., Giles, K., Legname, G., Wille, H., Baskakov, I. V., DeArmond, S. J., & Prusiner, S. B. (2009). Design and construction of diverse mammalian prion strains. *Proc Natl Acad Sci U S A*, *106*(48), 20417-20422.

Colby, D. W., & Prusiner, S. B. (2011). Prions. *Cold Spring Harb Perspect Biol*, *3*(1), a006833.

Colby, D. W., Wain, R., Baskakov, I. V., Legname, G., Palmer, C. G., Nguyen, H. O., Lemus, A., Cohen, F. E., DeArmond, S. J., & Prusiner, S. B. (2010). Protease-sensitive synthetic prions. *PLoS Pathog*, *6*(1), e1000736.

Cole, S., & Kimberlin, R. H. (1985). Pathogenesis of mouse scrapie: dynamics of vacuolation in brain and spinal cord after intraperitoneal infection. *Neuropathol Appl Neurobiol*, *11*(3), 213-227.

Collinge, J. (1999). Variant Creutzfeldt-Jakob disease. *Lancet*, *354*(9175), 317-323.

Collinge, J., & Clarke, A. R. (2007). A general model of prion strains and their pathogenicity. *Science*, *318*(5852), 930-936.

Collinge, J., Gorham, M., Hudson, F., Kennedy, A., Keogh, G., Pal, S., Rossor, M., Rudge, P., Siddique, D., Spyer, M., Thomas, D., Walker, S., Webb, T., Wroe, S., & Darbyshire, J. (2009). Safety and efficacy of quinacrine in human prion disease (PRION-1 study): a patient-preference trial. *Lancet Neurol*, *8*(4), 334-344.

Collinge, J., Palmer, M. S., & Dryden, A. J. (1991). Genetic predisposition to iatrogenic Creutzfeldt-Jakob disease. *Lancet*, *337*(8755), 1441-1442.

Collinge, J., Palmer, M. S., Sidle, K. C., Gowland, I., Medori, R., Ironside, J., & Lantos, P. (1995a). Transmission of fatal familial insomnia to laboratory animals. *Lancet*, *346*(8974), 569.

Collinge, J., Palmer, M. S., Sidle, K. C., Hill, A. F., Gowland, I., Meads, J., Asante, E., Bradley, R., Doey, L. J., & Lantos, P. L. (1995b). Unaltered susceptibility to BSE in transgenic mice expressing human prion protein. *Nature*, *378*(6559), 779-783.

Collinge, J., Sidle, K. C., Meads, J., Ironside, J., & Hill, A. F. (1996). Molecular analysis of prion strain variation and the aetiology of 'new variant' CJD. *Nature*, *383*(6602), 685-690.

Collinge, J., Whitfield, J., McKintosh, E., Frosh, A., Mead, S., Hill, A. F., Brandner, S., Thomas, D., & Alpers, M. P. (2008). A clinical study of kuru patients with long incubation periods at the end of the epidemic in Papua New Guinea. *Philos Trans R Soc Lond B Biol Sci*, *363*(1510), 3725-3739.

Combs, C. K., Johnson, D. E., Cannady, S. B., Lehman, T. M., & Landreth, G. E. (1999). Identification of microglial signal transduction pathways mediating a neurotoxic response to amyloidogenic fragments of beta-amyloid and prion proteins. *J Neurosci*, *19*(3), 928-939.

Comoy, E. E., Mikol, J., Luccantoni-Freire, S., Correia, E., Lescoutra-Etchegaray, N., Durand, V., Dehen, C., Andreoletti, O., Casalone, C., Richt, J. A., Greenlee, J. J., Baron, T., Benestad, S. L., Brown, P., & Deslys, J. P. (2015). Transmission of scrapie prions to primate after an extended silent incubation period. *Sci Rep*, *5*, 11573.

Cooney, S. J., Bermudez-Sabogal, S. L., & Byrnes, K. R. (2013). Cellular and temporal expression of NADPH oxidase (NOX) isotypes after brain injury. *J Neuroinflammation*, *10*, 155.

Copp, J., Manning, G., & Hunter, T. (2009). TORC-specific phosphorylation of mammalian target of rapamycin (mTOR): phospho-Ser2481 is a marker for intact mTOR signaling complex 2. *Cancer Res*, *69*(5), 1821-1827.

Corsaro, A., Thellung, S., Villa, V., Principe, D. R., Paludi, D., Arena, S., Millo, E., Schettini, D., Damonte, G., Aceto, A., Schettini, G., & Florio, T. (2003). Prion protein fragment 106-126 induces a p38 MAP kinase-dependent apoptosis in SH-SY5Y neuroblastoma cells independently from the amyloid fibril formation. *Ann N Y Acad Sci*, *1010*, 610-622.

Cortes, C. J., Qin, K., Cook, J., Solanki, A., & Mastrianni, J. A. (2012). Rapamycin delays disease onset and prevents PrP plaque deposition in a mouse model of Gerstmann-Sträussler-Scheinker disease. *J Neurosci*, *32*(36), 12396-12405.

Crecelius, A. C., Helmstetter, D., Strangmann, J., Mitteregger, G., Fröhlich, T., Arnold, G. J., & Kretzschmar, H. A. (2008). The brain proteome profile is highly conserved between Prnp-/- and Prnp+/+ mice. *Neuroreport*, *19*(10), 1027-1031.

Cuadrado, A., Molloy, C. J., & Pech, M. (1990). Expression of protein kinase CI in NIH 3T3 cells increases its growth response to specific activators. *FEBS Lett*, *260*(2), 281-284.

Cuillé, J., & Chelle, P.-L. (1936). La maladie dite tremblante du mouton est-elle inoculable. *CR Acad Sci*, *203*, 1552-1554.

Cunningham, C., Boche, D., & Perry, V. H. (2002). Transforming growth factor beta1, the dominant cytokine in murine prion disease: influence on inflammatory cytokine synthesis and alteration of vascular extracellular matrix. *Neuropathol Appl Neurobiol*, *28*(2), 107-119.

Czymai, T., Viemann, D., Sticht, C., Molema, G., Goebeler, M., & Schmidt, M. (2010). FOXO3 modulates endothelial gene expression and function by classical and alternative mechanisms. *J Biol Chem*, *285*(14), 10163-10178.

Daigle, J., Van Wyk, B., Trost, B., Scruten, E., Arsenault, R., Kusalik, A., Griebel, P. J., & Napper, S. (2014). Peptide Arrays for Kinome Analysis of Livestock Species. *Front Vet Sci*, *1*, 4.

Dalby, K. N., Morrice, N., Caudwell, F. B., Avruch, J., & Cohen, P. (1998). Identification of regulatory phosphorylation sites in mitogen-activated protein kinase (MAPK)-activated protein kinase-1a/p90rsk that are inducible by MAPK. *J Biol Chem*, *273*(3), 1496-1505.

Dametto, P., Lakkaraju, A. K., Bridel, C., Villiger, L., O'Connor, T., Herrmann, U. S., Pelczar, P., Rülicke, T., McHugh, D., Adili, A., & Aguzzi, A. (2015). Neurodegeneration and unfolded-protein response in mice expressing a membrane-tethered flexible tail of PrP. *PLoS One*, *10*(2), e0117412.

Das, I., Krzyzosiak, A., Schneider, K., Wrabetz, L., D'Antonio, M., Barry, N., Sigurdardottir, A., & Bertolotti, A. (2015). Preventing proteostasis diseases by selective inhibition of a phosphatase regulatory subunit. *Science*, *348*(6231), 239-242.

Daude, N., Marella, M., & Chabry, J. (2003). Specific inhibition of pathological prion protein accumulation by small interfering RNAs. *J Cell Sci*, *116*(Pt 13), 2775-2779.

Daude, N., Wohlgemuth, S., Brown, R., Pitstick, R., Gapeshina, H., Yang, J., Carlson, G. A., & Westaway, D. (2012). Knockout of the prion protein (PrP)-like Sprn gene does not produce embryonic lethality in combination with PrP(C)-deficiency. *Proc Natl Acad Sci U S A*, *109*(23), 9035-9040.

Davidson, B. L., & McCray, P. B. J. (2011). Current prospects for RNA interference-based therapies. *Nat Rev Genet*, *12*(5), 329-340.

de Hoon, M. J., Imoto, S., Nolan, J., & Miyano, S. (2004). Open source clustering software. *Bioinformatics*, *20*(9), 1453-1454.

de la Monte, S. M. (2012). Brain insulin resistance and deficiency as therapeutic targets in Alzheimer's disease. *Curr Alzheimer Res*, *9*(1), 35-66.

De Strooper, B., Annaert, W., Cupers, P., Saftig, P., Craessaerts, K., Mumm, J. S., Schroeter, E. H., Schrijvers, V., Wolfe, M. S., Ray, W. J., Goate, A., & Kopan, R. (1999). A presenilin-1-dependent gamma-secretase-like protease mediates release of Notch intracellular domain. *Nature*, *398*(6727), 518-522.

DeArmond, S. J., Sánchez, H., Yehiely, F., Qiu, Y., Ninchak-Casey, A., Daggett, V., Camerino, A. P., Cayetano, J., Rogers, M., Groth, D., Torchia, M., Tremblay, P., Scott, M. R., Cohen, F. E., & Prusiner, S. B. (1997). Selective neuronal targeting in prion disease. *Neuron*, *19*(6), 1337-1348.

Deighton, R. F., Short, D. M., McGregor, R. J., Gow, A. J., Whittle, I. R., & McCulloch, J. (2009). The utility of functional interaction and cluster analysis in CNS proteomics. *J Neurosci Methods*, *180*(2), 321-329.

Deisseroth, K., Heist, E. K., & Tsien, R. W. (1998). Translocation of calmodulin to the nucleus supports CREB phosphorylation in hippocampal neurons. *Nature*, *392*(6672), 198-202.

Deleault, N. R., Harris, B. T., Rees, J. R., & Supattapone, S. (2007). Formation of native prions from minimal components in vitro. *Proc Natl Acad Sci U S A*, *104*(23), 9741-9746.

Deleault, N. R., Piro, J. R., Walsh, D. J., Wang, F., Ma, J., Geoghegan, J. C., & Supattapone, S. (2012). Isolation of phosphatidylethanolamine as a solitary cofactor for prion formation in the absence of nucleic acids. *Proc Natl Acad Sci U S A*, *109*(22), 8546-8551.

Demaimay, R., Adjou, K. T., Beringue, V., Demart, S., Lasmezas, C. I., Deslys, J. P., Seman, M., & Dormont, D. (1997). Late treatment with polyene antibiotics can prolong the survival time of scrapie-infected animals. *J Virol*, *71*(12), 9685-9689.

Deribe, Y. L., Pawson, T., & Dikic, I. (2010). Post-translational modifications in signal integration. *Nat Struct Mol Biol*, *17*(6), 666-672.

Deriziotis, P., Andre, R., Smith, D. M., Goold, R., Kinghorn, K. J., Kristiansen, M., Nathan, J. A., Rosenzweig, R., Krutauz, D., Glickman, M. H., Collinge, J., Goldberg, A. L., & Tabrizi, S. J. (2011). Misfolded PrP impairs the UPS by interaction with the 20S proteasome and inhibition of substrate entry. *EMBO J*, *30*(15), 3065-3077.

Dhillon, A. S., Hagan, S., Rath, O., & Kolch, W. (2007). MAP kinase signalling pathways in cancer. *Oncogene*, *26*(22), 3279-3290.

Diaz-Espinoza, R., & Soto, C. (2012). High-resolution structure of infectious prion protein: the final frontier. *Nat Struct Mol Biol*, *19*(4), 370-377.

Dickinson, A. G., & Outram, G. W. (1979). The scrapie replication-site hypothesis and its implications for pathogenesis. *Slow transmissible diseases of the nervous system*, *2*, 13-31.

Dlouhy, S. R., Hsiao, K., Farlow, M. R., Foroud, T., Conneally, P. M., Johnson, P., Prusiner, S. B., Hodes, M. E., & Ghetti, B. (1992). Linkage of the Indiana kindred of Gerstmann-Sträussler-Scheinker disease to the prion protein gene. *Nat Genet*, *1*(1), 64-67.

Doh-ura, K., Ishikawa, K., Murakami-Kubo, I., Sasaki, K., Mohri, S., Race, R., & Iwaki, T. (2004). Treatment of transmissible spongiform encephalopathy by intraventricular drug infusion in animal models. *J Virol*, *78*(10), 4999-5006.

Doh-Ura, K., Iwaki, T., & Caughey, B. (2000). Lysosomotropic agents and cysteine protease inhibitors inhibit scrapie-associated prion protein accumulation. *J Virol*, *74*(10), 4894-4897.

Doolan, K. M., & Colby, D. W. (2015). Conformation-dependent epitopes recognized by prion protein antibodies probed using mutational scanning and deep sequencing. *J Mol Biol*, *427*(2), 328-340.

Dorandeu, A., Wingertsmann, L., Chretien, F., Delisle, M. B., Vital, C., Parchi, P., Montagna, P., Lugaresi, E., Ironside, J. W., Budka, H., Gambetti, P., & Gray, F. (1998). Neuronal apoptosis in fatal familial insomnia. *Brain Pathol*, *8*(3), 531-537.

Dorsey, K., Zou, S., Schonberger, L. B., Sullivan, M., Kessler, D., Notari, E., Fang, C. T., & Dodd, R. Y. (2009). Lack of evidence of transfusion transmission of Creutzfeldt-Jakob disease in a US surveillance study. *Transfusion*, *49*(5), 977-984.

Dossena, S., Imeri, L., Mangieri, M., Garofoli, A., Ferrari, L., Senatore, A., Restelli, E., Balducci, C., Fiordaliso, F., Salio, M., Bianchi, S., Fioriti, L., Morbin, M., Pincherle, A., Marcon, G., Villani, F., Carli, M., Tagliavini, F., Forloni, G., & Chiesa, R. (2008). Mutant prion protein expression causes motor and memory deficits and abnormal sleep patterns in a transgenic mouse model. *Neuron*, *60*(4), 598-609.

Douet, J. Y., Zafar, S., Perret-Liaudet, A., Lacroux, C., Lugan, S., Aron, N., Cassard, H., Ponto, C., Corbière, F., Torres, J. M., Zerr, I., & Andreoletti, O. (2014). Detection of infectivity in blood of persons with variant and sporadic Creutzfeldt-Jakob disease. *Emerg Infect Dis*, *20*(1), 114-117.

Drisaldi, B., Coomaraswamy, J., Mastrangelo, P., Strome, B., Yang, J., Watts, J. C., Chishti, M. A., Marvi, M., Windl, O., Ahrens, R., Major, F., Sy, M. S., Kretzschmar, H., Fraser, P. E., Mount, H. T., & Westaway, D. (2004). Genetic mapping of activity determinants within cellular prion proteins: N-terminal modules in PrP^{C} offset pro-apoptotic activity of the Doppel helix B/B' region. *J Biol Chem*, *279*(53), 55443-55454.

Drisaldi, B., Stewart, R. S., Adles, C., Stewart, L. R., Quaglio, E., Biasini, E., Fioriti, L., Chiesa, R., & Harris, D. A. (2003). Mutant PrP is delayed in its exit from the endoplasmic reticulum, but neither wild-type nor mutant PrP undergoes retrotranslocation prior to proteasomal degradation. *J Biol Chem*, *278*(24), 21732-21743.

Druker, B. J., Guilhot, F., O'Brien, S. G., Gathmann, I., Kantarjian, H., Gattermann, N., Deininger, M. W., Silver, R. T., Goldman, J. M., Stone, R. M., Cervantes, F., Hochhaus, A., Powell, B. L., Gabrilove, J. L., Rousselot, P., Reiffers, J., Cornelissen, J. J., Hughes, T., Agis, H., Fischer, T., Verhoef, G., Shepherd, J., Saglio, G., Gratwohl, A., Nielsen, J. L., Radich, J. P., Simonsson, B., Taylor, K., Baccarani, M., So, C., Letvak, L., Larson, R. A., & IRIS, I. (2006). Five-year follow-up of patients receiving imatinib for chronic myeloid leukemia. *N Engl J Med*, *355*(23), 2408-2417.

Druker, B. J., Talpaz, M., Resta, D. J., Peng, B., Buchdunger, E., Ford, J. M., Lydon, N. B., Kantarjian, H., Capdeville, R., Ohno-Jones, S., & Sawyers, C. L. (2001). Efficacy and safety of a specific inhibitor of the BCR-ABL tyrosine kinase in chronic myeloid leukemia. *N Engl J Med*, *344*(14), 1031-1037.

Duffy, P., Wolf, J., Collins, G., DeVoe, A. G., Streeten, B., & Cowen, D. (1974). Letter: Possible person-to-person transmission of Creutzfeldt-Jakob disease. *N Engl J Med*, *290*(12), 692-693.

Duguid, J. R., Bohmont, C. W., Liu, N. G., & Tourtellotte, W. W. (1989). Changes in brain gene expression shared by scrapie and Alzheimer disease. *Proc Natl Acad Sci U S A*, *86*(18), 7260-7264.

Duguid, J. R., Rohwer, R. G., & Seed, B. (1988). Isolation of cDNAs of scrapie-modulated RNAs by subtractive hybridization of a cDNA library. *Proc Natl Acad Sci U S A*, *85*(15), 5738-5742.

Emerman, A. B., Zhang, Z. R., Chakrabarti, O., & Hegde, R. S. (2010). Compartment-restricted biotinylation reveals novel features of prion protein metabolism in vivo. *Mol Biol Cell*, *21*(24), 4325-4337.

Enari, M., Flechsig, E., & Weissmann, C. (2001). Scrapie prion protein accumulation by scrapie-infected neuroblastoma cells abrogated by exposure to a prion protein antibody. *Proc Natl Acad Sci U S A*, *98*(16), 9295-9299.

Engelstein, R., Grigoriadis, N., Greig, N. H., Ovadia, H., & Gabizon, R. (2005). Inhibition of P53-related apoptosis had no effect on PrP(Sc) accumulation and prion disease incubation time. *Neurobiol Dis*, *18*(2), 282-285.

Ertmer, A., Gilch, S., Yun, S. W., Flechsig, E., Klebl, B., Stein-Gerlach, M., Klein, M. A., & Schatzl, H. M. (2004). The tyrosine kinase inhibitor STI571 induces cellular clearance of PrP^{Sc} in prion-infected cells. *J Biol Chem*, *279*(40), 41918-41927.

Ettaiche, M., Pichot, R., Vincent, J. P., & Chabry, J. (2000). In vivo cytotoxicity of the prion protein fragment 106-126. *J Biol Chem*, *275*(47), 36487-36490.

Fabbro, D., Cowan-Jacob, S. W., Mobitz, H., & Martiny-Baron, G. (2012). Targeting cancer with small-molecular-weight kinase inhibitors. *Methods Mol Biol*, *795*, 1-34.

Falsig, J., Sonati, T., Herrmann, U. S., Saban, D., Li, B., Arroyo, K., Ballmer, B., Liberski, P. P., & Aguzzi, A. (2012). Prion pathogenesis is faithfully reproduced in cerebellar organotypic slice cultures. *PLoS Pathog*, *8*(11), e1002985.

Fernandez-Borges, N., Brun, A., Whitton, J. L., Parra, B., Diaz-San Segundo, F., Salguero, F. J., Torres, J. M., & Rodriguez, F. (2006). DNA vaccination can break immunological tolerance to PrP in wild-type mice and attenuates prion disease after intracerebral challenge. *J Virol*, *80*(20), 9970-9976.

Ferrari, S., Bandi, H. R., Hofsteenge, J., Bussian, B. M., & Thomas, G. (1991). Mitogen-activated 70K S6 kinase. Identification of in vitro 40 S ribosomal S6 phosphorylation sites. *J Biol Chem*, *266*(33), 22770-22775.

Ferreiro, E., Resende, R., Costa, R., Oliveira, C. R., & Pereira, C. M. (2006). An endoplasmic-reticulum-specific apoptotic pathway is involved in prion and amyloid-beta peptides neurotoxicity. *Neurobiol Dis*, *23*(3), 669-678.

Fevrier, B., Vilette, D., Archer, F., Loew, D., Faigle, W., Vidal, M., Laude, H., & Raposo, G. (2004). Cells release prions in association with exosomes. *Proc Natl Acad Sci U S A*, *101*(26), 9683-9688.

Filali, H., Martin-Burriel, I., Harders, F., Varona, L., Lyahyai, J., Zaragoza, P., Pumarola, M., Badiola, J. J., Bossers, A., & Bolea, R. (2011). Gene expression profiling and association with prion-related lesions in the medulla oblongata of symptomatic natural scrapie animals. *PLoS One*, *6*(5), e19909.

Fischer, M., Rulicke, T., Raeber, A., Sailer, A., Moser, M., Oesch, B., Brandner, S., Aguzzi, A., & Weissmann, C. (1996). Prion protein (PrP) with amino-proximal deletions restoring susceptibility of PrP knockout mice to scrapie. *EMBO J*, *15*(6), 1255-1264.

Flechsig, E., Shmerling, D., Hegyi, I., Raeber, A. J., Fischer, M., Cozzio, A., von Mering, C., Aguzzi, A., & Weissmann, C. (2000). Prion protein devoid of the octapeptide repeat region restores susceptibility to scrapie in PrP knockout mice. *Neuron*, *27*(2), 399-408.

Folch, J., Petrov, D., Ettcheto, M., Abad, S., Sánchez-López, E., García, M. L., Olloquequi, J., Beas-Zarate, C., Auladell, C., & Camins, A. (2016). Current Research Therapeutic Strategies for Alzheimer's Disease Treatment. *Neural Plast*, *2016*, 8501693.

Ford, M. J., Burton, L. J., Morris, R. J., & Hall, S. M. (2002). Selective expression of prion protein in peripheral tissues of the adult mouse. *Neuroscience*, *113*(1), 177-192.

Forloni, G., Angeretti, N., Chiesa, R., Monzani, E., Salmona, M., Bugiani, O., & Tagliavini, F. (1993). Neurotoxicity of a prion protein fragment. *Nature*, *362*(6420), 543-546.

Forloni, G., Del Bo, R., Angeretti, N., Chiesa, R., Smiroldo, S., Doni, R., Ghibaudi, E., Salmona, M., Porro, M., Verga, L., & et, A. (1994). A neurotoxic prion protein fragment induces rat astroglial proliferation and hypertrophy. *Eur J Neurosci*, *6*(9), 1415-1422.

Foster, K. G., & Fingar, D. C. (2010). Mammalian target of rapamycin (mTOR): conducting the cellular signaling symphony. *J Biol Chem*, *285*(19), 14071-14077.

Fraser, H., & Dickinson, A. G. (1973). Scrapie in mice. Agent-strain differences in the distribution and intensity of grey matter vacuolation. *J Comp Pathol*, *83*(1), 29-40.

Freude, S., Schilbach, K., & Schubert, M. (2009). The role of IGF-1 receptor and insulin receptor signaling for the pathogenesis of Alzheimer's disease: from model organisms to human disease. *Curr Alzheimer Res*, *6*(3), 213-223.

Friedman-Levi, Y., Meiner, Z., Canello, T., Frid, K., Kovacs, G. G., Budka, H., Avrahami, D., & Gabizon, R. (2011). Fatal prion disease in a mouse model of genetic E200K Creutzfeldt-Jakob disease. *PLoS Pathog*, *7*(11), e1002350.

Friedman, R. C., Farh, K. K., Burge, C. B., & Bartel, D. P. (2009). Most mammalian mRNAs are conserved targets of microRNAs. *Genome Res*, *19*(1), 92-105.

Frisch, J., Houchins, J. P., Grahek, M., Schoephoerster, J., Hagen, J., Sweet, J., Mendoza, L., Schwartz, D., & Kalyuzhny, A. E. (2011). Novel multicolor immunofluorescence technique using primary antibodies raised in the same host species. *Methods Mol Biol*, *717*, 233-244.

Fu, Y., Rusznak, Z., Herculano-Houzel, S., Watson, C., & Paxinos, G. (2013). Cellular composition characterizing postnatal development and maturation of the mouse brain and spinal cord. *Brain Struct Funct*, *218*, 1337-1354.

Fuller, A. D., & Van Eldik, L. J. (2008). MFG-E8 regulates microglial phagocytosis of apoptotic neurons. *J Neuroimmune Pharmacol*, *3*(4), 246-256.

Gabizon, R., McKinley, M. P., Groth, D., & Prusiner, S. B. (1988). Immunoaffinity purification and neutralization of scrapie prion infectivity. *Proc Natl Acad Sci U S A*, *85*(18), 6617-6621.

Gajdusek, D. C., Gibbs, C. J., & Alpers, M. (1966). Experimental transmission of a Kuru-like syndrome to chimpanzees. *Nature*, *209*(5025), 794-796.

Gambetti, P., Parchi, P., & Chen, S. G. (2003). Hereditary Creutzfeldt-Jakob disease and fatal familial insomnia. *Clin Lab Med*, *23*(1), 43-64.

Gasset, M., Baldwin, M. A., Fletterick, R. J., & Prusiner, S. B. (1993). Perturbation of the secondary structure of the scrapie prion protein under conditions that alter infectivity. *Proc Natl Acad Sci U S A*, *90*(1), 1-5.

Genoud, N., Behrens, A., Miele, G., Robay, D., Heppner, F. L., Freigang, S., & Aguzzi, A. (2004). Disruption of Doppel prevents neurodegeneration in mice with extensive Prnp deletions. *Proc Natl Acad Sci U S A*, *101*(12), 4198-4203.

Geschwind, M. D., Kuo, A. L., Wong, K. S., Haman, A., Devereux, G., Raudabaugh, B. J., Johnson, D. Y., Torres-Chae, C. C., Finley, R., Garcia, P., Thai, J. N., Cheng, H. Q., Neuhaus, J. M., Forner, S. A., Duncan, J. L., Possin, K. L., Dearmond, S. J., Prusiner, S. B., & Miller, B. L. (2013). Quinacrine treatment trial for sporadic Creutzfeldt-Jakob disease. *Neurology*, *81*(23), 2015-2023.

Gibbs, C. J. J. (1967). Search for infectious etiology in chronic and subacute degenerative diseases of the central nervous system. *Curr Top Microbiol Immunol*, *40*, 44-58.

Gibbs, C. J. J., Gajdusek, D. C., Asher, D. M., Alpers, M. P., Beck, E., Daniel, P. M., & Matthews, W. B. (1968). Creutzfeldt-Jakob disease (spongiform encephalopathy): transmission to the chimpanzee. *Science*, *161*(3839), 388-389.

Giese, A., Brown, D. R., Groschup, M. H., Feldmann, C., Haist, I., & Kretzschmar, H. A. (1998). Role of microglia in neuronal cell death in prion disease. *Brain Pathol*, *8*(3), 449-457.

Giese, A., Groschup, M. H., Hess, B., & Kretzschmar, H. A. (1995). Neuronal cell death in scrapie-infected mice is due to apoptosis. *Brain Pathol*, *5*(3), 213-221.

Giles, K., Berry, D. B., Condello, C., Hawley, R. C., Gallardo-Godoy, A., Bryant, C., Oehler, A., Elepano, M., Bhardwaj, S., Patel, S., Silber, B. M., Guan, S., DeArmond, S. J., Renslo, A. R., & Prusiner, S. B. (2015). Different 2-Aminothiazole Therapeutics Produce Distinct Patterns of Scrapie Prion Neuropathology in Mouse Brains. *J Pharmacol Exp Ther*, *355*(1), 2-12.

Gill, O. N., Spencer, Y., Richard-Loendt, A., Kelly, C., Dabaghian, R., Boyes, L., Linehan, J., Simmons, M., Webb, P., Bellerby, P., Andrews, N., Hilton, D. A., Ironside, J. W., Beck, J., Poulter, M., Mead, S., & Brandner, S. (2013). Prevalent abnormal prion protein in human appendixes after bovine spongiform encephalopathy epizootic: large scale survey. *BMJ*, *347*, f5675.

Glantschnig, H., Rodan, G. A., & Reszka, A. A. (2002). Mapping of MST1 kinase sites of phosphorylation. Activation and autophosphorylation. *J Biol Chem*, *277*(45), 42987-42996.

Godsave, S. F., Wille, H., Kujala, P., Latawiec, D., DeArmond, S. J., Serban, A., Prusiner, S. B., & Peters, P. J. (2008). Cryo-immunogold electron microscopy for prions: toward identification of a conversion site. *J Neurosci*, *28*(47), 12489-12499.

Godsave, S. F., Wille, H., Pierson, J., Prusiner, S. B., & Peters, P. J. (2013). Plasma membrane invaginations containing clusters of full-length PrP^{Sc} are an early form of prion-associated neuropathology in vivo. *Neurobiol Aging*, *34*(6), 1621-1631.

Goggin, K., Beaudoin, S., Grenier, C., Brown, A. A., & Roucou, X. (2008). Prion protein aggresomes are poly(A)+ ribonucleoprotein complexes that induce a PKR-mediated deficient cell stress response. *Biochim Biophys Acta*, *1783*(3), 479-491.

Gómez-Nicola, D., Fransen, N. L., Suzzi, S., & Perry, V. H. (2013). Regulation of microglial proliferation during chronic neurodegeneration. *J Neurosci*, *33*(6), 2481-2493.

Goni, F., Knudsen, E., Schreiber, F., Scholtzova, H., Pankiewicz, J., Carp, R., Meeker, H. C., Rubenstein, R., Brown, D. R., Sy, M. S., Chabalgoity, J. A., Sigurdsson, E. M., & Wisniewski, T. (2005). Mucosal vaccination delays or prevents prion infection via an oral route. *Neuroscience*, *133*(2), 413-421.

Goni, F., Prelli, F., Schreiber, F., Scholtzova, H., Chung, E., Kascsak, R., Brown, D. R., Sigurdsson, E. M., Chabalgoity, J. A., & Wisniewski, T. (2008). High titers of mucosal and systemic anti-PrP antibodies abrogate oral prion infection in mucosal-vaccinated mice. *Neuroscience*, *153*(3), 679-686.

Goold, R., Rabbanian, S., Sutton, L., Andre, R., Arora, P., Moonga, J., Clarke, A. R., Schiavo, G., Jat, P., Collinge, J., & Tabrizi, S. J. (2011). Rapid cell-surface prion protein conversion revealed using a novel cell system. *Nat Commun*, *2*, 281.

Gordon, W. S. (1946). Louping ill, tickborne fever and scrapie. *Vet Rec*, *58*, 516-525.

Gorodinsky, A., & Harris, D. A. (1995). Glycolipid-anchored proteins in neuroblastoma cells form detergent-resistant complexes without caveolin. *J Cell Biol*, *129*(3), 619-627.

Gossert, A. D., Bonjour, S., Lysek, D. A., Fiorito, F., & Wuthrich, K. (2005). Prion protein NMR structures of elk and of mouse/elk hybrids. *Proc Natl Acad Sci U S A*, *102*(3), 646-650.

Govaerts, C., Wille, H., Prusiner, S. B., & Cohen, F. E. (2004). Evidence for assembly of prions with left-handed beta-helices into trimers. *Proc Natl Acad Sci U S A*, *101*(22), 8342-8347.

Graves, J. D., Draves, K. E., Gotoh, Y., Krebs, E. G., & Clark, E. A. (2001). Both phosphorylation and caspase-mediated cleavage contribute to regulation of the Ste20-like protein kinase Mst1 during CD95/Fas-induced apoptosis. *J Biol Chem*, *276*(18), 14909-14915.

Graves, J. D., Gotoh, Y., Draves, K. E., Ambrose, D., Han, D. K., Wright, M., Chernoff, J., Clark, E. A., & Krebs, E. G. (1998). Caspase-mediated activation and induction of apoptosis by the mammalian Ste20-like kinase Mst1. *EMBO J*, *17*(8), 2224-2234.

Gray, F., Chretien, F., Adle-Biassette, H., Dorandeu, A., Ereau, T., Delisle, M. B., Kopp, N., Ironside, J. W., & Vital, C. (1999). Neuronal apoptosis in Creutzfeldt-Jakob disease. *J Neuropathol Exp Neurol*, *58*(4), 321-328.

Grenier, C., Bissonnette, C., Volkov, L., & Roucou, X. (2006). Molecular morphology and toxicity of cytoplasmic prion protein aggregates in neuronal and non-neuronal cells. *J Neurochem*, *97*(5), 1456-1466.

Grienberger, C., & Konnerth, A. (2012). Imaging calcium in neurons. *Neuron*, *73*(5), 862-885.

Griffith, J. S. (1967). Self-replication and scrapie. *Nature*, *215*(5105), 1043-1044.

Groffen, J., Stephenson, J. R., Heisterkamp, N., de Klein, A., Bartram, C. R., & Grosveld, G. (1984). Philadelphia chromosomal breakpoints are clustered within a limited region, bcr, on chromosome 22. *Cell*, *36*(1), 93-99.

Gu, Y., Verghese, S., Mishra, R. S., Xu, X., Shi, Y., & Singh, N. (2003). Mutant prion protein-mediated aggregation of normal prion protein in the endoplasmic reticulum: implications for prion propagation and neurotoxicity. *J Neurochem*, *84*(1), 10-22.

Guillot-Sestier, M. V., Sunyach, C., Druon, C., Scarzello, S., & Checler, F. (2009). The alpha-secretase-derived N-terminal product of cellular prion, N1, displays neuroprotective function in vitro and in vivo. *J Biol Chem*, *284*(51), 35973-35986.

Guo, Y., Gong, H. S., Zhang, J., Xie, W. L., Tian, C., Chen, C., Shi, Q., Wang, S. B., Xu, Y., Zhang, B. Y., & Dong, X. P. (2012). Remarkable reduction of MAP2 in the brains of scrapie-infected rodents and human prion disease possibly correlated with the increase of calpain. *PLoS One*, *7*(1), e30163.

Gygi, S. P., Rochon, Y., Franza, B. R., & Aebersold, R. (1999). Correlation between protein and mRNA abundance in yeast. *Mol Cell Biol*, *19*(3), 1720-1730.

Hadlow, W. J. (1959). Scrapie and kuru. *The Lancet*, *274*(7097), 289-290.

Hadlow, W. J., Kennedy, R. C., & Race, R. E. (1982). Natural infection of Suffolk sheep with scrapie virus. *J Infect Dis*, *146*(5), 657-664.

Hadlow, W. J., Kennedy, R. C., Race, R. E., & Eklund, C. M. (1980). Virologic and neurohistologic findings in dairy goats affected with natural scrapie. *Vet Pathol*, *17*(2), 187-199.

Haik, S., Brandel, J. P., Salomon, D., Sazdovitch, V., Delasnerie-Laupretre, N., Laplanche, J. L., Faucheux, B. A., Soubrie, C., Boher, E., Belorgey, C., Hauw, J. J., & Alperovitch, A. (2004). Compassionate use of quinacrine in Creutzfeldt-Jakob disease fails to show significant effects. *Neurology*, *63*(12), 2413-2415.

Haïk, S., Peyrin, J. M., Lins, L., Rosseneu, M. Y., Brasseur, R., Langeveld, J. P., Tagliavini, F., Deslys, J. P., Lasmézas, C., & Dormont, D. (2000). Neurotoxicity of the putative transmembrane domain of the prion protein. *Neurobiol Dis*, *7*(6 Pt B), 644-656.

Hanks, S. K., & Hunter, T. (1995). Protein kinases 6. The eukaryotic protein kinase superfamily: kinase (catalytic) domain structure and classification. *FASEB J*, *9*(8), 576-596.

Hannon, G. J. (2002). RNA interference. *Nature*, *418*(6894), 244-251.

Hara, T., Nakamura, K., Matsui, M., Yamamoto, A., Nakahara, Y., Suzuki-Migishima, R., Yokoyama, M., Mishima, K., Saito, I., Okano, H., & Mizushima, N. (2006). Suppression of basal autophagy in neural cells causes neurodegenerative disease in mice. *Nature*, *441*(7095), 885-889.

Haraguchi, T., Fisher, S., Olofsson, S., Endo, T., Groth, D., Tarentino, A., Borchelt, D. R., Teplow, D., Hood, L., Burlingame, A., & et, A. (1989). Asparagine-linked glycosylation of the scrapie and cellular prion proteins. *Arch Biochem Biophys*, *274*(1), 1-13.

Harischandra, D. S., Kondru, N., Martin, D., Kanthasamy, A., Jin, H., Anantharam, V., & Kanthasamy, A. (2014). Role of proteolytic activation of protein kinase Cdelta in the pathogenesis of prion disease. *Prion*, *8*(1), 143-153.

Harlow, E., & Lane, D. (1999). *Using Antibodies: A Laboratory Manual*. New York: Cold Spring Harbor Laboratory Press.

Harris, D. A., Huber, M. T., van Dijken, P., Shyng, S. L., Chait, B. T., & Wang, R. (1993). Processing of a cellular prion protein: identification of N- and C-terminal cleavage sites. *Biochemistry*, *32*(4), 1009-1016.

Hawley, S. A., Davison, M., Woods, A., Davies, S. P., Beri, R. K., Carling, D., & Hardie, D. G. (1996). Characterization of the AMP-activated protein kinase kinase from rat liver and identification of threonine 172 as the major site at which it phosphorylates AMP-activated protein kinase. *J Biol Chem*, *271*(44), 27879-27887.

He, L., Lu, X. Y., Jolly, A. F., Eldridge, A. G., Watson, S. J., Jackson, P. K., Barsh, G. S., & Gunn, T. M. (2003). Spongiform degeneration in mahoganoid mutant mice. *Science*, *299*(5607), 710-712.

Hedlin, P., Taschuk, R., Potter, A., Griebel, P., & Napper, S. (2012). Detection and control of prion diseases in food animals. *ISRN Vet Sci*, *2012*, 254739.

Hegde, R. S., Mastrianni, J. A., Scott, M. R., DeFea, K. A., Tremblay, P., Torchia, M., DeArmond, S. J., Prusiner, S. B., & Lingappa, V. R. (1998). A transmembrane form of the prion protein in neurodegenerative disease. *Science*, *279*(5352), 827-834.

Hegde, R. S., & Rane, N. S. (2003). Prion protein trafficking and the development of neurodegeneration. *Trends Neurosci*, *26*(7), 337-339.

Hegde, R. S., Tremblay, P., Groth, D., DeArmond, S. J., Prusiner, S. B., & Lingappa, V. R. (1999). Transmissible and genetic prion diseases share a common pathway of neurodegeneration. *Nature*, *402*(6763), 822-826.

Heiseke, A., Aguib, Y., Riemer, C., Baier, M., & Schatzl, H. M. (2009). Lithium induces clearance of protease resistant prion protein in prion-infected cells by induction of autophagy. *J Neurochem*, *109*(1), 25-34.

Heisterkamp, N., Stephenson, J. R., Groffen, J., Hansen, P. F., de Klein, A., Bartram, C. R., & Grosveld, G. (1983). Localization of the c-ab1 oncogene adjacent to a translocation break point in chronic myelocytic leukaemia. *Nature*, *306*(5940), 239-242.

Heneka, M. T., Kummer, M. P., & Latz, E. (2014). Innate immune activation in neurodegenerative disease. *Nat Rev Immunol*, *14*(7), 463-477.

Heppner, F. L., Musahl, C., Arrighi, I., Klein, M. A., Rulicke, T., Oesch, B., Zinkernagel, R. M., Kalinke, U., & Aguzzi, A. (2001). Prevention of scrapie pathogenesis by transgenic expression of anti-prion protein antibodies. *Science*, *294*(5540), 178-182.

Herbst, A., Ness, A., Johnson, C. J., McKenzie, D., & Aiken, J. M. (2015). Transcriptomic responses to prion disease in rats. *BMC Genomics*, *16*(1), 682.

Herrmann, U. S., Schütz, A. K., Shirani, H., Huang, D., Saban, D., Nuvolone, M., Li, B., Ballmer, B., Åslund, A. K., Mason, J. J., Rushing, E., Budka, H., Nyström, S., Hammarström, P., Böckmann, A., Caflisch, A., Meier, B. H., Nilsson, K. P., Hornemann, S., & Aguzzi, A. (2015). Structure-based drug design identifies polythiophenes as antiprion compounds. *Sci Transl Med*, *7*(299), 299ra123.

Hetz, C., Lee, A. H., Gonzalez-Romero, D., Thielen, P., Castilla, J., Soto, C., & Glimcher, L. H. (2008). Unfolded protein response transcription factor XBP-1 does not influence prion replication or pathogenesis. *Proc Natl Acad Sci U S A*, *105*(2), 757-762.

Hetz, C., Russelakis-Carneiro, M., Maundrell, K., Castilla, J., & Soto, C. (2003). Caspase-12 and endoplasmic reticulum stress mediate neurotoxicity of pathological prion protein. *EMBO J*, *22*(20), 5435-5445.

Hill, A. F., Butterworth, R. J., Joiner, S., Jackson, G., Rossor, M. N., Thomas, D. J., Frosh, A., Tolley, N., Bell, J. E., Spencer, M., King, A., Al-Sarraj, S., Ironside, J. W., Lantos, P. L., & Collinge, J. (1999). Investigation of variant Creutzfeldt-Jakob disease and other human prion diseases with tonsil biopsy samples. *Lancet*, *353*(9148), 183-189.

Hill, A. F., Joiner, S., Wadsworth, J. D., Sidle, K. C., Bell, J. E., Budka, H., Ironside, J. W., & Collinge, J. (2003). Molecular classification of sporadic Creutzfeldt-Jakob disease. *Brain*, *126*(Pt 6), 1333-1346.

Hilton, D. A., Fathers, E., Edwards, P., Ironside, J. W., & Zajicek, J. (1998). Prion immunoreactivity in appendix before clinical onset of variant Creutzfeldt-Jakob disease. *Lancet*, *352*(9129), 703-704.

Hilton, D. A., Ghani, A. C., Conyers, L., Edwards, P., McCardle, L., Penney, M., Ritchie, D., & Ironside, J. W. (2002). Accumulation of prion protein in tonsil and appendix: review of tissue samples. *BMJ*, *325*(7365), 633-634.

Holman, R. C., Belay, E. D., Christensen, K. Y., Maddox, R. A., Minino, A. M., Folkema, A. M., Haberling, D. L., Hammett, T. A., Kochanek, K. D., Sejvar, J. J., & Schonberger, L. B. (2010). Human prion diseases in the United States. *PLoS One*, *5*(1), e8521.

Holscher, C., Delius, H., & Burkle, A. (1998). Overexpression of nonconvertible PrP^{C} delta114-121 in scrapie-infected mouse neuroblastoma cells leads to trans-dominant inhibition of wild-type PrP(Sc) accumulation. *J Virol*, *72*(2), 1153-1159.

Homma, T., Ishibashi, D., Nakagaki, T., Satoh, K., Sano, K., Atarashi, R., & Nishida, N. (2014). Increased expression of p62/SQSTM1 in prion diseases and its association with pathogenic prion protein. *Sci Rep*, *4*, 4504.

Honda, H., Sasaki, K., Minaki, H., Masui, K., Suzuki, S. O., Doh-Ura, K., & Iwaki, T. (2012). Protease-resistant PrP and PrP oligomers in the brain in human prion diseases after intraventricular pentosan polysulfate infusion. *Neuropathology*, *32*(2), 124-132.

Horiuchi, M., Yamazaki, N., Ikeda, T., Ishiguro, N., & Shinagawa, M. (1995). A cellular form of prion protein (PrPC) exists in many non-neuronal tissues of sheep. *J Gen Virol*, *76*(Pt 10), 2583-2587.

Hornemann, S., Schorn, C., & Wuthrich, K. (2004). NMR structure of the bovine prion protein isolated from healthy calf brains. *EMBO Rep*, *5*(12), 1159-1164.

Hsiao, K., Baker, H. F., Crow, T. J., Poulter, M., Owen, F., Terwilliger, J. D., Westaway, D., Ott, J., & Prusiner, S. B. (1989). Linkage of a prion protein missense variant to Gerstmann-Straussler syndrome. *Nature*, *338*(6213), 342-345.

Hsiao, K. K., Groth, D., Scott, M., Yang, S. L., Serban, H., Rapp, D., Foster, D., Torchia, M., Dearmond, S. J., & Prusiner, S. B. (1994). Serial transmission in rodents of neurodegeneration from transgenic mice expressing mutant prion protein. *Proc Natl Acad Sci U S A*, *91*(19), 9126-9130.

Hsiao, K. K., Scott, M., Foster, D., Groth, D. F., DeArmond, S. J., & Prusiner, S. B. (1990). Spontaneous neurodegeneration in transgenic mice with mutant prion protein. *Science*, *250*(4987), 1587-1590.

Hunter, G. D., Millson, G. C., & Meek, G. (1964). The intracellular location of the agent of mouse scrapie. *J Gen Microbiol*, *34*, 319-325.

Hwang, D., Lee, I. Y., Yoo, H., Gehlenborg, N., Cho, J. H., Petritis, B., Baxter, D., Pitstick, R., Young, R., Spicer, D., Price, N. D., Hohmann, J. G., Dearmond, S. J., Carlson, G. A., & Hood, L. E. (2009). A systems approach to prion disease. *Mol Syst Biol*, *5*, 252.

Impey, S., Fong, A. L., Wang, Y., Cardinaux, J. R., Fass, D. M., Obrietan, K., Wayman, G. A., Storm, D. R., Soderling, T. R., & Goodman, R. H. (2002). Phosphorylation of CBP mediates transcriptional activation by neural activity and CaM kinase IV. *Neuron*, *34*(2), 235-244.

Imran, M., & Mahmood, S. (2011). An overview of animal prion diseases. *Virol J*, *8*, 493.

Ishibashi, D., Yamanaka, H., Yamaguchi, N., Yoshikawa, D., Nakamura, R., Okimura, N., Yamaguchi, Y., Shigematsu, K., Katamine, S., & Sakaguchi, S. (2007). Immunization with recombinant bovine but not mouse prion protein delays the onset of disease in mice inoculated with a mouse-adapted prion. *Vaccine*, *25*(6), 985-992.

Ishikura, N., Clever, J. L., Bouzamondo-Bernstein, E., Samayoa, E., Prusiner, S. B., Huang, E. J., & DeArmond, S. J. (2005). Notch-1 activation and dendritic atrophy in prion disease. *Proc Natl Acad Sci U S A*, *102*(3), 886-891.

Jackson, W. S., Borkowski, A. W., Faas, H., Steele, A. D., King, O. D., Watson, N., Jasanoff, A., & Lindquist, S. (2009). Spontaneous generation of prion infectivity in fatal familial insomnia knockin mice. *Neuron*, *63*(4), 438-450.

Jackson, W. S., Borkowski, A. W., Watson, N. E., King, O. D., Faas, H., Jasanoff, A., & Lindquist, S. (2013). Profoundly different prion diseases in knock-in mice carrying single PrP codon substitutions associated with human diseases. *Proc Natl Acad Sci U S A*, *110*(36), 14759-14764.

Jackson, W. S., Krost, C., Borkowski, A. W., & Kaczmarczyk, L. (2014). Translation of the prion protein mRNA is robust in astrocytes but does not amplify during reactive astrocytosis in the mouse brain. *PLoS One*, *9*(4), e95958.

Jamieson, E., Jeffrey, M., Ironside, J. W., & Fraser, J. R. (2001). Activation of Fas and caspase 3 precedes PrP accumulation in 87V scrapie. *Neuroreport*, *12*(16), 3567-3572.

Jancic, D., Lopez de Armentia, M., Valor, L. M., Olivares, R., & Barco, A. (2009). Inhibition of cAMP response element-binding protein reduces neuronal excitability and plasticity, and triggers neurodegeneration. *Cereb Cortex*, *19*(11), 2535-2547.

Jang, B., Kim, E., Choi, J. K., Jin, J. K., Kim, J. I., Ishigami, A., Maruyama, N., Carp, R. I., Kim, Y. S., & Choi, E. K. (2008). Accumulation of citrullinated proteins by up-regulated peptidylarginine deiminase 2 in brains of scrapie-infected mice: a possible role in pathogenesis. *Am J Pathol*, *173*(4), 1129-1142.

Jeffrey, M., & Fraser, J. R. (2000a). Tubulovesicular particles occur early in the incubation period of murine scrapie. *Acta Neuropathol*, *99*(5), 525-528.

Jeffrey, M., Halliday, W. G., Bell, J., Johnston, A. R., MacLeod, N. K., Ingham, C., Sayers, A. R., Brown, D. A., & Fraser, J. R. (2000b). Synapse loss associated with abnormal PrP precedes neuronal degeneration in the scrapie-infected murine hippocampus. *Neuropathol Appl Neurobiol*, *26*(1), 41-54.

Jendroska, K., Heinzel, F. P., Torchia, M., Stowring, L., Kretzschmar, H. A., Kon, A., Stern, A., Prusiner, S. B., & DeArmond, S. J. (1991). Proteinase-resistant prion protein accumulation in Syrian hamster brain correlates with regional pathology and scrapie infectivity. *Neurology*, *41*(9), 1482-1490.

Jesionek-Kupnicka, D., Buczynski, J., Kordek, R., & Liberski, P. P. (1999). Neuronal loss and apoptosis in experimental Creutzfeldt-Jakob disease in mice. *Folia Neuropathol*, *37*(4), 283-286.

Jesionek-Kupnicka, D., Buczynski, J., Kordek, R., Sobow, T., Kloszewska, I., Papierz, W., & Liberski, P. P. (1997). Programmed cell death (apoptosis) in Alzheimer's disease and Creutzfeldt-Jakob disease. *Folia Neuropathol*, *35*(4), 233-235.

Jesionek-Kupnicka, D., Kordek, R., Buczynski, J., & Liberski, P. P. (2001). Apoptosis in relation to neuronal loss in experimental Creutzfeldt-Jakob disease in mice. *Acta Neurobiol Exp (Wars)*, *61*(1), 13-19.

Jiang, B., Liang, P., Deng, G., Tu, Z., Liu, M., & Xiao, X. (2011). Increased stability of Bcl-2 in HSP70-mediated protection against apoptosis induced by oxidative stress. *Cell Stress Chaperones*, *16*(2), 143-152.

Jin, J. K., Choi, J. K., Lee, H. G., Kim, Y. S., Carp, R. I., & Choi, E. K. (1999). Increased expression of CaM kinase II alpha in the brains of scrapie-infected mice. *Neurosci Lett*, *273*(1), 37-40.

Johannessen, M., Delghandi, M. P., & Moens, U. (2004). What turns CREB on? *Cell Signal*, *16*(11), 1211-1227.

Johnson, S. A., & Hunter, T. (2005). Kinomics: methods for deciphering the kinome. *Nat Methods*, *2*(1), 17-25.

Joiner, S., Linehan, J., Brandner, S., Wadsworth, J. D., & Collinge, J. (2002). Irregular presence of abnormal prion protein in appendix in variant Creutzfeldt-Jakob disease. *J Neurol Neurosurg Psychiatry*, *73*(5), 597-598.

Jones, D. R., Taylor, W. A., Bate, C., David, M., & Tayebi, M. (2010). A camelid anti-PrP antibody abrogates PrP replication in prion-permissive neuroblastoma cell lines. *PLoS One*, *5*(3), e9804.

Jones, M., Peden, A. H., Prowse, C. V., Gröner, A., Manson, J. C., Turner, M. L., Ironside, J. W., MacGregor, I. R., & Head, M. W. (2007). In vitro amplification and detection of variant Creutzfeldt-Jakob disease PrP^{Sc}. *J Pathol*, *213*(1), 21-26.

Juanes, M. E., Elvira, G., Garcia-Grande, A., Calero, M., & Gasset, M. (2009). Biosynthesis of prion protein nucleocytoplasmic isoforms by alternative initiation of translation. *J Biol Chem*, *284*(5), 2787-2794.

Kakeya, H., Onose, R., & Osada, H. (1998). Caspase-mediated activation of a 36-kDa myelin basic protein kinase during anticancer drug-induced apoptosis. *Cancer Res*, *58*(21), 4888-4894.

Kalia, L. V., & Salter, M. W. (2003). Interactions between Src family protein tyrosine kinases and PSD-95. *Neuropharmacology*, *45*(6), 720-728.

Kanaani, J., Prusiner, S. B., Diacovo, J., Baekkeskov, S., & Legname, G. (2005). Recombinant prion protein induces rapid polarization and development of synapses in embryonic rat hippocampal neurons in vitro. *J Neurochem*, *95*(5), 1373-1386.

Kaneko, K., Ball, H. L., Wille, H., Zhang, H., Groth, D., Torchia, M., Tremblay, P., Safar, J., Prusiner, S. B., DeArmond, S. J., Baldwin, M. A., & Cohen, F. E. (2000). A synthetic peptide initiates Gerstmann-Straussler-Scheinker (GSS) disease in transgenic mice. *J Mol Biol*, *295*(4), 997-1007.

Kaneko, K., Vey, M., Scott, M., Pilkuhn, S., Cohen, F. E., & Prusiner, S. B. (1997). COOH-terminal sequence of the cellular prion protein directs subcellular trafficking and controls conversion into the scrapie isoform. *Proc Natl Acad Sci U S A*, *94*(6), 2333-2338.

Kang, S. C., Brown, D. R., Whiteman, M., Li, R., Pan, T., Perry, G., Wisniewski, T., Sy, M. S., & Wong, B. S. (2004). Prion protein is ubiquitinated after developing protease resistance in the brains of scrapie-infected mice. *J Pathol*, *203*(1), 603-608.

Kang, Y. S., Zhao, X., Lovaas, J., Eisenberg, E., & Greene, L. E. (2009). Clathrin-independent internalization of normal cellular prion protein in neuroblastoma cells is associated with the Arf6 pathway. *J Cell Sci*, *122*(Pt 22), 4062-4069.

Karapetyan, Y. E., Sferrazza, G. F., Zhou, M., Ottenberg, G., Spicer, T., Chase, P., Fallahi, M., Hodder, P., Weissmann, C., & Lasmezas, C. I. (2013). Unique drug screening approach for prion diseases identifies tacrolimus and astemizole as antiprion agents. *Proc Natl Acad Sci U S A*, *110*(17), 7044-7049.

Kasahara, J., Fukunaga, K., & Miyamoto, E. (1999). Differential effects of a calcineurin inhibitor on glutamate-induced phosphorylation of Ca2+/calmodulin-dependent protein kinases in cultured rat hippocampal neurons. *J Biol Chem*, *274*(13), 9061-9067.

Kascsak, R. J., Rubenstein, R., Merz, P. A., Carp, R. I., Robakis, N. K., Wisniewski, H. M., & Diringer, H. (1986). Immunological comparison of scrapie-associated fibrils isolated from animals infected with four different scrapie strains. *J Virol*, *59*(3), 676-683.

Kaufman, A. C., Salazar, S. V., Haas, L. T., Yang, J., Kostylev, M. A., Jeng, A. T., Robinson, S. A., Gunther, E. C., van Dyck, C. H., Nygaard, H. B., & Strittmatter, S. M. (2015). Fyn inhibition rescues established memory and synapse loss in Alzheimer mice. *Ann Neurol*, *77*(6), 953-971.

Kawasaki, Y., Kawagoe, K., Chen, C. J., Teruya, K., Sakasegawa, Y., & Doh-ura, K. (2007). Orally administered amyloidophilic compound is effective in prolonging the incubation periods of animals cerebrally infected with prion diseases in a prion strain-dependent manner. *J Virol*, *81*(23), 12889-12898.

Kellings, K., Meyer, N., Mirenda, C., Prusiner, S. B., & Riesner, D. (1992). Further analysis of nucleic acids in purified scrapie prion preparations by improved return refocusing gel electrophoresis. *J Gen Virol*, *73*(Pt 4), 1025-1029.

Kelly, S., Zhang, Z. J., Zhao, H., Xu, L., Giffard, R. G., Sapolsky, R. M., Yenari, M. A., & Steinberg, G. K. (2002). Gene transfer of HSP72 protects cornu ammonis 1 region of the hippocampus neurons from global ischemia: influence of Bcl-2. *Ann Neurol*, *52*(2), 160-167.

Khalifé, M., Young, R., Passet, B., Halliez, S., Vilotte, M., Jaffrezic, F., Marthey, S., Béringue, V., Vaiman, D., Le Provost, F., Laude, H., & Vilotte, J. L. (2011). Transcriptomic analysis brings new insight into the biological role of the prion protein during mouse embryogenesis. *PLoS One*, *6*(8), e23253.

Khosravani, H., Zhang, Y., Tsutsui, S., Hameed, S., Altier, C., Hamid, J., Chen, L., Villemaire, M., Ali, Z., Jirik, F. R., & Zamponi, G. W. (2008). Prion protein attenuates excitotoxicity by inhibiting NMDA receptors. *J Cell Biol*, *181*(3), 551-565.

Kim, H. O., Snyder, G. P., Blazey, T. M., Race, R. E., Chesebro, B., & Skinner, P. J. (2008). Prion disease induced alterations in gene expression in spleen and brain prior to clinical symptoms. *Adv Appl Bioinform Chem*, *1*, 29-50.

Kimberlin, R. H. (1982). Scrapie agent: prions or virinos? *Nature*, *297*(5862), 107-108.
Kimberlin, R. H., Millson, G. C., & Hunter, G. D. (1971). An experimental examination of the scrapie agent in cell membrane mixtures. 3. Studies of the operational size. *J Comp Pathol*, *81*(3), 383-391.
Kimberlin, R. H., & Walker, C. A. (1978). Pathogenesis of mouse scrapie: effect of route of inoculation on infectivity titres and dose-response curves. *J Comp Pathol*, *88*(1), 39-47.
Kimberlin, R. H., & Walker, C. A. (1979). Pathogenesis of mouse scrapie: dynamics of agent replication in spleen, spinal cord and brain after infection by different routes. *J Comp Pathol*, *89*(4), 551-562.
Kimberlin, R. H., & Walker, C. A. (1982). Pathogenesis of mouse scrapie: patterns of agent replication in different parts of the CNS following intraperitoneal infection. *J R Soc Med*, *75*(8), 618-624.
Kimberlin, R. H., & Walker, C. A. (1986). Pathogenesis of scrapie (strain 263K) in hamsters infected intracerebrally, intraperitoneally or intraocularly. *J Gen Virol*, *67*(Pt 2), 255-263.
Kimberlin, R. H., & Walker, C. A. (1977). Characteristics of a short incubation model of scrapie in the golden hamster. *Journal of General Virology*, *34*(2), 295-304.
Klein, R., Nanduri, V., Jing, S. A., Lamballe, F., Tapley, P., Bryant, S., Cordon-Cardo, C., Jones, K. R., Reichardt, L. F., & Barbacid, M. (1991). The trkB tyrosine protein kinase is a receptor for brain-derived neurotrophic factor and neurotrophin-3. *Cell*, *66*(2), 395-403.
Kmiecik, T. E., Johnson, P. J., & Shalloway, D. (1988). Regulation by the autophosphorylation site in overexpressed pp60c-src. *Mol Cell Biol*, *8*(10), 4541-4546.
Kmiecik, T. E., & Shalloway, D. (1987). Activation and suppression of pp60c-src transforming ability by mutation of its primary sites of tyrosine phosphorylation. *Cell*, *49*(1), 65-73.
Knight, Z. A., Lin, H., & Shokat, K. M. (2010). Targeting the cancer kinome through polypharmacology. *Nat Rev Cancer*, *10*(2), 130-137.
Koch, T. K., Berg, B. O., De Armond, S. J., & Gravina, R. F. (1985). Creutzfeldt-Jakob disease in a young adult with idiopathic hypopituitarism. Possible relation to the administration of cadaveric human growth hormone. *N Engl J Med*, *313*(12), 731-733.
Kocisko, D. A., Baron, G. S., Rubenstein, R., Chen, J., Kuizon, S., & Caughey, B. (2003). New inhibitors of scrapie-associated prion protein formation in a library of 2000 drugs and natural products. *J Virol*, *77*(19), 10288-10294.
Kocisko, D. A., & Caughey, B. (2006). Searching for anti-prion compounds: cell-based high-throughput in vitro assays and animal testing strategies. *Methods Enzymol*, *412*, 223-234.
Kocisko, D. A., Come, J. H., Priola, S. A., Chesebro, B., Raymond, G. J., Lansbury, P. T., & Caughey, B. (1994). Cell-free formation of protease-resistant prion protein. *Nature*, *370*(6489), 471-474.
Komatsu, M., Waguri, S., Chiba, T., Murata, S., Iwata, J., Tanida, I., Ueno, T., Koike, M., Uchiyama, Y., Kominami, E., & Tanaka, K. (2006). Loss of autophagy in the central nervous system causes neurodegeneration in mice. *Nature*, *441*(7095), 880-884.
Komatsu, M., Waguri, S., Ueno, T., Iwata, J., Murata, S., Tanida, I., Ezaki, J., Mizushima, N., Ohsumi, Y., Uchiyama, Y., Kominami, E., Tanaka, K., & Chiba, T. (2005). Impairment of starvation-induced and constitutive autophagy in Atg7-deficient mice. *J Cell Biol*, *169*(3), 425-434.

Kourie, J. I., & Culverson, A. (2000). Prion peptide fragment PrP[106-126] forms distinct cation channel types. *J Neurosci Res*, *62*(1), 120-133.

Kranich, J., Krautler, N. J., Falsig, J., Ballmer, B., Li, S., Hutter, G., Schwarz, P., Moos, R., Julius, C., Miele, G., & Aguzzi, A. (2010). Engulfment of cerebral apoptotic bodies controls the course of prion disease in a mouse strain-dependent manner. *J Exp Med*, *207*(10), 2271-2281.

Krebs, B., Dorner-Ciossek, C., Schmalzbauer, R., Vassallo, N., Herms, J., & Kretzschmar, H. A. (2006). Prion protein induced signaling cascades in monocytes. *Biochem Biophys Res Commun*, *340*(1), 13-22.

Kretzschmar, H. A., Prusiner, S. B., Stowring, L. E., & DeArmond, S. J. (1986). Scrapie prion proteins are synthesized in neurons. *Am J Pathol*, *122*(1), 1-5.

Kristiansen, M., Deriziotis, P., Dimcheff, D. E., Jackson, G. S., Ovaa, H., Naumann, H., Clarke, A. R., van Leeuwen, F. W., Menendez-Benito, V., Dantuma, N. P., Portis, J. L., Collinge, J., & Tabrizi, S. J. (2007). Disease-associated prion protein oligomers inhibit the 26S proteasome. *Mol Cell*, *26*(2), 175-188.

Küffer, A., Lakkaraju, A. K., Mogha, A., Petersen, S. C., Airich, K., Doucerain, C., Marpakwar, R., Bakirci, P., Senatore, A., Monnard, A., Schiavi, C., Nuvolone, M., Grosshans, B., Hornemann, S., Bassilana, F., Monk, K. R., & Aguzzi, A. (2016). The prion protein is an agonistic ligand of the G protein-coupled receptor Adgrg6. *Nature*, *536*(7617), 464-468.

Kuma, A., Hatano, M., Matsui, M., Yamamoto, A., Nakaya, H., Yoshimori, T., Ohsumi, Y., Tokuhisa, T., & Mizushima, N. (2004). The role of autophagy during the early neonatal starvation period. *Nature*, *432*(7020), 1032-1036.

Kumar, R., McClain, D., Young, R., & Carlson, G. A. (2008). Cholesterol transporter ATP-binding cassette A1 (ABCA1) is elevated in prion disease and affects PrP^{C} and PrP^{Sc} concentrations in cultured cells. *J Gen Virol*, *89*(Pt 6), 1525-1532.

Lacroux, C., Comoy, E., Moudjou, M., Perret-Liaudet, A., Lugan, S., Litaise, C., Simmons, H., Jas-Duval, C., Lantier, I., Béringue, V., Groschup, M., Fichet, G., Costes, P., Streichenberger, N., Lantier, F., Deslys, J. P., Vilette, D., & Andréoletti, O. (2014). Preclinical detection of variant CJD and BSE prions in blood. *PLoS Pathog*, *10*(6), e1004202.

Langevin, C., Andreoletti, O., Le Dur, A., Laude, H., & Beringue, V. (2011). Marked influence of the route of infection on prion strain apparent phenotype in a scrapie transgenic mouse model. *Neurobiol Dis*, *41*(1), 219-225.

Lasmezas, C. I., Deslys, J. P., Demaimay, R., Adjou, K. T., Hauw, J. J., & Dormont, D. (1996a). Strain specific and common pathogenic events in murine models of scrapie and bovine spongiform encephalopathy. *J Gen Virol*, *77*(Pt 7), 1601-1609.

Lasmezas, C. I., Deslys, J. P., Demaimay, R., Adjou, K. T., Lamoury, F., Dormont, D., Robain, O., Ironside, J., & Hauw, J. J. (1996b). BSE transmission to macaques. *Nature*, *381*(6585), 743-744.

Lau, A., McDonald, A., Daude, N., Mays, C. E., Walter, E. D., Aglietti, R., Mercer, R. C., Wohlgemuth, S., van der Merwe, J., Yang, J., Gapeshina, H., Kim, C., Grams, J., Shi, B., Wille, H., Balachandran, A., Schmitt-Ulms, G., Safar, J. G., Millhauser, G. L., & Westaway, D. (2015). Octarepeat region flexibility impacts prion function, endoproteolysis and disease manifestation. *EMBO Mol Med, 7*(3), 339-356.

Lee, H. P., Jun, Y. C., Choi, J. K., Kim, J. I., Carp, R. I., & Kim, Y. S. (2005). Activation of mitogen-activated protein kinases in hamster brains infected with 263K scrapie agent. *J Neurochem*, *95*(2), 584-593.

Lee, J. K., Park, J., Lee, Y. D., Lee, S. H., & Han, P. L. (1999). Distinct localization of SAPK isoforms in neurons of adult mouse brain implies multiple signaling modes of SAPK pathway. *Brain Res Mol Brain Res*, *70*(1), 116-124.

Lee, J. K., Shin, J. H., Hwang, S. G., Gwag, B. J., McKee, A. C., Lee, J., Kowall, N. W., Ryu, H., Lim, D. S., & Choi, E. J. (2013). MST1 functions as a key modulator of neurodegeneration in a mouse model of ALS. *Proc Natl Acad Sci U S A*, *110*(29), 12066-12071.

Lee, K. K., Ohyama, T., Yajima, N., Tsubuki, S., & Yonehara, S. (2001). MST, a physiological caspase substrate, highly sensitizes apoptosis both upstream and downstream of caspase activation. *J Biol Chem*, *276*(22), 19276-19285.

Lee, S. J., Seo, B. R., Choi, E. J., & Koh, J. Y. (2014). The role of reciprocal activation of cAbl and Mst1 in the oxidative death of cultured astrocytes. *Glia*, *62*(4), 639-648.

Legname, G., Baskakov, I. V., Nguyen, H. O., Riesner, D., Cohen, F. E., DeArmond, S. J., & Prusiner, S. B. (2004). Synthetic mammalian prions. *Science*, *305*(5684), 673-676.

Legname, G., Nguyen, H. O., Peretz, D., Cohen, F. E., DeArmond, S. J., & Prusiner, S. B. (2006). Continuum of prion protein structures enciphers a multitude of prion isolate-specified phenotypes. *Proc Natl Acad Sci U S A*, *103*(50), 19105-19110.

Lehmann, S., Relano-Gines, A., Resina, S., Brillaud, E., Casanova, D., Vincent, C., Hamela, C., Poupeau, S., Laffont, M., Gabelle, A., Delaby, C., Belondrade, M., Arnaud, J. D., Alvarez, M. T., Maurel, J. C., Maurel, P., & Crozet, C. (2014). Systemic delivery of siRNA down regulates brain prion protein and ameliorates neuropathology in prion disorder. *PLoS One*, *9*(2), e88797.

Lehtinen, M. K., Yuan, Z., Boag, P. R., Yang, Y., Villen, J., Becker, E. B., DiBacco, S., de la Iglesia, N., Gygi, S., Blackwell, T. K., & Bonni, A. (2006). A conserved MST-FOXO signaling pathway mediates oxidative-stress responses and extends life span. *Cell*, *125*(5), 987-1001.

Lemrow, S. M., Anderson, K. A., Joseph, J. D., Ribar, T. J., Noeldner, P. K., & Means, A. R. (2004). Catalytic activity is required for calcium/calmodulin-dependent protein kinase IV to enter the nucleus. *J Biol Chem*, *279*(12), 11664-11671.

Levine, C. G., Mitra, D., Sharma, A., Smith, C. L., & Hegde, R. S. (2005). The efficiency of protein compartmentalization into the secretory pathway. *Mol Biol Cell*, *16*(1), 279-291.

Lewis, V., Johanssen, V. A., Crouch, P. J., Klug, G. M., Hooper, N. M., & Collins, S. J. (2015). Prion protein "gamma-cleavage": characterizing a novel endoproteolytic processing event. *Cell Mol Life Sci*, *73*(3), 667-683.

Li, A., Christensen, H. M., Stewart, L. R., Roth, K. A., Chiesa, R., & Harris, D. A. (2007). Neonatal lethality in transgenic mice expressing prion protein with a deletion of residues 105-125. *EMBO J*, *26*(2), 548-558.

Li, S., Ju, C., Han, C., Li, Z., Liu, W., Ye, X., Xu, J., Xulong, L., Wang, X., Chen, Z., Meng, K., & Wan, J. (2014). Unchanged survival rates of Shadoo knockout mice after infection with mouse-adapted scrapie. *Prion*, *8*(5), 339-343.

Li, X., Wilmanns, M., Thornton, J., & Köhn, M. (2013). Elucidating human phosphatase-substrate networks. *Sci Signal*, *6*(275), rs10.

Liang, J., Wang, W., Sorensen, D., Medina, S., Ilchenko, S., Kiselar, J., Surewicz, W. K., Booth, S. A., & Kong, Q. (2012). Cellular prion protein regulates its own alpha-cleavage through ADAM8 in skeletal muscle. *J Biol Chem*, *287*(20), 16510-16520.

Liberski, P. (2008). The tubulovesicular structures - the ultrastructural hallmark for all prion diseases. *Acta Neurobiol Exp (Wars)*, *68*(1), 113-121.

Liberski, P. P., Gajdusek, D. C., & Brown, P. (2002). How do neurons degenerate in prion diseases or transmissible spongiform encephalopathies (TSEs): neuronal autophagy revisited. *Acta Neurobiol Exp (Wars)*, *62*(3), 141-147.

Liberski, P. P., Jeffrey, M., & Goodsir, C. (1997). Tubulovesicular structures are not labeled using antibodies to prion protein (PrP) with the immunogold electron microscopy techniques. *Acta Neuropathol*, *93*(3), 260-264.

Liberski, P. P., Streichenberger, N., Giraud, P., Soutrenon, M., Meyronnet, D., Sikorska, B., & Kopp, N. (2005). Ultrastructural pathology of prion diseases revisited: brain biopsy studies. *Neuropathol Appl Neurobiol*, *31*(1), 88-96.

Liberski, P. P., Yanagihara, R., Gibbs, C. J., & Gajdusek, D. C. (1990). Appearance of tubulovesicular structures in experimental Creutzfeldt-Jakob disease and scrapie precedes the onset of clinical disease. *Acta Neuropathol*, *79*(4), 349-354.

Liberski, P. P., Yanagihara, R., Gibbs, C. J. J., & Gajdusek, D. C. (1992). Neuronal autophagic vacuoles in experimental scrapie and Creutzfeldt-Jakob disease. *Acta Neuropathol*, *83*(2), 134-139.

Liemann, S., & Glockshuber, R. (1999). Influence of amino acid substitutions related to inherited human prion diseases on the thermodynamic stability of the cellular prion protein. *Biochemistry*, *38*(11), 3258-3267.

Lilienbaum, A. (2013). Relationship between the proteasomal system and autophagy. *Int J Biochem Mol Biol*, *4*(1), 1-26.

Lin, M. C., Mirzabekov, T., & Kagan, B. L. (1997). Channel formation by a neurotoxic prion protein fragment. *J Biol Chem*, *272*(1), 44-47.

Lin, Y., Skeberdis, V. A., Francesconi, A., Bennett, M. V., & Zukin, R. S. (2004). Postsynaptic density protein-95 regulates NMDA channel gating and surface expression. *J Neurosci*, *24*(45), 10138-10148.

Linden, R., Martins, V. R., Prado, M. A., Cammarota, M., Izquierdo, I., & Brentani, R. R. (2008). Physiology of the prion protein. *Physiol Rev*, *88*(2), 673-728.

Llewelyn, C. A., Hewitt, P. E., Knight, R. S., Amar, K., Cousens, S., Mackenzie, J., & Will, R. G. (2004). Possible transmission of variant Creutzfeldt-Jakob disease by blood transfusion. *Lancet*, *363*(9407), 417-421.

Lopes, J. P., Oliveira, C. R., & Agostinho, P. (2007). Role of cyclin-dependent kinase 5 in the neurodegenerative process triggered by amyloid-Beta and prion peptides: implications for Alzheimer's disease and prion-related encephalopathies. *Cell Mol Neurobiol*, *27*(7), 943-957.

Lopes, M. H., Hajj, G. N., Muras, A. G., Mancini, G. L., Castro, R. M., Ribeiro, K. C., Brentani, R. R., Linden, R., & Martins, V. R. (2005). Interaction of cellular prion and stress-inducible protein 1 promotes neuritogenesis and neuroprotection by distinct signaling pathways. *J Neurosci*, *25*(49), 11330-11339.

Lowe, J., Fergusson, J., Kenward, N., Laszlo, L., Landon, M., Farquhar, C., Brown, J., Hope, J., & Mayer, R. J. (1992). Immunoreactivity to ubiquitin-protein conjugates is present early in the disease process in the brains of scrapie-infected mice. *J Pathol*, *168*(2), 169-177.

Lucassen, P. J., Williams, A., Chung, W. C., & Fraser, H. (1995). Detection of apoptosis in murine scrapie. *Neurosci Lett*, *198*(3), 185-188.

Lugo, T. G., Pendergast, A. M., Muller, A. J., & Witte, O. N. (1990). Tyrosine kinase activity and transformation potency of bcr-abl oncogene products. *Science*, *247*(4946), 1079-1082.

Luhrs, T., Riek, R., Guntert, P., & Wuthrich, K. (2003). NMR structure of the human doppel protein. *J Mol Biol*, *326*(5), 1549-1557.

Lund, C., Olsen, C. M., Skogtvedt, S., Tveit, H., Prydz, K., & Tranulis, M. A. (2009). Alternative translation initiation generates cytoplasmic sheep prion protein. *J Biol Chem*, *284*(29), 19668-19678.

Lyahyai, J., Bolea, R., Serrano, C., Monleon, E., Moreno, C., Osta, R., Zaragoza, P., Badiola, J. J., & Martin-Burriel, I. (2006). Correlation between Bax overexpression and prion deposition in medulla oblongata from natural scrapie without evidence of apoptosis. *Acta Neuropathol*, *112*(4), 451-460.

Ma, J., & Lindquist, S. (2001). Wild-type PrP and a mutant associated with prion disease are subject to retrograde transport and proteasome degradation. *Proc Natl Acad Sci U S A*, *98*(26), 14955-14960.

Ma, J., & Lindquist, S. (2002a). Conversion of PrP to a self-perpetuating PrP^{Sc}-like conformation in the cytosol. *Science*, *298*(5599), 1785-1788.

Ma, J., Wollmann, R., & Lindquist, S. (2002b). Neurotoxicity and neurodegeneration when PrP accumulates in the cytosol. *Science*, *298*(5599), 1781-1785.

Mabuchi, T., Kitagawa, K., Kuwabara, K., Takasawa, K., Ohtsuki, T., Xia, Z., Storm, D., Yanagihara, T., Hori, M., & Matsumoto, M. (2001). Phosphorylation of cAMP response element-binding protein in hippocampal neurons as a protective response after exposure to glutamate in vitro and ischemia in vivo. *J Neurosci*, *21*(23), 9204-9213.

Magalhaes, A. C., Silva, J. A., Lee, K. S., Martins, V. R., Prado, V. F., Ferguson, S. S., Gomez, M. V., Brentani, R. R., & Prado, M. A. (2002). Endocytic intermediates involved with the intracellular trafficking of a fluorescent cellular prion protein. *J Biol Chem*, *277*(36), 33311-33318.

Magill, S. T., Cambronne, X. A., Luikart, B. W., Lioy, D. T., Leighton, B. H., Westbrook, G. L., Mandel, G., & Goodman, R. H. (2010). microRNA-132 regulates dendritic growth and arborization of newborn neurons in the adult hippocampus. *Proc Natl Acad Sci U S A*, *107*(47), 20382-20387.

Magri, G., Clerici, M., Dall'Ara, P., Biasin, M., Caramelli, M., Casalone, C., Giannino, M. L., Longhi, R., Piacentini, L., Della Bella, S., Gazzuola, P., Martino, P. A., Della Bella, S., Pollera, C., Puricelli, M., Servida, F., Crescio, I., Boasso, A., Ponti, W., & Poli, G. (2005). Decrease in pathology and progression of scrapie after immunisation with synthetic prion protein peptides in hamsters. *Vaccine*, *23*(22), 2862-2868.

Majer, A., Medina, S. J., Niu, Y., Abrenica, B., Manguiat, K. J., Frost, K. L., Philipson, C. S., Sorensen, D. L., & Booth, S. A. (2012). Early mechanisms of pathobiology are revealed by transcriptional temporal dynamics in hippocampal CA1 neurons of prion infected mice. *PLoS Pathog*, *8*(11), e1003002.

Makarava, N., Kovacs, G. G., Savtchenko, R., Alexeeva, I., Ostapchenko, V. G., Budka, H., Rohwer, R. G., & Baskakov, I. V. (2012). A new mechanism for transmissible prion diseases. *J Neurosci*, *32*(21), 7345-7355.

Makrinou, E., Collinge, J., & Antoniou, M. (2002). Genomic characterization of the human prion protein (PrP) gene locus. *Mamm Genome*, *13*(12), 696-703.

Malaga-Trillo, E., Solis, G. P., Schrock, Y., Geiss, C., Luncz, L., Thomanetz, V., & Stuermer, C. A. (2009). Regulation of embryonic cell adhesion by the prion protein. *PLoS Biol*, *7*(3), e55.

Mallucci, G., Dickinson, A., Linehan, J., Klohn, P. C., Brandner, S., & Collinge, J. (2003). Depleting neuronal PrP in prion infection prevents disease and reverses spongiosis. *Science*, *302*(5646), 871-874.

Mallucci, G. R., Ratte, S., Asante, E. A., Linehan, J., Gowland, I., Jefferys, J. G., & Collinge, J. (2002). Post-natal knockout of prion protein alters hippocampal CA1 properties, but does not result in neurodegeneration. *EMBO J*, *21*(3), 202-210.

Mange, A., Beranger, F., Peoc'h, K., Onodera, T., Frobert, Y., & Lehmann, S. (2004). Alpha- and beta- cleavages of the amino-terminus of the cellular prion protein. *Biol Cell*, *96*(2), 125-132.

Manning, C. F., Bundros, A. M., & Trimmer, J. S. (2012). Benefits and pitfalls of secondary antibodies: why choosing the right secondary is of primary importance. *PLoS One*, *7*(6), e38313.

Manning, G., Whyte, D. B., Martinez, R., Hunter, T., & Sudarsanam, S. (2002). The protein kinase complement of the human genome. *Science*, *298*(5600), 1912-1934.

Manson, J. C., Clarke, A. R., Hooper, M. L., Aitchison, L., McConnell, I., & Hope, J. (1994). 129/Ola mice carrying a null mutation in PrP that abolishes mRNA production are developmentally normal. *Mol Neurobiol*, *8*(2-3), 121-127.

Mantamadiotis, T., Lemberger, T., Bleckmann, S. C., Kern, H., Kretz, O., Martin Villalba, A., Tronche, F., Kellendonk, C., Gau, D., Kapfhammer, J., Otto, C., Schmid, W., & Schutz, G. (2002). Disruption of CREB function in brain leads to neurodegeneration. *Nat Genet*, *31*(1), 47-54.

Marijanovic, Z., Caputo, A., Campana, V., & Zurzolo, C. (2009). Identification of an intracellular site of prion conversion. *PLoS Pathog*, *5*(5), e1000426.

Marsh, R. F., Kincaid, A. E., Bessen, R. A., & Bartz, J. C. (2005). Interspecies transmission of chronic wasting disease prions to squirrel monkeys (Saimiri sciureus). *J Virol*, *79*(21), 13794-13796.

Martin, J., Masri, J., Bernath, A., Nishimura, R. N., & Gera, J. (2008). Hsp70 associates with Rictor and is required for mTORC2 formation and activity. *Biochem Biophys Res Commun*, *372*(4), 578-583.

Martin, L., Latypova, X., Wilson, C. M., Magnaudeix, A., Perrin, M. L., Yardin, C., & Terro, F. (2013). Tau protein kinases: involvement in Alzheimer's disease. *Ageing Res Rev*, *12*(1), 289-309.

Martínez-Lage, J. F., Rábano, A., Bermejo, J., Martínez Pérez, M., Guerrero, M. C., Contreras, M. A., & Lunar, A. (2005). Creutzfeldt-Jakob disease acquired via a dural graft: failure of therapy with quinacrine and chlorpromazine. *Surg Neurol*, *64*(6), 542-5, discussion 545.

Massignan, T., Stewart, R. S., Biasini, E., Solomon, I. H., Bonetto, V., Chiesa, R., & Harris, D. A. (2010). A novel, drug-based, cellular assay for the activity of neurotoxic mutants of the prion protein. *J Biol Chem*, *285*(10), 7752-7765.

Masters, C. L., & Richardson, E. P. (1978). Subacute spongiform encephalopathy (Creutzfeldt-Jakob disease). The nature and progression of spongiform change. *Brain*, *101*(2), 333-344.

Masullo, C., Macchi, G., Xi, Y. G., & Pocchiari, M. (1992). Failure to ameliorate Creutzfeldt-Jakob disease with amphotericin B therapy. *J Infect Dis*, *165*(4), 784-785.

Mathews, J. D., Glasse, R., & Lindenbaum, S. (1968). Kuru and cannibalism. *Lancet*, *2*(7565), 449-452.

Matthews, R. P., Guthrie, C. R., Wailes, L. M., Zhao, X., Means, A. R., & McKnight, G. S. (1994). Calcium/calmodulin-dependent protein kinase types II and IV differentially regulate CREB-dependent gene expression. *Mol Cell Biol*, *14*(9), 6107-6116.

Mawhinney, S., Pape, W. J., Forster, J. E., Anderson, C. A., Bosque, P., & Miller, M. W. (2006). Human prion disease and relative risk associated with chronic wasting disease. *Emerg Infect Dis*, *12*(10), 1527-1535.

Mays, C. E., van der Merwe, J., Kim, C., Haldiman, T., McKenzie, D., Safar, J. G., & Westaway, D. (2015). Prion infectivity plateaus and conversion to symptomatic disease originate from falling precursor levels and increased oligomeric PrP^{Sc} species. *J Virol*, *89*(24), 12418-12426.

Mays, C. E., Kim, C., Haldiman, T., van der Merwe, J., Lau, A., Yang, J., Grams, J., Di Bari, M. A., Nonno, R., & Telling, G. C. (2014). Prion disease tempo determined by host-dependent substrate reduction. *The Journal of clinical investigation*, *124*(2), 847-858.

McDonald, A. J., Dibble, J. P., Evans, E. G., & Millhauser, G. L. (2014). A new paradigm for enzymatic control of alpha-cleavage and beta-cleavage of the prion protein. *J Biol Chem*, *289*(2), 803-813.

McGinnis, K. M., Whitton, M. M., Gnegy, M. E., & Wang, K. K. (1998). Calcium/calmodulin-dependent protein kinase IV is cleaved by caspase-3 and calpain in SH-SY5Y human neuroblastoma cells undergoing apoptosis. *J Biol Chem*, *273*(32), 19993-20000.

McGuire, L. I., Peden, A. H., Orrú, C. D., Wilham, J. M., Appleford, N. E., Mallinson, G., Andrews, M., Head, M. W., Caughey, B., Will, R. G., Knight, R. S., & Green, A. J. (2012). Real time quaking-induced conversion analysis of cerebrospinal fluid in sporadic Creutzfeldt-Jakob disease. *Ann Neurol*, *72*(2), 278-285.

McKinley, M. P., Bolton, D. C., & Prusiner, S. B. (1983a). A protease-resistant protein is a structural component of the scrapie prion. *Cell*, *35*(1), 57-62.

McKinley, M. P., Masiarz, F. R., Isaacs, S. T., Hearst, J. E., & Prusiner, S. B. (1983b). Resistance of the scrapie agent to inactivation by psoralens. *Photochem Photobiol*, *37*(5), 539-545.

McKinley, M. P., Masiarz, F. R., & Prusiner, S. B. (1981). Reversible chemical modification of the scrapie agent. *Science*, *214*(4526), 1259-1261.

McKinnon, C., Goold, R., Andre, R., Devoy, A., Ortega, Z., Moonga, J., Linehan, J. M., Brandner, S., Lucas, J. J., Collinge, J., & Tabrizi, S. J. (2015). Prion-mediated neurodegeneration is associated with early impairment of the ubiquitin-proteasome system. *Acta Neuropathol*, *131*(3), 411-425.

McLennan, N. F., Brennan, P. M., McNeill, A., Davies, I., Fotheringham, A., Rennison, K. A., Ritchie, D., Brannan, F., Head, M. W., Ironside, J. W., Williams, A., & Bell, J. E. (2004). Prion protein accumulation and neuroprotection in hypoxic brain damage. *Am J Pathol*, *165*(1), 227-235.

McLennan, N. F., Rennison, K. A., Bell, J. E., & Ironside, J. W. (2001). In situ hybridization analysis of PrP mRNA in human CNS tissues. *Neuropathol Appl Neurobiol*, *27*(5), 373-383.

McMahon, H. E., Mange, A., Nishida, N., Creminon, C., Casanova, D., & Lehmann, S. (2001). Cleavage of the amino terminus of the prion protein by reactive oxygen species. *J Biol Chem*, *276*(3), 2286-2291.

Mead, S., Poulter, M., Beck, J., Webb, T. E., Campbell, T. A., Linehan, J. M., Desbruslais, M., Joiner, S., Wadsworth, J. D., King, A., Lantos, P., & Collinge, J. (2006). Inherited prion disease with six octapeptide repeat insertional mutation--molecular analysis of phenotypic heterogeneity. *Brain*, *129*(Pt 9), 2297-2317.

Mead, S., Webb, T. E., Campbell, T. A., Beck, J., Linehan, J. M., Rutherfoord, S., Joiner, S., Wadsworth, J. D., Heckmann, J., Wroe, S., Doey, L., King, A., & Collinge, J. (2007). Inherited prion disease with 5-OPRI: phenotype modification by repeat length and codon 129. *Neurology*, *69*(8), 730-738.

Mead, S., Whitfield, J., Poulter, M., Shah, P., Uphill, J., Beck, J., Campbell, T., Al-Dujaily, H., Hummerich, H., Alpers, M. P., & Collinge, J. (2008). Genetic susceptibility, evolution and the kuru epidemic. *Philos Trans R Soc Lond B Biol Sci*, *363*(1510), 3741-3746.

Mead, S., Whitfield, J., Poulter, M., Shah, P., Uphill, J., Campbell, T., Al-Dujaily, H., Hummerich, H., Beck, J., Mein, C. A., Verzilli, C., Whittaker, J., Alpers, M. P., & Collinge, J. (2009). A novel protective prion protein variant that colocalizes with kuru exposure. *N Engl J Med*, *361*(21), 2056-2065.

Mendes, K. N., Nicorici, D., Cogdell, D., Tabus, I., Yli-Harja, O., Guerra, R., Hamilton, S. R., & Zhang, W. (2007). Analysis of signaling pathways in 90 cancer cell lines by protein lysate array. *J Proteome Res*, *6*(7), 2753-2767.

Methot, N., Pickett, G., Keene, J. D., & Sonenberg, N. (1996a). In vitro RNA selection identifies RNA ligands that specifically bind to eukaryotic translation initiation factor 4B: the role of the RNA remotif. *RNA*, *2*(1), 38-50.

Methot, N., Song, M. S., & Sonenberg, N. (1996b). A region rich in aspartic acid, arginine, tyrosine, and glycine (DRYG) mediates eukaryotic initiation factor 4B (eIF4B) self-association and interaction with eIF3. *Mol Cell Biol*, *16*(10), 5328-5334.

Meyer, N., Rosenbaum, V., Schmidt, B., Gilles, K., Mirenda, C., Groth, D., Prusiner, S. B., & Riesner, D. (1991). Search for a putative scrapie genome in purified prion fractions reveals a paucity of nucleic acids. *J Gen Virol*, *72*(Pt 1), 37-49.

Meyer, R. K., McKinley, M. P., Bowman, K. A., Braunfeld, M. B., Barry, R. A., & Prusiner, S. B. (1986). Separation and properties of cellular and scrapie prion proteins. *Proc Natl Acad Sci U S A*, *83*(8), 2310-2314.

Miller, M. B., Wang, D. W., Wang, F., Noble, G. P., Ma, J., Woods, V. L. J., Li, S., & Supattapone, S. (2013). Cofactor molecules induce structural transformation during infectious prion formation. *Structure*, *21*(11), 2061-2068.

Millson, G. C., Hunter, G. D., & Kimberlin, R. H. (1971). An experimental examination of the scrapie agent in cell membrane mixtures. II. The association of scrapie activity with membrane fractions. *J Comp Pathol*, *81*(2), 255-265.

Millson, G. C., Hunter, G. D., & Kimberlin, R. H. (1976). The physico-chemical nature of the scrapie agent. *Front Biol*, *44*, 243-266.

Mironov, A. J., Latawiec, D., Wille, H., Bouzamondo-Bernstein, E., Legname, G., Williamson, R. A., Burton, D., DeArmond, S. J., Prusiner, S. B., & Peters, P. J. (2003). Cytosolic prion protein in neurons. *J Neurosci*, *23*(18), 7183-7193.

Mitteregger, G., Vosko, M., Krebs, B., Xiang, W., Kohlmannsperger, V., Nölting, S., Hamann, G. F., & Kretzschmar, H. A. (2007). The role of the octarepeat region in neuroprotective function of the cellular prion protein. *Brain Pathol*, *17*(2), 174-183.

Moda, F., Gambetti, P., Notari, S., Concha-Marambio, L., Catania, M., Park, K. W., Maderna, E., Suardi, S., Haik, S., Brandel, J. P., Ironside, J., Knight, R., Tagliavini, F., & Soto, C. (2014). Prions in the urine of patients with variant Creutzfeldt-Jakob disease. *N Engl J Med*, *371*(6), 530-539.

Moda, F., Vimercati, C., Campagnani, I., Ruggerone, M., Giaccone, G., Morbin, M., Zentilin, L., Giacca, M., Zucca, I., Legname, G., & Tagliavini, F. (2012). Brain delivery of AAV9 expressing an anti-PrP monovalent antibody delays prion disease in mice. *Prion*, *6*(4), 383-390.

Mok, S. W., Thelen, K. M., Riemer, C., Bamme, T., Gultner, S., Lutjohann, D., & Baier, M. (2006). Simvastatin prolongs survival times in prion infections of the central nervous system. *Biochem Biophys Res Commun*, *348*(2), 697-702.

Monnet, C., Gavard, J., Mege, R. M., & Sobel, A. (2004). Clustering of cellular prion protein induces ERK1/2 and stathmin phosphorylation in GT1-7 neuronal cells. *FEBS Lett*, *576*(1-2), 114-118.

Montag, J., Hitt, R., Opitz, L., Schulz-Schaeffer, W. J., Hunsmann, G., & Motzkus, D. (2009). Upregulation of miRNA hsa-miR-342-3p in experimental and idiopathic prion disease. *Mol Neurodegener*, *4*, 36.

Moody, L. R., Herbst, A. J., Yoo, H. S., Vanderloo, J. P., & Aiken, J. M. (2009). Comparative prion disease gene expression profiling using the prion disease mimetic, cuprizone. *Prion*, *3*(2), 99-109.

Moore, R. C., Lee, I. Y., Silverman, G. L., Harrison, P. M., Strome, R., Heinrich, C., Karunaratne, A., Pasternak, S. H., Chishti, M. A., Liang, Y., Mastrangelo, P., Wang, K., Smit, A. F., Katamine, S., Carlson, G. A., Cohen, F. E., Prusiner, S. B., Melton, D. W., Tremblay, P., Hood, L. E., & Westaway, D. (1999). Ataxia in prion protein (PrP)-deficient mice is associated with upregulation of the novel PrP-like protein doppel. *J Mol Biol*, *292*(4), 797-817.

Moreno, J. A., Halliday, M., Molloy, C., Radford, H., Verity, N., Axten, J. M., Ortori, C. A., Willis, A. E., Fischer, P. M., Barrett, D. A., & Mallucci, G. R. (2013). Oral treatment targeting the unfolded protein response prevents neurodegeneration and clinical disease in prion-infected mice. *Sci Transl Med*, *5*(206), 206ra138.

Moreno, J. A., Radford, H., Peretti, D., Steinert, J. R., Verity, N., Martin, M. G., Halliday, M., Morgan, J., Dinsdale, D., Ortori, C. A., Barrett, D. A., Tsaytler, P., Bertolotti, A., Willis, A. E., Bushell, M., & Mallucci, G. R. (2012). Sustained translational repression by eIF2alpha-P mediates prion neurodegeneration. *Nature*, *485*(7399), 507-511.

Moroncini, G., Kanu, N., Solforosi, L., Abalos, G., Telling, G. C., Head, M., Ironside, J., Brockes, J. P., Burton, D. R., & Williamson, R. A. (2004). Motif-grafted antibodies containing the replicative interface of cellular PrP are specific for PrP^{Sc}. *Proc Natl Acad Sci U S A*, *101*(28), 10404-10409.

Mouillet-Richard, S., Ermonval, M., Chebassier, C., Laplanche, J. L., Lehmann, S., Launay, J. M., & Kellermann, O. (2000). Signal transduction through prion protein. *Science*, *289*(5486), 1925-1928.

Mukherjee, A., Morales-Scheihing, D., Gonzalez-Romero, D., Green, K., Taglialatela, G., & Soto, C. (2010). Calcineurin inhibition at the clinical phase of prion disease reduces neurodegeneration, improves behavioral alterations and increases animal survival. *PLoS Pathog*, *6*(10), e1001138.

Mulcahy, E. R., & Bessen, R. A. (2004). Strain-specific kinetics of prion protein formation in vitro and in vivo. *J Biol Chem*, *279*(3), 1643-1649.

Müller, M., Cárdenas, C., Mei, L., Cheung, K. H., & Foskett, J. K. (2011). Constitutive cAMP response element binding protein (CREB) activation by Alzheimer's disease presenilin-driven inositol trisphosphate receptor (InsP3R) Ca2+ signaling. *Proc Natl Acad Sci U S A*, *108*(32), 13293-13298.

Müller, W. E., Ushijima, H., Schröder, H. C., Forrest, J. M., Schatton, W. F., Rytik, P. G., & Heffner-Lauc, M. (1993). Cytoprotective effect of NMDA receptor antagonists on prion protein (PrionSc)-induced toxicity in rat cortical cell cultures. *Eur J Pharmacol*, *246*(3), 261-267.

Mumm, J. S., Schroeter, E. H., Saxena, M. T., Griesemer, A., Tian, X., Pan, D. J., Ray, W. J., & Kopan, R. (2000). A ligand-induced extracellular cleavage regulates gamma-secretase-like proteolytic activation of Notch1. *Mol Cell*, *5*(2), 197-206.

Muramoto, T., DeArmond, S. J., Scott, M., Telling, G. C., Cohen, F. E., & Prusiner, S. B. (1997). Heritable disorder resembling neuronal storage disease in mice expressing prion protein with deletion of an alpha-helix. *Nat Med*, *3*(7), 750-755.

Muramoto, T., Scott, M., Cohen, F. E., & Prusiner, S. B. (1996). Recombinant scrapie-like prion protein of 106 amino acids is soluble. *Proc Natl Acad Sci U S A*, *93*(26), 15457-15462.

Murray, P. D., Kingsbury, T. J., & Krueger, B. K. (2009). Failure of Ca2+-activated, CREB-dependent transcription in astrocytes. *Glia*, *57*(8), 828-834.

Nakagaki, T., Satoh, K., Ishibashi, D., Fuse, T., Sano, K., Kamatari, Y. O., Kuwata, K., Shigematsu, K., Iwamaru, Y., Takenouchi, T., Kitani, H., Nishida, N., & Atarashi, R. (2013). FK506 reduces abnormal prion protein through the activation of autolysosomal degradation and prolongs survival in prion-infected mice. *Autophagy*, *9*(9), 1386-1394.

Naslavsky, N., Stein, R., Yanai, A., Friedlander, G., & Taraboulos, A. (1997). Characterization of detergent-insoluble complexes containing the cellular prion protein and its scrapie isoform. *J Biol Chem*, *272*(10), 6324-6331.

National CJD Research and Surveillance Unit. Number of Variant CJD cases worldwide. Retreived May 4, 2016, from www.cjd.ed.ac.uk/documents/worldfigs.pdf.

Nishida, N., Tremblay, P., Sugimoto, T., Shigematsu, K., Shirabe, S., Petromilli, C., Erpel, S. P., Nakaoke, R., Atarashi, R., Houtani, T., Torchia, M., Sakaguchi, S., DeArmond, S. J., Prusiner, S. B., & Katamine, S. (1999). A mouse prion protein transgene rescues mice deficient for the prion protein gene from purkinje cell degeneration and demyelination. *Lab Invest*, *79*(6), 689-697.

Nishizawa, Y. (2001). Glutamate release and neuronal damage in ischemia. *Life Sci*, *69*(4), 369-381.

Nixon, R. R. (2005). Prion-associated increases in Src-family kinases. *J Biol Chem*, *280*(4), 2455-2462.

Nordstrom, E., Fisone, G., & Kristensson, K. (2009). Opposing effects of ERK and p38-JNK MAP kinase pathways on formation of prions in GT1-1 cells. *FASEB J*, *23*(2), 613-622.

Nordstrom, E. K., Luhr, K. M., Ibanez, C., & Kristensson, K. (2005). Inhibitors of the mitogen-activated protein kinase kinase 1/2 signaling pathway clear prion-infected cells from PrP^{Sc}. *J Neurosci*, *25*(37), 8451-8456.

Norstrom, E. M., Ciaccio, M. F., Rassbach, B., Wollmann, R., & Mastrianni, J. A. (2007). Cytosolic prion protein toxicity is independent of cellular prion protein expression and prion propagation. *J Virol*, *81*(6), 2831-2837.

Norstrom, E. M., & Mastrianni, J. A. (2005). The AGAAAAGA palindrome in PrP is required to generate a productive PrP^{Sc}-PrPC complex that leads to prion propagation. *J Biol Chem*, *280*(29), 27236-27243.

Novitskaya, V., Bocharova, O. V., Bronstein, I., & Baskakov, I. V. (2006). Amyloid fibrils of mammalian prion protein are highly toxic to cultured cells and primary neurons. *J Biol Chem*, *281*(19), 13828-13836.

Nudelman, A. S., DiRocco, D. P., Lambert, T. J., Garelick, M. G., Le, J., Nathanson, N. M., & Storm, D. R. (2010). Neuronal activity rapidly induces transcription of the CREB-regulated microRNA-132, in vivo. *Hippocampus*, *20*(4), 492-498.

O'Donovan, C. N., Tobin, D., & Cotter, T. G. (2001). Prion protein fragment PrP-(106-126) induces apoptosis via mitochondrial disruption in human neuronal SH-SY5Y cells. *J Biol Chem*, *276*(47), 43516-43523.

Obexer, P., Geiger, K., Ambros, P. F., Meister, B., & Ausserlechner, M. J. (2007). FKHRL1-mediated expression of Noxa and Bim induces apoptosis via the mitochondria in neuroblastoma cells. *Cell Death Differ*, *14*(3), 534-547.

Oesch, B., Groth, D. F., Prusiner, S. B., & Weissmann, C. (1988). Search for a scrapie-specific nucleic acid: a progress report. *Ciba Found Symp*, *135*, 209-223.

Oesch, B., Westaway, D., Walchli, M., McKinley, M. P., Kent, S. B., Aebersold, R., Barry, R. A., Tempst, P., Teplow, D. B., Hood, L. E., & et, A. (1985). A cellular gene encodes scrapie PrP 27-30 protein. *Cell*, *40*(4), 735-746.

Oetjen, E., Lechleiter, A., Blume, R., Nihalani, D., Holzman, L., & Knepel, W. (2006). Inhibition of membrane depolarisation-induced transcriptional activity of cyclic AMP response element binding protein (CREB) by the dual-leucine-zipper-bearing kinase in a pancreatic islet beta cell line. *Diabetologia*, *49*(2), 332-342.

Office International des Epizooties (a). Number of cases of BSE in farmed cattle worldwide excluding the UK by year of confirmation. Retrieved October 25, 2015, from http://www.oie.int/animal-health-in-the-world/bse-specific-data/number-of-reported-cases-worldwide-excluding-the-united-kingdom/.

Office International des Epizooties (b). Number of cases of BSE in the UK by year of restriction. Retrieved October 25, 2015, from http://www.oie.int/animal-health-in-the-world/bse-specific-data/number-of-cases-in-the-united-kingdom/.

Oh, S., Lee, D., Kim, T., Kim, T. S., Oh, H. J., Hwang, C. Y., Kong, Y. Y., Kwon, K. S., & Lim, D. S. (2009). Crucial role for Mst1 and Mst2 kinases in early embryonic development of the mouse. *Mol Cell Biol*, *29*(23), 6309-6320.

Ohsawa, N., Song, C. H., Suzuki, A., Furuoka, H., Hasebe, R., & Horiuchi, M. (2013). Therapeutic effect of peripheral administration of an anti-prion protein antibody on mice infected with prions. *Microbiol Immunol*, *57*(4), 288-297.

Oliveira-Martins, J. B., Yusa, S., Calella, A. M., Bridel, C., Baumann, F., Dametto, P., & Aguzzi, A. (2010). Unexpected tolerance of alpha-cleavage of the prion protein to sequence variations. *PLoS One*, *5*(2), e9107.

Orru, C. D., Bongianni, M., Tonoli, G., Ferrari, S., Hughson, A. G., Groveman, B. R., Fiorini, M., Pocchiari, M., Monaco, S., Caughey, B., & Zanusso, G. (2014). A test for Creutzfeldt-Jakob disease using nasal brushings. *N Engl J Med*, *371*(6), 519-529.

Otter, T., King, S. M., & Witman, G. B. (1987). A two-step procedure for efficient electrotransfer of both high-molecular-weight (greater than 400,000) and low-molecular-weight (less than 20,000) proteins. *Anal Biochem*, *162*(2), 370-377.

Paisley, D., Banks, S., Selfridge, J., McLennan, N. F., Ritchie, A. M., McEwan, C., Irvine, D. S., Saunders, P. T., Manson, J. C., & Melton, D. W. (2004). Male infertility and DNA damage in Doppel knockout and prion protein/Doppel double-knockout mice. *Am J Pathol*, *164*(6), 2279-2288.

Palmer, M. S., Dryden, A. J., Hughes, J. T., & Collinge, J. (1991). Homozygous prion protein genotype predisposes to sporadic Creutzfeldt-Jakob disease. *Nature*, *352*(6333), 340-342.

Pan, B., Yang, L., Wang, J., Wang, Y., Wang, J., Zhou, X., Yin, X., Zhang, Z., & Zhao, D. (2014). c-Abl Tyrosine Kinase Mediates Neurotoxic Prion Peptide-Induced Neuronal Apoptosis via Regulating Mitochondrial Homeostasis. *Mol Neurobiol*, *49*(2), 1102-1116.

Pan, K. M., Baldwin, M., Nguyen, J., Gasset, M., Serban, A., Groth, D., Mehlhorn, I., Huang, Z., Fletterick, R. J., Cohen, F. E., & et, A. (1993). Conversion of alpha-helices into beta-sheets features in the formation of the scrapie prion proteins. *Proc Natl Acad Sci U S A*, *90*(23), 10962-10966.

Pankiv, S., Clausen, T. H., Lamark, T., Brech, A., Bruun, J. A., Outzen, H., Øvervatn, A., Bjørkøy, G., & Johansen, T. (2007). p62/SQSTM1 binds directly to Atg8/LC3 to facilitate degradation of ubiquitinated protein aggregates by autophagy. *J Biol Chem*, *282*(33), 24131-24145.

Park, I. K., & Soderling, T. R. (1995). Activation of Ca2+/calmodulin-dependent protein kinase (CaM-kinase) IV by CaM-kinase kinase in Jurkat T lymphocytes. *J Biol Chem*, *270*(51), 30464-30469.

Park, S. K., Choi, S. I., Jin, J. K., Choi, E. K., Kim, J. I., Carp, R. I., & Kim, Y. S. (2000). Differential expression of Bax and Bcl-2 in the brains of hamsters infected with 263K scrapie agent. *Neuroreport*, *11*(8), 1677-1682.

Paterson, R. W., Takada, L. T., & Geschwind, M. D. (2012a). Diagnosis and treatment of rapidly progressive dementias. *Neurol Clin Pract*, *2*(3), 187-200.

Paterson, R. W., Torres-Chae, C. C., Kuo, A. L., Ando, T., Nguyen, E. A., Wong, K., Dearmond, S. J., Haman, A., Garcia, P., Johnson, D. Y., Miller, B. L., & Geschwind, M. D. (2012b). Differential diagnosis of jakob-creutzfeldt disease. *Arch Neurol*, *69*(12), 1578-1582.

Pattison, I. H., & Jones, K. M. (1967). The possible nature of the transmissible agent of scrapie. *Vet Rec*, *80*(1), 2-9.

Pauly, P. C., & Harris, D. A. (1998). Copper stimulates endocytosis of the prion protein. *J Biol Chem*, *273*(50), 33107-33110.

Pearce, L. R., Komander, D., & Alessi, D. R. (2010). The nuts and bolts of AGC protein kinases. *Nat Rev Mol Cell Biol*, *11*(1), 9-22.

Peden, A., McCardle, L., Head, M. W., Love, S., Ward, H. J., Cousens, S. N., Keeling, D. M., Millar, C. M., Hill, F. G., & Ironside, J. W. (2010). Variant CJD infection in the spleen of a neurologically asymptomatic UK adult patient with haemophilia. *Haemophilia*, *16*(2), 296-304.

Peden, A. H., Head, M. W., Ritchie, D. L., Bell, J. E., & Ironside, J. W. (2004). Preclinical vCJD after blood transfusion in a PRNP codon 129 heterozygous patient. *Lancet*, *364*(9433), 527-529.

Pekny, M., & Pekna, M. (2014). Astrocyte reactivity and reactive astrogliosis: costs and benefits. *Physiol Rev*, *94*(4), 1077-1098.

Pelech, S., Sutter, C., & Zhang, H. (2003). Kinetworks protein kinase multiblot analysis. *Methods Mol Biol*, *218*, 99-111.

Peppelenbosch, M. P. (2012). Kinome profiling. *Scientifica (Cairo)*, *2012*, 306798.

Peralta, O. A., & Eyestone, W. H. (2009). Quantitative and qualitative analysis of cellular prion protein (PrP(C)) expression in bovine somatic tissues. *Prion*, *3*(3), 161-170.

Perera, W. S., & Hooper, N. M. (2001). Ablation of the metal ion-induced endocytosis of the prion protein by disease-associated mutation of the octarepeat region. *Curr Biol*, *11*(7), 519-523.

Peretz, D., Scott, M. R., Groth, D., Williamson, R. A., Burton, D. R., Cohen, F. E., & Prusiner, S. B. (2001a). Strain-specified relative conformational stability of the scrapie prion protein. *Protein Sci*, *10*(4), 854-863.

Peretz, D., Williamson, R. A., Kaneko, K., Vergara, J., Leclerc, E., Schmitt-Ulms, G., Mehlhorn, I. R., Legname, G., Wormald, M. R., Rudd, P. M., Dwek, R. A., Burton, D. R., & Prusiner, S. B. (2001b). Antibodies inhibit prion propagation and clear cell cultures of prion infectivity. *Nature*, *412*(6848), 739-743.

Perrier, V., Solassol, J., Crozet, C., Frobert, Y., Mourton-Gilles, C., Grassi, J., & Lehmann, S. (2004). Anti-PrP antibodies block PrP^{Sc} replication in prion-infected cell cultures by accelerating PrP^{C} degradation. *J Neurochem*, *89*(2), 454-463.

Peters, P. J., Mironov, A. J., Peretz, D., van Donselaar, E., Leclerc, E., Erpel, S., DeArmond, S. J., Burton, D. R., Williamson, R. A., Vey, M., & Prusiner, S. B. (2003). Trafficking of prion proteins through a caveolae-mediated endosomal pathway. *J Cell Biol*, *162*(4), 703-717.

Pfeifer, A., Eigenbrod, S., Al-Khadra, S., Hofmann, A., Mitteregger, G., Moser, M., Bertsch, U., & Kretzschmar, H. (2006). Lentivector-mediated RNAi efficiently suppresses prion protein and prolongs survival of scrapie-infected mice. *J Clin Invest*, *116*(12), 3204-3210.

Pietri, M., Dakowski, C., Hannaoui, S., Alleaume-Butaux, A., Hernandez-Rapp, J., Ragagnin, A., Mouillet-Richard, S., Haik, S., Bailly, Y., Peyrin, J. M., Launay, J. M., Kellermann, O., & Schneider, B. (2013). PDK1 decreases TACE-mediated alpha-secretase activity and promotes disease progression in prion and Alzheimer's diseases. *Nat Med*, *19*(9), 1124-1131.

Pillot, T., Lins, L., Goethals, M., Vanloo, B., Baert, J., Vandekerckhove, J., Rosseneu, M., & Brasseur, R. (1997). The 118-135 peptide of the human prion protein forms amyloid fibrils and induces liposome fusion. *J Mol Biol*, *274*(3), 381-393.

Pimpinelli, F., Lehmann, S., & Maridonneau-Parini, I. (2005). The scrapie prion protein is present in flotillin-1-positive vesicles in central- but not peripheral-derived neuronal cell lines. *Eur J Neurosci*, *21*(8), 2063-2072.

Piro, J. R., Harris, B. T., & Supattapone, S. (2011). In situ photodegradation of incorporated polyanion does not alter prion infectivity. *PLoS Pathog*, *7*(2), e1002001.

Plaumann, S., Blume, R., Börchers, S., Steinfelder, H. J., Knepel, W., & Oetjen, E. (2008). Activation of the dual-leucine-zipper-bearing kinase and induction of beta-cell apoptosis by the immunosuppressive drug cyclosporin A. *Mol Pharmacol*, *73*(3), 652-659.

Poli, G., Corda, E., Lucchini, B., Puricelli, M., Martino, P. A., Dall'ara, P., Villetti, G., Bareggi, S. R., Corona, C., Vallino Costassa, E., Gazzuola, P., Iulini, B., Mazza, M., Acutis, P., Mantegazza, P., Casalone, C., & Imbimbo, B. P. (2012). Therapeutic effect of CHF5074, a new γ-secretase modulator, in a mouse model of scrapie. *Prion*, *6*(1), 62-72.

Pozniak, C. D., Sengupta Ghosh, A., Gogineni, A., Hanson, J. E., Lee, S. H., Larson, J. L., Solanoy, H., Bustos, D., Li, H., Ngu, H., Jubb, A. M., Ayalon, G., Wu, J., Scearce-Levie, K., Zhou, Q., Weimer, R. M., Kirkpatrick, D. S., & Lewcock, J. W. (2013). Dual leucine zipper kinase is required for excitotoxicity-induced neuronal degeneration. *J Exp Med*, *210*(12), 2553-2567.

Praskova, M., Khoklatchev, A., Ortiz-Vega, S., & Avruch, J. (2004). Regulation of the MST1 kinase by autophosphorylation, by the growth inhibitory proteins, RASSF1 and NORE1, and by Ras. *Biochem J*, *381*(Pt 2), 453-462.

Premzl, M., Sangiorgio, L., Strumbo, B., Marshall Graves, J. A., Simonic, T., & Gready, J. E. (2003). Shadoo, a new protein highly conserved from fish to mammals and with similarity to prion protein. *Gene*, *314*, 89-102.

Price, J. C., Guan, S., Burlingame, A., Prusiner, S. B., & Ghaemmaghami, S. (2010). Analysis of proteome dynamics in the mouse brain. *Proc Natl Acad Sci U S A*, *107*(32), 14508-14513.

Priola, S. A., Caughey, B., Race, R. E., & Chesebro, B. (1994). Heterologous PrP molecules interfere with accumulation of protease-resistant PrP in scrapie-infected murine neuroblastoma cells. *J Virol*, *68*(8), 4873-4878.

Prusiner, S. B. (1982). Novel proteinaceous infectious particles cause scrapie. *Science*, *216*(4542), 136-144.

Prusiner, S. B. (1998). Prions. *Proc Natl Acad Sci U S A*, *95*(23), 13363-13383.

Prusiner, S. B., Bolton, D. C., Groth, D. F., Bowman, K. A., Cochran, S. P., & McKinley, M. P. (1982). Further purification and characterization of scrapie prions. *Biochemistry*, *21*(26), 6942-6950.

Prusiner, S. B., Groth, D. F., Cochran, S. P., Masiarz, F. R., McKinley, M. P., & Martinez, H. M. (1980a). Molecular properties, partial purification, and assay by incubation period measurements of the hamster scrapie agent. *Biochemistry*, *19*(21), 4883-4891.

Prusiner, S. B., Groth, D. F., Cochran, S. P., McKinley, M. P., & Masiarz, F. R. (1980b). Gel electrophoresis and glass permeation chromatography of the hamster scrapie agent after enzymatic digestion and detergent extraction. *Biochemistry*, *19*(21), 4892-4898.

Prusiner, S. B., Groth, D. F., McKinley, M. P., Cochran, S. P., Bowman, K. A., & Kasper, K. C. (1981a). Thiocyanate and hydroxyl ions inactivate the scrapie agent. *Proc Natl Acad Sci U S A*, *78*(7), 4606-4610.

Prusiner, S. B., Hadlow, W. J., Eklund, C. M., & Race, R. E. (1977). Sedimentation properties of the scrapie agent. *Proc Natl Acad Sci U S A*, *74*(10), 4656-4660.

Prusiner, S. B., Hadlow, W. J., Eklund, C. M., Race, R. E., & Cochran, S. P. (1978a). Sedimentation characteristics of the scrapie agent from murine spleen and brain. *Biochemistry*, *17*(23), 4987-4992.

Prusiner, S. B., Hadlow, W. J., Garfin, D. E., Cochran, S. P., Baringer, J. R., Race, R. E., & Eklund, C. M. (1978b). Partial purification and evidence for multiple molecular forms of the scrapie agent. *Biochemistry*, *17*(23), 4993-4999.

Prusiner, S. B., McKinley, M. P., Groth, D. F., Bowman, K. A., Mock, N. I., Cochran, S. P., & Masiarz, F. R. (1981b). Scrapie agent contains a hydrophobic protein. *Proc Natl Acad Sci U S A*, *78*(11), 6675-6679.

Prusiner, S. B., Scott, M., Foster, D., Pan, K. M., Groth, D., Mirenda, C., Torchia, M., Yang, S. L., Serban, D., Carlson, G. A., & et, A. (1990). Transgenetic studies implicate interactions between homologous PrP isoforms in scrapie prion replication. *Cell*, *63*(4), 673-686.

Puig, B., & Ferrer, I. (2001). Cell death signaling in the cerebellum in Creutzfeldt-Jakob disease. *Acta Neuropathol*, *102*(3), 207-215.

Qiu, J. H., Asai, A., Chi, S., Saito, N., Hamada, H., & Kirino, T. (2000). Proteasome inhibitors induce cytochrome c-caspase-3-like protease-mediated apoptosis in cultured cortical neurons. *J Neurosci*, *20*(1), 259-265.

Quaglio, E., Restelli, E., Garofoli, A., Dossena, S., De Luigi, A., Tagliavacca, L., Imperiale, D., Migheli, A., Salmona, M., Sitia, R., Forloni, G., & Chiesa, R. (2011). Expression of mutant or cytosolic PrP in transgenic mice and cells is not associated with endoplasmic reticulum stress or proteasome dysfunction. *PLoS One*, *6*(4), e19339.

Race, B., Meade-White, K. D., Miller, M. W., Barbian, K. D., Rubenstein, R., LaFauci, G., Cervenakova, L., Favara, C., Gardner, D., Long, D., Parnell, M., Striebel, J., Priola, S. A., Ward, A., Williams, E. S., Race, R., & Chesebro, B. (2009). Susceptibilities of nonhuman primates to chronic wasting disease. *Emerg Infect Dis*, *15*(9), 1366-1376.

Race, B., Meade-White, K. D., Phillips, K., Striebel, J., Race, R., & Chesebro, B. (2014). Chronic wasting disease agents in nonhuman primates. *Emerg Infect Dis*, *20*(5), 833-837.

Race, R. E., Priola, S. A., Bessen, R. A., Ernst, D., Dockter, J., Rall, G. F., Mucke, L., Chesebro, B., & Oldstone, M. B. (1995). Neuron-specific expression of a hamster prion protein minigene in transgenic mice induces susceptibility to hamster scrapie agent. *Neuron*, *15*(5), 1183-1191.

Raeber, A. J., Race, R. E., Brandner, S., Priola, S. A., Sailer, A., Bessen, R. A., Mucke, L., Manson, J., Aguzzi, A., Oldstone, M. B., Weissmann, C., & Chesebro, B. (1997). Astrocyte-specific expression of hamster prion protein (PrP) renders PrP knockout mice susceptible to hamster scrapie. *EMBO J*, *16*(20), 6057-6065.

Rambold, A. S., Miesbauer, M., Rapaport, D., Bartke, T., Baier, M., Winklhofer, K. F., & Tatzelt, J. (2006). Association of Bcl-2 with misfolded prion protein is linked to the toxic potential of cytosolic PrP. *Mol Biol Cell*, *17*(8), 3356-3368.

Rambold, A. S., Muller, V., Ron, U., Ben-Tal, N., Winklhofer, K. F., & Tatzelt, J. (2008). Stress-protective signalling of prion protein is corrupted by scrapie prions. *EMBO J*, *27*(14), 1974-1984.

Rane, N. S., Kang, S. W., Chakrabarti, O., Feigenbaum, L., & Hegde, R. S. (2008). Reduced translocation of nascent prion protein during ER stress contributes to neurodegeneration. *Dev Cell*, *15*(3), 359-370.

Rane, N. S., Yonkovich, J. L., & Hegde, R. S. (2004). Protection from cytosolic prion protein toxicity by modulation of protein translocation. *EMBO J*, *23*(23), 4550-4559.

Rangel, A., Burgaya, F., Gavín, R., Soriano, E., Aguzzi, A., & Del, R., JA. (2007). Enhanced susceptibility of Prnp-deficient mice to kainate-induced seizures, neuronal apoptosis, and death: Role of AMPA/kainate receptors. *J Neurosci Res*, *85*(12), 2741-2755.

Rangel, A., Madroñal, N., Gruart, A., Gruart i Massó, A., Gavín, R., Llorens, F., Sumoy, L., Torres, J. M., Delgado-García, J. M., & Del, R., JA. (2009). Regulation of GABA(A) and glutamate receptor expression, synaptic facilitation and long-term potentiation in the hippocampus of prion mutant mice. *PLoS One*, *4*(10), e7592.

Rapoport, T. A. (2007). Protein translocation across the eukaryotic endoplasmic reticulum and bacterial plasma membranes. *Nature*, *450*(7170), 663-669.

Raught, B., Peiretti, F., Gingras, A. C., Livingstone, M., Shahbazian, D., Mayeur, G. L., Polakiewicz, R. D., Sonenberg, N., & Hershey, J. W. (2004). Phosphorylation of eucaryotic translation initiation factor 4B Ser422 is modulated by S6 kinases. *EMBO J*, *23*(8), 1761-1769.

Rawat, S. J., & Chernoff, J. (2015). Regulation of mammalian Ste20 (Mst) kinases. *Trends Biochem Sci*, *40*(3), 149-156.

Raymond, G. J., Bossers, A., Raymond, L. D., O'Rourke, K. I., McHolland, L. E., Bryant, P. K., Miller, M. W., Williams, E. S., Smits, M., & Caughey, B. (2000). Evidence of a molecular barrier limiting susceptibility of humans, cattle and sheep to chronic wasting disease. *EMBO J*, *19*(17), 4425-4430.

Raymond, G. J., Race, B., Hollister, J. R., Offerdahl, D. K., Moore, R. A., Kodali, R., Raymond, L. D., Hughson, A. G., Rosenke, R., Long, D., Dorward, D. W., & Baron, G. S. (2012). Isolation of novel synthetic prion strains by amplification in transgenic mice coexpressing wild-type and anchorless prion proteins. *J Virol*, *86*(21), 11763-11778.

Redpath, N. T., Price, N. T., Severinov, K. V., & Proud, C. G. (1993). Regulation of elongation factor-2 by multisite phosphorylation. *Eur J Biochem*, *213*(2), 689-699.

European Commission Directorate-General for Health and Food Safety. Report on the monitoring and testing of ruminants for the presence of transmissible spongiform encephalopathies (TSEs) in the EU in 2013. Retrieved October 25, 2015, from http://ec.europa.eu/food/food/biosafety/tse_bse/docs/annual_report_tse2013_en.pdf.

Requena, J. R., & Wille, H. (2014). The structure of the infectious prion protein: experimental data and molecular models. *Prion*, *8*(1), 60-66.

Resenberger, U. K., Harmeier, A., Woerner, A. C., Goodman, J. L., Müller, V., Krishnan, R., Vabulas, R. M., Kretzschmar, H. A., Lindquist, S., Hartl, F. U., Multhaup, G., Winklhofer, K. F., & Tatzelt, J. (2011). The cellular prion protein mediates neurotoxic signalling of β-sheet-rich conformers independent of prion replication. *EMBO J*, *30*(10), 2057-2070.

Ribar, T. J., Rodriguiz, R. M., Khiroug, L., Wetsel, W. C., Augustine, G. J., & Means, A. R. (2000). Cerebellar defects in Ca2+/calmodulin kinase IV-deficient mice. *J Neurosci*, *20*(22), RC107.

Richt, J. A., Kasinathan, P., Hamir, A. N., Castilla, J., Sathiyaseelan, T., Vargas, F., Sathiyaseelan, J., Wu, H., Matsushita, H., Koster, J., Kato, S., Ishida, I., Soto, C., Robl, J. M., & Kuroiwa, Y. (2007). Production of cattle lacking prion protein. *Nat Biotechnol*, *25*(1), 132-138.

Riek, R., Hornemann, S., Wider, G., Billeter, M., Glockshuber, R., & Wuthrich, K. (1996). NMR structure of the mouse prion protein domain PrP(121-231). *Nature*, *382*(6587), 180-182.

Riek, R., Hornemann, S., Wider, G., Glockshuber, R., & Wuthrich, K. (1997). NMR characterization of the full-length recombinant murine prion protein, mPrP(23-231). *FEBS Lett*, *413*(2), 282-288.

Riemer, C., Burwinkel, M., Schwarz, A., Gultner, S., Mok, S. W., Heise, I., Holtkamp, N., & Baier, M. (2008). Evaluation of drugs for treatment of prion infections of the central nervous system. *J Gen Virol*, *89*(Pt 2), 594-597.

Riemer, C., Neidhold, S., Burwinkel, M., Schwarz, A., Schultz, J., Kratzschmar, J., Monning, U., & Baier, M. (2004). Gene expression profiling of scrapie-infected brain tissue. *Biochem Biophys Res Commun*, *323*(2), 556-564.

Ritchie, D. L., Boyle, A., McConnell, I., Head, M. W., Ironside, J. W., & Bruce, M. E. (2009). Transmissions of variant Creutzfeldt-Jakob disease from brain and lymphoreticular tissue show uniform and conserved bovine spongiform encephalopathy-related phenotypic properties on primary and secondary passage in wild-type mice. *J Gen Virol*, *90*(Pt 12), 3075-3082.

Roberts, G. W., Lofthouse, R., Brown, R., Crow, T. J., Barry, R. A., & Prusiner, S. B. (1986). Prion-protein immunoreactivity in human transmissible dementias. *N Engl J Med*, *315*(19), 1231-1233.

Roffe, M., Beraldo, F. H., Bester, R., Nunziante, M., Bach, C., Mancini, G., Gilch, S., Vorberg, I., Castilho, B. A., Martins, V. R., & Hajj, G. N. (2010). Prion protein interaction with stress-inducible protein 1 enhances neuronal protein synthesis via mTOR. *Proc Natl Acad Sci U S A*, *107*(29), 13147-13152.

Ron, D., & Walter, P. (2007). Signal integration in the endoplasmic reticulum unfolded protein response. *Nat Rev Mol Cell Biol*, *8*(7), 519-529.

Rosner, M., Fuchs, C., Siegel, N., Valli, A., & Hengstschlager, M. (2009). Functional interaction of mammalian target of rapamycin complexes in regulating mammalian cell size and cell cycle. *Hum Mol Genet*, *18*(17), 3298-3310.

Rossi, D., Cozzio, A., Flechsig, E., Klein, M. A., Rülicke, T., Aguzzi, A., & Weissmann, C. (2001). Onset of ataxia and Purkinje cell loss in PrP null mice inversely correlated with Dpl level in brain. *EMBO J*, *20*(4), 694-702.

Roucou, X., Guo, Q., Zhang, Y., Goodyer, C. G., & LeBlanc, A. C. (2003). Cytosolic prion protein is not toxic and protects against Bax-mediated cell death in human primary neurons. *J Biol Chem*, *278*(42), 40877-40881.

Rozen, F., Edery, I., Meerovitch, K., Dever, T. E., Merrick, W. C., & Sonenberg, N. (1990). Bidirectional RNA helicase activity of eucaryotic translation initiation factors 4A and 4F. *Mol Cell Biol*, *10*(3), 1134-1144.

Rozovsky, N., Butterworth, A. C., & Moore, M. J. (2008). Interactions between eIF4AI and its accessory factors eIF4B and eIF4H. *RNA*, *14*(10), 2136-2148.

Ruiz, A., Matute, C., & Alberdi, E. (2009). Endoplasmic reticulum Ca(2+) release through ryanodine and IP(3) receptors contributes to neuronal excitotoxicity. *Cell Calcium*, *46*(4), 273-281.

Rutala, W. A., Weber, D. J., & Society, F. H. E. O. A. (2010). Guideline for disinfection and sterilization of prion-contaminated medical instruments. *Infect Control Hosp Epidemiol*, *31*(2), 107-117.

Rymer, D. L., & Good, T. A. (2000). The role of prion peptide structure and aggregation in toxicity and membrane binding. *J Neurochem*, *75*(6), 2536-2545.

Saba, R., Goodman, C. D., Huzarewich, R. L., Robertson, C., & Booth, S. A. (2008). A miRNA signature of prion induced neurodegeneration. *PLoS One*, *3*(11), e3652.

Sabio, G., Reuver, S., Feijoo, C., Hasegawa, M., Thomas, G. M., Centeno, F., Kuhlendahl, S., Leal-Ortiz, S., Goedert, M., Garner, C., & Cuenda, A. (2004). Stress- and mitogen-induced phosphorylation of the synapse-associated protein SAP90/PSD-95 by activation of SAPK3/p38gamma and ERK1/ERK2. *Biochem J*, *380*(Pt 1), 19-30.

Saborio, G. P., Permanne, B., & Soto, C. (2001). Sensitive detection of pathological prion protein by cyclic amplification of protein misfolding. *Nature*, *411*(6839), 810-813.

Saez-Valero, J., Angeretti, N., & Forloni, G. (2000). Caspase-3 activation by beta-amyloid and prion protein peptides is independent from their neurotoxic effect. *Neurosci Lett*, *293*(3), 207-210.

Safar, J., Roller, P. P., Gajdusek, D. C., & Gibbs, C. J. J. (1993). Conformational transitions, dissociation, and unfolding of scrapie amyloid (prion) protein. *J Biol Chem*, *268*(27), 20276-20284.

Safar, J., Wille, H., Itri, V., Groth, D., Serban, H., Torchia, M., Cohen, F. E., & Prusiner, S. B. (1998). Eight prion strains have PrP(Sc) molecules with different conformations. *Nat Med*, *4*(10), 1157-1165.

Safar, J. G., DeArmond, S. J., Kociuba, K., Deering, C., Didorenko, S., Bouzamondo-Bernstein, E., Prusiner, S. B., & Tremblay, P. (2005a). Prion clearance in bigenic mice. *J Gen Virol*, *86*(Pt 10), 2913-2923.

Safar, J. G., Geschwind, M. D., Deering, C., Didorenko, S., Sattavat, M., Sanchez, H., Serban, A., Vey, M., Baron, H., Giles, K., Miller, B. L., Dearmond, S. J., & Prusiner, S. B. (2005b). Diagnosis of human prion disease. *Proc Natl Acad Sci U S A*, *102*(9), 3501-3506.

Safar, J. G., Kellings, K., Serban, A., Groth, D., Cleaver, J. E., Prusiner, S. B., & Riesner, D. (2005c). Search for a prion-specific nucleic acid. *J Virol*, *79*(16), 10796-10806.

Sage, E. (1993). Distribution and repair of photolesions in DNA: genetic consequences and the role of sequence context. *Photochem Photobiol*, *57*(1), 163-174.

Sailer, A., Bueler, H., Fischer, M., Aguzzi, A., & Weissmann, C. (1994). No propagation of prions in mice devoid of PrP. *Cell*, *77*(7), 967-968.

Sakagami, H., Umemiya, M., Kobayashi, T., Saito, S., & Kondo, H. (1999). Immunological evidence that the beta isoform of Ca2+/calmodulin-dependent protein kinase IV is a cerebellar granule cell-specific product of the CaM kinase IV gene. *Eur J Neurosci*, *11*(7), 2531-2536.

Sakaguchi, S. (2009). [Systematic review of the therapeutics for prion diseases]. *Brain Nerve*, *61*(8), 929-938.

Sakaguchi, S., Katamine, S., Nishida, N., Moriuchi, R., Shigematsu, K., Sugimoto, T., Nakatani, A., Kataoka, Y., Houtani, T., Shirabe, S., Okada, H., Hasegawa, S., Miyamoto, T., & Noda, T. (1996). Loss of cerebellar Purkinje cells in aged mice homozygous for a disrupted PrP gene. *Nature*, *380*(6574), 528-531.

Sakai, K., Hasebe, R., Takahashi, Y., Song, C. H., Suzuki, A., Yamasaki, T., & Horiuchi, M. (2013). Absence of CD14 delays progression of prion diseases accompanied by increased microglial activation. *J Virol*, *87*(24), 13433-13445.

Sakthivelu, V., Seidel, R. P., Winklhofer, K. F., & Tatzelt, J. (2011). Conserved stress-protective activity between prion protein and Shadoo. *J Biol Chem*, *286*(11), 8901-8908.

Saldanha, A. J. (2004). Java Treeview-extensible visualization of microarray data. *Bioinformatics*, *20*(17), 3246-3248.

Salojin, K. V., Hamman, B. D., Chang, W. C., Jhaver, K. G., Al-Shami, A., Crisostomo, J., Wilkins, C., Digeorge-Foushee, A. M., Allen, J., Patel, N., Gopinathan, S., Zhou, J., Nouraldeen, A., Jessop, T. C., Bagdanoff, J. T., Augeri, D. J., Read, R., Vogel, P., Swaffield, J., Wilson, A., Platt, K. A., Carson, K. G., Main, A., Zambrowicz, B. P., & Oravecz, T. (2014). Genetic deletion of Mst1 alters T cell function and protects against autoimmunity. *PLoS One*, *9*(5), e98151.

Sandberg, M. K., Al-Doujaily, H., Sharps, B., Clarke, A. R., & Collinge, J. (2011). Prion propagation and toxicity in vivo occur in two distinct mechanistic phases. *Nature*, *470*(7335), 540-542.

Sandberg, M. K., Al-Doujaily, H., Sharps, B., De Oliveira, M. W., Schmidt, C., Richard-Londt, A., Lyall, S., Linehan, J. M., Brandner, S., Wadsworth, J. D., Clarke, A. R., & Collinge, J. (2014). Prion neuropathology follows the accumulation of alternate prion protein isoforms after infective titre has peaked. *Nat Commun*, *5*, 4347.

Sandberg, M. K., Al-Doujaily, H., Sigurdson, C. J., Glatzel, M., O'Malley, C., Powell, C., Asante, E. A., Linehan, J. M., Brandner, S., Wadsworth, J. D., & Collinge, J. (2010). Chronic wasting disease prions are not transmissible to transgenic mice overexpressing human prion protein. *J Gen Virol*, *91*(Pt 10), 2651-2657.

Sarbassov, D. D., Ali, S. M., Kim, D. H., Guertin, D. A., Latek, R. R., Erdjument-Bromage, H., Tempst, P., & Sabatini, D. M. (2004). Rictor, a novel binding partner of mTOR, defines a rapamycin-insensitive and raptor-independent pathway that regulates the cytoskeleton. *Curr Biol*, *14*(14), 1296-1302.

Sarbassov, D. D., Guertin, D. A., Ali, S. M., & Sabatini, D. M. (2005). Phosphorylation and regulation of Akt/PKB by the rictor-mTOR complex. *Science*, *307*(5712), 1098-1101.

Sarnataro, D., Caputo, A., Casanova, P., Puri, C., Paladino, S., Tivodar, S. S., Campana, V., Tacchetti, C., & Zurzolo, C. (2009). Lipid rafts and clathrin cooperate in the internalization of PrP in epithelial FRT cells. *PLoS One*, *4*(6), e5829.

Sasaki, K., Minaki, H., & Iwaki, T. (2009). Development of oligomeric prion-protein aggregates in a mouse model of prion disease. *J Pathol*, *219*(1), 123-130.

Sattler, R., Xiong, Z., Lu, W. Y., Hafner, M., MacDonald, J. F., & Tymianski, M. (1999). Specific coupling of NMDA receptor activation to nitric oxide neurotoxicity by PSD-95 protein. *Science*, *284*(5421), 1845-1848.

Saunders, S. E., Bartelt-Hunt, S. L., & Bartz, J. C. (2012). Occurrence, transmission, and zoonotic potential of chronic wasting disease. *Emerg Infect Dis*, *18*(3), 369-376.

Sawiris, G. P., Becker, K. G., Elliott, E. J., Moulden, R., & Rohwer, R. G. (2007). Molecular analysis of bovine spongiform encephalopathy infection by cDNA arrays. *J Gen Virol*, *88*(Pt 4), 1356-1362.

Schatzl, H. M., Da Costa, M., Taylor, L., Cohen, F. E., & Prusiner, S. B. (1995). Prion protein gene variation among primates. *J Mol Biol*, *245*(4), 362-374.

Schatzl, H. M., Laszlo, L., Holtzman, D. M., Tatzelt, J., DeArmond, S. J., Weiner, R. I., Mobley, W. C., & Prusiner, S. B. (1997). A hypothalamic neuronal cell line persistently infected with scrapie prions exhibits apoptosis. *J Virol*, *71*(11), 8821-8831.

Schmued, L. C., Stowers, C. C., Scallet, A. C., & Xu, L. (2005). Fluoro-Jade C results in ultra high resolution and contrast labeling of degenerating neurons. *Brain Res*, *1035*(1), 24-31.

Schneider, B., Mutel, V., Pietri, M., Ermonval, M., Mouillet-Richard, S., & Kellermann, O. (2003). NADPH oxidase and extracellular regulated kinases 1/2 are targets of prion protein signaling in neuronal and nonneuronal cells. *Proc Natl Acad Sci U S A*, *100*(23), 13326-13331.

Schneider, K., Fangerau, H., Michaelsen, B., & Raab, W. H. (2008). The early history of the transmissible spongiform encephalopathies exemplified by scrapie. *Brain Res Bull*, *77*(6), 343-355.

Schultz, J., Schwarz, A., Neidhold, S., Burwinkel, M., Riemer, C., Simon, D., Kopf, M., Otto, M., & Baier, M. (2004). Role of interleukin-1 in prion disease-associated astrocyte activation. *Am J Pathol*, *165*(2), 671-678.

Schwarz, A., Burwinkel, M., Riemer, C., Schultz, J., & Baier, M. (2004). Unchanged scrapie pathology in brain tissue of tyrosine kinase Fyn-deficient mice. *Neurodegener Dis*, *1*(6), 266-268.

Schwarz, A., Kratke, O., Burwinkel, M., Riemer, C., Schultz, J., Henklein, P., Bamme, T., & Baier, M. (2003). Immunisation with a synthetic prion protein-derived peptide prolongs survival times of mice orally exposed to the scrapie agent. *Neurosci Lett*, *350*(3), 187-189.

Scott, M., Foster, D., Mirenda, C., Serban, D., Coufal, F., Walchli, M., Torchia, M., Groth, D., Carlson, G., DeArmond, S. J., Westaway, D., & Prusiner, S. B. (1989). Transgenic mice expressing hamster prion protein produce species-specific scrapie infectivity and amyloid plaques. *Cell*, *59*(5), 847-857.

Scott, M., Groth, D., Foster, D., Torchia, M., Yang, S. L., DeArmond, S. J., & Prusiner, S. B. (1993). Propagation of prions with artificial properties in transgenic mice expressing chimeric PrP genes. *Cell*, *73*(5), 979-988.

See, V., & Loeffler, J. P. (2001). Oxidative stress induces neuronal death by recruiting a protease and phosphatase-gated mechanism. *J Biol Chem*, *276*(37), 35049-35059.

Selvaggini, C., De Gioia, L., Cantu, L., Ghibaudi, E., Diomede, L., Passerini, F., Forloni, G., Bugiani, O., Tagliavini, F., & Salmona, M. (1993). Molecular characteristics of a protease-resistant, amyloidogenic and neurotoxic peptide homologous to residues 106-126 of the prion protein. *Biochem Biophys Res Commun*, *194*(3), 1380-1386.

Senatore, A., Colleoni, S., Verderio, C., Restelli, E., Morini, R., Condliffe, S. B., Bertani, I., Mantovani, S., Canovi, M., Micotti, E., Forloni, G., Dolphin, A. C., Matteoli, M., Gobbi, M., & Chiesa, R. (2012). Mutant PrP suppresses glutamatergic neurotransmission in cerebellar granule neurons by impairing membrane delivery of VGCC α(2)δ-1 Subunit. *Neuron*, *74*(2), 300-313.

Shahbazian, D., Parsyan, A., Petroulakis, E., Topisirovic, I., Martineau, Y., Gibbs, B. F., Svitkin, Y., & Sonenberg, N. (2010). Control of cell survival and proliferation by mammalian eukaryotic initiation factor 4B. *Mol Cell Biol*, *30*(6), 1478-1485.

Shibuya, S., Higuchi, J., Shin, R. W., Tateishi, J., & Kitamoto, T. (1998). Codon 219 Lys allele of PRNP is not found in sporadic Creutzfeldt-Jakob disease. *Ann Neurol*, *43*(6), 826-828.

Shikiya, R. A., & Bartz, J. C. (2011). In vitro generation of high-titer prions. *J Virol*, *85*(24), 13439-13442.

Shmerling, D., Hegyi, I., Fischer, M., Blattler, T., Brandner, S., Gotz, J., Rulicke, T., Flechsig, E., Cozzio, A., von Mering, C., Hangartner, C., Aguzzi, A., & Weissmann, C. (1998). Expression of amino-terminally truncated PrP in the mouse leading to ataxia and specific cerebellar lesions. *Cell*, *93*(2), 203-214.

Shyng, S. L., Heuser, J. E., & Harris, D. A. (1994). A glycolipid-anchored prion protein is endocytosed via clathrin-coated pits. *J Cell Biol*, *125*(6), 1239-1250.

Shyu, W. C., Lin, S. Z., Chiang, M. F., Ding, D. C., Li, K. W., Chen, S. F., Yang, H. I., & Li, H. (2005). Overexpression of PrP^{C} by adenovirus-mediated gene targeting reduces ischemic injury in a stroke rat model. *J Neurosci*, *25*(39), 8967-8977.

Sigurdson, C. J., Manco, G., Schwarz, P., Liberski, P., Hoover, E. A., Hornemann, S., Polymenidou, M., Miller, M. W., Glatzel, M., & Aguzzi, A. (2006). Strain fidelity of chronic wasting disease upon murine adaptation. *J Virol*, *80*(24), 12303-12311.

Sigurdson, C. J., Nilsson, K. P., Hornemann, S., Manco, G., Fernandez-Borges, N., Schwarz, P., Castilla, J., Wuthrich, K., & Aguzzi, A. (2010). A molecular switch controls interspecies prion disease transmission in mice. *J Clin Invest*, *120*(7), 2590-2599.

Sigurðsson, B. (1954). Rida, a chronic encephalitis of sheep: With general remarks on infections which develop slowly and some of their special characteristics. *Br Vet J*, *110*, 341-354.

Sigurdsson, E. M., Brown, D. R., Daniels, M., Kascsak, R. J., Kascsak, R., Carp, R., Meeker, H. C., Frangione, B., & Wisniewski, T. (2002). Immunization delays the onset of prion disease in mice. *Am J Pathol*, *161*(1), 13-17.

Sikorska, B., Liberski, P. P., Giraud, P., Kopp, N., & Brown, P. (2004). Autophagy is a part of ultrastructural synaptic pathology in Creutzfeldt-Jakob disease: a brain biopsy study. *Int J Biochem Cell Biol*, *36*(12), 2563-2573.

Silveira, J. R., Raymond, G. J., Hughson, A. G., Race, R. E., Sim, V. L., Hayes, S. F., & Caughey, B. (2005). The most infectious prion protein particles. *Nature*, *437*(7056), 257-261.

Silverman, G. L., Qin, K., Moore, R. C., Yang, Y., Mastrangelo, P., Tremblay, P., Prusiner, S. B., Cohen, F. E., & Westaway, D. (2000). Doppel is an N-glycosylated, glycosylphosphatidylinositol-anchored protein. Expression in testis and ectopic production in the brains of Prnp(0/0) mice predisposed to Purkinje cell loss. *J Biol Chem*, *275*(35), 26834-26841.

Silvius, D., Pitstick, R., Ahn, M., Meishery, D., Oehler, A., Barsh, G. S., DeArmond, S. J., Carlson, G. A., & Gunn, T. M. (2013). Levels of the Mahogunin Ring Finger 1 E3 ubiquitin ligase do not influence prion disease. *PLoS One*, *8*(1), e55575.

Sim, V. L. (2012). Prion disease: chemotherapeutic strategies. *Infect Disord Drug Targets*, *12*(2), 144-160.

Siso, S., Puig, B., Varea, R., Vidal, E., Acin, C., Prinz, M., Montrasio, F., Badiola, J., Aguzzi, A., Pumarola, M., & Ferrer, I. (2002). Abnormal synaptic protein expression and cell death in murine scrapie. *Acta Neuropathol*, *103*(6), 615-626.

Skinner, P. J., Abbassi, H., Chesebro, B., Race, R. E., Reilly, C., & Haase, A. T. (2006). Gene expression alterations in brains of mice infected with three strains of scrapie. *BMC Genomics*, *7*, 114.

Skinner, P. J., Kim, H. O., Bryant, D., Kinzel, N. J., Reilly, C., Priola, S. A., Ward, A. E., Goodman, P. A., Olson, K., & Seelig, D. M. (2015). Treatment of Prion Disease with Heterologous Prion Proteins. *PLoS One*, *10*(7), e0131993.

Sofroniew, M. V., & Vinters, H. V. (2010). Astrocytes: biology and pathology. *Acta Neuropathol*, *119*(1), 7-35.

Solforosi, L., Bellon, A., Schaller, M., Cruite, J. T., Abalos, G. C., & Williamson, R. A. (2007). Toward molecular dissection of PrP^{C}-PrPSc interactions. *J Biol Chem*, *282*(10), 7465-7471.

Solforosi, L., Milani, M., Mancini, N., Clementi, M., & Burioni, R. (2013). A closer look at prion strains: characterization and important implications. *Prion*, *7*(2), 99-108.

Solomon, I. H., Huettner, J. E., & Harris, D. A. (2010). Neurotoxic mutants of the prion protein induce spontaneous ionic currents in cultured cells. *J Biol Chem*, *285*(34), 26719-26726.

Solomon, I. H., Khatri, N., Biasini, E., Massignan, T., Huettner, J. E., & Harris, D. A. (2011). An N-terminal polybasic domain and cell surface localization are required for mutant prion protein toxicity. *J Biol Chem*, *286*(16), 14724-14736.

Sonati, T., Reimann, R. R., Falsig, J., Baral, P. K., O'Connor, T., Hornemann, S., Yaganoglu, S., Li, B., Herrmann, U. S., Wieland, B., Swayampakula, M., Rahman, M. H., Das, D., Kav, N., Riek, R., Liberski, P. P., James, M. N., & Aguzzi, A. (2013). The toxicity of antiprion antibodies is mediated by the flexible tail of the prion protein. *Nature*, *501*(7465), 102-106.

Song, C. H., Furuoka, H., Kim, C. L., Ogino, M., Suzuki, A., Hasebe, R., & Horiuchi, M. (2008). Effect of intraventricular infusion of anti-prion protein monoclonal antibodies on disease progression in prion-infected mice. *J Gen Virol*, *89*(Pt 6), 1533-1544.

Song, D., Cui, M., Zhao, G., Fan, Z., Nolan, K., Yang, Y., Lee, P., Ye, F., & Zhang, D. Y. (2014). Pathway-based analysis of breast cancer. *Am J Transl Res*, *6*(3), 302-311.

Song, T., Sugimoto, K., Ihara, H., Mizutani, A., Hatano, N., Kume, K., Kambe, T., Yamaguchi, F., Tokuda, M., & Watanabe, Y. (2007). p90 RSK-1 associates with and inhibits neuronal nitric oxide synthase. *Biochem J*, *401*(2), 391-398.

Soppet, D., Escandon, E., Maragos, J., Middlemas, D. S., Reid, S. W., Blair, J., Burton, L. E., Stanton, B. R., Kaplan, D. R., Hunter, T., Nikolics, K., & Parada, L. F. (1991). The neurotrophic factors brain-derived neurotrophic factor and neurotrophin-3 are ligands for the trkB tyrosine kinase receptor. *Cell*, *65*(5), 895-903.

Sorce, S., Nuvolone, M., Keller, A., Falsig, J., Varol, A., Schwarz, P., Bieri, M., Budka, H., & Aguzzi, A. (2014). The role of the NADPH oxidase NOX2 in prion pathogenesis. *PLoS Pathog*, *10*(12), e1004531.

Sorensen, G., Medina, S., Parchaliuk, D., Phillipson, C., Robertson, C., & Booth, S. A. (2008). Comprehensive transcriptional profiling of prion infection in mouse models reveals networks of responsive genes. *BMC Genomics*, *9*, 114.

Sparkes, R. S., Simon, M., Cohn, V. H., Fournier, R. E., Lem, J., Klisak, I., Heinzmann, C., Blatt, C., Lucero, M., Mohandas, T., & et, A. (1986). Assignment of the human and mouse prion protein genes to homologous chromosomes. *Proc Natl Acad Sci U S A*, *83*(19), 7358-7362.

Spencer, T. K., Mellado, W., & Filbin, M. T. (2008). BDNF activates CaMKIV and PKA in parallel to block MAG-mediated inhibition of neurite outgrowth. *Mol Cell Neurosci*, *38*(1), 110-116.

Spilman, P., Lessard, P., Sattavat, M., Bush, C., Tousseyn, T., Huang, E. J., Giles, K., Golde, T., Das, P., Fauq, A., Prusiner, S. B., & Dearmond, S. J. (2008). A gamma-secretase inhibitor and quinacrine reduce prions and prevent dendritic degeneration in murine brains. *Proc Natl Acad Sci U S A*, *105*(30), 10595-10600.

Spudich, A., Frigg, R., Kilic, E., Kilic, U., Oesch, B., Raeber, A., Bassetti, C. L., & Hermann, D. M. (2005). Aggravation of ischemic brain injury by prion protein deficiency: role of ERK-1/-2 and STAT-1. *Neurobiol Dis*, *20*(2), 442-449.

Spurrier, B., Ramalingam, S., & Nishizuka, S. (2008). Reverse-phase protein lysate microarrays for cell signaling analysis. *Nat Protoc*, *3*(11), 1796-1808.

Stahl, N., Baldwin, M. A., Teplow, D. B., Hood, L., Gibson, B. W., Burlingame, A. L., & Prusiner, S. B. (1993). Structural studies of the scrapie prion protein using mass spectrometry and amino acid sequencing. *Biochemistry*, *32*(8), 1991-2002.

Stahl, N., Borchelt, D. R., Hsiao, K., & Prusiner, S. B. (1987). Scrapie prion protein contains a phosphatidylinositol glycolipid. *Cell*, *51*(2), 229-240.

Stahl, N., Borchelt, D. R., & Prusiner, S. B. (1990). Differential release of cellular and scrapie prion proteins from cellular membranes by phosphatidylinositol-specific phospholipase C. *Biochemistry*, *29*(22), 5405-5412.

Steele, A. D., Emsley, J. G., Ozdinler, P. H., Lindquist, S., & Macklis, J. D. (2006). Prion protein (PrPc) positively regulates neural precursor proliferation during developmental and adult mammalian neurogenesis. *Proc Natl Acad Sci U S A*, *103*(9), 3416-3421.

Steele, A. D., Hetz, C., Yi, C. H., Jackson, W. S., Borkowski, A. W., Yuan, J., Wollmann, R. H., & Lindquist, S. (2007a). Prion pathogenesis is independent of caspase-12. *Prion*, *1*(4), 243-247.

Steele, A. D., King, O. D., Jackson, W. S., Hetz, C. A., Borkowski, A. W., Thielen, P., Wollmann, R., & Lindquist, S. (2007b). Diminishing apoptosis by deletion of Bax or overexpression of Bcl-2 does not protect against infectious prion toxicity in vivo. *J Neurosci*, *27*(47), 13022-13027.

Stewart, R. S., & Harris, D. A. (2001). Most pathogenic mutations do not alter the membrane topology of the prion protein. *J Biol Chem*, *276*(3), 2212-2220.

Stewart, R. S., & Harris, D. A. (2003). Mutational analysis of topological determinants in prion protein (PrP) and measurement of transmembrane and cytosolic PrP during prion infection. *J Biol Chem*, *278*(46), 45960-45968.

Stewart, R. S., Piccardo, P., Ghetti, B., & Harris, D. A. (2005). Neurodegenerative illness in transgenic mice expressing a transmembrane form of the prion protein. *J Neurosci*, *25*(13), 3469-3477.

Stockman, S. (1913). Scrapie: an obscure disease of sheep. *Journal of Comparative Pathology and Therapeutics*, *26*, 317-327.

Sunyach, C., Cisse, M. A., da Costa, C. A., Vincent, B., & Checler, F. (2007). The C-terminal products of cellular prion protein processing, C1 and C2, exert distinct influence on p53-dependent staurosporine-induced caspase-3 activation. *J Biol Chem*, *282*(3), 1956-1963.

Sunyach, C., Jen, A., Deng, J., Fitzgerald, K. T., Frobert, Y., Grassi, J., McCaffrey, M. W., & Morris, R. (2003). The mechanism of internalization of glycosylphosphatidylinositol-anchored prion protein. *EMBO J*, *22*(14), 3591-3601.

Supattapone, S., Muramoto, T., Legname, G., Mehlhorn, I., Cohen, F. E., DeArmond, S. J., Prusiner, S. B., & Scott, M. R. (2001). Identification of two prion protein regions that modify scrapie incubation time. *J Virol*, *75*(3), 1408-1413.

Swietnicki, W., Petersen, R. B., Gambetti, P., & Surewicz, W. K. (1998). Familial mutations and the thermodynamic stability of the recombinant human prion protein. *J Biol Chem*, *273*(47), 31048-31052.

Tagliavini, F., Prelli, F., Verga, L., Giaccone, G., Sarma, R., Gorevic, P., Ghetti, B., Passerini, F., Ghibaudi, E., Forloni, G., & et, A. (1993). Synthetic peptides homologous to prion protein residues 106-147 form amyloid-like fibrils in vitro. *Proc Natl Acad Sci U S A*, *90*(20), 9678-9682.

Tamgüney, G., Giles, K., Bouzamondo-Bernstein, E., Bosque, P. J., Miller, M. W., Safar, J., DeArmond, S. J., & Prusiner, S. B. (2006). Transmission of elk and deer prions to transgenic mice. *J Virol*, *80*(18), 9104-9114.

Tamguney, G., Giles, K., Glidden, D. V., Lessard, P., Wille, H., Tremblay, P., Groth, D. F., Yehiely, F., Korth, C., Moore, R. C., Tatzelt, J., Rubinstein, E., Boucheix, C., Yang, X., Stanley, P., Lisanti, M. P., Dwek, R. A., Rudd, P. M., Moskovitz, J., Epstein, C. J., Cruz, T. D., Kuziel, W. A., Maeda, N., Sap, J., Ashe, K. H., Carlson, G. A., Tesseur, I., Wyss-Coray, T., Mucke, L., Weisgraber, K. H., Mahley, R. W., Cohen, F. E., & Prusiner, S. B. (2008). Genes contributing to prion pathogenesis. *J Gen Virol*, *89*(Pt 7), 1777-1788.

Tan, Y. W., Zhang, S. J., Hoffmann, T., & Bading, H. (2012). Increasing levels of wild-type CREB up-regulates several activity-regulated inhibitor of death (AID) genes and promotes neuronal survival. *BMC Neurosci*, *13*, 48.

Tang, Y., Xiang, W., Hawkins, S. A., Kretzschmar, H. A., & Windl, O. (2009). Transcriptional changes in the brains of cattle orally infected with the bovine spongiform encephalopathy agent precede detection of infectivity. *J Virol*, *83*(18), 9464-9473.

Tang, Y., Xiang, W., Terry, L., Kretzschmar, H. A., & Windl, O. (2010). Transcriptional analysis implicates endoplasmic reticulum stress in bovine spongiform encephalopathy. *PLoS One*, *5*(12), e14207.

Taraboulos, A., Scott, M., Semenov, A., Avrahami, D., Laszlo, L., & Prusiner, S. B. (1995). Cholesterol depletion and modification of COOH-terminal targeting sequence of the prion protein inhibit formation of the scrapie isoform. *J Cell Biol*, *129*(1), 121-132.

Taschuk, R., Marciniuk, K., Määttänen, P., Madampage, C., Hedlin, P., Potter, A., Lee, J., Cashman, N. R., Griebel, P. J., & Napper, S. (2014). Safety, specificity and immunogenicity of a PrP(Sc)-specific prion vaccine based on the YYR disease specific epitope. *Prion*, *8*(1), 51-59.

Tateishi, J., Brown, P., Kitamoto, T., Hoque, Z. M., Roos, R., Wollman, R., Cervenáková, L., & Gajdusek, D. C. (1995a). First experimental transmission of fatal familial insomnia. *Nature*, *376*(6539), 434-435.

Tateishi, J., & Kitamoto, T. (1995b). Inherited prion diseases and transmission to rodents. *Brain Pathol*, *5*(1), 53-59.

Tayebi, M., Collinge, J., & Hawke, S. (2009). Unswitched immunoglobulin M response prolongs mouse survival in prion disease. *J Gen Virol*, *90*(Pt 3), 777-782.

Tayebi, M., Enever, P., Sattar, Z., Collinge, J., & Hawke, S. (2004). Disease-associated prion protein elicits immunoglobulin M responses in vivo. *Mol Med*, *10*(7-12), 104-111.
Taylor, D. R., Parkin, E. T., Cocklin, S. L., Ault, J. R., Ashcroft, A. E., Turner, A. J., & Hooper, N. M. (2009). Role of ADAMs in the ectodomain shedding and conformational conversion of the prion protein. *J Biol Chem*, *284*(34), 22590-22600.
Taylor, D. R., Watt, N. T., Perera, W. S., & Hooper, N. M. (2005). Assigning functions to distinct regions of the N-terminus of the prion protein that are involved in its copper-stimulated, clathrin-dependent endocytosis. *J Cell Sci*, *118*(Pt 21), 5141-5153.
Taylor, R. C., Cullen, S. P., & Martin, S. J. (2008). Apoptosis: controlled demolition at the cellular level. *Nat Rev Mol Cell Biol*, *9*(3), 231-241.
Taylor, S. S., Keshwani, M. M., Steichen, J. M., & Kornev, A. P. (2012). Evolution of the eukaryotic protein kinases as dynamic molecular switches. *Philos Trans R Soc Lond B Biol Sci*, *367*(1602), 2517-2528.
Telling, G. C., Haga, T., Torchia, M., Tremblay, P., DeArmond, S. J., & Prusiner, S. B. (1996). Interactions between wild-type and mutant prion proteins modulate neurodegeneration in transgenic mice. *Genes Dev*, *10*(14), 1736-1750.
Telling, G. C., Scott, M., Hsiao, K. K., Foster, D., Yang, S. L., Torchia, M., Sidle, K. C., Collinge, J., DeArmond, S. J., & Prusiner, S. B. (1994). Transmission of Creutzfeldt-Jakob disease from humans to transgenic mice expressing chimeric human-mouse prion protein. *Proc Natl Acad Sci U S A*, *91*(21), 9936-9940.
Telling, G. C., Scott, M., Mastrianni, J., Gabizon, R., Torchia, M., Cohen, F. E., DeArmond, S. J., & Prusiner, S. B. (1995). Prion propagation in mice expressing human and chimeric PrP transgenes implicates the interaction of cellular PrP with another protein. *Cell*, *83*(1), 79-90.
ter Meulen, V., & Hall, W. W. (1978). Slow virus infections of the nervous system: virological, immunological and pathogenetic considerations. *J Gen Virol*, *41*(1), 1-25.
Terada, T., Tsuboi, Y., Obi, T., Doh-ura, K., Murayama, S., Kitamoto, T., Yamada, T., & Mizoguchi, K. (2010). Less protease-resistant PrP in a patient with sporadic CJD treated with intraventricular pentosan polysulphate. *Acta Neurol Scand*, *121*(2), 127-130.
Thackray, A. M., Hopkins, L., Klein, M. A., & Bujdoso, R. (2007). Mouse-adapted ovine scrapie prion strains are characterized by different conformers of PrP^{Sc}. *J Virol*, *81*(22), 12119-12127.
Thackray, A. M., Klein, M. A., Aguzzi, A., & Bujdoso, R. (2002). Chronic subclinical prion disease induced by low-dose inoculum. *J Virol*, *76*(5), 2510-2517.
Thackray, A. M., Klein, M. A., & Bujdoso, R. (2003). Subclinical prion disease induced by oral inoculation. *J Virol*, *77*(14), 7991-7998.
Thackray, A. M., McKenzie, A. N., Klein, M. A., Lauder, A., & Bujdoso, R. (2004). Accelerated prion disease in the absence of interleukin-10. *J Virol*, *78*(24), 13697-13707.
Thackray, A. M., Zhang, C., Arndt, T., & Bujdoso, R. (2014). Cytosolic PrP can participate in prion-mediated toxicity. *J Virol*, *88*(14), 8129-8138.
Thadani, V., Penar, P. L., Partington, J., Kalb, R., Janssen, R., Schonberger, L. B., Rabkin, C. S., & Prichard, J. W. (1988). Creutzfeldt-Jakob disease probably acquired from a cadaveric dura mater graft. Case report. *J Neurosurg*, *69*(5), 766-769.

Thellung, S., Florio, T., Villa, V., Corsaro, A., Arena, S., Amico, C., Robello, M., Salmona, M., Forloni, G., Bugiani, O., Tagliavini, F., & Schettini, G. (2000). Apoptotic cell death and impairment of L-type voltage-sensitive calcium channel activity in rat cerebellar granule cells treated with the prion protein fragment 106-126. *Neurobiol Dis*, *7*(4), 299-309.

Tilly, G., Chapuis, J., Vilette, D., Laude, H., & Vilotte, J. L. (2003). Efficient and specific down-regulation of prion protein expression by RNAi. *Biochem Biophys Res Commun*, *305*(3), 548-551.

Tintner, R., Brown, P., Hedley-Whyte, E. T., Rappaport, E. B., Piccardo, C. P., & Gajdusek, D. C. (1986). Neuropathologic verification of Creutzfeldt-Jakob disease in the exhumed American recipient of human pituitary growth hormone: epidemiologic and pathogenetic implications. *Neurology*, *36*(7), 932-936.

Tobler, I., Gaus, S. E., Deboer, T., Achermann, P., Fischer, M., Rulicke, T., Moser, M., Oesch, B., McBride, P. A., & Manson, J. C. (1996). Altered circadian activity rhythms and sleep in mice devoid of prion protein. *Nature*, *380*(6575), 639-642.

Tokumitsu, H., & Soderling, T. R. (1996). Requirements for calcium and calmodulin in the calmodulin kinase activation cascade. *J Biol Chem*, *271*(10), 5617-5622.

Torres, J. M., Castilla, J., Pintado, B., Gutierrez-Adan, A., Andreoletti, O., Aguilar-Calvo, P., Arroba, A. I., Parra-Arrondo, B., Ferrer, I., Manzanares, J., & Espinosa, J. C. (2013). Spontaneous generation of infectious prion disease in transgenic mice. *Emerg Infect Dis*, *19*(12), 1938-1947.

Torres, M., Castillo, K., Armisén, R., Stutzin, A., Soto, C., & Hetz, C. (2010). Prion protein misfolding affects calcium homeostasis and sensitizes cells to endoplasmic reticulum stress. *PLoS One*, *5*(12), e15658.

Tremblay, P., Ball, H. L., Kaneko, K., Groth, D., Hegde, R. S., Cohen, F. E., DeArmond, S. J., Prusiner, S. B., & Safar, J. G. (2004). Mutant PrP^{Sc} conformers induced by a synthetic peptide and several prion strains. *J Virol*, *78*(4), 2088-2099.

Trevitt, C. R., & Collinge, J. (2006). A systematic review of prion therapeutics in experimental models. *Brain*, *129*(Pt 9), 2241-2265.

Tribouillard-Tanvier, D., Striebel, J. F., Peterson, K. E., & Chesebro, B. (2009). Analysis of protein levels of 24 cytokines in scrapie agent-infected brain and glial cell cultures from mice differing in prion protein expression levels. *J Virol*, *83*(21), 11244-11253.

Trost, B., Kindrachuk, J., Määttänen, P., Napper, S., & Kusalik, A. (2013). PIIKA 2: an expanded, web-based platform for analysis of kinome microarray data. *PLoS One*, *8*(11), e80837.

Turk, E., Teplow, D. B., Hood, L. E., & Prusiner, S. B. (1988). Purification and properties of the cellular and scrapie hamster prion proteins. *Eur J Biochem*, *176*(1), 21-30.

Turnbaugh, J. A., Unterberger, U., Saa, P., Massignan, T., Fluharty, B. R., Bowman, F. P., Miller, M. B., Supattapone, S., Biasini, E., & Harris, D. A. (2012). The N-terminal, polybasic region of PrP(C) dictates the efficiency of prion propagation by binding to PrP(Sc). *J Neurosci*, *32*(26), 8817-8830.

Tuzi, N. L., Gall, E., Melton, D., & Manson, J. C. (2002). Expression of doppel in the CNS of mice does not modulate transmissible spongiform encephalopathy disease. *J Gen Virol*, *83*(Pt 3), 705-711.

United States Geological Survey, National Wildlife Health Center. Distribution of Chronic Wasting Disease in North America. Retrieved October 25, 2015, from http://www.nwhc.usgs.gov/images/cwd/cwd_map.jpg.

United States National Institutes of Health (a). A Phase 3 Study to Evaluate the Safety and Efficacy of Masitinib in Patients with Mild to Moderate Alzheimer's Disease. Retrieved April 15, 2016, from https://clinicaltrials.gov/ct2/show/NCT01872598?term=nct01872598&rank=1.

United States National Institutes of Health (b). A Phase IIa Multi-Center Study of 18F-FDG PET, Safety, and Tolerability of AZD0530 in Mild Alzheimer's Disease. Retrieved April 15, 2016, from https://clinicaltrials.gov/ct2/show/NCT02167256?term=nct02167256&rank=1.

United States National Institutes of Health (c). Clinical Trials of Protein Kinase Inhibitors. Retrieved September 28, 2016, from https://clinicaltrials.gov/ct2/results?term=protein+kinase+inhibitor&Search=Search.

Unterberger, U., Hoftberger, R., Gelpi, E., Flicker, H., Budka, H., & Voigtlander, T. (2006). Endoplasmic reticulum stress features are prominent in Alzheimer disease but not in prion diseases in vivo. *J Neuropathol Exp Neurol*, *65*(4), 348-357.

Ura, S., Masuyama, N., Graves, J. D., & Gotoh, Y. (2001). Caspase cleavage of MST1 promotes nuclear translocation and chromatin condensation. *Proc Natl Acad Sci U S A*, *98*(18), 10148-10153.

Urano, F., Wang, X., Bertolotti, A., Zhang, Y., Chung, P., Harding, H. P., & Ron, D. (2000). Coupling of stress in the ER to activation of JNK protein kinases by transmembrane protein kinase IRE1. *Science*, *287*(5453), 664-666.

Urwin, P. J., Mackenzie, J. M., Llewelyn, C. A., Will, R. G., & Hewitt, P. E. (2015). Creutzfeldt-Jakob disease and blood transfusion: updated results of the UK Transfusion Medicine Epidemiology Review Study. *Vox Sang*, vox.12371.

Valin, A., Cook, J. D., Ross, S., Saklad, C. L., & Gill, G. (2009). Sp1 and Sp3 regulate transcription of the cyclin-dependent kinase 5 regulatory subunit 2 (p39) promoter in neuronal cells. *Biochim Biophys Acta*, *1789*(3), 204-211.

van der Kamp, M. W., & Daggett, V. (2009). The consequences of pathogenic mutations to the human prion protein. *Protein Eng Des Sel*, *22*(8), 461-468.

van Rheede, T., Smolenaars, M. M., Madsen, O., & de Jong, W. W. (2003). Molecular evolution of the mammalian prion protein. *Mol Biol Evol*, *20*(1), 111-121.

Vanderperre, B., Staskevicius, A. B., Tremblay, G., McCoy, M., O'Neill, M. A., Cashman, N. R., & Roucou, X. (2011). An overlapping reading frame in the PRNP gene encodes a novel polypeptide distinct from the prion protein. *FASEB J*, *25*(7), 2373-2386.

Vella, L. J., Sharples, R. A., Lawson, V. A., Masters, C. L., Cappai, R., & Hill, A. F. (2007). Packaging of prions into exosomes is associated with a novel pathway of PrP processing. *J Pathol*, *211*(5), 582-590.

Vey, M., Pilkuhn, S., Wille, H., Nixon, R., DeArmond, S. J., Smart, E. J., Anderson, R. G., Taraboulos, A., & Prusiner, S. B. (1996). Subcellular colocalization of the cellular and scrapie prion proteins in caveolae-like membranous domains. *Proc Natl Acad Sci U S A*, *93*(25), 14945-14949.

Vik, T. A., & Ryder, J. W. (1997). Identification of serine 380 as the major site of autophosphorylation of Xenopus pp90rsk. *Biochem Biophys Res Commun*, *235*(2), 398-402.
Vilches, S., Vergara, C., Nicolás, O., Mata, Á., Del Río, J. A., & Gavín, R. (2015). Domain-Specific Activation of Death-Associated Intracellular Signalling Cascades by the Cellular Prion Protein in Neuroblastoma Cells. *Mol Neurobiol*.
Vilches, S., Vergara, C., Nicolas, O., Sanclimens, G., Merino, S., Varon, S., Acosta, G. A., Albericio, F., Royo, M., Del Rio, J. A., & Gavin, R. (2013). Neurotoxicity of prion peptides mimicking the central domain of the cellular prion protein. *PLoS One*, *8*(8), e70881.
Vincent, B., Paitel, E., Saftig, P., Frobert, Y., Hartmann, D., De Strooper, B., Grassi, J., Lopez-Perez, E., & Checler, F. (2001). The disintegrins ADAM10 and TACE contribute to the constitutive and phorbol ester-regulated normal cleavage of the cellular prion protein. *J Biol Chem*, *276*(41), 37743-37746.
Vo, N., Klein, M. E., Varlamova, O., Keller, D. M., Yamamoto, T., Goodman, R. H., & Impey, S. (2005). A cAMP-response element binding protein-induced microRNA regulates neuronal morphogenesis. *Proc Natl Acad Sci U S A*, *102*(45), 16426-16431.
Vorberg, I., Chan, K., & Priola, S. A. (2001). Deletion of beta-strand and alpha-helix secondary structure in normal prion protein inhibits formation of its protease-resistant isoform. *J Virol*, *75*(21), 10024-10032.
Wadsworth, J. D., Hill, A. F., Beck, J. A., & Collinge, J. (2003). Molecular and clinical classification of human prion disease. *Br Med Bull*, *66*, 241-254.
Wadsworth, J. D., Joiner, S., Hill, A. F., Campbell, T. A., Desbruslais, M., Luthert, P. J., & Collinge, J. (2001). Tissue distribution of protease resistant prion protein in variant Creutzfeldt-Jakob disease using a highly sensitive immunoblotting assay. *Lancet*, *358*(9277), 171-180.
Wadsworth, J. D., Joiner, S., Linehan, J. M., Desbruslais, M., Fox, K., Cooper, S., Cronier, S., Asante, E. A., Mead, S., Brandner, S., Hill, A. F., & Collinge, J. (2008). Kuru prions and sporadic Creutzfeldt-Jakob disease prions have equivalent transmission properties in transgenic and wild-type mice. *Proc Natl Acad Sci U S A*, *105*(10), 3885-3890.
Wadzinski, B. E., Wheat, W. H., Jaspers, S., Peruski, L. F. J., Lickteig, R. L., Johnson, G. L., & Klemm, D. J. (1993). Nuclear protein phosphatase 2A dephosphorylates protein kinase A-phosphorylated CREB and regulates CREB transcriptional stimulation. *Mol Cell Biol*, *13*(5), 2822-2834.
Wagner, J., Ryazanov, S., Leonov, A., Levin, J., Shi, S., Schmidt, F., Prix, C., Pan-Montojo, F., Bertsch, U., Mitteregger-Kretzschmar, G., Geissen, M., Eiden, M., Leidel, F., Hirschberger, T., Deeg, A. A., Krauth, J. J., Zinth, W., Tavan, P., Pilger, J., Zweckstetter, M., Frank, T., Bahr, M., Weishaupt, J. H., Uhr, M., Urlaub, H., Teichmann, U., Samwer, M., Botzel, K., Groschup, M., Kretzschmar, H., Griesinger, C., & Giese, A. (2013). Anle138b: a novel oligomer modulator for disease-modifying therapy of neurodegenerative diseases such as prion and Parkinson's disease. *Acta Neuropathol*, *125*(6), 795-813.
Walmsley, A. R., Watt, N. T., Taylor, D. R., Perera, W. S., & Hooper, N. M. (2009). alpha-cleavage of the prion protein occurs in a late compartment of the secretory pathway and is independent of lipid rafts. *Mol Cell Neurosci*, *40*(2), 242-248.

Walter, P., & Ron, D. (2011). The unfolded protein response: from stress pathway to homeostatic regulation. *Science*, *334*(6059), 1081-1086.

Walz, R., Amaral, O. B., Rockenbach, I. C., Roesler, R., Izquierdo, I., Cavalheiro, E. A., Martins, V. R., & Brentani, R. R. (1999). Increased sensitivity to seizures in mice lacking cellular prion protein. *Epilepsia*, *40*(12), 1679-1682.

Wang, F., Wang, X., Yuan, C. G., & Ma, J. (2010a). Generating a prion with bacterially expressed recombinant prion protein. *Science*, *327*(5969), 1132-1135.

Wang, F., Yang, F., Hu, Y., Wang, X., Wang, X., Jin, C., & Ma, J. (2007). Lipid interaction converts prion protein to a PrP^{Sc}-like proteinase K-resistant conformation under physiological conditions. *Biochemistry*, *46*(23), 7045-7053.

Wang, J., & Maldonado, M. A. (2006). The ubiquitin-proteasome system and its role in inflammatory and autoimmune diseases. *Cell Mol Immunol*, *3*(4), 255-261.

Wang, X., McGovern, G., Zhang, Y., Wang, F., Zha, L., Jeffrey, M., & Ma, J. (2015). Intraperitoneal Infection of Wild-Type Mice with Synthetically Generated Mammalian Prion. *PLoS Pathog*, *11*(7), e1004958.

Wang, X., Shi, Q., Xu, K., Gao, C., Chen, C., Li, X. L., Wang, G. R., Tian, C., Han, J., & Dong, X. P. (2011). Familial CJD associated PrP mutants within transmembrane region induced Ctm-PrP retention in ER and triggered apoptosis by ER stress in SH-SY5Y cells. *PLoS One*, *6*(1), e14602.

Wang, Y., & Qin, Z. H. (2010b). Molecular and cellular mechanisms of excitotoxic neuronal death. *Apoptosis*, *15*(11), 1382-1402.

Waskiewicz, A. J., Johnson, J. C., Penn, B., Mahalingam, M., Kimball, S. R., & Cooper, J. A. (1999). Phosphorylation of the cap-binding protein eukaryotic translation initiation factor 4E by protein kinase Mnk1 in vivo. *Mol Cell Biol*, *19*(3), 1871-1880.

Watt, F., & Molloy, P. L. (1993). Specific cleavage of transcription factors by the thiol protease, m-calpain. *Nucleic Acids Res*, *21*(22), 5092-5100.

Watt, N. T., Taylor, D. R., Gillott, A., Thomas, D. A., Perera, W. S., & Hooper, N. M. (2005). Reactive oxygen species-mediated beta-cleavage of the prion protein in the cellular response to oxidative stress. *J Biol Chem*, *280*(43), 35914-35921.

Watts, J. C., Drisaldi, B., Ng, V., Yang, J., Strome, B., Horne, P., Sy, M. S., Yoong, L., Young, R., Mastrangelo, P., Bergeron, C., Fraser, P. E., Carlson, G. A., Mount, H. T., Schmitt-Ulms, G., & Westaway, D. (2007). The CNS glycoprotein Shadoo has PrP(C)-like protective properties and displays reduced levels in prion infections. *EMBO J*, *26*(17), 4038-4050.

Watts, J. C., Stöhr, J., Bhardwaj, S., Wille, H., Oehler, A., Dearmond, S. J., Giles, K., & Prusiner, S. B. (2011). Protease-resistant prions selectively decrease Shadoo protein. *PLoS Pathog*, *7*(11), e1002382.

Weise, J., Doeppner, T. R., Müller, T., Wrede, A., Schulz-Schaeffer, W., Zerr, I., Witte, O. W., & Bähr, M. (2008). Overexpression of cellular prion protein alters postischemic Erk1/2 phosphorylation but not Akt phosphorylation and protects against focal cerebral ischemia. *Restor Neurol Neurosci*, *26*(1), 57-64.

Weise, J., Sandau, R., Schwarting, S., Crome, O., Wrede, A., Schulz-Schaeffer, W., Zerr, I., & Bahr, M. (2006). Deletion of cellular prion protein results in reduced Akt activation, enhanced postischemic caspase-3 activation, and exacerbation of ischemic brain injury. *Stroke*, *37*(5), 1296-1300.

Wells, G. A., Scott, A. C., Johnson, C. T., Gunning, R. F., Hancock, R. D., Jeffrey, M., Dawson, M., & Bradley, R. (1987). A novel progressive spongiform encephalopathy in cattle. *Vet Rec*, *121*(18), 419-420.

Westaway, D., Goodman, P. A., Mirenda, C. A., McKinley, M. P., Carlson, G. A., & Prusiner, S. B. (1987). Distinct prion proteins in short and long scrapie incubation period mice. *Cell*, *51*(4), 651-662.

Westergard, L., Turnbaugh, J. A., & Harris, D. A. (2011). A naturally occurring C-terminal fragment of the prion protein (PrP) delays disease and acts as a dominant-negative inhibitor of PrP^{Sc} formation. *J Biol Chem*, *286*(51), 44234-44242.

Westphal, R. S., Anderson, K. A., Means, A. R., & Wadzinski, B. E. (1998). A signaling complex of Ca2+-calmodulin-dependent protein kinase IV and protein phosphatase 2A. *Science*, *280*(5367), 1258-1261.

White, A. R., Enever, P., Tayebi, M., Mushens, R., Linehan, J., Brandner, S., Anstee, D., Collinge, J., & Hawke, S. (2003). Monoclonal antibodies inhibit prion replication and delay the development of prion disease. *Nature*, *422*(6927), 80-83.

White, A. R., Guirguis, R., Brazier, M. W., Jobling, M. F., Hill, A. F., Beyreuther, K., Barrow, C. J., Masters, C. L., Collins, S. J., & Cappai, R. (2001). Sublethal concentrations of prion peptide PrP106-126 or the amyloid beta peptide of Alzheimer's disease activates expression of proapoptotic markers in primary cortical neurons. *Neurobiol Dis*, *8*(2), 299-316.

Whitehouse, I. J., Jackson, C., Turner, A. J., & Hooper, N. M. (2010). Prion protein is reduced in aging and in sporadic but not in familial Alzheimer's disease. *J Alzheimers Dis*, *22*(3), 1023-1031.

Wietgrefe, S., Zupancic, M., Haase, A., Chesebro, B., Race, R., Frey, W., Rustan, T., & Friedman, R. L. (1985). Cloning of a gene whose expression is increased in scrapie and in senile plaques in human brain. *Science*, *230*(4730), 1177-1179.

Wik, L., Klingeborn, M., Willander, H., & Linne, T. (2012). Separate mechanisms act concurrently to shed and release the prion protein from the cell. *Prion*, *6*(5), 498-509.

Will, R. G. (2003). Acquired prion disease: iatrogenic CJD, variant CJD, kuru. *Br Med Bull*, *66*, 255-265.

Will, R. G., Ironside, J. W., Zeidler, M., Cousens, S. N., Estibeiro, K., Alperovitch, A., Poser, S., Pocchiari, M., Hofman, A., & Smith, P. G. (1996). A new variant of Creutzfeldt-Jakob disease in the UK. *Lancet*, *347*(9006), 921-925.

Williams, A., Lucassen, P. J., Ritchie, D., & Bruce, M. (1997). PrP deposition, microglial activation, and neuronal apoptosis in murine scrapie. *Exp Neurol*, *144*(2), 433-438.

Williams, W. M., Stadtman, E. R., & Moskovitz, J. (2004). Ageing and exposure to oxidative stress in vivo differentially affect cellular levels of PrP in mouse cerebral microvessels and brain parenchyma. *Neuropathol Appl Neurobiol*, *30*(2), 161-168.

Wiseman, F. K., Cancellotti, E., Piccardo, P., Iremonger, K., Boyle, A., Brown, D., Ironside, J. W., Manson, J. C., & Diack, A. B. (2015). The Glycosylation Status of PrP^{C} Is a Key Factor in Determining Transmissible Spongiform Encephalopathy Transmission between Species. *J Virol*, *89*(9), 4738-4747.

Wood-Kaczmar, A., Gandhi, S., & Wood, N. W. (2006). Understanding the molecular causes of Parkinson's disease. *Trends Mol Med*, *12*(11), 521-528.

World Health Organization. Dementia - Fact Sheet. Retrieved April 15, 2016, from http://www.who.int/mediacentre/factsheets/fs362/en/.

Wroe, S. J., Pal, S., Siddique, D., Hyare, H., Macfarlane, R., Joiner, S., Linehan, J. M., Brandner, S., Wadsworth, J. D., Hewitt, P., & Collinge, J. (2006). Clinical presentation and pre-mortem diagnosis of variant Creutzfeldt-Jakob disease associated with blood transfusion: a case report. *Lancet*, *368*(9552), 2061-2067.

Wu, P., Nielsen, T. E., & Clausen, M. H. (2015). FDA-approved small-molecule kinase inhibitors. *Trends Pharmacol Sci*, *36*(7), 422-439.

Xiang, W., Hummel, M., Mitteregger, G., Pace, C., Windl, O., Mansmann, U., & Kretzschmar, H. A. (2007). Transcriptome analysis reveals altered cholesterol metabolism during the neurodegeneration in mouse scrapie model. *J Neurochem*, *102*(3), 834-847.

Xiang, W., Windl, O., Wunsch, G., Dugas, M., Kohlmann, A., Dierkes, N., Westner, I. M., & Kretzschmar, H. A. (2004). Identification of differentially expressed genes in scrapie-infected mouse brains by using global gene expression technology. *J Virol*, *78*(20), 11051-11060.

Xu, Y., Tian, C., Wang, S. B., Xie, W. L., Guo, Y., Zhang, J., Shi, Q., Chen, C., & Dong, X. P. (2012). Activation of the macroautophagic system in scrapie-infected experimental animals and human genetic prion diseases. *Autophagy*, *8*(11), 1604-1620.

Yadavalli, R., Guttmann, R. P., Seward, T., Centers, A. P., Williamson, R. A., & Telling, G. C. (2004). Calpain-dependent endoproteolytic cleavage of PrP^{Sc} modulates scrapie prion propagation. *J Biol Chem*, *279*(21), 21948-21956.

Yamaguchi, H., & Shen, J. (2013). Histological analysis of neurodegeneration in the mouse brain. *Methods Mol Biol*, *1004*, 91-113.

Yang, W., Cook, J., Rassbach, B., Lemus, A., DeArmond, S. J., & Mastrianni, J. A. (2009). A New Transgenic Mouse Model of Gerstmann-Straussler-Scheinker Syndrome Caused by the A117V Mutation of PRNP. *J Neurosci*, *29*(32), 10072-10080.

Yang, Z., & Klionsky, D. J. (2010). Eaten alive: a history of macroautophagy. *Nat Cell Biol*, *12*(9), 814-822.

Yao, Z., Diener, K., Wang, X. S., Zukowski, M., Matsumoto, G., Zhou, G., Mo, R., Sasaki, T., Nishina, H., Hui, C. C., Tan, T. H., Woodgett, J. P., & Penninger, J. M. (1997). Activation of stress-activated protein kinases/c-Jun N-terminal protein kinases (SAPKs/JNKs) by a novel mitogen-activated protein kinase kinase. *J Biol Chem*, *272*(51), 32378-32383.

Ye, F., Che, Y., McMillen, E., Gorski, J., Brodman, D., Saw, D., Jiang, B., & Zhang, D. Y. (2009). The effect of Scutellaria baicalensis on the signaling network in hepatocellular carcinoma cells. *Nutr Cancer*, *61*(4), 530-537.

Yedidia, Y., Horonchik, L., Tzaban, S., Yanai, A., & Taraboulos, A. (2001). Proteasomes and ubiquitin are involved in the turnover of the wild-type prion protein. *EMBO J*, *20*(19), 5383-5391.

Yeung, Y. G., & Stanley, E. R. (2009). A solution for stripping antibodies from polyvinylidene fluoride immunoblots for multiple reprobing. *Anal Biochem*, *389*(1), 89-91.

Yim, Y. I., Park, B. C., Yadavalli, R., Zhao, X., Eisenberg, E., & Greene, L. E. (2015). The multivesicular body is the major internal site of prion conversion. *J Cell Sci*, *128*(7), 1434-1443.

Yin, F., Ye, F., Tan, L., Liu, K., Xuan, Z., Zhang, J., Wang, W., Zhang, Y., Jiang, X., & Zhang, D. Y. (2012). Alterations of signaling pathways in muscle tissues of patients with amyotrophic lateral sclerosis. *Muscle Nerve*, *46*(6), 861-870.

Ying, Y. S., Anderson, R. G., & Rothberg, K. G. (1992). Each caveola contains multiple glycosyl-phosphatidylinositol-anchored membrane proteins. *Cold Spring Harb Symp Quant Biol*, *57*, 593-604.

Yokoyama, T., Kimura, K. M., Ushiki, Y., Yamada, S., Morooka, A., Nakashiba, T., Sassa, T., & Itohara, S. (2001). In vivo conversion of cellular prion protein to pathogenic isoforms, as monitored by conformation-specific antibodies. *J Biol Chem*, *276*(14), 11265-11271.

You, H., Pellegrini, M., Tsuchihara, K., Yamamoto, K., Hacker, G., Erlacher, M., Villunger, A., & Mak, T. W. (2006). FOXO3a-dependent regulation of Puma in response to cytokine/growth factor withdrawal. *J Exp Med*, *203*(7), 1657-1663.

Yu, G., Chen, J., Xu, Y., Zhu, C., Yu, H., Liu, S., Sha, H., Chen, J., Xu, X., Wu, Y., Zhang, A., Ma, J., & Cheng, G. (2009). Generation of goats lacking prion protein. *Mol Reprod Dev*, *76*(1), 3.

Yuan, Z., Lehtinen, M. K., Merlo, P., Villen, J., Gygi, S., & Bonni, A. (2009). Regulation of neuronal cell death by MST1-FOXO1 signaling. *J Biol Chem*, *284*(17), 11285-11292.

Yun, H. J., Yoon, J. H., Lee, J. K., Noh, K. T., Yoon, K. W., Oh, S. P., Oh, H. J., Chae, J. S., Hwang, S. G., Kim, E. H., Maul, G. G., Lim, D. S., & Choi, E. J. (2011). Daxx mediates activation-induced cell death in microglia by triggering MST1 signalling. *EMBO J*, *30*(12), 2465-2476.

Yun, S. W., Ertmer, A., Flechsig, E., Gilch, S., Riederer, P., Gerlach, M., Schatzl, H. M., & Klein, M. A. (2007). The tyrosine kinase inhibitor imatinib mesylate delays prion neuroinvasion by inhibiting prion propagation in the periphery. *J Neurovirol*, *13*(4), 328-337.

Yun, S. W., Gerlach, M., Riederer, P., & Klein, M. A. (2006). Oxidative stress in the brain at early preclinical stages of mouse scrapie. *Exp Neurol*, *201*(1), 90-98.

Zahn, R., Liu, A., Luhrs, T., Riek, R., von Schroetter, C., Lopez Garcia, F., Billeter, M., Calzolai, L., Wider, G., & Wuthrich, K. (2000). NMR solution structure of the human prion protein. *Proc Natl Acad Sci U S A*, *97*(1), 145-150.

Zhang, J., Wang, K., Guo, Y., Shi, Q., Tian, C., Chen, C., Gao, C., Zhang, B. Y., & Dong, X. P. (2012). Heat shock protein 70 selectively mediates the degradation of cytosolic PrPs and restores the cytosolic PrP-induced cytotoxicity via a molecular interaction. *Virol J*, *9*, 303.

Zhang, S. J., Zou, M., Lu, L., Lau, D., Ditzel, D. A., Delucinge-Vivier, C., Aso, Y., Descombes, P., & Bading, H. (2009). Nuclear calcium signaling controls expression of a large gene pool: identification of a gene program for acquired neuroprotection induced by synaptic activity. *PLoS Genet*, *5*(8), e1000604.

Zhang, X., Gao, X., Coots, R. A., Conn, C. S., Liu, B., & Qian, S. B. (2015). Translational control of the cytosolic stress response by mitochondrial ribosomal protein L18. *Nat Struct Mol Biol*, *22*(5), 404-410.

Zhang, Z., Zhang, Y., Wang, F., Wang, X., Xu, Y., Yang, H., Yu, G., Yuan, C., & Ma, J. (2013). De novo generation of infectious prions with bacterially expressed recombinant prion protein. *FASEB J*, *27*(12), 4768-4775.

Zhao, M., Tang, D., Lechpammer, S., Hoffman, A., Asea, A., Stevenson, M. A., & Calderwood, S. K. (2002). Double-stranded RNA-dependent protein kinase (pkr) is essential for thermotolerance, accumulation of HSP70, and stabilization of ARE-containing HSP70 mRNA during stress. *J Biol Chem*, *277*(46), 44539-44547.

Zhou, D., Medoff, B. D., Chen, L., Li, L., Zhang, X. F., Praskova, M., Liu, M., Landry, A., Blumberg, R. S., Boussiotis, V. A., Xavier, R., & Avruch, J. (2008). The Nore1B/Mst1 complex restrains antigen receptor-induced proliferation of naïve T cells. *Proc Natl Acad Sci U S A*, *105*(51), 20321-20326.

Zhou, Q., Wang, M., Du, Y., Zhang, W., Bai, M., Zhang, Z., Li, Z., & Miao, J. (2015). Inhibition of c-Jun N-terminal kinase activation reverses Alzheimer disease phenotypes in APPswe/PS1dE9 mice. *Ann Neurol*, *77*(4), 637-654.

Zurawel, A. A., Walsh, D. J., Fortier, S. M., Chidawanyika, T., Sengupta, S., Zilm, K., & Supattapone, S. (2014). Prion nucleation site unmasked by transient interaction with phospholipid cofactor. *Biochemistry*, *53*(1), 68-76.

APPENDICES

Appendix 1 – The expression levels of 99 protein kinases or regulatory subunits in cells expressing cytoplasmic PrP mutants analyzed by primary screens.

	Absolute (arbitrary units)				Ratio		
	Vector	CyPrP	124stop	124-230	CyPrP	124stop	124-230
Akt1	2.77	3.12	2.86	2.47	1.13	1.03	0.89
Akt2	4.61	4.07	4.21	NQ	0.88	0.91	–
Akt3	2.30	1.78	2.02	1.41	0.77	0.88	0.61
AMPKα1	3.95	4.96	4.20	3.72	1.26	1.06	0.94
B-Raf	4.78	4.26	4.35	4.27	0.89	0.91	0.89
c-Abl	0.70	0.50	0.30	0.31	0.71	0.43	0.44
CaMK1α	0.48	0.48	0.41	0.37	1.00	0.85	0.77
CaMK2γ	0.07	0.06	0.04	0.05	0.86	0.57	0.71
CaMK4	NQ	0.74	0.73	0.66	–	–	–
CASK	3.98	3.83	3.51	3.53	0.96	0.88	0.89
CDK1	12.25	9.90	11.40	8.41	0.81	0.93	0.69
CDK2	25.14	21.13	21.11	19.72	0.84	0.84	0.78
CDK4	19.48	19.56	19.54	16.51	1.00	1.00	0.85
CDK5	1.09	0.83	0.91	0.75	0.76	0.83	0.69
CDK7	12.94	11.81	NQ	10.24	0.91	–	0.79
CDKL1	0.73	NQ	0.79	0.62	–	1.08	0.85
CHK1	9.98	9.46	9.08	9.22	0.95	0.91	0.92
CK1α	2.25	2.10	1.92	2.15	0.93	0.85	0.96
CK1ε	11.09	11.67	10.29	10.59	1.05	0.93	0.95
CK2α1	0.68	0.77	0.68	0.65	1.13	1.00	0.96
CRIK	2.13	2.49	1.88	2.57	1.17	0.88	1.21
cyclin D1	0.15	0.04	0.01	0.02	0.27	0.07	0.13
cyclin D3	3.08	3.71	2.64	2.88	1.20	0.86	0.94
cyclin E1	2.50	2.39	2.14	NQ	0.96	0.86	–
cyclin G1	0.30	0.31	0.34	0.32	1.03	1.13	1.07
DAPK1	0.07	0.07	0.09	0.05	1.00	1.29	0.71
DDR1	2.35	2.09	2.04	2.01	0.89	0.87	0.86
DLK	2.03	2.19	NQ	1.77	1.08	–	0.87
DYRK1A	1.25	1.03	1.04	0.84	0.82	0.83	0.67
EphA1	0.98	1.02	0.85	NQ	1.04	0.87	–
EphA3	0.16	NQ	0.16	0.15	–	1.00	0.94
EphA4	NQ	0.33	0.37	0.24	–	–	–
Erk1	0.35	0.24	0.34	0.40	0.69	0.97	1.14
Erk2	22.89	20.41	23.34	24.14	0.89	1.02	1.05
Erk5	3.95	3.99	4.18	3.84	1.01	1.06	0.97
FAK	1.17	1.06	1.04	1.03	0.91	0.89	0.88
FGFR1	0.09	0.08	0.07	0.09	0.89	0.78	1.00
Fms/CSF1R	0.97	0.97	0.77	NQ	1.00	0.79	–
GRK2	0.80	0.64	0.63	0.75	0.80	0.79	0.94
GSK3α	NQ	8.56	7.86	7.70	–	–	–
GSK3β	32.81	28.58	28.46	26.41	0.87	0.87	0.80
HER3	0.03	0.04	0.03	0.06	1.33	1.00	2.00
IKKα	2.32	1.99	2.23	2.16	0.86	0.96	0.93
IKKβ	1.57	1.70	1.43	1.71	1.08	0.91	1.09
IRAK4	0.71	1.01	1.11	0.85	1.42	1.56	1.20
JAK1	0.72	0.65	0.74	0.87	0.90	1.03	1.21
JNK1α1	5.21	5.06	4.96	4.68	0.97	0.95	0.90
JNK2α1/β1	1.28	1.17	1.11	1.15	0.91	0.87	0.90
JNK2α2/β2	2.49	2.30	2.15	2.19	0.92	0.86	0.88
Lck	0.04	0.07	0.10	0.08	1.75	2.50	2.00
LIMK1	4.34	3.82	4.16	4.25	0.88	0.96	0.98
Lkb1	10.57	9.38	NQ	8.10	0.89	–	0.77
MAPKAPK2	0.14	0.12	0.16	0.18	0.86	1.14	1.29
MARK4	0.40	NQ	0.36	0.30	–	0.90	0.75
MEK1	7.25	NQ	7.77	6.30	–	1.07	0.87

MEK2	24.44	22.94	23.97	22.34	0.94	0.98	0.91
MEK5α	24.43	NQ	21.73	21.00	–	0.89	0.86
MEK5β	6.07	6.18	6.01	5.92	1.02	0.99	0.98
MEKK1	0.07	0.05	0.09	0.10	0.71	1.29	1.43
MKK6	3.80	3.42	4.07	3.48	0.90	1.07	0.92
MKK7	0.19	0.18	0.15	0.15	0.95	0.79	0.79
MLK3	0.11	0.15	0.11	0.13	1.36	1.00	1.18
MSK1	0.26	0.18	0.18	0.41	0.69	0.69	1.58
MST1	6.93	6.61	6.47	6.20	0.95	0.93	0.89
p25	1.89	1.91	1.66	1.96	1.01	0.88	1.04
p38α	11.20	11.35	10.74	10.09	1.01	0.96	0.90
p38δ	0.15	0.11	0.12	0.14	0.73	0.80	0.93
p38γ	7.01	6.75	6.12	5.74	0.96	0.87	0.82
p70S6K	3.44	2.39	2.96	3.01	0.69	0.86	0.88
PAK1	13.23	12.64	NQ	11.15	0.96	–	0.84
PAK3	0.34	0.29	0.29	0.22	0.85	0.85	0.65
PCTAIRE3	0.53	0.50	0.62	0.52	0.94	1.17	0.98
PDK1	0.34	0.38	0.38	0.35	1.12	1.12	1.03
PINK1	0.36	0.31	0.39	0.26	0.86	1.08	0.72
PKACα	18.63	19.29	19.38	19.44	1.04	1.04	1.04
PKACβ	1.16	1.00	1.41	1.31	0.86	1.22	1.13
PKACγ	12.20	12.49	NQ	11.96	1.02	–	0.98
PKCα	4.62	3.51	4.21	3.77	0.76	0.91	0.82
PKCδ	NQ	2.63	2.33	2.41	–	–	–
PKCε	0.31	0.40	0.43	0.37	1.29	1.39	1.19
PKCι	21.03	19.23	18.91	20.05	0.91	0.90	0.95
PKCθ	0.44	0.54	0.41	NQ	1.23	0.93	–
PKCζ	18.58	17.09	15.42	17.47	0.92	0.83	0.94
PKD1	0.67	0.67	0.80	0.88	1.00	1.19	1.31
PKR	0.71	0.64	0.77	0.81	0.90	1.08	1.14
PLK1	10.71	NQ	9.78	9.67	–	0.91	0.90
PRK1	7.57	6.36	6.62	5.37	0.84	0.87	0.71
PRK2	1.99	1.61	1.55	1.75	0.81	0.78	0.88
Raf-1	9.25	NQ	9.66	NQ	–	1.04	–
RIPK2	0.35	0.19	0.28	0.21	0.54	0.80	0.60
ROCK1	1.04	1.08	0.99	1.04	1.04	0.95	1.00
RSK1	5.22	5.22	5.12	5.15	1.00	0.98	0.99
RSK2	NQ	12.09	10.29	11.51	–	–	–
SGK3	13.12	12.73	14.12	12.74	0.97	1.08	0.97
SLK	2.07	1.79	1.59	1.52	0.86	0.77	0.73
Src	10.83	8.89	9.74	NQ	0.82	0.90	–
TNIK	2.99	3.24	2.43	2.48	1.08	0.81	0.83
TrkA	0.06	0.05	0.04	0.05	0.83	0.67	0.83
Yes	3.55	3.60	3.92	3.41	1.01	1.10	0.96

Equivalent amounts of protein from N2a cells transfected with empty vector (vector), or vector encoding CyPrP^{EGFP} (CyPrP), CyPrP^{EGFP}124stop (124stop), or CyPrP^{EGFP}124-230 (124-230) were resolved and transferred to membranes. Primary multiplex Western blots analyzed the expression levels of 137 protein kinases or regulatory subunits; 99 were detected in cells expressing one or more construct. The 76 proteins detected in cells expressing each construct (in bold) were further analyzed by hierarchical clustering. Ratios were calculated relative to the absolute levels in cells expressing empty vector. NQ, not quantitated due to artifacts from transfer or blotting.

		EGFP			CyPrP^{EGFP}								
		Absolute (arbitrary units)			Absolute (arbitrary units)			Normalized absolute (arbitrary units)			Ratio		
		12	24	48	12	24	48	12	24	48	12	24	48
Akt1	Repeat 1	0.02	0.07	0.06	0.04	0.07	0.06	0.06	0.07	0.06	3.12	1.00	1.00
	Repeat 2	0.03	0.05	0.06	0.05	0.05	0.04	0.07	0.05	0.02	2.47	1.00	0.26
	Repeat 3	0.04	0.06	0.05	0.05	0.06	0.04	0.07	0.06	0.02	1.74	1.00	0.41
AMPK1α1	Repeat 1	3.13	3.53	2.38	2.61	2.43	2.31	2.03	1.20	2.23	0.65	0.34	0.94
	Repeat 2	0.32	0.29	0.29	0.22	0.21	0.29	0.10	0.11	0.29	0.31	0.39	1.00
	Repeat 3	0.41	0.40	0.46	0.40	0.38	0.39	0.38	0.34	0.25	0.93	0.85	0.55
eEF2	Repeat 1	5.44	5.49	4.04	6.26	5.08	4.91	7.18	4.62	5.88	1.32	0.84	1.46
	Repeat 2	0.48	0.51	0.54	0.58	0.36	0.42	0.70	0.18	0.28	1.46	0.35	0.51
	Repeat 3	0.37	0.38	0.41	0.40	0.39	0.28	0.46	0.41	0.03	1.24	1.08	0.06
eIF4B	Repeat 1	4.06	3.66	3.99	3.87	2.09	1.70	3.66	0.33	*0.001*	0.90	0.09	0.00
	Repeat 2	0.41	0.15	0.04	0.08	0.03	0.01	*0.001*	*0.001*	*0.001*	0.00	0.01	0.03
	Repeat 3	2.65	2.12	2.19	2.58	1.77	1.29	2.44	1.09	*0.001*	0.92	0.51	0.00
eIF4E	Repeat 1	2.14	4.59	2.50	2.29	4.11	2.70	2.46	3.57	2.92	1.15	0.78	1.17
	Repeat 2	0.72	1.01	0.70	0.64	0.66	0.65	0.54	0.24	0.59	0.75	0.24	0.84
	Repeat 3	0.95	1.21	1.03	0.90	0.93	0.92	0.80	0.38	0.71	0.84	0.32	0.68
Mnk1	Repeat 1	2.85	3.03	2.91	2.35	2.07	2.55	1.79	1.00	2.15	0.63	0.33	0.74
	Repeat 2	0.25	0.22	0.21	0.20	0.14	0.14	0.14	0.04	0.06	0.56	0.20	0.26
	Repeat 3	0.53	0.25	0.48	0.49	0.20	0.35	0.41	0.10	0.10	0.78	0.41	0.20
mTOR	Repeat 1	0.45	0.53	0.47	0.49	0.44	0.35	0.53	0.34	0.22	1.19	0.64	0.46
	Repeat 2	0.05	0.07	0.05	0.06	0.06	0.04	0.07	0.05	0.03	1.44	0.68	0.56
	Repeat 3	0.25	0.31	0.20	0.28	0.28	0.18	0.34	0.22	0.14	1.35	0.71	0.71
p70S6K	Repeat 1	0.21	0.51	0.36	0.28	0.39	0.30	0.36	0.26	0.23	1.71	0.50	0.65
	Repeat 2	0.12	0.14	0.22	0.15	0.08	0.08	0.19	0.01	*0.001*	1.55	0.05	0.00
	Repeat 3	0.54	0.52	0.51	0.60	0.46	0.37	0.72	0.34	0.10	1.33	0.66	0.19
PKCα	Repeat 1	0.47	0.54	0.39	0.61	0.48	0.56	0.77	0.41	0.75	1.63	0.76	1.92
	Repeat 2	0.07	0.06	0.05	0.08	0.05	0.06	0.09	0.04	0.07	1.32	0.63	1.44
	Repeat 3	0.10	0.10	0.09	0.11	0.09	0.09	0.13	0.07	0.09	1.29	0.71	1.00
S6	Repeat 1	6.06	6.52	5.41	5.96	5.81	4.34	5.85	5.02	3.14	0.97	0.77	0.58
	Repeat 2	1.02	1.16	1.15	0.93	0.90	1.06	0.82	0.59	0.95	0.81	0.51	0.83
	Repeat 3	1.01	1.01	1.04	0.93	0.81	0.87	0.77	0.42	0.54	0.77	0.42	0.52

Appendix 2 – The expression levels of 10 protein kinases and substrates in cells expressing CyPrP^{EGFP} analyzed by targeted secondary analyses. Secondary analyses of the mTOR signaling pathway in N2a cells expressing EGFP or CyPrP^{EGFP} (CyPrP) for 12, 24, or 48 h from three biological repeats. The raw (absolute) levels in cells expressing CyPrP^{EGFP} were corrected for differences in transfection efficiency in each biological repeat (normalized absolute) and expressed relative to the levels in cells expressing EGFP, as described in **Section 2.9**. Normalized absolute levels below detection were assigned a value of 0.001 (indicated in italics), 10-fold below the detection limit. Ratios were calculated from the normalized absolute levels relative to levels in cells expressing EGFP from the same biological repeat at each time point, used as internal control. Ratios below 0.005 were assigned a value of 0.

		EGFP			CyPrP^{EGFP}								
		Absolute (arbitrary units)			Absolute (arbitrary units)			Normalized absolute (arbitrary units)			Ratio		
		12	24	48	12	24	48	12	24	48	12	24	48
p-Akt (S473)	Repeat 1	NS	0.06	0.08	NS	0.04	0.04	–	0.02	*0.001*	–	0.29	0.01
	Repeat 2	0.11	0.11	0.06	0.09	0.07	0.05	0.07	0.02	0.04	0.64	0.20	0.63
	Repeat 3	0.45	0.11	0.23	0.25	0.11	0.20	*0.001*	0.08	0.14	0.00	0.73	0.62
p-AMPKα (T172)	Repeat 1	0.14	0.46	2.10	0.26	0.26	0.50	0.39	0.04	*0.001*	2.82	0.08	0.00
	Repeat 2	0.33	0.32	2.48	0.35	0.30	0.83	0.37	0.28	*0.001*	1.13	0.86	0.00
	Repeat 3	4.70	3.20	2.44	2.49	2.66	2.62	*0.001*	1.61	2.97	0.00	0.50	1.22
p-eEF2 (T56)	Repeat 1	0.04	0.06	0.07	0.07	0.06	0.06	0.10	0.06	0.05	2.59	1.00	0.70
	Repeat 2	0.06	0.06	0.21	0.06	0.06	0.04	0.06	0.06	*0.001*	1.00	1.00	0.00
	Repeat 3	0.09	0.06	0.05	0.05	0.06	0.05	*0.001*	0.06	0.05	0.01	1.00	1.00
p-eIF4B (S422)	Repeat 1	0.09	0.10	0.08	0.08	0.02	0.01	0.07	*0.001*	*0.001*	0.76	0.01	0.01
	Repeat 2	0.10	0.02	0.02	0.04	0.01	0.01	*0.001*	*0.001*	*0.001*	0.01	0.05	0.05
	Repeat 3	0.16	0.07	0.03	0.14	0.03	0.01	0.10	*0.001*	*0.001*	0.63	0.01	0.03
p-eIF4E (S209)	Repeat 1	1.94	3.00	3.10	2.22	2.71	2.80	2.53	2.39	2.46	1.31	0.80	0.79
	Repeat 2	0.35	0.37	0.43	0.38	0.41	0.44	0.42	0.46	0.45	1.19	1.24	1.05
	Repeat 3	0.55	0.55	0.50	0.56	0.54	0.53	0.58	0.52	0.59	1.05	0.95	1.18
p-Mnk1 (T197/202)	Repeat 1	0.46	0.38	0.31	0.27	0.45	0.31	0.06	0.53	0.31	0.12	1.39	1.00
	Repeat 2	0.03	0.02	0.02	0.02	0.02	0.02	0.01	0.02	0.02	0.26	1.00	1.00
	Repeat 3	0.04	0.03	0.02	0.02	0.02	0.02	*0.001*	0.00	0.02	0.03	0.02	1.00
p-mTOR (S2448)	Repeat 1	0.10	0.08	0.08	0.07	0.06	0.04	0.04	0.04	*0.001*	0.40	0.50	0.01
	Repeat 2	0.13	0.08	0.08	0.13	0.08	0.10	0.13	0.08	0.12	1.00	1.00	1.50
	Repeat 3	0.28	0.14	0.07	0.27	0.12	0.07	0.25	0.08	0.07	0.89	0.57	1.00
p-p70S6K (T389)	Repeat 1	0.89	1.36	1.16	0.76	1.09	0.98	0.61	0.79	0.78	0.69	0.58	0.67
	Repeat 2	0.29	0.30	0.29	0.23	0.28	0.22	0.16	0.26	0.14	0.54	0.85	0.48
	Repeat 3	0.31	0.29	0.32	0.25	0.28	0.27	0.13	0.26	0.17	0.43	0.90	0.54
p-PKCα (S657)	Repeat 1	0.94	1.65	1.74	1.23	2.02	2.24	1.55	2.43	2.80	1.65	1.48	1.61
	Repeat 2	0.40	0.33	0.30	0.38	0.29	0.39	0.36	0.24	0.50	0.89	0.73	1.66
	Repeat 3	0.29	0.35	0.30	0.28	0.31	0.31	0.26	0.23	0.33	0.90	0.66	1.10
p-S6 (S235/236)	Repeat 1	0.74	1.03	0.50	1.34	0.46	0.15	2.01	*0.001*	*0.001*	2.72	0.00	0.00
	Repeat 2	0.57	0.36	0.03	0.66	0.17	0.07	0.77	*0.001*	0.12	1.35	0.00	3.94
	Repeat 3	1.64	0.17	0.04	1.48	0.14	0.14	1.17	0.08	0.33	0.71	0.48	8.37
p-S6 (S240/244)	Repeat 1	2.50	2.54	1.17	3.18	1.01	0.27	3.94	*0.001*	*0.001*	1.58	0.00	0.00
	Repeat 2	1.53	1.02	0.04	1.66	0.60	0.19	1.82	0.09	0.37	1.19	0.09	9.28
	Repeat 3	1.51	0.21	0.13	1.57	0.34	0.32	1.69	0.59	0.69	1.12	2.83	5.31

Appendix 3 – The phosphorylation levels of 10 protein kinases and substrates in cells expressing CyPrP^{EGFP} analyzed by targeted tertiary analyses. Tertiary analyses of the mTOR signaling pathway in N2a cells expressing EGFP or CyPrP^{EGFP} (CyPrP) for 12, 24, or 48 h from three biological repeats. The raw (absolute) levels in cells expressing CyPrP^{EGFP} were corrected for differences in transfection efficiency in each biological repeat (normalized absolute) and expressed relative to the levels in cells expressing EGFP, as described in **Section 2.9**. Normalized absolute levels below detection were assigned a value of 0.001 (indicated in italics), 10-fold below the detection limit. Ratios were calculated from the normalized absolute levels relative to levels in cells expressing EGFP from the same biological repeat at each time point, used as internal control. Ratios below 0.005 were assigned a value of 0. The ratio of p-Akt (S473) at 12 h from repeat 1 could not be calculated due to the lack of available sample (NS, no sample).

Appendix 4 – The expression levels of 109 protein kinases or regulatory subunits in brainstem-cerebellum homogenates from scrapie-infected mice.

		Mock-infected					RML-infected									
		Absolute (arbitrary units)					Absolute (arbitrary units)					Ratio				
		70	90	110	130	TER	70	90	110	130	TER	70	90	110	130	TER
Akt1	Set 1	0.25	0.42	0.35	0.29	0.54	0.22	0.25	0.35	0.27	0.39	0.88	0.60	1.00	0.93	0.72
	Set 2	0.12	0.37	0.24	0.15	0.35	0.14	0.18	0.19	0.11	0.24	1.17	0.49	0.79	0.73	0.69
	Set 3	0.34	0.40	0.31	0.22	0.34	0.33	0.47	0.29	0.17	0.35	0.97	1.18	0.94	0.77	1.03
Akt2	Set 1	1.20	1.69	1.87	1.45	0.86	1.46	1.67	1.45	1.11	1.00	1.22	0.99	0.78	0.77	1.16
	Set 2	1.00	0.92	0.57	0.54	0.82	0.73	0.65	0.54	0.51	0.63	0.73	0.71	0.95	0.94	0.77
	Set 3	0.83	0.70	0.63	0.39	0.68	0.66	0.68	0.72	0.38	0.70	0.80	0.97	1.14	0.97	1.03
Akt3	Set 1	0.77	1.11	1.02	1.22	0.99	0.78	0.92	1.01	1.09	0.69	1.01	0.83	0.99	0.89	0.70
	Set 2	0.64	0.48	0.35	0.34	0.44	0.47	0.43	0.38	0.47	0.32	0.73	0.90	1.09	1.38	0.73
	Set 3	0.60	0.61	0.46	0.46	0.44	0.51	0.70	0.45	0.37	0.41	0.85	1.15	0.98	0.80	0.93
AMPKα2	Set 1	0.25	0.15	0.24	0.23	0.16	0.17	0.23	0.26	0.15	0.13	0.68	1.53	1.08	0.65	0.81
	Set 2	0.37	0.09	0.10	0.12	0.13	0.15	0.11	0.11	0.08	0.17	0.41	1.22	1.10	0.67	1.31
	Set 3	0.67	0.20	0.15	0.13	0.18	0.20	0.21	0.23	0.18	0.24	0.30	1.05	1.53	1.38	1.33
ASK1	Set 1	0.90	1.14	0.98	1.01	0.73	1.22	1.08	0.91	0.48	0.60	1.36	0.95	0.93	0.48	0.82
	Set 2	0.57	0.39	0.41	0.34	0.48	0.45	NQ	0.40	0.13	0.45	0.79	–	0.98	0.38	0.94
	Set 3	1.01	0.80	0.77	0.25	0.81	0.77	0.92	0.94	0.17	0.43	0.76	1.15	1.22	0.68	0.53
B-Raf	Set 1	0.07	0.08	0.06	0.05	0.01	0.08	0.14	0.08	0.05	0.01	1.14	1.75	1.33	1.00	1.00
	Set 2	0.02	0.02	0.02	0.02	0.04	0.01	0.03	0.02	0.01	0.01	0.50	1.50	1.00	0.50	0.25
	Set 3	0.01	0.01	0.02	ND	0.02	0.01	0.01	0.01	ND	0.02	1.00	1.00	0.50	–	1.00
c-Abl	Set 1	0.04	0.08	0.18	0.16	0.09	0.05	0.11	0.15	0.07	0.02	1.25	1.38	0.83	0.44	0.22
	Set 2	0.13	0.04	0.06	0.10	0.07	0.05	0.05	0.10	0.02	0.05	0.38	1.25	1.67	0.20	0.71
	Set 3	0.14	0.06	0.06	0.01	0.04	0.07	0.06	0.09	0.02	0.05	0.50	1.00	1.50	2.00	1.25
CaMK1α	Set 1	NR	NR	NR	NR	0.15	NR	NR	NR	NR	0.09	–	–	–	–	0.60
	Set 2	0.07	0.07	0.09	0.09	0.12	0.06	0.08	0.07	0.10	0.10	0.86	1.14	0.78	1.11	0.83
	Set 3	0.10	0.10	0.12	0.11	0.14	0.12	0.11	0.13	0.12	0.16	1.20	1.10	1.08	1.09	1.14
CaMK1δ	Set 1	0.14	0.13	0.11	0.16	0.05	0.10	0.06	0.07	0.08	0.06	0.71	0.46	0.64	0.50	1.20
	Set 2	0.05	0.06	0.07	0.04	0.08	0.07	0.07	0.03	0.03	0.05	1.40	1.17	0.43	0.75	0.63
	Set 3	0.09	0.10	0.08	0.10	0.12	0.12	0.11	0.08	0.06	0.08	1.33	1.10	1.00	0.60	0.67
CaMK2γ	Set 1	0.17	0.19	0.27	0.32	0.22	0.16	0.21	0.41	0.19	0.11	0.94	1.11	1.52	0.59	0.50
	Set 2	0.23	0.11	0.10	0.09	0.18	0.15	0.12	0.11	0.08	0.11	0.65	1.09	1.10	0.89	0.61
	Set 3	0.52	0.30	0.20	0.26	0.26	0.22	0.34	0.27	0.24	0.18	0.42	1.13	1.35	0.92	0.69
CaMK4	Set 1	2.64	2.47	2.14	2.27	2.06	2.15	1.97	1.54	1.67	2.39	0.81	0.80	0.72	0.74	1.16
	Set 2	1.67	2.16	1.81	1.62	2.09	2.06	1.94	1.48	1.33	1.63	1.23	0.90	0.82	0.82	0.78
	Set 3	1.57	1.67	1.84	1.46	2.90	1.99	1.65	1.68	1.07	1.68	1.27	0.99	0.91	0.73	0.58
CaMK4β	Set 1	1.63	1.75	1.19	1.19	1.11	1.54	1.22	1.14	1.20	1.12	0.94	0.70	0.96	1.01	1.01
	Set 2	0.29	0.99	1.11	0.69	1.60	1.32	1.10	0.85	0.72	0.61	4.55	1.11	0.77	1.04	0.38
	Set 3	0.40	1.24	1.10	0.81	1.92	1.31	1.20	1.18	0.47	1.42	3.28	0.97	1.07	0.58	0.74
CaMKK2	Set 1	0.06	0.08	0.03	0.02	0.04	0.07	0.07	0.05	0.04	0.05	1.17	0.88	1.67	2.00	1.25
	Set 2	0.08	0.05	0.02	0.05	0.05	0.03	0.05	0.03	0.03	0.03	0.38	1.00	1.50	0.60	0.60
	Set 3	0.13	0.06	0.03	0.05	0.11	0.06	0.06	0.05	0.03	0.04	0.46	1.00	1.67	0.60	0.36
CASK	Set 1	0.95	1.15	1.18	1.00	0.96	1.29	1.03	1.13	0.89	0.86	1.36	0.90	0.96	0.89	0.90
	Set 2	0.99	0.71	0.65	0.54	0.74	0.83	0.65	0.60	0.52	0.60	0.84	0.92	0.92	0.96	0.81
	Set 3	1.21	1.00	0.97	0.77	1.03	0.98	1.02	1.02	0.84	0.82	0.81	1.02	1.05	1.09	0.80
CDK5	Set 1	0.69	1.01	0.86	0.94	0.45	0.61	0.80	0.61	0.76	0.41	0.88	0.79	0.71	0.81	0.91
	Set 2	0.45	0.22	0.33	0.44	0.58	0.32	0.35	0.30	0.30	0.25	0.71	1.59	0.91	0.68	0.43
	Set 3	0.71	0.53	0.42	0.32	0.61	0.61	0.44	0.34	0.48	0.45	0.86	0.83	0.81	1.50	0.74

CDK7	Set 1	0.14	0.21	0.14	0.07	0.22	0.20	0.11	0.05	0.08	0.18	1.43	0.52	0.36	1.14	0.82
	Set 2	0.11	0.11	0.17	0.11	0.14	0.13	0.11	0.12	0.12	0.07	1.18	1.00	0.71	1.09	0.50
	Set 3	0.13	0.14	0.17	0.13	0.15	0.17	0.18	0.18	0.13	0.12	1.31	1.29	1.06	1.00	0.80
CDKL1	Set 1	0.11	0.23	0.39	0.37	0.52	0.21	0.26	0.25	0.36	0.33	1.91	1.13	0.64	0.97	0.63
	Set 2	0.15	0.07	0.14	0.24	0.16	0.08	0.14	0.14	0.17	0.13	0.53	2.00	1.00	0.71	0.81
	Set 3	0.27	0.17	0.16	0.25	0.14	0.13	0.16	0.16	0.19	0.06	0.48	0.94	1.00	0.76	0.43
CHK2	Set 1	0.10	0.09	0.10	0.15	0.09	0.13	0.13	0.11	0.13	0.07	1.30	1.44	1.10	0.87	0.78
	Set 2	0.06	0.04	0.06	0.07	0.09	0.06	0.05	0.09	0.05	0.05	1.00	1.25	1.50	0.71	0.56
	Set 3	0.06	0.10	0.07	0.07	0.11	0.06	0.08	0.08	0.07	0.06	1.00	0.80	1.14	1.00	0.55
CK1ε	Set 1	0.62	0.97	1.74	1.64	1.41	1.16	1.32	1.19	1.32	0.84	1.87	1.36	0.68	0.80	0.60
	Set 2	1.14	0.76	0.99	1.29	1.00	0.87	0.85	1.00	0.97	0.91	0.76	1.12	1.01	0.75	0.91
	Set 3	1.08	1.16	1.16	1.28	0.86	1.01	0.77	1.15	1.41	0.69	0.94	0.66	0.99	1.10	0.80
CK1γ1	Set 1	0.08	0.18	0.18	0.19	0.11	0.11	0.15	0.21	0.11	0.05	1.38	0.83	1.17	0.58	0.45
	Set 2	0.18	0.10	0.05	0.07	0.11	0.12	0.09	0.06	0.03	0.08	0.67	0.90	1.20	0.43	0.73
	Set 3	0.25	0.10	0.13	0.06	0.13	0.10	0.12	0.16	0.07	0.11	0.40	1.20	1.23	1.17	0.85
cyclin D1	Set 1	NR	NR	NR	NR	0.19	NR	NR	NR	NR	0.13	–	–	–	–	0.68
	Set 2	0.09	0.08	0.08	0.09	0.15	0.04	0.07	0.05	0.02	0.04	0.44	0.88	0.63	0.22	0.27
	Set 3	0.04	0.05	0.03	0.01	0.05	0.05	0.06	0.02	*0.001*	0.04	1.25	1.20	0.67	0.10	0.80
cyclin E1	Set 1	0.04	0.07	0.07	0.06	0.08	0.03	0.08	0.07	0.06	0.06	0.75	1.14	1.00	1.00	0.75
	Set 2	0.05	0.07	0.07	0.08	0.08	0.09	0.08	0.07	0.11	0.05	1.80	1.14	1.00	1.38	0.63
	Set 3	0.08	0.09	0.10	0.12	0.12	0.13	0.15	0.10	0.17	0.10	1.63	1.67	1.00	1.42	0.83
cyclin G1	Set 1	NR	NR	NR	NR	0.17	NR	NR	NR	NR	0.20	–	–	–	–	1.18
	Set 2	0.21	0.09	0.08	0.20	0.08	0.12	0.15	0.14	0.10	0.12	0.57	1.67	1.75	0.50	1.50
	Set 3	0.28	0.15	0.15	0.24	0.13	0.16	0.13	0.20	0.16	0.08	0.57	0.87	1.33	0.67	0.62
CRIK	Set 1	0.02	0.10	0.21	0.10	0.14	0.07	0.13	0.09	0.07	0.06	3.50	1.30	0.43	0.70	0.43
	Set 2	0.13	0.06	0.07	0.09	0.07	0.03	0.07	0.05	0.02	0.10	0.23	1.17	0.71	0.22	1.43
	Set 3	0.15	0.10	0.10	0.03	0.09	0.09	0.06	0.08	0.03	0.02	0.60	0.60	0.80	1.00	0.22
DDR1	Set 1	0.65	0.62	0.72	0.62	0.67	0.79	0.75	0.58	0.68	0.86	1.22	1.21	0.81	1.10	1.28
	Set 2	0.42	0.44	0.42	0.37	0.48	0.53	0.44	0.46	0.28	0.74	1.26	1.00	1.10	0.76	1.54
	Set 3	0.59	0.58	0.69	0.39	0.57	0.73	0.81	0.85	0.38	1.23	1.24	1.40	1.23	0.97	2.16
DLK	Set 1	1.21	1.31	1.36	1.73	1.35	1.24	1.17	1.26	0.50	1.35	1.02	0.89	0.93	0.29	1.00
	Set 2	2.19	1.31	1.46	1.65	1.50	1.46	1.40	1.49	0.63	1.29	0.67	1.07	1.02	0.38	0.86
	Set 3	3.15	2.43	2.09	1.17	2.04	2.35	1.98	2.50	0.54	1.95	0.75	0.81	1.20	0.46	0.96
DYRK1A	Set 1	0.33	0.40	0.49	0.44	0.48	0.28	0.55	0.51	0.15	0.15	0.85	1.38	1.04	0.34	0.31
	Set 2	0.39	0.19	0.24	0.23	0.31	0.26	0.26	0.28	0.02	0.26	0.67	1.37	1.17	0.09	0.84
	Set 3	0.52	0.40	0.34	0.08	0.36	0.42	0.42	0.41	0.05	0.34	0.81	1.05	1.21	0.63	0.94
EphA3	Set 1	0.46	0.32	0.35	0.42	0.51	0.41	0.41	0.41	0.07	0.24	0.89	1.28	1.17	0.17	0.47
	Set 2	0.47	0.29	0.39	0.29	0.36	0.31	0.25	0.32	0.01	0.29	0.66	0.86	0.82	0.03	0.81
	Set 3	0.71	0.39	0.37	0.01	0.56	0.57	0.60	0.53	0.02	0.43	0.80	1.54	1.43	2.00	0.77
EphA4	Set 1	0.35	0.35	0.88	0.89	0.41	0.39	0.54	0.90	0.40	0.13	1.11	1.54	1.02	0.45	0.32
	Set 2	1.34	0.15	0.20	0.29	0.26	0.18	0.19	0.20	0.13	0.38	0.13	1.27	1.00	0.45	1.46
	Set 3	1.65	0.39	0.27	0.28	0.28	0.42	0.35	0.47	0.67	0.37	0.25	0.90	1.74	2.39	1.32
EphA7	Set 1	0.04	0.07	0.08	0.04	0.07	0.09	0.08	0.05	0.06	0.04	2.25	1.14	0.63	1.50	0.57
	Set 2	0.01	0.02	0.04	0.03	0.05	0.02	0.02	0.02	0.02	0.02	2.00	1.00	0.50	0.67	0.40
	Set 3	0.03	0.05	0.05	0.04	0.04	0.03	0.03	0.04	0.03	0.03	1.00	0.60	0.80	0.75	0.75
EphB3	Set 1	0.06	0.05	0.08	0.05	0.05	0.06	0.08	0.10	0.05	0.04	1.00	1.60	1.25	1.00	0.80
	Set 2	0.08	0.03	0.04	0.04	0.04	0.04	0.04	0.03	0.04	0.04	0.50	1.33	0.75	1.00	1.00
	Set 3	0.17	0.06	0.06	0.05	0.04	0.09	0.07	0.07	0.11	0.04	0.53	1.17	1.17	2.20	1.00
Erk1	Set 1	1.26	1.19	1.21	1.35	1.15	1.23	1.20	1.22	1.29	1.18	0.98	1.01	1.01	0.96	1.03
	Set 2	0.80	0.71	0.70	0.67	0.82	0.70	0.76	0.72	0.64	0.95	0.88	1.07	1.03	0.96	1.16
	Set 3	1.19	1.09	0.91	0.93	0.87	1.03	1.11	0.99	0.98	1.12	0.87	1.02	1.09	1.05	1.29

Erk2	Set 1	1.33	1.35	1.63	1.66	1.56	1.37	1.26	1.42	1.24	1.54	1.03	0.93	0.87	0.75	0.99
	Set 2	2.04	1.31	1.18	1.26	1.44	1.27	1.26	1.12	1.09	1.81	0.62	0.96	0.95	0.87	1.26
	Set 3	2.15	1.49	1.31	1.14	1.43	1.23	1.32	1.27	1.39	1.17	0.57	0.89	0.97	1.22	0.82
Erk5	Set 1	0.12	0.20	0.22	0.16	0.14	0.16	0.18	0.23	0.18	0.11	1.33	0.90	1.05	1.13	0.79
	Set 2	0.10	0.09	0.08	0.09	0.11	0.09	0.10	0.06	0.05	0.07	0.90	1.11	0.75	0.56	0.64
	Set 3	0.14	0.11	0.11	0.05	0.13	0.12	0.10	0.12	0.06	0.07	0.86	0.91	1.09	1.20	0.54
GRK2	Set 1	0.29	0.70	0.62	0.55	0.39	0.41	0.56	0.61	0.67	0.34	1.41	0.80	0.98	1.22	0.87
	Set 2	0.22	0.26	0.18	0.23	0.21	0.25	0.25	0.20	0.31	0.22	1.14	0.96	1.11	1.35	1.05
	Set 3	0.27	0.31	0.28	0.32	0.27	0.31	0.30	0.34	0.39	0.22	1.15	0.97	1.21	1.22	0.81
GRK5	Set 1	0.06	0.06	0.05	0.05	0.08	0.03	0.05	0.04	0.03	0.03	0.50	0.83	0.80	0.60	0.38
	Set 2	0.13	0.09	0.15	0.13	0.21	0.14	0.16	0.12	0.09	0.08	1.08	1.78	0.80	0.69	0.38
	Set 3	0.45	0.27	0.18	0.24	0.27	0.18	0.30	0.21	0.19	0.31	0.40	1.11	1.17	0.79	1.15
GSK3α	Set 1	2.49	3.20	3.32	3.15	2.28	2.81	2.93	2.68	2.70	1.84	1.13	0.92	0.81	0.86	0.81
	Set 2	1.83	1.45	1.58	1.59	1.37	1.74	1.61	1.68	1.22	1.35	0.95	1.11	1.06	0.77	0.99
	Set 3	2.50	2.26	2.07	1.75	1.96	2.27	2.21	2.46	1.84	1.63	0.91	0.98	1.19	1.05	0.83
GSK3β	Set 1	4.56	4.82	5.44	5.21	4.99	4.70	4.58	4.62	4.50	4.09	1.04	0.94	0.86	0.87	0.80
	Set 2	4.44	3.58	3.69	3.74	4.00	3.63	3.76	3.38	2.85	3.72	0.83	1.05	0.91	0.73	0.91
	Set 3	4.18	3.82	3.62	3.27	3.77	3.74	3.52	3.98	3.23	3.03	0.90	0.90	1.12	0.94	0.79
HER2	Set 1	0.11	0.10	0.14	0.19	0.32	0.17	0.15	0.14	0.01	0.19	1.55	1.50	1.00	0.05	0.59
	Set 2	0.52	0.15	0.14	0.11	0.32	0.24	0.14	0.14	0.04	0.31	0.46	0.93	1.00	0.36	0.97
	Set 3	0.51	0.17	0.14	0.02	0.26	0.28	0.34	0.16	0.07	0.31	0.55	2.00	1.14	3.50	1.19
HER3	Set 1	0.03	0.05	0.09	0.09	0.05	0.04	0.07	0.09	0.02	0.02	1.33	1.40	1.00	0.22	0.40
	Set 2	0.10	0.04	0.07	0.05	0.05	0.05	0.06	0.05	0.01	0.13	0.50	1.50	0.71	0.20	2.60
	Set 3	0.17	0.13	0.08	0.02	0.11	0.13	0.14	0.07	0.02	0.11	0.76	1.08	0.88	1.00	1.00
HER4	Set 1	0.03	0.07	0.05	0.07	0.02	0.05	0.05	0.03	0.04	0.02	1.67	0.71	0.60	0.57	1.00
	Set 2	0.02	0.05	0.03	0.02	0.01	0.03	0.06	0.02	0.01	0.01	1.50	1.20	0.67	0.50	1.00
	Set 3	0.03	0.06	0.02	0.02	0.02	0.02	0.05	0.01	0.02	0.02	0.67	0.83	0.50	1.00	1.00
HGK	Set 1	0.02	0.10	0.31	0.18	0.29	0.13	0.21	0.10	0.01	*0.001*	6.50	2.10	0.32	0.06	0.00
	Set 2	0.51	0.14	0.17	0.16	0.36	0.29	0.16	0.16	*0.001*	0.28	0.57	1.14	0.94	0.01	0.78
	Set 3	0.99	0.35	0.27	0.01	0.55	0.63	0.56	0.48	*0.001*	0.49	0.64	1.60	1.78	0.10	0.89
IKKα	Set 1	0.36	0.38	0.35	0.29	0.25	0.36	0.33	0.39	0.35	0.22	1.00	0.87	1.11	1.21	0.88
	Set 2	0.18	0.18	0.15	0.16	0.18	0.18	0.15	0.14	0.09	0.17	1.00	0.83	0.93	0.56	0.94
	Set 3	0.24	0.16	0.18	0.13	0.22	0.20	0.21	0.19	0.14	0.20	0.83	1.31	1.06	1.08	0.91
IKKβ	Set 1	0.14	0.21	0.19	0.16	0.07	0.15	0.17	0.13	0.22	0.06	1.07	0.81	0.68	1.38	0.86
	Set 2	0.10	0.08	0.11	0.10	0.08	0.15	0.12	0.07	0.06	0.09	1.50	1.50	0.64	0.60	1.13
	Set 3	0.10	0.13	0.09	0.04	0.11	0.11	0.10	0.09	0.04	0.10	1.10	0.77	1.00	1.00	0.91
JAK1	Set 1	0.01	0.05	0.09	0.03	0.05	0.02	0.05	0.05	0.05	0.06	2.00	1.00	0.56	1.67	1.20
	Set 2	0.04	0.02	0.02	0.03	0.04	0.02	0.02	0.02	0.04	0.05	0.50	1.00	1.00	1.33	1.25
	Set 3	0.04	0.05	0.04	0.03	0.04	0.04	0.03	0.02	0.03	0.04	1.00	0.60	0.50	1.00	1.00
JAK2	Set 1	0.02	0.02	0.03	0.03	0.03	0.04	*0.001*	0.04	0.02	0.03	2.00	0.05	1.33	0.67	1.00
	Set 2	0.01	0.01	0.02	0.02	0.02	0.01	0.01	0.01	0.02	0.03	1.00	1.00	0.50	1.00	1.50
	Set 3	0.03	0.01	0.02	0.01	0.04	0.06	0.04	0.03	0.03	0.03	2.00	4.00	1.50	3.00	0.75
JNK1α1	Set 1	2.20	1.68	1.73	1.71	1.58	1.64	1.62	1.60	1.39	1.42	0.75	0.96	0.92	0.81	0.90
	Set 2	1.20	1.16	1.21	1.12	1.28	1.17	1.15	1.11	1.17	1.12	0.98	0.99	0.92	1.04	0.88
	Set 3	1.43	1.38	1.50	1.50	1.45	1.56	1.58	1.51	1.61	1.42	1.09	1.14	1.01	1.07	0.98
JNK2α1/β1	Set 1	0.39	0.49	0.39	0.46	0.45	0.37	0.30	0.27	0.28	0.30	0.95	0.61	0.69	0.61	0.67
	Set 2	0.39	0.40	0.45	0.38	1.16	0.31	0.38	0.30	0.28	1.01	0.79	0.95	0.67	0.74	0.87
	Set 3	0.92	0.81	0.71	0.48	1.05	1.13	1.17	0.55	0.37	0.79	1.23	1.44	0.77	0.77	0.75
JNK2α2/β2	Set 1	0.22	0.33	0.37	0.42	0.21	0.26	0.28	0.26	0.10	0.14	1.18	0.85	0.70	0.24	0.67
	Set 2	0.29	0.21	0.22	0.20	0.27	0.26	0.30	0.24	0.06	0.21	0.90	1.43	1.09	0.30	0.78
	Set 3	0.31	0.27	0.17	0.06	0.23	0.22	0.26	0.19	0.02	0.19	0.71	0.96	1.12	0.33	0.83

LIMK1	Set 1	2.25	2.17	2.34	2.39	1.66	2.40	2.20	2.08	2.20	1.61	1.07	1.01	0.89	0.92	0.97
	Set 2	0.89	1.20	1.34	1.23	1.32	0.97	1.22	1.43	1.18	1.09	1.09	1.02	1.07	0.96	0.83
	Set 3	1.19	1.64	1.57	1.66	1.60	1.54	2.05	1.58	1.42	1.61	1.29	1.25	1.01	0.86	1.01
Lkb1	Set 1	0.34	0.37	0.32	0.21	0.30	0.39	0.31	0.33	0.02	0.22	1.15	0.84	1.03	0.10	0.73
	Set 2	0.12	0.29	0.20	0.14	0.27	0.33	0.33	0.19	0.01	0.12	2.75	1.14	0.95	0.07	0.44
	Set 3	0.19	0.41	0.41	0.03	0.47	0.34	0.46	0.37	0.01	0.32	1.79	1.12	0.90	0.33	0.68
Lyn	Set 1	0.18	0.31	0.10	0.16	0.12	0.23	0.17	0.08	0.14	0.26	1.28	0.55	0.80	0.88	2.17
	Set 2	0.01	0.15	0.08	0.08	0.10	0.11	0.12	0.06	0.10	0.14	11.00	0.80	0.75	1.25	1.40
	Set 3	0.01	0.10	0.12	0.06	0.23	0.10	0.11	0.14	0.08	0.19	10.00	1.10	1.17	1.33	0.83
MAPKAPK2	Set 1	0.03	0.03	0.02	0.02	0.02	0.03	0.01	0.03	0.03	0.04	1.00	0.33	1.50	1.50	2.00
	Set 2	0.01	0.01	0.02	0.02	0.01	0.02	0.02	0.01	0.01	0.01	2.00	2.00	0.50	0.50	1.00
	Set 3	0.01	0.02	0.01	0.02	0.01	0.02	0.01	0.01	0.01	0.01	2.00	0.50	1.00	0.50	1.00
MARK1	Set 1	0.07	0.07	0.08	0.09	0.05	0.08	0.10	0.10	0.09	0.05	1.14	1.43	1.25	1.00	1.00
	Set 2	0.03	0.04	0.03	0.04	0.03	0.03	0.04	0.02	0.04	0.02	1.00	1.00	0.67	1.00	0.67
	Set 3	0.03	0.03	0.04	0.03	0.03	0.04	0.02	0.03	0.03	0.02	1.33	0.67	0.75	1.00	0.67
MARK4	Set 1	0.02	0.05	0.15	0.06	0.08	0.03	0.08	0.14	0.07	0.08	1.50	1.60	0.93	1.17	1.00
	Set 2	0.15	0.02	0.06	0.06	0.03	0.06	0.04	0.08	0.02	0.04	0.40	2.00	1.33	0.33	1.33
	Set 3	0.13	0.06	0.05	0.06	0.04	0.07	0.07	0.08	0.04	0.05	0.54	1.17	1.60	0.67	1.25
MEK1	Set 1	1.67	1.31	1.63	1.67	1.43	1.16	1.31	1.44	1.14	0.96	0.69	1.00	0.88	0.68	0.67
	Set 2	2.66	1.12	1.02	1.29	1.43	1.10	1.08	0.99	0.82	1.32	0.41	0.96	0.97	0.64	0.92
	Set 3	2.58	1.60	1.26	1.11	1.33	1.37	1.36	1.43	1.31	1.24	0.53	0.85	1.13	1.18	0.93
MEK2	Set 1	1.19	1.19	1.30	1.38	1.16	1.11	1.12	1.06	1.06	0.87	0.93	0.94	0.82	0.77	0.75
	Set 2	1.44	0.98	0.90	0.99	0.97	0.93	0.90	0.87	0.71	1.01	0.65	0.92	0.97	0.72	1.04
	Set 3	1.87	1.47	1.33	1.21	1.19	1.42	1.53	1.36	1.23	1.14	0.76	1.04	1.02	1.02	0.96
MEK5α	Set 1	2.58	2.16	1.74	2.43	1.93	2.70	1.90	1.81	0.56	1.43	1.05	0.88	1.04	0.23	0.74
	Set 2	2.34	2.62	2.67	2.43	2.86	3.02	3.12	2.62	0.30	1.90	1.29	1.19	0.98	0.12	0.66
	Set 3	2.59	2.81	2.44	0.19	2.87	2.82	2.59	2.93	0.06	1.98	1.09	0.92	1.20	0.32	0.69
MEK5β	Set 1	0.43	0.43	0.46	0.44	0.29	0.39	0.36	0.40	0.39	0.26	0.91	0.84	0.87	0.89	0.90
	Set 2	0.26	0.28	0.28	0.26	0.33	0.23	0.26	0.19	0.21	0.31	0.88	0.93	0.68	0.81	0.94
	Set 3	0.24	0.25	0.28	0.24	0.30	0.26	0.25	0.27	0.35	0.17	1.08	1.00	0.96	1.46	0.57
MEKK1	Set 1	0.04	0.04	0.07	0.06	0.10	0.09	0.04	0.09	0.02	0.13	2.25	1.00	1.29	0.33	1.30
	Set 2	0.10	0.03	0.04	0.04	0.07	0.07	0.04	0.04	0.01	NQ	0.70	1.33	1.00	0.25	–
	Set 3	0.10	0.07	0.06	0.06	0.08	0.16	0.04	0.06	0.01	NQ	1.60	0.57	1.00	0.17	–
MKK6	Set 1	0.82	0.63	0.66	0.76	0.75	0.72	0.62	0.67	0.56	0.68	0.88	0.98	1.02	0.74	0.91
	Set 2	0.59	0.52	0.56	0.54	0.61	0.60	0.51	0.54	0.41	0.55	1.02	0.98	0.96	0.76	0.90
	Set 3	0.88	0.85	0.83	0.69	0.81	0.88	0.86	0.89	0.75	0.74	1.00	1.01	1.07	1.09	0.91
MKK7	Set 1	0.78	1.23	1.65	1.55	1.29	0.93	1.29	1.37	1.32	0.78	1.19	1.05	0.83	0.85	0.60
	Set 2	0.77	0.61	0.53	0.65	0.68	0.61	0.66	0.60	0.51	0.51	0.79	1.08	1.13	0.78	0.75
	Set 3	0.80	0.69	0.71	0.63	0.63	0.70	0.82	0.88	0.63	0.60	0.88	1.19	1.24	1.00	0.95
MLK3	Set 1	0.02	0.03	0.07	0.06	0.07	0.03	0.05	0.06	0.04	0.04	1.50	1.67	0.86	0.67	0.57
	Set 2	0.03	0.03	0.03	0.04	0.03	0.03	0.03	0.03	0.02	0.03	1.00	1.00	1.00	0.50	1.00
	Set 3	0.03	0.03	0.05	0.02	0.04	0.04	0.04	0.06	0.01	0.03	1.33	1.33	1.20	0.50	0.75
MSK1	Set 1	0.39	0.34	0.34	0.24	0.33	0.64	0.48	0.39	0.27	0.31	1.64	1.41	1.15	1.13	0.94
	Set 2	0.12	0.31	0.26	0.23	0.32	0.33	0.29	0.31	0.13	0.21	2.75	0.94	1.19	0.57	0.66
	Set 3	0.19	0.44	0.33	0.19	0.43	0.52	0.47	0.38	0.13	0.37	2.74	1.07	1.15	0.68	0.86
MST1	Set 1	0.12	0.14	0.15	0.17	0.10	0.13	0.15	0.12	0.07	0.08	1.08	1.07	0.80	0.41	0.80
	Set 2	0.07	0.07	0.07	0.07	0.08	0.07	0.06	0.07	0.02	0.07	1.00	0.86	1.00	0.29	0.88
	Set 3	0.15	0.15	0.14	0.03	0.12	0.13	0.18	0.17	0.01	0.17	0.87	1.20	1.21	0.33	1.42
Myt1	Set 1	0.02	0.04	0.13	0.11	0.06	0.05	0.06	0.17	0.03	0.03	2.50	1.50	1.31	0.27	0.50
	Set 2	0.27	0.05	ND	0.05	0.03	0.05	0.03	ND	0.05	0.05	0.19	0.60	–	1.00	1.67
	Set 3	0.19	0.06	0.05	0.04	0.05	0.05	0.04	0.10	0.08	0.08	0.26	0.67	2.00	2.00	1.60

	Set 1	2.10	2.22	2.16	2.07	1.94	1.81	1.98	2.32	2.27	1.69	0.86	0.89	1.07	1.10	0.87
Nek6	Set 2	0.56	0.85	0.79	0.77	0.77	0.77	0.83	0.64	0.75	0.54	1.38	0.98	0.81	0.97	0.70
	Set 3	0.62	0.69	0.78	0.75	0.83	0.55	0.80	0.76	0.59	0.63	0.89	1.16	0.97	0.79	0.76
	Set 1	NR	NR	NR	NR	0.08	NR	NR	NR	NR	0.12	–	–	–	–	1.50
p25	Set 2	0.13	0.10	0.01	0.07	0.10	0.14	0.11	0.04	0.10	0.10	1.08	1.10	4.00	1.43	1.00
	Set 3	0.11	0.09	0.07	0.07	0.06	0.07	0.07	0.14	0.09	0.06	0.64	0.78	2.00	1.29	1.00
	Set 1	NR	NR	NR	NR	0.20	NR	NR	NR	NR	0.13	–	–	–	–	0.65
p35	Set 2	0.31	0.10	0.09	0.11	0.08	0.11	0.11	0.10	0.05	0.09	0.35	1.10	1.11	0.45	1.13
	Set 3	0.38	0.16	0.12	0.07	0.13	0.15	0.14	0.19	0.05	0.11	0.39	0.88	1.58	0.71	0.85
	Set 1	0.33	0.28	0.27	0.39	0.27	0.25	0.27	0.18	0.26	0.62	0.76	0.96	0.67	0.67	2.30
p38α	Set 2	0.21	0.23	0.20	0.20	0.32	0.25	0.25	0.16	0.27	0.44	1.19	1.09	0.80	1.35	1.38
	Set 3	0.24	0.34	0.31	0.31	0.39	0.31	0.26	0.35	0.33	0.47	1.29	0.76	1.13	1.06	1.21
	Set 1	0.11	0.10	0.09	0.11	0.10	0.10	0.09	0.11	0.08	0.11	0.91	0.90	1.22	0.73	1.10
p38β	Set 2	0.25	0.12	0.25	0.12	0.28	0.12	0.14	0.14	0.11	0.21	0.48	1.17	0.56	0.92	0.75
	Set 3	0.41	0.16	0.19	0.16	0.23	0.22	0.24	0.19	0.11	0.37	0.54	1.50	1.00	0.69	1.61
	Set 1	0.67	0.43	0.55	0.57	0.54	0.71	0.43	0.38	0.54	0.33	1.06	1.00	0.69	0.95	0.61
p38γ	Set 2	0.10	0.33	0.32	0.26	0.46	0.38	0.26	0.30	0.41	0.35	3.80	0.79	0.94	1.58	0.76
	Set 3	0.13	0.45	0.39	0.38	0.40	0.63	0.47	0.52	0.47	0.45	4.85	1.04	1.33	1.24	1.13
	Set 1	0.02	0.03	0.02	0.03	0.03	0.03	0.03	0.02	0.01	0.03	1.50	1.00	1.00	0.33	1.00
p39	Set 2	0.10	0.02	0.02	0.02	0.03	0.02	0.02	0.02	0.01	0.02	0.20	1.00	1.00	0.50	0.67
	Set 3	0.21	0.07	0.06	0.03	0.04	0.03	0.08	0.07	0.03	0.04	0.14	1.14	1.17	1.00	1.00
	Set 1	0.07	0.12	0.06	0.07	0.07	0.04	0.08	0.07	0.04	0.04	0.57	0.67	1.17	0.57	0.57
p70S6K	Set 2	0.09	0.08	0.04	0.06	0.07	0.06	0.05	0.05	*0.001*	0.05	0.67	0.63	1.25	0.02	0.71
	Set 3	0.05	0.06	0.03	ND	0.06	0.08	0.08	0.04	ND	0.03	1.60	1.33	1.33	–	0.50
	Set 1	3.79	3.36	3.44	3.30	1.78	3.73	3.20	2.89	3.03	1.73	0.98	0.95	0.84	0.92	0.97
PAK1	Set 2	1.21	1.13	1.11	0.99	1.27	1.19	1.32	1.27	1.30	1.11	0.98	1.17	1.14	1.31	0.87
	Set 3	1.36	1.55	1.77	1.59	1.60	1.34	1.56	1.64	1.58	1.61	0.99	1.01	0.93	0.99	1.01
	Set 1	0.26	0.25	0.51	0.45	0.38	0.25	0.45	0.54	0.34	0.14	0.96	1.80	1.06	0.76	0.37
PAK3	Set 2	0.73	0.28	0.28	0.36	0.27	0.26	0.25	0.35	0.21	0.30	0.36	0.89	1.25	0.58	1.11
	Set 3	0.96	0.41	0.32	0.32	0.22	0.36	0.40	0.41	0.28	0.31	0.38	0.98	1.28	0.88	1.41
	Set 1	0.51	1.17	2.06	2.04	1.12	0.93	1.01	1.92	1.29	0.73	1.82	0.86	0.93	0.63	0.65
PCTAIRE3	Set 2	0.81	0.54	0.60	0.67	0.62	0.65	0.78	0.79	0.40	0.68	0.80	1.44	1.32	0.60	1.10
	Set 3	1.00	0.76	0.85	0.70	0.54	0.69	0.97	0.99	0.61	0.80	0.69	1.28	1.16	0.87	1.48
	Set 1	0.11	0.12	0.12	0.08	0.12	0.11	0.12	0.16	0.10	0.10	1.00	1.00	1.33	1.25	0.83
PDK1	Set 2	0.07	0.06	0.05	0.06	0.06	0.07	0.08	0.05	0.04	0.04	1.00	1.33	1.00	0.67	0.67
	Set 3	0.06	0.06	0.08	0.04	0.06	0.07	0.06	0.06	0.02	0.05	1.17	1.00	0.75	0.50	0.83
	Set 1	0.49	0.46	0.60	0.55	0.41	0.36	0.57	0.57	0.45	0.28	0.73	1.24	0.95	0.82	0.68
PKACα	Set 2	0.70	0.32	0.29	0.42	0.46	0.32	0.26	0.27	0.31	0.40	0.46	0.81	0.93	0.74	0.87
	Set 3	0.87	0.48	0.37	0.44	0.43	0.40	0.42	0.47	0.50	0.47	0.46	0.88	1.27	1.14	1.09
	Set 1	3.18	2.32	3.23	3.43	2.38	3.11	3.30	3.13	1.76	2.17	0.98	1.42	0.97	0.51	0.91
PKACβ	Set 2	3.20	1.51	1.57	1.95	2.17	1.92	1.93	2.07	0.71	2.13	0.60	1.28	1.32	0.36	0.98
	Set 3	4.53	3.07	2.57	1.55	3.20	3.47	2.71	3.56	1.05	3.03	0.77	0.88	1.39	0.68	0.95
	Set 1	0.87	0.90	1.00	1.07	0.73	0.71	0.76	0.88	0.62	0.46	0.82	0.84	0.88	0.58	0.63
PKACγ	Set 2	1.33	0.56	0.46	0.59	0.68	0.40	0.51	0.44	0.39	0.46	0.30	0.91	0.96	0.66	0.68
	Set 3	1.30	0.64	0.54	0.59	0.65	0.65	0.69	0.68	0.82	0.58	0.50	1.08	1.26	1.39	0.89
	Set 1	1.18	1.17	1.31	1.15	0.99	1.60	1.43	1.54	0.98	0.77	1.36	1.22	1.18	0.85	0.78
PKCα	Set 2	1.92	1.07	0.75	0.60	1.11	0.81	0.55	0.69	0.62	1.18	0.42	0.51	0.92	1.03	1.06
	Set 3	1.46	0.83	0.65	0.49	0.82	0.67	0.81	0.75	0.68	0.31	0.46	0.98	1.15	1.39	0.38
	Set 1	1.08	1.42	1.25	0.92	0.88	1.30	1.20	1.26	0.90	0.60	1.20	0.85	1.01	0.98	0.68
PKCβ	Set 2	1.41	0.79	0.60	0.44	0.84	0.54	0.38	0.48	0.37	0.78	0.38	0.48	0.80	0.84	0.93
	Set 3	1.39	0.72	0.65	0.43	0.83	0.70	0.85	0.60	0.70	0.17	0.50	1.18	0.92	1.63	0.20

PKCε	Set 1	0.63	0.74	0.70	0.84	0.68	0.99	0.81	0.57	0.65	0.58	1.57	1.09	0.81	0.77	0.85
	Set 2	1.02	0.49	0.34	0.45	0.54	0.41	0.32	0.33	0.32	0.67	0.40	0.65	0.97	0.71	1.24
	Set 3	0.86	0.49	0.33	0.27	0.51	0.46	0.52	0.46	0.44	0.45	0.53	1.06	1.39	1.63	0.88
PKCγ	Set 1	0.67	0.77	0.56	0.57	0.49	0.71	0.44	0.40	0.43	0.21	1.06	0.57	0.71	0.75	0.43
	Set 2	0.23	0.31	0.29	0.23	0.50	0.36	0.27	0.25	0.20	0.24	1.57	0.87	0.86	0.87	0.48
	Set 3	0.38	0.42	0.42	0.21	0.83	0.56	0.39	0.45	0.20	0.19	1.47	0.93	1.07	0.95	0.23
PKCι	Set 1	0.28	0.29	0.22	0.22	0.26	0.28	0.22	0.23	0.17	0.23	1.00	0.76	1.05	0.77	0.88
	Set 2	0.15	0.15	0.23	0.15	0.23	0.20	0.19	0.12	0.11	0.17	1.33	1.27	0.52	0.73	0.74
	Set 3	0.23	0.23	0.20	0.18	0.35	0.28	0.31	0.23	0.16	0.16	1.22	1.35	1.15	0.89	0.46
PKCθ	Set 1	0.04	0.07	0.05	0.10	0.06	0.05	0.06	0.08	0.08	0.03	1.25	0.86	1.60	0.80	0.50
	Set 2	0.02	0.05	0.05	0.05	0.03	0.04	0.05	0.04	0.03	0.01	2.00	1.00	0.80	0.60	0.33
	Set 3	0.02	0.05	0.05	0.02	0.03	0.03	0.06	0.05	0.03	0.04	1.50	1.20	1.00	1.50	1.33
PKCζ	Set 1	0.48	0.51	0.47	0.29	0.39	0.62	0.48	0.46	0.40	0.24	1.29	0.94	0.98	1.38	0.62
	Set 2	0.35	0.29	0.42	0.27	0.47	0.29	0.28	0.30	0.28	0.41	0.83	0.97	0.71	1.04	0.87
	Set 3	0.54	0.52	0.44	0.44	0.55	0.65	0.60	0.47	0.57	0.50	1.20	1.15	1.07	1.30	0.91
PKD1	Set 1	0.35	0.69	0.95	1.15	0.76	0.62	0.83	1.08	0.57	0.32	1.77	1.20	1.14	0.50	0.42
	Set 2	0.57	0.40	0.32	0.33	0.36	0.41	0.43	0.35	0.06	0.38	0.72	1.08	1.09	0.18	1.06
	Set 3	0.63	0.49	0.38	0.08	0.37	0.47	0.46	0.52	0.06	0.57	0.75	0.94	1.37	0.75	1.54
PKD3	Set 1	0.02	0.06	0.07	0.06	0.07	0.04	0.06	0.13	0.03	0.05	2.00	1.00	1.86	0.50	0.71
	Set 2	0.02	0.04	0.01	0.02	0.07	0.03	0.03	0.01	0.01	0.04	1.50	0.75	1.00	0.50	0.57
	Set 3	0.02	0.03	0.03	ND	0.03	0.03	0.03	0.04	ND	0.04	1.50	1.00	1.33	−	1.33
PKG1	Set 1	0.06	0.06	0.02	0.02	0.02	0.04	0.06	0.02	0.04	0.02	0.67	1.00	1.00	2.00	1.00
	Set 2	0.01	0.02	0.01	0.01	0.01	0.03	0.02	0.01	0.01	0.01	3.00	1.00	1.00	1.00	1.00
	Set 3	0.01	0.02	0.02	0.01	0.02	0.02	0.02	0.02	0.01	0.01	2.00	1.00	1.00	1.00	0.50
PKR	Set 1	0.01	0.01	0.02	0.01	0.06	0.02	0.04	0.03	0.01	0.04	2.00	4.00	1.50	1.00	0.67
	Set 2	0.01	0.02	0.05	0.06	0.05	0.01	0.01	0.05	0.01	0.04	1.00	0.50	1.00	0.17	0.80
	Set 3	0.01	0.03	0.02	ND	0.02	0.02	0.03	0.04	ND	0.04	2.00	1.00	2.00	−	2.00
PLK1	Set 1	0.06	0.10	0.05	0.07	0.09	0.03	0.07	0.08	0.08	0.06	0.50	0.70	1.60	1.14	0.67
	Set 2	0.03	0.01	0.03	0.01	0.04	0.01	0.02	0.03	0.03	0.02	0.33	2.00	1.00	3.00	0.50
	Set 3	0.05	0.07	0.04	0.03	0.06	0.04	0.11	0.05	0.01	0.05	0.80	1.57	1.25	0.33	0.83
PRK1	Set 1	0.41	0.56	0.59	0.46	0.43	0.59	0.61	0.56	0.48	0.45	1.44	1.09	0.95	1.04	1.05
	Set 2	0.35	0.31	0.30	0.28	0.38	0.27	0.26	0.29	0.31	0.33	0.77	0.84	0.97	1.11	0.87
	Set 3	0.44	0.35	0.44	0.29	0.49	0.42	0.47	0.42	0.35	0.52	0.95	1.34	0.95	1.21	1.06
PRK2	Set 1	0.02	0.02	0.04	0.02	0.09	0.02	0.02	0.02	0.01	0.05	1.00	1.00	0.50	0.50	0.56
	Set 2	0.01	0.02	0.04	0.02	0.02	0.02	0.02	0.03	*0.001*	0.01	2.00	1.00	0.75	0.05	0.50
	Set 3	0.01	0.02	0.03	ND	0.02	0.03	0.02	0.03	ND	0.01	3.00	1.00	1.00	−	0.50
Pyk2	Set 1	0.07	0.09	0.84	0.60	0.21	0.06	0.36	0.67	0.14	0.04	0.86	4.00	0.80	0.23	0.19
	Set 2	1.24	0.07	0.07	0.34	0.10	0.06	0.06	0.11	0.04	0.58	0.05	0.86	1.57	0.12	5.80
	Set 3	1.75	0.47	0.17	0.12	0.11	0.18	0.22	0.44	0.47	0.51	0.10	0.47	2.59	3.92	4.64
Raf1	Set 1	0.74	0.89	0.79	1.10	0.70	0.89	0.74	0.87	0.64	0.55	1.20	0.83	1.10	0.58	0.79
	Set 2	0.76	0.65	0.57	0.57	0.66	0.62	0.67	0.55	0.25	0.50	0.82	1.03	0.96	0.44	0.76
	Set 3	0.76	0.65	0.72	0.37	0.74	0.73	0.78	0.71	0.30	0.50	0.96	1.20	0.99	0.81	0.68
ROCK1	Set 1	0.09	0.10	0.10	0.07	0.08	0.10	0.08	0.05	0.10	0.07	1.11	0.80	0.50	1.43	0.88
	Set 2	0.05	0.04	0.06	0.04	0.05	0.04	0.03	0.04	0.05	0.06	0.80	0.75	0.67	1.25	1.20
	Set 3	0.04	0.05	0.06	0.04	0.07	0.07	0.07	0.05	0.03	0.07	1.75	1.40	0.83	0.75	1.00
ROCK2	Set 1	1.96	1.87	2.27	2.18	1.88	2.35	2.10	2.46	1.60	1.56	1.20	1.12	1.08	0.73	0.83
	Set 2	1.43	1.10	1.08	1.06	1.47	1.48	1.09	1.40	1.21	1.37	1.03	0.99	1.30	1.14	0.93
	Set 3	1.69	1.52	1.42	1.38	1.84	1.85	1.60	2.01	1.77	1.56	1.09	1.05	1.42	1.28	0.85
RSK1	Set 1	3.55	3.40	2.26	2.87	2.62	4.12	2.86	2.48	2.80	1.33	1.16	0.84	1.10	0.98	0.51
	Set 2	0.23	2.02	1.72	1.32	2.15	2.12	1.75	1.78	1.86	0.68	9.22	0.87	1.03	1.41	0.32
	Set 3	0.54	2.26	2.29	2.15	3.27	2.95	2.65	2.43	2.06	2.27	5.46	1.17	1.06	0.96	0.69

	Set 1	0.09	0.09	0.05	0.07	0.08	0.09	0.08	0.08	0.12	0.08	1.00	0.89	1.60	1.71	1.00
RSK2	Set 2	0.04	0.05	0.05	0.04	0.04	0.06	0.04	0.05	0.05	0.04	1.50	0.80	1.00	1.25	1.00
	Set 3	0.06	0.06	0.06	0.07	0.07	0.06	0.08	0.05	0.05	0.08	1.00	1.33	0.83	0.71	1.14
	Set 1	0.91	0.81	1.08	0.91	0.77	1.04	0.92	1.05	0.64	0.75	1.14	1.14	0.97	0.70	0.97
SGK3	Set 2	0.63	0.40	0.43	0.52	0.52	0.48	0.47	0.49	0.19	0.45	0.76	1.18	1.14	0.37	0.87
	Set 3	1.11	0.90	0.85	0.49	0.92	0.89	0.92	0.98	0.51	0.74	0.80	1.02	1.15	1.04	0.80
	Set 1	0.80	0.92	0.89	0.78	0.72	0.86	0.82	0.85	0.10	0.48	1.08	0.89	0.96	0.13	0.67
SLK	Set 2	0.45	0.41	0.47	0.34	0.50	0.33	0.41	0.28	0.01	0.37	0.73	1.00	0.60	0.03	0.74
	Set 3	0.71	0.55	0.58	ND	0.47	0.65	0.63	0.65	ND	0.44	0.92	1.15	1.12	–	0.94
	Set 1	0.42	1.03	1.37	1.71	1.01	0.49	1.45	1.01	0.88	0.78	1.17	1.41	0.74	0.51	0.77
Src	Set 2	1.41	0.96	0.43	0.91	0.68	0.92	0.70	0.56	0.98	1.00	0.65	0.73	1.30	1.08	1.47
	Set 3	1.64	1.08	0.83	0.80	1.17	1.03	0.95	1.37	0.97	1.27	0.63	0.88	1.65	1.21	1.09
	Set 1	0.84	1.04	1.50	1.56	1.01	1.15	1.22	1.53	0.23	0.45	1.37	1.17	1.02	0.15	0.45
TNIK	Set 2	1.06	0.57	0.74	0.72	0.90	0.62	0.63	0.65	0.03	0.80	0.58	1.11	0.88	0.04	0.89
	Set 3	1.23	0.89	0.79	ND	0.72	0.81	0.95	1.05	ND	0.45	0.66	1.07	1.33	–	0.63
	Set 1	0.20	0.27	0.30	0.28	0.20	0.33	0.22	0.34	0.15	0.06	1.65	0.81	1.13	0.54	0.30
TrkA	Set 2	0.21	0.10	0.12	0.08	0.13	0.12	0.10	0.12	0.02	0.09	0.57	1.00	1.00	0.25	0.69
	Set 3	0.32	0.17	0.16	0.03	0.21	0.21	0.30	0.14	0.04	0.20	0.66	1.76	0.88	1.33	0.95
	Set 1	ND	0.06	0.09	0.11	0.08	ND	0.05	0.13	0.01	0.04	–	0.83	1.44	0.09	0.50
TrkB	Set 2	0.22	0.03	0.01	0.06	0.04	0.02	0.03	0.04	0.03	0.10	0.09	1.00	4.00	0.50	2.50
	Set 3	0.21	0.06	0.04	0.03	0.06	0.05	0.05	0.07	0.04	0.04	0.24	0.83	1.75	1.33	0.67
	Set 1	0.03	0.09	0.09	0.12	0.09	0.03	0.09	0.10	0.15	0.06	1.00	1.00	1.11	1.25	0.67
TrkB T	Set 2	0.02	0.08	0.09	0.06	0.04	0.01	0.05	0.06	0.06	0.08	0.50	0.63	0.67	1.00	2.00
	Set 3	0.02	0.07	0.08	0.05	0.06	0.02	0.07	0.05	0.08	0.07	1.00	1.00	0.63	1.60	1.17
	Set 1	0.01	0.01	0.02	0.01	0.02	0.01	0.02	0.01	*0.001*	0.01	1.00	2.00	0.50	0.10	0.50
TrkC	Set 2	0.01	0.02	0.01	0.03	0.02	0.02	0.02	0.01	*0.001*	0.01	2.00	1.00	1.00	0.03	0.50
	Set 3	0.01	0.01	0.01	ND	0.02	0.03	0.02	0.02	ND	0.01	3.00	2.00	2.00	–	0.50
	Set 1	0.23	0.21	0.23	0.15	0.13	0.27	0.26	0.24	0.21	0.12	1.17	1.24	1.04	1.40	0.92
Wee1	Set 2	0.10	0.09	0.07	0.10	0.10	0.10	0.08	0.11	0.07	0.07	1.00	0.89	1.57	0.70	0.70
	Set 3	0.13	0.14	0.18	0.14	0.15	0.23	0.20	0.21	0.13	0.15	1.77	1.43	1.17	0.93	1.00

Equivalent amounts of protein from the brainstem-cerebellum of three mock- and three scrapie-infected mice (Sets 1-3) at 70, 90, 110, 130 dpi, or at terminal stage of disease (TER) were resolved and transferred to membranes. Primary multiplex Western blots analyzed the expression levels of 139 protein kinases or regulatory subunits; 109 were detected. A truncated TrkB product (TrkB T) was also detected. Ratios were calculated relative to the absolute levels in mock-infected mice from the same set at each time point. Proteins below detection in scrapie-infected samples were assigned a value of 0.001 (indicated in italics), 10-fold below the detection limit. ND, not detected in mock- or scrapie-infected samples. NR, not resolved in mock- or scrapie-infected samples. NQ, not quantitated due to transfer (ASK1) or blotting (MEKK1) artifacts.

Appendix 5 – The expression levels of 12 protein kinases and substrates in scrapie-infected mice analyzed by targeted secondary analyses.

			Mock-infected					RML-infected									
			Absolute (arbitrary units)					Absolute (arbitrary units)					Ratio				
			70	90	110	130	TER	70	90	110	130	TER	70	90	110	130	TER
	BC*	Set 1	1.63	1.75	1.19	1.19	1.11	1.54	1.22	1.14	1.20	1.12	0.94	0.70	0.96	1.01	1.01
		Set 2	0.29	0.99	1.11	0.69	1.60	1.32	1.10	0.85	0.72	0.61	4.55	1.11	0.77	1.04	0.38
		Set 3	0.40	1.24	1.10	0.81	1.92	1.31	1.20	1.18	0.47	1.42	3.28	0.97	1.07	0.58	0.74
CaMK4β	S	Set 1	0.53	0.41	0.58	0.43	0.89	0.59	0.49	0.52	0.42	0.55	1.11	1.20	0.90	0.98	0.62
		Set 2	0.43	0.56	0.43	0.60	0.40	0.73	0.64	0.61	0.58	0.61	1.70	1.14	1.42	0.97	1.53
		Set 3	0.54	0.64	0.70	0.54	0.56	0.65	0.61	0.53	0.57	0.68	1.20	0.95	0.76	1.06	1.21
	C	Set 1	0.72	0.87	0.68	0.54	0.68	0.74	0.69	0.69	0.67	0.59	1.03	0.79	1.01	1.24	0.87
		Set 2	2.12	0.45	0.43	0.39	0.58	0.63	0.41	0.51	0.53	0.57	0.30	0.91	1.19	1.36	0.98
		Set 3	2.02	0.65	0.64	0.62	0.55	0.51	0.55	0.43	0.55	0.51	0.25	0.85	0.67	0.89	0.93
	BC	Set 1	0.06	0.10	0.22	0.13	0.16	0.20	0.33	0.13	0.33	0.17	3.33	3.30	0.59	2.54	1.06
		Set 2	0.19	0.18	0.53	0.59	0.48	0.40	0.44	0.46	0.40	0.36	2.11	2.44	0.87	0.68	0.75
		Set 3	0.16	0.52	0.49	0.42	0.30	0.71	0.20	0.68	0.22	0.01	4.44	0.38	1.39	0.52	0.03
CREB	S	Set 1	0.48	0.72	0.54	0.63	0.68	0.57	0.90	0.35	0.76	0.40	1.19	1.25	0.65	1.21	0.59
		Set 2	0.14	0.49	0.50	0.59	0.61	0.52	0.71	0.56	0.39	0.70	3.71	1.45	1.12	0.66	1.15
		Set 3	0.72	0.53	0.34	0.57	0.80	0.58	0.73	0.45	0.40	0.67	0.81	1.38	1.32	0.70	0.84
	C	Set 1	0.16	0.14	0.10	0.29	0.21	0.31	0.33	0.27	0.07	0.27	1.94	2.36	2.70	0.24	1.29
		Set 2	0.50	0.24	0.36	0.45	0.29	0.20	0.43	0.17	0.17	0.45	0.40	1.79	0.47	0.38	1.55
		Set 3	0.26	0.41	0.27	0.41	0.44	0.50	0.60	0.35	0.44	0.34	1.92	1.46	1.30	1.07	0.77
	BC*	Set 1	1.21	1.31	1.36	1.73	1.35	1.24	1.17	1.26	0.50	1.35	1.02	0.89	0.93	0.29	1.00
		Set 2	2.19	1.31	1.46	1.65	1.50	1.46	1.40	1.49	0.63	1.29	0.67	1.07	1.02	0.38	0.86
		Set 3	3.15	2.43	2.09	1.17	2.04	2.35	1.98	2.50	0.54	1.95	0.75	0.81	1.20	0.46	0.96
DLK	S	Set 1	3.04	2.77	3.14	3.45	3.58	3.30	3.27	3.48	2.92	3.03	1.09	1.18	1.11	0.85	0.85
		Set 2	4.07	3.70	3.55	3.69	3.52	3.71	4.10	4.14	3.52	3.54	0.91	1.11	1.17	0.95	1.01
		Set 3	3.49	3.28	3.56	3.39	2.94	3.13	3.55	3.37	3.33	3.43	0.90	1.08	0.95	0.98	1.17
	C	Set 1	3.59	3.49	3.67	3.35	2.90	3.89	3.81	3.93	3.54	3.16	1.08	1.09	1.07	1.06	1.09
		Set 2	2.20	2.78	2.77	3.18	3.21	3.45	3.36	3.63	3.03	3.49	1.57	1.21	1.31	0.95	1.09
		Set 3	2.59	3.11	3.24	3.74	3.79	3.43	3.65	3.66	3.57	3.65	1.32	1.17	1.13	0.95	0.96
	BC	Set 1	0.01	0.01	0.02	0.02	0.03	0.02	0.02	0.01	0.01	0.03	2.00	2.00	0.50	0.50	1.00
		Set 2	0.03	0.04	0.04	0.06	0.09	0.05	NQ	0.04	0.03	NQ	1.67	–	1.00	0.50	–
		Set 3	0.05	0.06	0.10	0.04	0.07	0.11	0.11	0.10	0.02	0.05	2.20	1.83	1.00	0.50	0.71
FOXO3	S	Set 1	0.03	0.03	0.03	0.02	0.05	0.03	0.03	0.03	0.02	0.05	1.00	1.00	1.00	1.00	1.00
		Set 2	0.04	0.07	0.06	0.07	0.06	0.04	0.08	0.07	0.05	NQ	1.00	1.14	1.17	0.71	–
		Set 3	0.10	0.12	0.10	0.08	0.05	0.10	0.19	0.08	0.04	0.06	1.00	1.58	0.80	0.50	1.20
	C	Set 1	0.07	0.07	0.06	0.06	0.05	0.07	0.05	0.05	0.02	0.03	1.00	0.71	0.83	0.33	0.60
		Set 2	0.11	0.07	0.06	0.06	0.06	0.07	0.06	0.04	0.02	0.07	0.64	0.86	0.67	0.33	1.17
		Set 3	0.10	0.09	0.05	0.09	0.08	0.07	0.08	0.06	0.04	0.06	0.70	0.89	1.20	0.44	0.75
	BC*	Set 1	0.22	0.33	0.37	0.42	0.21	0.26	0.28	0.26	0.10	0.14	1.18	0.85	0.70	0.24	0.67
		Set 2	0.29	0.21	0.22	0.20	0.27	0.26	0.30	0.24	0.06	0.21	0.90	1.43	1.09	0.30	0.78
		Set 3	0.31	0.27	0.17	0.06	0.23	0.22	0.26	0.19	0.02	0.19	0.71	0.96	1.12	0.33	0.83
JNK2 α2/β2	S	Set 1	1.17	1.14	1.38	1.06	1.27	1.46	1.44	1.27	1.36	1.17	1.25	1.26	0.92	1.28	0.92
		Set 2	1.45	1.77	1.55	1.63	1.24	1.69	1.74	1.43	1.61	1.56	1.17	0.98	0.92	0.99	1.26
		Set 3	1.37	1.52	1.51	1.46	1.70	1.82	1.43	1.00	1.19	1.67	1.33	0.94	0.66	0.82	0.98
	C	Set 1	1.20	1.13	1.35	1.04	1.21	1.32	1.39	1.54	1.23	1.19	1.10	1.23	1.14	1.18	0.98
		Set 2	0.91	0.84	1.01	0.91	0.96	0.80	1.13	1.13	1.04	1.37	0.88	1.35	1.12	1.14	1.43
		Set 3	1.17	1.03	1.20	1.07	1.01	0.93	1.16	1.19	0.93	0.83	0.79	1.13	0.99	0.87	0.82

		Set 1	0.18	0.31	0.10	0.16	0.12	0.23	0.17	0.08	0.14	0.26	1.28	0.55	0.80	0.88	2.17
	BC*	Set 2	0.01	0.15	0.08	0.08	0.10	0.11	0.12	0.06	0.10	0.14	11.00	0.80	0.75	1.25	1.40
		Set 3	0.01	0.10	0.12	0.06	0.23	0.10	0.11	0.14	0.08	0.19	10.00	1.10	1.17	1.33	0.83
		Set 1	0.05	NQ	0.06	0.06	0.06	0.04	0.05	0.06	0.05	0.07	0.80	–	1.00	0.83	1.17
Lyn	S	Set 2	0.04	0.04	0.05	0.05	0.04	0.04	0.03	0.04	0.04	0.11	1.00	0.75	0.80	0.80	2.75
		Set 3	0.04	0.05	0.05	0.05	0.04	0.04	0.04	0.04	0.04	NQ	1.00	0.80	0.80	0.80	–
		Set 1	0.04	0.06	0.06	0.06	0.05	0.07	0.07	NQ	0.04	0.05	1.75	1.17	–	0.67	1.00
	C	Set 2	0.19	0.04	0.07	0.05	0.04	0.04	0.06	0.06	0.04	0.08	0.21	1.50	0.86	0.80	2.00
		Set 3	0.28	0.09	0.09	0.12	0.05	0.09	0.11	0.08	0.05	0.10	0.32	1.22	0.89	0.42	2.00
		Set 1	0.78	1.23	1.65	1.55	1.29	0.93	1.29	1.37	1.32	0.78	1.19	1.05	0.83	0.85	0.60
	BC*	Set 2	0.77	0.61	0.53	0.65	0.68	0.61	0.66	0.60	0.51	0.51	0.79	1.08	1.13	0.78	0.75
		Set 3	0.80	0.69	0.71	0.63	0.63	0.70	0.82	0.88	0.63	0.60	0.88	1.19	1.24	1.00	0.95
		Set 1	1.19	1.26	1.25	1.13	1.15	1.23	1.32	1.21	1.29	1.01	1.03	1.05	0.97	1.14	0.88
MKK7	S	Set 2	1.10	1.37	1.45	1.29	1.34	1.38	1.52	1.38	1.35	1.05	1.25	1.11	0.95	1.05	0.78
		Set 3	1.23	1.16	1.20	1.21	1.21	1.25	1.37	1.20	1.13	1.04	1.02	1.18	1.00	0.93	0.86
		Set 1	0.83	0.96	0.87	0.79	0.76	0.93	0.97	0.85	0.96	0.76	1.12	1.01	0.98	1.22	1.00
	C	Set 2	0.73	0.71	0.79	0.77	0.81	0.87	0.85	0.81	0.77	0.74	1.19	1.20	1.03	1.00	0.91
		Set 3	0.80	1.02	0.99	0.99	0.97	0.96	1.01	0.96	0.97	0.80	1.20	0.99	0.97	0.98	0.82
		Set 1	0.12	0.14	0.15	0.17	0.10	0.13	0.15	0.12	0.07	0.08	1.08	1.07	0.80	0.41	0.80
	BC*	Set 2	0.07	0.07	0.07	0.07	0.08	0.07	0.06	0.07	0.02	0.07	1.00	0.86	1.00	0.29	0.88
		Set 3	0.15	0.15	0.14	0.03	0.12	0.13	0.18	0.17	0.01	0.17	0.87	1.20	1.21	0.33	1.42
		Set 1	0.45	0.37	0.47	0.38	0.36	0.36	0.45	0.48	0.39	0.40	0.80	1.22	1.02	1.03	1.11
MST1	S	Set 2	0.40	0.45	0.49	0.51	0.39	0.42	0.54	0.45	0.34	0.44	1.05	1.20	0.92	0.67	1.13
		Set 3	0.42	0.43	0.43	0.34	0.35	0.36	0.43	0.40	0.29	0.45	0.86	1.00	0.93	0.85	1.29
		Set 1	0.30	0.36	0.33	0.31	0.23	0.35	0.35	0.34	0.20	0.28	1.17	0.97	1.03	0.65	1.22
	C	Set 2	0.20	0.24	0.22	0.24	0.24	0.22	0.26	0.26	0.12	0.26	1.10	1.08	1.18	0.50	1.08
		Set 3	0.28	0.32	0.29	0.33	0.30	0.31	0.35	0.34	0.23	0.31	1.11	1.09	1.17	0.70	1.03
		Set 1	0.06	0.10	0.07	0.05	0.05	0.07	0.07	0.05	0.06	0.04	1.17	0.70	0.71	1.20	0.80
	BC	Set 2	0.15	0.26	0.17	0.19	0.15	0.20	0.21	0.21	0.20	NQ	1.33	0.81	1.24	1.05	–
		Set 3	0.17	0.25	0.33	0.19	0.18	0.24	0.31	0.25	0.19	0.24	1.41	1.24	0.76	1.00	1.33
		Set 1	0.38	0.35	0.36	0.31	0.33	0.36	0.37	0.35	0.35	0.26	0.95	1.06	0.97	1.13	0.79
nNOS	S	Set 2	0.39	0.44	0.43	0.35	0.35	0.37	0.43	0.40	0.33	0.40	0.95	0.98	0.93	0.94	1.14
		Set 3	0.29	0.33	0.29	0.31	0.24	0.33	0.33	0.29	0.21	0.26	1.14	1.00	1.00	0.68	1.08
		Set 1	0.28	0.27	0.24	0.22	0.21	0.26	0.23	0.27	0.19	0.20	0.93	0.85	1.13	0.86	0.95
	C	Set 2	0.35	0.22	0.25	0.23	0.22	0.21	0.18	0.23	0.18	0.27	0.60	0.82	0.92	0.78	1.23
		Set 3	0.57	0.35	0.34	0.34	0.30	0.31	0.35	0.34	0.30	0.36	0.54	1.00	1.00	0.88	1.20
		Set 1	0.67	0.43	0.55	0.57	0.54	0.71	0.43	0.38	0.54	0.33	1.06	1.00	0.69	0.95	0.61
	BC*	Set 2	0.10	0.33	0.32	0.26	0.46	0.38	0.26	0.30	0.41	0.35	3.80	0.79	0.94	1.58	0.76
		Set 3	0.13	0.45	0.39	0.38	0.40	0.63	0.47	0.52	0.47	0.45	4.85	1.04	1.33	1.24	1.13
		Set 1	0.30	0.22	0.31	0.27	0.34	0.30	0.29	0.29	0.31	0.27	1.00	1.32	0.94	1.15	0.79
p38γ	S	Set 2	0.28	0.30	0.30	0.29	0.36	0.32	0.31	0.33	0.47	0.43	1.14	1.03	1.10	1.62	1.19
		Set 3	0.21	0.28	0.24	0.19	0.21	0.26	0.25	0.24	0.25	0.29	1.24	0.89	1.00	1.32	1.38
		Set 1	0.22	0.22	0.24	0.25	0.26	0.25	0.23	0.22	0.23	0.18	1.14	1.05	0.92	0.92	0.69
	C	Set 2	0.57	0.14	0.15	0.18	0.18	0.18	0.17	0.19	0.24	0.25	0.32	1.21	1.27	1.33	1.39
		Set 3	0.60	0.24	0.20	0.19	0.19	0.23	0.21	0.22	0.22	0.18	0.38	0.88	1.10	1.16	0.95

PSD-95	BC	Set 1	0.04	0.04	0.06	0.03	0.03	0.03	0.05	0.04	0.02	0.03	0.75	1.25	0.67	0.67	1.00
		Set 2	0.10	0.05	0.06	0.06	0.06	0.06	NQ	0.04	0.04	NQ	0.60	–	0.67	0.67	–
		Set 3	0.11	0.07	0.08	0.05	0.06	0.07	0.07	0.09	0.04	0.06	0.64	1.00	1.13	0.80	1.00
	S	Set 1	0.28	0.31	0.36	0.26	0.28	0.30	0.36	0.28	0.28	0.27	1.07	1.16	0.78	1.08	0.96
		Set 2	0.32	0.38	0.35	0.35	0.27	0.34	0.38	0.45	0.29	0.31	1.06	1.00	1.29	0.83	1.15
		Set 3	0.32	0.29	0.29	0.20	0.23	0.27	0.34	0.24	0.21	0.21	0.84	1.17	0.83	1.05	0.91
	C	Set 1	0.31	0.29	0.30	0.24	0.23	0.31	0.33	0.24	0.15	0.28	1.00	1.14	0.80	0.63	1.22
		Set 2	0.16	0.24	0.42	0.25	0.23	0.20	0.26	0.20	0.19	0.33	1.25	1.08	0.48	0.76	1.43
		Set 3	0.17	0.31	0.23	0.26	0.32	0.30	0.33	0.22	0.28	0.26	1.76	1.06	0.96	1.08	0.81
RSK1	BC*	Set 1	3.55	3.40	2.26	2.87	2.62	4.12	2.86	2.48	2.80	1.33	1.16	0.84	1.10	0.98	0.51
		Set 2	0.23	2.02	1.72	1.32	2.15	2.12	1.75	1.78	1.86	0.68	9.22	0.87	1.03	1.41	0.32
		Set 3	0.54	2.26	2.29	2.15	3.27	2.95	2.65	2.43	2.06	2.27	5.46	1.17	1.06	0.96	0.69
	S	Set 1	2.78	2.77	2.61	2.30	2.53	3.10	2.90	3.08	3.00	2.29	1.12	1.05	1.18	1.30	0.91
		Set 2	2.53	3.17	3.11	3.14	3.07	2.83	3.86	3.38	3.39	2.42	1.12	1.22	1.09	1.08	0.79
		Set 3	2.55	2.70	2.62	2.22	2.73	2.58	2.94	2.28	2.27	2.52	1.01	1.09	0.87	1.02	0.92
	C	Set 1	1.64	1.99	1.90	1.75	1.77	2.16	1.82	1.86	1.96	1.75	1.32	0.91	0.98	1.12	0.99
		Set 2	6.05	1.59	1.70	1.74	1.81	1.78	1.91	1.82	1.82	1.79	0.29	1.20	1.07	1.05	0.99
		Set 3	7.06	2.38	2.25	1.98	2.36	2.05	2.02	1.92	2.10	2.04	0.29	0.85	0.85	1.06	0.86

Secondary analyses of the NMDAR-regulated CaMK4β and MST1 signaling pathways in brainstem-cerebellum (**BC**), subcortical (**S**), and cortical (**C**) homogenates from three mock- and three scrapie-infected mice (Sets 1-3) at 70, 90, 110, 130 dpi, or at terminal stage of disease (TER). Asterisks indicate data obtained form primary screens. Ratios were calculated relative to the absolute levels in mock-infected mice from the same set at each time point. NQ, not quantitated due to blotting artifacts.

Appendix 6 – The levels of cleaved MST1 and phosphorylation levels of 10 protein kinases and substrates in scrapie-infected mice analyzed by targeted tertiary analyses.

			Mock-infected					RML-infected									
			Absolute (arbitrary units)					Absolute (arbitrary units)					Ratio				
			70	90	110	130	TER	70	90	110	130	TER	70	90	110	130	TER
Cleaved MST1	BC*	Set 1	0.01	0.05	0.02	0.04	0.01	0.01	0.05	0.03	0.10	0.01	1.00	1.00	1.50	2.50	1.00
		Set 2	0.01	0.01	0.01	0.01	0.01	0.01	0.01	0.01	0.02	0.01	1.00	1.00	1.00	2.00	1.00
		Set 3	0.01	0.01	0.01	0.12	0.01	0.01	0.01	0.01	0.18	0.01	1.00	1.00	1.00	1.50	1.00
	S	Set 1	0.01	0.01	0.01	0.01	0.01	0.01	0.01	0.01	0.04	0.01	1.00	1.00	1.00	4.00	1.00
		Set 2	0.02	0.02	0.02	0.02	0.02	0.02	0.02	0.02	0.10	0.02	1.00	1.00	1.00	5.00	1.00
		Set 3	0.02	0.01	0.01	0.02	0.01	0.02	0.01	0.01	0.05	0.01	1.00	1.00	1.00	2.50	1.00
	C	Set 1	0.01	0.01	0.01	0.01	0.01	0.01	0.01	0.01	0.07	0.01	1.00	1.00	1.00	7.00	1.00
		Set 2	0.01	0.01	0.01	0.01	0.01	0.01	0.01	0.01	0.03	0.01	1.00	1.00	1.00	3.00	1.00
		Set 3	0.01	0.01	0.01	0.01	0.01	0.01	0.01	0.01	0.05	0.02	1.00	1.00	1.00	5.00	2.00
p-CaMK4 (T196)	BC	Set 1	0.01	0.01	0.01	0.01	0.01	0.01	0.01	0.01	0.01	0.01	1.00	1.00	1.00	1.00	1.00
		Set 2	0.04	0.04	0.02	0.02	0.03	0.03	0.03	0.04	0.02	0.01	0.75	0.75	2.00	1.00	0.33
		Set 3	0.02	0.02	0.02	0.02	0.02	0.02	0.02	0.02	0.02	0.03	1.00	1.00	1.00	1.00	1.50
	S	Set 1	0.01	0.01	0.01	0.01	0.01	0.02	0.01	0.02	0.01	0.04	2.00	1.00	2.00	1.00	4.00
		Set 2	0.02	0.01	0.05	0.03	0.03	0.03	0.03	0.02	0.03	0.05	1.50	3.00	0.40	1.00	1.67
		Set 3	0.05	0.02	0.01	0.03	0.03	0.04	0.04	0.03	0.04	0.05	0.80	2.00	3.00	1.33	1.67
	C	Set 1	0.05	0.02	0.02	0.02	0.04	0.02	0.02	0.03	0.03	0.03	0.40	1.00	1.50	1.50	0.75
		Set 2	0.03	0.02	0.03	0.02	0.03	0.04	0.02	0.03	0.02	0.03	1.33	1.00	1.00	1.00	1.00
		Set 3	0.02	0.02	0.01	0.02	0.02	0.02	0.02	0.04	0.02	0.03	1.00	1.00	4.00	1.00	1.50
p-CaMK4β (T196)	BC	Set 1	0.01	0.01	0.01	0.01	0.01	0.02	0.02	0.01	0.01	0.01	2.00	2.00	1.00	1.00	1.00
		Set 2	0.01	0.02	0.02	0.02	0.01	0.03	0.03	0.03	0.02	0.01	3.00	1.50	1.50	1.00	1.00
		Set 3	0.02	0.02	NQ	0.03	0.03	0.04	0.04	0.02	0.03	0.06	2.00	2.00	–	1.00	2.00
	S	Set 1	0.01	0.01	0.01	0.01	0.01	0.01	0.01	0.01	0.01	0.01	1.00	1.00	1.00	1.00	1.00
		Set 2	0.02	0.01	0.03	0.01	0.01	0.03	NQ	0.01	0.01	0.01	1.50	–	0.33	1.00	1.00
		Set 3	0.01	0.01	0.03	0.02	0.01	0.01	0.01	0.02	0.02	0.01	1.00	1.00	0.67	1.00	1.00
	C	Set 1	0.01	0.01	0.01	0.01	0.01	0.01	0.01	0.01	0.01	0.01	1.00	1.00	1.00	1.00	1.00
		Set 2	0.02	0.01	0.01	0.01	0.01	0.01	0.01	0.01	0.01	0.01	0.50	1.00	1.00	1.00	1.00
		Set 3	0.01	0.01	0.01	0.01	0.01	0.01	0.01	0.01	0.01	0.01	1.00	1.00	1.00	1.00	1.00
p-CREB (S133)	BC	Set 1	0.01	0.02	0.02	NQ	0.02	0.02	0.03	0.03	0.03	0.04	2.00	1.50	1.50	–	2.00
		Set 2	0.05	0.04	0.07	0.07	0.07	0.11	0.07	0.07	0.07	0.05	2.20	1.75	1.00	1.00	0.71
		Set 3	0.03	0.05	0.09	0.09	0.06	0.09	0.08	0.09	0.10	0.06	3.00	1.60	1.00	1.11	1.00
	S	Set 1	0.07	0.09	0.12	0.12	0.08	0.11	0.11	0.14	0.11	0.16	1.57	1.22	1.17	0.92	2.00
		Set 2	0.04	0.10	0.22	0.06	0.16	0.15	0.13	0.21	0.15	0.13	3.75	1.30	0.95	2.50	0.81
		Set 3	0.09	0.10	0.20	0.21	0.09	0.17	0.15	0.22	0.17	0.23	1.89	1.50	1.10	0.81	2.56
	C	Set 1	0.03	0.02	0.04	0.04	0.04	0.06	0.03	0.04	0.04	0.08	2.00	1.50	1.00	1.00	2.00
		Set 2	0.02	0.02	0.06	0.02	0.05	0.05	0.04	0.06	0.03	0.03	2.50	2.00	1.00	1.50	0.60
		Set 3	0.03	0.03	0.07	0.08	0.05	0.06	0.07	0.08	0.08	0.12	2.00	2.33	1.14	1.00	2.40
p-FOXO3 (S208)	BC	Set 1	0.02	0.02	0.02	0.02	0.01	0.02	0.02	0.02	0.02	0.02	1.00	1.00	1.00	1.00	2.00
		Set 2	0.03	0.03	0.03	0.03	0.03	0.03	0.03	0.03	NQ	0.04	1.00	1.00	1.00	–	1.33
		Set 3	0.03	0.04	0.03	0.03	0.03	0.03	0.04	0.03	0.03	0.03	1.00	1.00	1.00	1.00	1.00
	S	Set 1	0.08	0.07	0.07	0.06	0.05	0.08	0.07	0.07	0.07	0.05	1.00	1.00	1.00	1.17	1.00
		Set 2	0.06	0.06	0.06	0.04	0.04	0.05	0.06	0.05	0.04	0.06	0.83	1.00	0.83	1.00	1.50
		Set 3	0.04	0.06	0.04	0.03	0.04	0.04	0.06	0.04	0.03	0.05	1.00	1.00	1.00	1.00	1.25
	C	Set 1	0.08	0.06	0.06	0.05	0.05	0.08	0.06	0.06	0.06	0.05	1.00	1.00	1.00	1.20	1.00
		Set 2	0.06	0.03	0.04	0.04	NQ	0.04	0.03	0.05	0.03	0.04	0.67	1.00	1.25	0.75	–
		Set 3	0.09	0.06	0.06	0.04	0.06	0.07	0.06	0.06	0.06	0.08	0.78	1.00	1.00	1.50	1.33

p-JNK (p54; T183/Y185)	**BC**	Set 1	0.26	0.19	0.28	0.19	0.26	0.22	0.16	0.25	0.18	0.22	0.85	0.84	0.89	0.95	0.85
		Set 2	0.62	0.45	0.50	0.45	0.56	0.61	0.50	0.58	0.44	0.43	0.98	1.11	1.16	0.98	0.77
		Set 3	0.67	0.49	0.58	0.50	0.56	0.71	0.52	0.70	0.54	0.63	1.06	1.06	1.21	1.08	1.13
	S	Set 1	0.94	0.78	0.90	1.02	0.56	1.27	0.84	1.32	1.12	1.26	1.35	1.08	1.47	1.10	2.25
		Set 2	0.98	0.97	1.12	0.86	1.11	1.15	1.01	1.51	1.07	0.95	1.17	1.04	1.35	1.24	0.86
		Set 3	0.92	0.93	0.82	1.04	0.91	1.13	1.02	1.37	1.07	1.30	1.23	1.10	1.67	1.03	1.43
	C	Set 1	0.79	0.86	0.84	0.73	0.78	0.96	0.74	0.93	0.76	1.07	1.22	0.86	1.11	1.04	1.37
		Set 2	0.51	0.49	0.87	0.53	0.87	0.99	0.80	1.07	0.62	0.89	1.94	1.63	1.23	1.17	1.02
		Set 3	0.61	0.70	0.90	0.84	1.02	0.95	1.04	0.94	0.95	0.94	1.56	1.49	1.04	1.13	0.92
p-Lyn (Y396)	**BC**	Set 1	0.01	0.01	0.01	0.01	0.01	0.01	0.01	0.01	0.01	0.01	1.00	1.00	1.00	1.00	1.00
		Set 2	0.02	0.01	0.01	0.01	0.01	0.02	0.01	0.01	0.01	0.01	1.00	1.00	1.00	1.00	1.00
		Set 3	0.02	0.02	0.02	0.02	0.01	0.02	0.02	0.02	0.02	0.01	1.00	1.00	1.00	1.00	1.00
	S	Set 1	0.02	0.02	0.02	0.02	NQ	0.02	0.02	0.02	0.02	0.02	1.00	1.00	1.00	1.00	–
		Set 2	0.04	0.03	0.03	0.03	0.02	0.04	0.03	0.03	0.02	0.02	1.00	1.00	1.00	0.67	1.00
		Set 3	0.01	0.02	0.02	0.02	0.02	0.02	0.02	0.02	0.02	0.02	2.00	1.00	1.00	1.00	1.00
	C	Set 1	0.02	0.02	0.03	0.02	0.02	0.02	0.02	0.02	0.02	0.02	1.00	1.00	0.67	1.00	1.00
		Set 2	0.02	0.02	0.01	0.01	NQ	0.02	0.02	0.01	0.01	0.02	1.00	1.00	1.00	1.00	–
		Set 3	0.02	0.02	0.02	0.02	0.02	0.02	0.02	0.01	0.02	0.02	1.00	1.00	0.50	1.00	1.00
p-MST1 (T183)	**BC**	Set 1	0.01	0.01	0.01	0.01	0.01	0.01	0.01	0.01	0.01	0.02	1.00	1.00	1.00	1.00	2.00
		Set 2	0.04	0.03	0.01	0.01	0.09	0.04	0.03	0.01	0.02	NQ	1.00	1.00	1.00	2.00	–
		Set 3	0.04	0.03	0.05	0.03	0.11	0.03	0.02	0.04	0.05	0.10	0.75	0.67	0.80	1.67	0.91
	S	Set 1	0.02	0.03	0.03	0.03	0.08	0.04	0.03	0.03	0.05	0.08	2.00	1.00	1.00	1.67	1.00
		Set 2	0.07	0.08	0.05	0.02	0.17	0.06	0.04	0.05	0.04	0.11	0.86	0.50	1.00	2.00	0.65
		Set 3	0.03	0.06	0.08	0.08	0.05	0.08	0.04	NQ	0.04	0.04	2.67	0.67	–	0.50	0.80
	C	Set 1	0.06	0.05	0.06	0.03	0.04	0.11	0.05	0.05	0.05	0.07	1.83	1.00	0.83	1.67	1.75
		Set 2	0.03	0.03	0.03	0.02	0.02	0.04	0.03	0.03	0.02	0.05	1.33	1.00	1.00	1.00	2.50
		Set 3	0.04	0.03	0.04	0.03	0.04	0.05	0.03	0.05	0.06	0.10	1.25	1.00	1.25	2.00	2.50
p-nNOS (S847)	**BC**	Set 1	0.06	0.05	0.03	0.03	0.05	0.10	0.06	0.03	0.04	0.10	1.67	1.20	1.00	1.33	2.00
		Set 2	0.03	0.08	0.09	0.07	0.11	0.02	0.06	0.07	0.09	0.14	0.67	0.75	0.78	1.29	1.27
		Set 3	0.06	0.15	0.04	0.08	0.08	0.07	0.16	0.03	0.07	0.15	1.17	1.07	0.75	0.88	1.88
	S	Set 1	0.02	0.02	0.01	0.01	0.10	0.02	0.07	0.01	0.03	0.01	1.00	3.50	1.00	3.00	0.10
		Set 2	0.01	0.11	0.04	0.04	NQ	NQ	0.09	0.02	0.02	0.07	–	0.82	0.50	0.50	–
		Set 3	0.13	0.10	0.05	0.05	0.04	0.04	0.02	0.05	0.08	0.07	0.31	0.20	1.00	1.60	1.75
	C	Set 1	0.03	0.03	0.01	0.02	0.06	0.03	0.07	0.04	0.02	0.07	1.00	2.33	4.00	1.00	1.17
		Set 2	0.18	0.05	0.06	0.07	0.10	0.02	0.09	0.03	0.07	0.15	0.11	1.80	0.50	1.00	1.50
		Set 3	0.03	0.03	0.02	0.03	0.05	0.03	0.02	0.02	0.09	0.03	1.00	0.67	1.00	3.00	0.60
p-p38 (T180/Y182)	**BC**	Set 1	0.03	0.01	0.04	0.04	0.05	0.04	0.02	0.05	0.03	0.06	1.33	2.00	1.25	0.75	1.20
		Set 2	0.25	0.10	0.18	0.19	0.26	0.24	0.19	0.21	0.14	0.13	0.96	1.90	1.17	0.74	0.50
		Set 3	0.25	0.18	0.20	0.22	0.20	0.30	0.27	0.28	0.25	0.20	1.20	1.50	1.40	1.14	1.00
	S	Set 1	0.22	0.18	0.21	0.23	0.19	0.37	0.21	0.34	0.35	0.52	1.68	1.17	1.62	1.52	2.74
		Set 2	0.31	0.34	0.57	0.34	0.55	0.54	0.42	0.58	0.46	0.33	1.74	1.24	1.02	1.35	0.60
		Set 3	0.40	0.55	0.42	0.49	0.40	0.59	0.57	0.82	0.56	0.46	1.48	1.04	1.95	1.14	1.15
	C	Set 1	0.24	0.24	0.29	0.25	0.31	0.51	0.27	0.33	0.35	0.36	2.13	1.13	1.14	1.40	1.16
		Set 2	0.14	0.15	0.30	0.16	0.38	0.33	0.24	0.35	0.25	0.21	2.36	1.60	1.17	1.56	0.55
		Set 3	0.19	0.33	0.31	0.32	0.47	0.42	0.40	0.31	0.44	0.40	2.21	1.21	1.00	1.38	0.85
p-RSK1 (S380)	**BC**	Set 1	0.69	0.30	0.56	0.26	0.46	0.43	0.39	0.39	0.38	0.56	0.62	1.30	0.70	1.46	1.22
		Set 2	1.22	0.87	1.24	0.67	1.44	1.51	1.13	1.43	0.77	1.09	1.24	1.30	1.15	1.15	0.76
		Set 3	1.11	1.00	1.48	1.01	1.70	1.67	1.37	1.26	1.21	0.78	1.50	1.37	0.85	1.20	0.46
	S	Set 1	1.63	0.59	0.96	1.73	0.52	1.41	1.91	1.54	1.52	1.40	0.87	3.24	1.60	0.88	2.69
		Set 2	1.31	1.05	1.83	1.68	0.90	1.17	0.73	1.47	1.46	1.97	0.89	0.70	0.80	0.87	2.19
		Set 3	2.06	1.07	0.53	0.94	1.31	1.18	0.85	1.24	1.48	2.25	0.57	0.79	2.34	1.57	1.72
	C	Set 1	2.50	2.09	1.87	1.25	2.42	1.74	1.54	1.70	2.19	1.16	0.70	0.74	0.91	1.75	0.48
		Set 2	0.81	0.82	0.51	0.73	0.83	1.40	0.69	1.42	0.71	1.04	1.73	0.84	2.78	0.97	1.25
		Set 3	1.36	1.60	1.54	0.76	0.89	1.42	1.72	0.81	1.48	0.67	1.04	1.08	0.53	1.95	0.75

Tertiary analyses of the CaMK4β/CREB and MST1 signaling pathways in brainstem-cerebellum (**BC**), subcortical (**S**), and cortical (**C**) homogenates from three mock- and three scrapie-infected mice (Sets 1-3) at 70, 90, 110, 130 dpi, or at terminal stage of disease (TER). Asterisks indicate data obtained form primary screens. Ratios were calculated relative to the absolute levels in mock-infected mice from the same set at each time point. NQ, not quantitated due to blotting artifacts.